Improved Thermodynamic Investigation of Asphaltene Precipitation

By

A thesis submitted to the school of Graduate Studies in partial fulfillment of the requirements for the degree of

Doctor of Philosophy

Faculty of Engineering and Applied Science

Memorial University of Newfoundland

May 2023

St. John's, Newfoundland and Labrador

Canada

Abstract

Asphaltenes are analogous to the "cholesterol" of crude oils, so they may cause significant flow assurance problems to various oil and gas processes and negatively affect the economy of the oil recovery, transportation, and processing by increasing operational expenditures (OPEX). Asphaltenes increase oil viscosity, decrease its market value, and, when they precipitate, cause flow assurance challenges. Understanding asphaltene precipitation and phase behaviour is important to avoid, prevent, and address asphaltene flow assurance challenges. An experimental investigation is time-consuming and requires laboratory expertise with limitations on how many experiments can reasonably be conducted over what range of feasible operating conditions. Furthermore, we need to predict asphaltene and fluid phase behaviour over the full range of operating conditions to avoid flow assurance issues. Therefore, having a thorough knowledge of the phenomenon and applying asphaltene modeling approaches is essential to foresee conditions leading to asphaltene precipitation to treat the phenomenon properly. Despite significant research, asphaltene behaviour in different operating conditions and the application of improved thermodynamic investigations have not been well understood. There is little research on the investigation of the operating conditions and improvement of the thermodynamic models (e.g., application of advanced optimization technique) on asphaltene precipitation. This thesis uses different modeling approaches (e.g., equation of state) to investigate crude oil asphaltene precipitation at operating conditions.

Asphaltene phase separation can be triggered by altering the operating conditions, e.g., temperature, composition, and adding n-alkanes. For instance, decreasing temperature from reservoir conditions leads to asphaltene precipitation due to alteration of the solubility of asphaltene in the oil mixture. Moreover, the composition of crude oil is upgraded or downgraded

by adding different hydrocarbons at the refinery inlet. Yet, the prediction of asphaltene precipitation and the impact of operating conditions are quite uncertain, and detailed thermodynamic investigations and appropriate techniques for adjusting the models are required.

Several research studies have used thermodynamic equations of state (EoS) to model asphaltene precipitation. Recently, advanced EoSs that take into account the association of hydrogen bonding has become popular. For example, Cubic Plus Association (CPA) has shown promising results in modeling asphaltene precipitation. There is uncertainty in using EoSs, e.g., tuning the adjustable parameters. Hence, there is a need to systematically study how to adjust the tunable parameters to predict asphaltene precipitation using advanced EoS.

The objective of this research is to investigate and improve the performance of EoS modeling of asphaltene precipitation. For this purpose, first, a comprehensive literature review was conducted to address asphaltene precipitation from different standpoints. While a comprehensive literature review to study asphaltene precipitation and deposition was missing in the literature, the focus of this research is to provide an overview of the nature and physical properties of asphaltenes, experimental and thermodynamic/simulation tools investigations, operating/fluid/reservoir impact, inhibition/treatment, and economic analysis of flow assurance. The literature review findings highlighted two main gaps in asphaltene thermodynamic modeling; 1) only gradient-based optimization techniques have been used to tune the EoS parameters, and 2) the effect of heteroatoms in asphaltene precipitation has not been considered. Therefore, the two other objectives of this thesis are tailored to address the gaps.

In order to address the fact that only gradient-based methods have been used to tune the parameters, we used a global optimization approach instead of gradient-based optimization to relate and correlate hydrogen bonding to the binary interaction parameters of the Cubic Plus Association

(CPA) EoS model. While the application of advanced optimization methods and a systematic sensitivity analysis of operational conditions/BIPs were missing in the literature, the focus of this section is to consider the association of hydrogen bonding in asphaltene precipitation while developing correlations for binary interactions (BIs) using global optimization. The advantages of using global optimization are to avoid entrapment in local minima while optimizing the parameters of the EoS and to improve the correlation/prediction capability of the EoS by finding the best fit of the adjustable parameters. The CPA EoS is validated by predicting unseen data, comparing with cubic EoSs, i.e., SRK and PR, using different oil characterization, e.g., SARA analysis, and drawing an analogy between scaling equation and CPA. Application of the proposed technique significantly improved the performance of the CPA EoS in modeling asphaltene precipitation (average deviation of less than 0.067 for correlation and prediction). The relative importance analysis revealed that the composition of the mixture (dilution ratio) is the most influential factor contributing to the asphaltene precipitation (other factors are temperature and carbon number of the diluents).

The effect of polar forces due to the presence of heteroatoms on asphaltene phase behaviour is investigated using a Cubic Plus Polar EoS (CPP). To the best of our knowledge, we have not found any literature focused on polar heteroatom forces in asphaltene thermodynamic modeling. In this novel work, we demonstrate how a single term that accounts for polarity can be added to the extension of the cubic EoS and be effectively applied to calculate asphaltene precipitation. Further, a simplified oil characterization method is adapted to reduce the number of adjustable parameters (binary interactions) and reduce the need for experimental measurements. A global optimization approach and molecular dynamic (MD) simulation have also been used to increase the reliability of the optimization and reduce the number of adjustable parameters for polar forces. This section

of the research finds that the CPP approach using global optimization to tune parameters of the EoS is the most reliable approach, followed by CPP EoS using MD to find dipole moment for the aryl-linked core asphaltene structure (average R2 for both modes are above 0.98).

The improved thermodynamic approaches (global optimization and including the effect of heteroatoms) introduced in this research can be used by other researchers to increase the efficiency of the asphaltene thermodynamic modeling.

ACKNOWLEDGMENTS

"This dissertation is dedicated to my family for their endless support."

My partner has been a constant source of support and encouragement throughout

the research journey, providing a listening ear, insightful feedback, and

unwavering belief in their success.

To my parents and siblings, I am eternally grateful for your constant support and

unwavering faith.

TABLE OF CONTENTS:

LIST OF TABLES

LIST OF FIGURES

Chapter 1 : Introduction and Overview

The steadily increasing demand for energy has caused an increase in new investment in fuels due to the energy crisis [1], even as we try to reduce our global GHG emissions. Even though the climate commitment and Net-Zero emissions by 2050 have been accepted by 33 countries, the European Union, and Canada, fossil fuels will still make up a majority of Canada's energy mix by 2050 [2]. The Canadian Association of Petroleum Producers (CAPP) projects an increase in oil production of 1.7 million barrels per day (b/d) by 2035. The total annual production of Canadian oil companies is expected to increase steadily by 1% annually [3]. To meet the production of oil rate forecasted for 2022 and years after, major oil and gas companies have increased investment in the upstream facilities, led by US oil companies, such as ExxonMobil and Chevron, by 34% and 24% of increased investments, respectively [1].

The majority of our energy still comes from oil and gas, and this trend will continue for the foreseeable future. Given the climate and energy crisis, it is even more important that we reduce the energy intensity of oil production. It has been predicted that the demand for energy in some leading importers of oil (China and India) will increase by almost 25%, while the oil demand will rise by almost 40% in the Americas [1]. With the growth of technology and the advent of modern products, especially in transportation, oil will continue to play a leading role in the world's energy mix until 2030, when it is predicted that fossil fuels will cover around 70% of the demanding energy and oil would be the leading source of energy [1]. Due to the high demand for oil and the need for massive production and transferring equipment, flow-assurance issues will become more substantial. Flow assurance includes maintaining sustainable hydrocarbon production from the reservoir to facilities for both onshore and offshore cases. Managing the hydrocarbon flow and preventing the formation of slug or blockage (solids formation, such as waxes, asphaltenes, hydrates, and scales) are the critical aspects of flow assurance in oil and gas energy and can be particularly challenging when longer subsea pipelines are used. Due to the ongoing demand for oil, new projects, and more effort to produce from extended fields, asphaltene flow-assurance issues will likely become more substantial [4-8].

Large chain molecules found in the oil, such as waxes and asphaltenes, challenge flow assurance and can impact production. Asphaltenic crudes and asphaltene-related issues are found worldwide. For instance, some regions of Alberta, west Texas, and Alaska in the US, the southern region of Mexico, and the North Sea, particularly the Norwegian sector, are affected by asphaltenic oils.

Moreover, fields in Venezuela, the Adriatic Sea, the Persian Gulf, and the US Gulf of Mexico have experienced (and are still experiencing) asphaltene precipitation/deposition and related problems [9, 10].

Asphaltene precipitation and deposition can negatively affect production systems' profitability in upstream or downstream sections (Figure 1). For example, asphaltene precipitation/deposition in upstream parts may block pore throats, decrease the fluid flow during gas injection recovery processes, alter reservoir wettability, stabilize water-in-oil emulsions, and lead to the creation of high viscosity fluids, and reduce oil relative permeability and mobility [11, 12]. In downstream operations, asphaltene precipitation/deposition results in unfavourable phenomena, such as the plugging of flow facilities, the formation of solids in storage tanks, and fouling safety valves. Moreover, asphaltene may cause severe issues in refineries, including a reduction in conversion level by deactivating catalysts, a higher formation rate of coke, and a decline in the overall rate of hydrotreating reactions [13]. Therefore, it is important to understand the asphaltene precipitation and deposition to avoid flow assurance issues during crude oil processing.
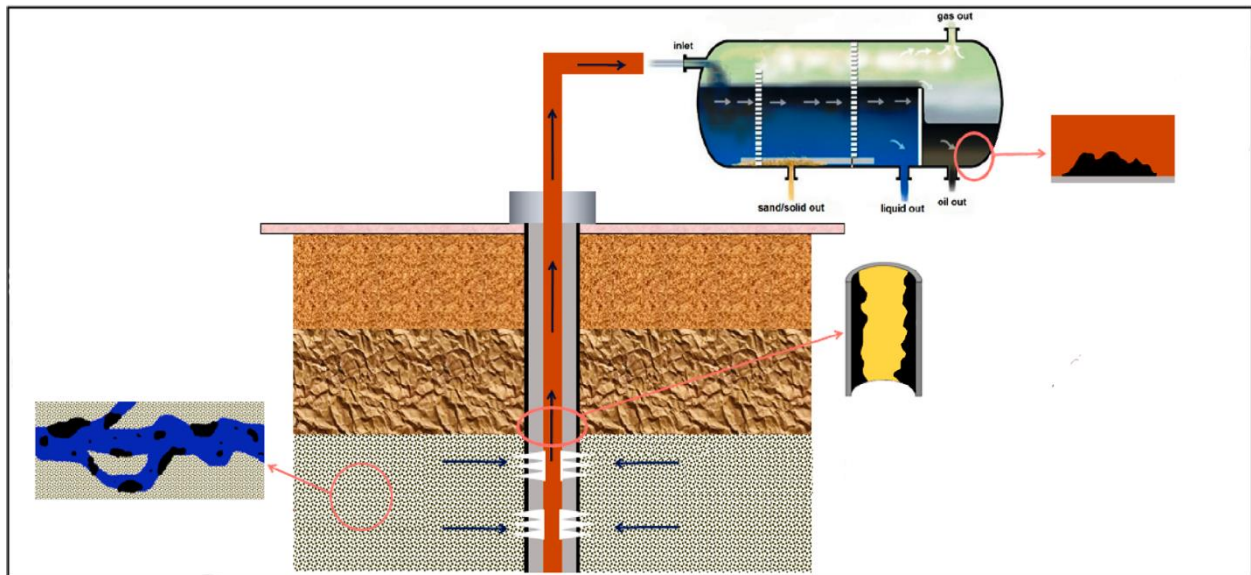
Figure 1-1. Asphaltene precipitation examples in oil production, reservoir, and equipment [14]

Oil is a complex mixture of several hydrocarbons, and its complexity is the reason to classify oil with respect to group analysis. Solution properties and polarity of petroleum residuum in various solvents are the basis of the classical definition of oil. Generally, crude oils are classified into two

fractions: maltene and asphaltene. Maltene consists of saturates, aromatics, and resins in the form of continuous oil, while asphaltene is dispersed or dissolved in crude oil [15]. Asphaltene has been named the "cholesterol" of petroleum due to its tendency to precipitate and deposit out of the oil [16, 17]. In 1837, J. B. Boussingault first introduced asphaltene, which is soluble in turpentine and insoluble in alcohol [18]. In fact, asphaltene is a complex and heavy molecule which is insoluble in nonpolar solvents such as light hydrocarbons, low-boiling naphtha, and hydrocarbon gas (methane). In contrast, it is soluble in solvents with high surface tension, for example, pyridine, carbon disulphide, benzene, and toluene [19]. Paraffin is also used to classify asphaltene, while the quantity of precipitation is a function of solvent type, dilution ratio (solvent/oil), thermodynamic conditions, and contact time [15]. While light oil samples have less asphaltene content, they are more prone to asphaltene related problems in comparison with the medium and heavy oil samples, which have a higher asphaltene content. This is because of the solubility of asphaltene in oil samples and the presence of light hydrocarbons. It has been shown that the solubility of light oils containing a small amount of asphaltene changes to a higher degree with changes in operating conditions in comparison with the heavier oils. Therefore, the probability of asphaltene precipitation is higher for the light oil samples, despite the fact that they predominantly have a smaller amount of asphaltene. Moreover, oil with a higher viscosity usually shows less asphaltene precipitation due to the presence of lighter hydrocarbons to stabilize asphaltene particles [23].

Intermolecular interactions between asphaltene-asphaltene and asphaltene-maltene have an essential impact on the stability of asphaltene in an oil mixture. It has been shown that non-polar van der Waals force is an important factor in asphaltene phase equilibrium. Moreover, the association of hydrogen bonding (bridge) as a result of the presence of hydrogen atoms (proton donor) bonded to an electronegative atom, i.e., oxygen (proton acceptor), can be considered a deterministic intermolecular force resulting in asphaltene phase separation. In addition, polar forces of heteroatoms, e.g., sulfur, can impart a dipole-dipole effect and assist with asphaltene phase separation. Asphaltenes molecules associate with each other and precipitate as a change in the operating conditions, including temperature, pressure and composition.

While applying flow assurance techniques to inhibit asphaltene phase separation is costly, the formation and removal of asphaltene deposition can cost even more and threaten the profitability

of oil production. Therefore, it is important to predict the occurrence and the amount of asphaltene phase separation in upstream and downstream. Asphaltene phase behaviour and precipitation have been investigated in the literature by considering various asphaltene states considering different oils/asphaltene content, solvents, and operating conditions experimentally and via mathematical modeling. There are two main modeling categories; thermodynamic solubility and colloidal theory-based models [20]. There are some difficulties in modeling asphaltene precipitation, first, optimization of the adjustable parameters, and second, considering the intermolecular forces in the modeling approach. The modeling approaches in asphaltene phase behavior, e.g., Equation of State (EoS), are highly nonlinear. To date, only gradient-based optimization methods have been used, e.g., Nelder-Mead (NM) simplex and Least Squares methods, but they are not necessarily well-suited to non-linear behaviour. Gradient-based optimization methods have a high chance of entrapment in local optima and cannot best-tune the adjustable parameters. Secondly, asphaltene precipitation is controlled by different intermolecular forces, e.g., the association of hydrogen bonding and polarity of heteroatoms; therefore, considering simple intermolecular forces (van der Waals force) may cause inaccurate results [21, 22].

Asphaltene modelings, such as EoS, enable us to accurately predict the asphaltene phase behaviour. However, the application of EoS models of asphaltene precipitation, particularly considering intermolecular forces (e.g., association) and advanced optimization, are still in its infancy. Most advanced EoS are too complex, with a high number of adjustable parameters. Therefore, there is a need for a simplified EoS while accounting for intermolecular forces, e.g, association, a few numbers of adjustable parameters, and global optimization.

Three research gaps are identified regarding the asphaltene literature review, optimization of the EoS, and intermolecular forces in asphaltene precipitation. Therefore, three main objectives are defined and addressed in three chapters of the thesis (chapters 2, 3, and 4) to study asphaltene phase separation.

1. Objective One - Comprehensive Literature Review

Research gap: While asphaltene related issues have been reviewed in the literature, there has been a lack of comprehensive studies focusing specifically on molecular investigations, operating conditions, modeling tools, and economic analysis in asphaltene precipitation and deposition. The

existing literature reviews focus on limited aspects of asphaltene; a comprehensive understanding of related issues is needed. For example, thermodynamic approaches are reviewed in literature; however, information regarding the molecular states, impact of operating conditions, and the relationship between asphaltene precipitation and deposition was lacking [23, 24]. Besides, molecular scale experimental investigations of asphaltene are reviewed in the literature [25]; the interconnection between asphaltene molecular state, modeling approaches/tools (e.g., MD calculations), and thermodynamic models were missing in the literature.

Contribution/novelty: In this research, an attempt is made to cover a wide range of research studies of asphaltene-related issues to address the missing comprehensive review in the literature. Our comprehensive review includes the following: physical properties of asphaltene; kinetics of precipitation; experimental and modeling studies (e.g., thermodynamic modeling) of precipitation/deposition; effects of different variables, including operational conditions, fluid properties, and reservoir characteristics; simulation and optimization tools at various scales; treatment and inhibition techniques; economic analysis of flow assurance; and theoretical and practical challenges of precipitation/deposition (chapter 2).

2. Objective Two - Optimize Parameters of the CPA EoS Using a Global Optimization Approach

Research gap: The majority of the studies use gradient-based optimization techniques to tune the EoS. While the EoSs are highly non-linear, a gradient-based optimization technique may cause entrapment in the local optima and result in poor modeling capabilities. Recently, there have been some research regarding using CPA EoS for either asphaltene onset or precipitation [24-27]. However, the research does not consider global optimization of CPA EoS (while an advanced optimization technique is required to tune the parameters of the EoS), model both weight percent of precipitation and onset, correlate binary interaction parameters, and consider limited operation conditions. Moreover, a systematic sensitivity analysis of operational conditions and BIPs was missing in the literature. Having a systematic sensitivity analysis helps to better understand asphaltene phase separation and validate the performance of the EoS under different conditions. Moreover, BIPs play an important role in the accuracy and prediction capability of the EoS that needs to be carefully studied.

Contribution/novelty: We have found very little research focused on optimizing EoS. We believe our implementation of global optimization (GO) to tune association and BI parameters in CPA to be novel. This research uses the CPA approach to study asphaltene precipitation. The GO approach uses global optimization techniques to develop a thorough optimization to find associations and BIPs, and to avoid entrapment in local minima. The novel developed algorithm and the step-by-step procedure are introduced. In this work, first, the BIPs are correlated with the temperature and carbon number of the n-alkane to increase the reliability and accuracy of the CPA model. Later, the CPA EoS is further validated by predicting unseen data, is compared with cubic EoSs, i.e., SRK and PR, oil characterization is compared with other approaches, e.g., using SARA analysis, and then an analogy is drawn between the CPA EoS and the scaling equation. Finally, the relative importance analysis is performed to explain the role of each independent variable, i.e., temperature, the carbon number of solvent, and quantity of solvent, on asphaltene precipitation and BIPs (chapter 3).

3. *Objective Three - Consider Heteroatoms in Asphaltene Precipitation Modeling*

Research gap: Considering the comprehensive literature review presented in chapter 2 of this research, it is shown that the presence of the heteroatoms (e.g., sulfur) and their impact on the phase separation of asphaltene has not been sufficiently investigated. The heteroatoms impart polarity to the asphaltene molecule, and polar interactions contribute to asphaltene aggregation and precipitation. Therefore, Cubic Plus Polar (CPP) EoS is used to study the impact of heteroatoms on asphaltene precipitation. CPP EoS is an extension of the cubic EoS that accounts for polar energy contributing to asphaltene phase separation.

Contribution/novelty: This objective aims to study the effect of polar forces on asphaltene phase behaviour using CPP EoS. To the best of our knowledge, we have not found any literature focused on polar heteroatom forces in asphaltene phase behaviour, and we believe our implementation of polar energy in the asphaltene system and the approach used here to be novel. In this work, we demonstrate how a single term can be added to the extension of cubic EoS to account for polar interactions and effectively be applied to calculate asphaltene precipitation. Furthermore, we make the model less complex using an oil characterization method adopted from the literature to reduce the number of adjustable parameters (binary interactions) and the need for experimental

measurements. A global optimization approach and molecular dynamic (MD) simulation have also been used to increase the reliability of the optimization and reduce the number of adjustable parameters for polar forces (chapter 4).

References

1. Iea. "World Energy Investment 2022 – Analysis." IEA, https://www.iea.org/reports/world-energy-investment-2022.

2. Government of Canada, Canada Energy Regulator. "Canada Energy Regulator / Régie De L'énergie Du Canada." *CER*, Canada Energy Regulator / Régie De L'énergie Du Canada, 11 Apr. 2022, https://www.cer-rec.gc.ca/en/data-analysis/canada-energy-future/2020/net-zero/index.html.

3. Oilgascanada. "Crude Oil Forecast: Canadian Association of Petroleum Producers." CAPP, https://www.capp.ca/resources/crude-oil-forecast/.

4. Civan, F., Reservoir formation damage. 2015: Gulf Professional Publishing.

5. Olayiwola, S.O. and M. Dejam, A comprehensive review on interaction of nanoparticles with low salinity water and surfactant for enhanced oil recovery in sandstone and carbonate reservoirs. Fuel, 2019. 241: p. 1045-1057.

6. Olayiwola, S.O. and M. Dejam, Mathematical modelling of surface tension of nanoparticles in electrolyte solutions. Chemical Engineering Science, 2019. 197: p. 345-356.

7. Saboorian-Jooybari, H., M. Dejam, and Z. Chen, Heavy oil polymer flooding from laboratory core floods to pilot tests and field applications: Half-century studies. Journal of Petroleum Science and Engineering, 2016. 142: p. 85-100.

8. Mashayekhizadeh, V., S. Kord, and M. Dejam, EOR potential within Iran. Special Topics & Reviews in Porous Media: An International Journal, 2014. 5(4)

9. Cenegy, L.M. Survey of successful world-wide asphaltene inhibitor treatments in oil production fields. in SPE Annual Technical Conference and Exhibition. 2001. Society of Petroleum Engineers.

10. Mohammadzadeh, O., et al. Experimental Investigation of Asphaltene Induced Formation Damage due to Pressure Depletion of Live Reservoir Fluids in Porous Media. in SPE Annual Technical Conference and Exhibition. 2017. Society of Petroleum Engineers.

11. Leontaritis, K., J. Amaefule, and R. Charles, A systematic approach for the prevention and treatment of formation damage caused by asphaltene deposition. SPE Production & Facilities, 1994. 9(03): p. 157-164.

12. Seifried, C.M., J. Crawshaw, and E.S. Boek, Kinetics of asphaltene aggregation in crude oil studied by confocal laser-scanning microscopy. Energy & Fuels, 2013. 27(4): p. 1865-1872.

13. Powers, D., et al., Regular solution based approach to modeling asphaltene precipitation from native and reacted oils: Part 1, molecular weight, density, and solubility parameter distributions of asphaltenes. Fuel, 2016. 178: p. 218-233.

14. Mahmoudi Alemi, Fatemeh, Saber Mohammadi, Seyed Ali Mousavi Dehghani, Alimorad Rashidi, Negahdar Hosseinpour, and Abdolvahab Seif., Experimental and DFT Studies on the Effect of Carbon Nanoparticles on Asphaltene Precipitation and Aggregation Phenomena. Chemical Engineering Journal 422 (2021): 130030.

15. Speight, J.G., The chemistry and technology of petroleum. 2014: CRC press.

16. Kokal, S.L. and S.G. Sayegh. Asphaltenes: The cholesterol of petroleum. in Middle East Oil Show. 1995. Society of Petroleum Engineers.

17. Lin, Y.-J., et al., Examining asphaltene solubility on deposition in model porous media. Langmuir, 2016. 32(34): p. 8729-8734.

18. Boussingault, J. Mémoire sur l'influence des défrichements dans la diminution des cours d'eau. in Annales de chimie. 1837.

19. Mullins, O.C. and E.Y. Sheu, Structures and dynamics of asphaltenes. 2013: Springer Science & Business Media.

20. Forte, E. and S.E. Taylor, Thermodynamic modelling of asphaltene precipitation and related phenomena. Advances in colloid and interface science, 2015. 217: p. 1-12.

21. Abunahman, S. S., dos Santos, L. C., Tavares, F. W., & Kontogeorgis, G. M., A computational tool for parameter estimation in EoS: New methodologies and natural gas phase equilibria calculations. Chemical Engineering Science, 2020. 215: p. 115437.

22. dos Santos, L. C., Abunahman, S. S., Tavares, F. W., Ahón, V. R. R., & Kontogeorgis, G. M., Modeling Water Saturation Points in Natural Gas Streams Containing CO2 and H2S-Comparisons with Different Equations of State. Industrial & Engineering Chemistry Research, 2015. 54(2): p. 743-757.

23. Zendehboudi, Sohrab, et al. "Asphaltene Precipitation and Deposition in Oil Reservoirs – Technical Aspects, Experimental and Hybrid Neural Network Predictive Tools." Chemical Engineering Research and Design, vol. 92, no. 5, 2014, pp. 857–875.

24. Shirani, B., Nikazar, M., Naseri, A., Mousavi-Dehghani, S.A., Modeling of asphaltene precipitation utilizing Association Equation of State. Fuel, 2012. 93: p. 59-66.

25. Behnous, D., Palma, A., Zeraibi, N., & Coutinho, J. A., Modeling asphaltene precipitation in Algerian oilfields with the CPA Eos. Journal of Petroleum Science and Engineering, 2020. 190, 107115.

26. Nazemi, R., Daryasafar, A., Bazyari, A., Shafiee Najafi, S. A., & Ashoori, S., Modeling Asphaltene Precipitation in live crude oil using cubic plus association (CPA) equation of State. Petroleum Science and Technology, 2019, 38(3), 257-265.

27. Zare Talavaki, M., Afsharpour, A., & Taherian, Z., Determination of asphaltene precipitation using a CPA equation of State. Petroleum Science and Technology, 2017, 35(9), 839-844.

Chapter 2 : Literature Review

(A comprehensive review of asphaltene deposition in petroleum reservoirs: Theory, challenges, and tips, (Published)

Preface

A version of this manuscript has been published in the Journal of Fuel 252 (2019): 753-791. I am the primary author of this paper. Along with the co-authors, Sohrab Zendehboudi and Lesley James, I carried out the literature review, data collection, and discussions on experimental and modeling studies on the asphaltene precipitation/deposition process. I prepared the first draft of the manuscript and subsequently revised the manuscript based on the co-authors' feedback as well as the comments received from the peer review process. The co-author, Sohrab Zendehboudi and Lesley James, contributed by providing the manuscript's outlines, comments on various parts of the manuscript, and assisted in reviewing and revising the manuscript.

ABSTRACT

Asphaltene is the heaviest and most polar fraction of crude oils, which is usually defined as a solubility class, soluble in light aromatics, benzene and toluene, and insoluble in paraffin. Asphaltene precipitation/deposition negatively affects a variety of oil and gas processes, including oil recovery, transportation, and petroleum processing, as it exhibits some undesirable impacts, such as an increase in the viscosity of crudes and stability of the emulsions, a decrease in the distillate yields, and unstable phase separation. Experimental and theoretical investigations have revealed that asphaltene precipitation/deposition is influenced by several parameters/variables, including pressure, temperature, characteristics of the involved mixtures, properties and amount of precipitant, and characteristics of porous media. Knowing the undeniable consequences of asphaltene precipitation/deposition, such as reduction of well productivity or blockage of the surface facilities, effective treatments or inhibition techniques have gained widespread attention in the petroleum industry so far. Hence, a comprehensive knowledge of previous findings and an adequate understanding of different aspects of asphaltene precipitation/deposition (e.g., mechanisms and characterization) seem to be pivotal. Various attempts have been made to investigate different aspects of this phenomenon, including the thermodynamics of precipitation, kinetics of flocculation, and deposition mechanisms. The previous studies and the importance of asphaltene in the oil and gas industry inspired us to provide a comprehensive review of the asphaltene precipitation/deposition that helps to understand further the governing mechanisms, thermodynamic behaviours, and transport phenomena prospects in this area. In this review work, the theories and mechanisms of precipitation/deposition, experimental and modeling approaches, the effects of operational parameters, and treatment/inhibition techniques are reviewed. Moreover, the economic analysis of flow assurance and the most common theoretical and practical challenges in asphaltene precipitation/deposition are studied.

Keywords: Asphaltene Precipitation/Deposition; Experimental Methods; Modeling Approaches; Inhibition and Treatment Methods; Economic Analysis

2-1. Introduction

An uninterrupted supply and high demands for oil are crucial for countries in which fossil fuels are considered the major part of energy consumption. It has been predicted that the demand for energy in some main importers of oil (China and India) will increase by almost 25%, while the oil demand will rise by almost 40% in the Americas [1]. With the growth of technology and the advent of modern products, especially in transportation, oil will continue to play a leading role in the world's energy mix

until 2030, when it is predicted that fossil fuels will cover around 70% of the demanding energy and oil would be the leading source of energy [1]. Due to the high demand for oil and the need for massive production and transferring equipment, the asphaltene flow-assurance issues will become more substantial. One of the operational risks of pipelines is the transportation of multiphase fluids. Asphaltene precipitation and deposition is one of the potential problems (other risks include wax formation, hydrate formation, corrosion, and severe slugging), which may occur and subsequently cause operational problems to downstream and upstream processing facilities [2-6]. Flow assurance is the practice of identifying the quantity and mitigating the risks associated with oil and gas systems [7]. A phase diagram of black oil from the Gulf of Mexico is shown in Figure 1, which indicates that different solids may form in the production and transfer of crude oil from the reservoir to the flow line, which can impede the movement of fluids [8]. Solid formations, especially asphaltene, can have detrimental effects on production systems' profitability. Hence, it is vital to control solids formation to address economic and environmental penalties [2].
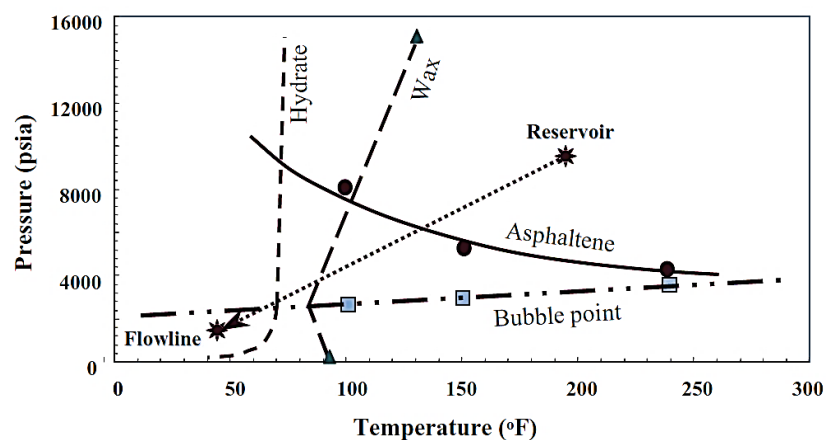
Figure 2-1. Phase diagram of a black oil obtained from the Gulf of Mexico [8]

Asphaltene has a complex structure and is qualitatively known as the heaviest and most polar fraction of crude oils. Generally, asphaltene is defined by its solubility and polarity characteristics, not by a specific chemical classification. Asphaltenes are operationally categorized as soluble in aromatic solvents such as toluene and benzene, while they are insoluble in light paraffinic solvents, including n-heptane and n-hexane [9-11]. The definition of asphaltene by its solubility characteristic is appropriate because not only it captures the aromatic fraction of crude oil, but it also includes asphaltene compounds that aggregate. Asphaltene may exist in other carbonaceous materials, such as coal, but coal-derived asphaltenes do not aggregate [12]. Asphaltene destabilization is influenced by several

parameters/variables, including pressure, temperature, characteristics of the mixture, and properties and amount of precipitant. Subsequently, solid aggregations may appear due to the changes in thermodynamic conditions, as well. It has been experimentally proven that the asphaltene precipitation is mainly affected by the pressure in comparison with other thermodynamic and process factors/characteristics [13]. A generic Pressure-Temperature (PT) diagram of the asphaltene (Asphaltene Precipitation Envelope or APE) is depicted in Figure 2. The two-phase diagram is started from points A to B. The former point is noted as a low-pressure dew point, where a rich phase of asphaltene is emerging from the vapour phase. Step-by-step, the pressure increases to the (T_3, P_3) point, at which three phases of vapour-liquid-asphaltene co-exist [14]. The APE, with its quality lines, can be regarded as a useful tool in finding the quantity of precipitation and mitigation ways of asphaltene related issues [15].
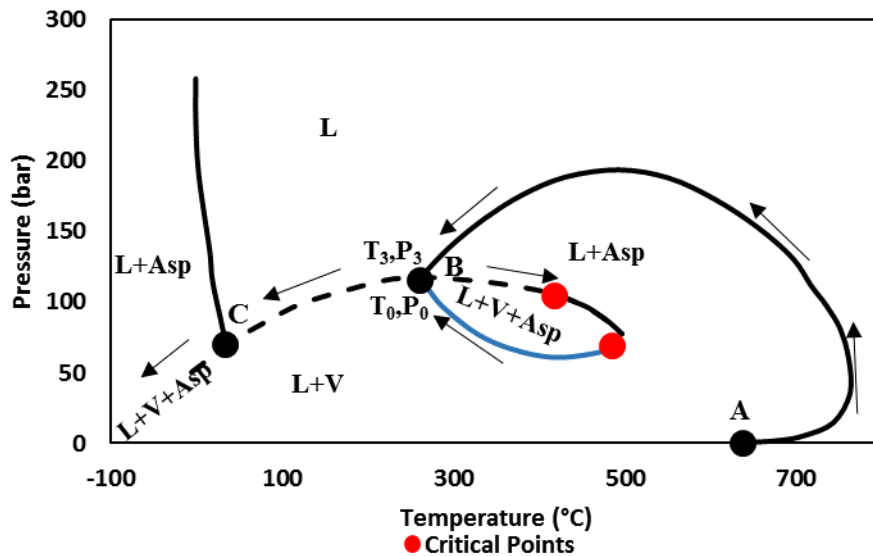
Figure 2-2. Generic Asphaltene Precipitation Envelope (APE) [14]

Light crudes are more prone to asphaltene precipitation in comparison with heavy oils. Although heavy oils have a higher asphaltene content, their lower tendency to precipitation is due to a high quantity of resin to stabilize asphaltene. From the colloidal point of view, asphaltene compounds are made of micelles, which are surrounded by resins and hydrocarbons, spreading in the oil medium. Asphaltene aggregation and phase separation generally occur due to the disconnection of resins from the asphaltene colloids [16].

Asphaltene precipitation and deposition may negatively affect the performance (and/or profitability) of production systems, in both upstream or downstream sections. For instance, the blockage of the pore

throats, alteration of reservoir wettability, and a decrease in permeability are the unfavourable consequences of the asphaltene precipitation and deposition. In addition, asphaltene precipitation/deposition in the downstream part leads to the plugging of flow facilities, the formation of solids in storage tanks, and fouling safety valves. Furthermore, asphaltene may reduce the conversion of catalysts and cause coke formation in refineries [17-19].

For more than half of a century, several researchers have focused on a variety of asphaltene-related issues (characterization, modeling, and mitigation) to address the main relevant concerns in the oil industry about the kinetics and quantity of precipitation/deposition [20-33]. Many experimental procedures and modeling approaches have been reported to describe the kinetic behaviours and thermodynamic states of asphaltene at different thermodynamic and process conditions [13, 16, 34-40]. In general, the common approaches to model asphaltene precipitation are classified into two main categories, including thermodynamic solubility techniques and colloidal-based models. In the former, asphaltene particles are considered to be dissolved in crude oil, which appears in the form of a real solution. The models categorize the oil mixture into two phases, asphaltenic and non-asphaltenic, using the solubility concept [20-24]. Thermodynamic operations (such as adding a solvent) disturb the phase equilibrium of the oil mixture and consequently cause phase separation, which is attributed to the changes in solubility of either of the two phases. However, the role of resins is not considered in this category and resins are modeled as separate molecules. Two distinguished groups are considered in the solubility-based approaches, including models using the lattice fluid theory and Equations of State (EoSs) [41]. One of the early models in asphaltene precipitation is the polymer models, particularly the lattice fluid theory. In this category, the Flory-Huggins polymer-solution theory and the regular-solution theory of Scatchard-Hildebrand have been more common in comparison with the Scott–Magat theory to study the precipitation of asphaltenes [21]. In the former, asphaltene is assumed to have a monodisperse nature, while the latter considers the polydispersity nature of asphaltenes [20]. Although the theory is simple to apply, it presents some limitations, for instance, the effect of pressure is not considered in theory, and the lattice fluid theory is combined with EOSs to tackle this limitation. In addition, the effect of temperature on the solubility parameters, densities, and mass distribution has been investigated only by the empirical correlations [21]. The regular solution theory considers the solubility parameters of the components as tuning parameters rather than measured values so that the parameters are determined by fitting through using experimental data [22-24].

The other category in the solubility-based models is the EoSs that consist of cubic, Cubic Plus Association (CPA), and Statistical Associating Fluid Theory (SAFT) equations of state. Peng Robinson

(PR) and Soave–Redlich–Kwong (SRK) are two simple EoS models whose simplicity and acceptable accuracy are the reasons for their wide applications in the oil industry. However, the limitation of cubic equations is their failure to model hydrogen bonding and association effects. It is important to note that the solid model is also considered in the category of EOSs, while the precipitated asphaltene phase is regarded as a pure solid, and the remaining part of the oil is modeled with EoSs [42]. To address the limitation of the cubic EOSs, the CPA EoS was introduced that takes into account the impact of association. The model consists of two parts, a physical term which stands for non-association (short-range interactions), and an association part [25, 43, 44]. One of the successful models to study the thermodynamic behaviours of complex mixtures (e.g., asphaltene) is the SAFT theory, which takes into account the influence of association and the non-spherical chain of molecules [45-48]. In this theory, it is assumed that the properties of a fluid of interest are obtained by the knowledge of the properties of a reference fluid. Considering the modeling of asphaltene precipitation by the SAFT theory, Perturbed-Chain SAFT (PC-SAF) has exhibited a successful performance. While utilizing the PC-SAFT without association, van der Waals interactions are considered to be dominant. Thus, the association term is not regarded in the calculations [22, 25-27]. Both CPA and PC-SAFT are powerful tools and can take into account the association of hydrogen bonding which leads to a higher accuracy and prediction capability of the EoS.

The second category of models to simulate the asphaltene precipitation is the colloidal-based models, which assume that the asphaltene particles are suspended in the oil mixture by lighter hydrocarbons, named peptizing agents [28, 29]. Asphaltene, which has a high molecular weight and aromaticity, constitutes the core of the micelles, while resins surround the core and peptize asphaltene in the oil mixture. In general, the insufficient amount of resins to peptize asphaltene is considered the reason for the attraction of asphaltenes and the formation of aggregations [28, 29].

Organic deposition (asphaltene) in the wellbore area is a damage that causes a decrease in oil production and imposes deposition treatment expenses on the Operating Expense/cost (OPEX). Asphaltene deposition reduces the permeability and porosity of the reservoirs by plugging pore throat and entrainment, alters the wettability of the rocks, and increases the hydrocarbon viscosity by stabilizing the water-oil emulsions. Porosity reduction and permeability impairment models are based on three main mechanisms, which are adsorption of asphaltene particles on the surface of capillary channels, entrainment, and pore throat plugging. It is important to note that these mechanisms are considered simultaneously, while deposition happens in the bigger pores, and the pore throat plugging is reported in the smaller throats. Wang [49], followed by Wang and Civan [50], proposed the most popular

asphaltene impairment model that considers these deposition mechanisms in their model. The main assumptions in their model include considering a single-phase flow in a horizontal direction, neglecting the gravity and capillary pressure, and assuming a constant temperature. They used mass balance equations for the oil phase and asphaltene, the model of asphaltene deposition rate, the momentum balance equation of Darcy's law, and the permeability and porosity models to represent the asphaltene deposition [49, 50]. Although the proposed model exhibited an acceptable accuracy, it has undeniable drawbacks, which result in oversimplification and non-realistic physics of the phenomenon. The effect of the kinetics of precipitation and deposition was not considered on the asphaltene impairment. In addition, the growth of asphaltene particles when passing through a porous medium or capillaries was not taken into account [49, 50].

Indeed, the best way to investigate the asphaltene behaviours at different thermodynamic/process conditions is to have a broad knowledge of the vital aspects of the phenomenon. To the best of our knowledge, no systematic reviews are found in the literature on asphaltene precipitation/deposition to cover the process mechanisms, controversial theoretical and experimental aspects, and mitigation and treatment ways.

In this review article, an attempt is made to cover a wide range of research studies of asphaltene-related matters. First, an overview of the nature and physical properties of asphaltenes is presented. Following that, the kinetics of precipitation, experimental studies of precipitation/deposition, and modeling approaches of the phenomena are reviewed. Then, the effects of different variables, including operational conditions, fluid properties, and reservoir characteristics on asphaltene precipitation/deposition are discussed. Next, the simulation and optimization tools in the lab-scale and field-scale, as well as the treatment and inhibition techniques to mitigate or hinder precipitation/deposition, are studied. After that, the economic analysis of flow assurance and theoretical and practical challenges of precipitation/deposition are also addressed. Eventually, the important points/conclusions of the previous research and engineering activities are listed in the last section.

2-2. Asphaltenes: Properties, Structures, and Thermodynamic Behaviours

The formation of solid particles (such as asphaltenes) causes serious operational, economic, and environmental problems in the petroleum industry, depending on the chemical and physical structures of petroleum, where the physical structure is highly influenced by the chemical structure. Having an adequate understanding of different species in the oil mixture, including their multi-phase behaviours

and interactions, is imperative to answer these important questions in the oil industry: when and how much solid-like particles will flocculate under certain thermodynamic conditions [51, 52].

The complexity of oil composition is the reason to classify oil with respect to the group analysis. The classical oil definition has been based on the solution properties of petroleum in various solvents and their polarity. Based on the SARA group analysis method, four main fractions are defined within oil, including Saturates, Aromatics, Resins, and Asphaltenes (SARA) [53]. SARA fractions and properties of some crude oil samples are listed in Table 1 [54].

Table 2-1. SARA fractions and physical properties of some crude oil samples [54]

Sample	API Gravity (°API)	Viscosity (cp)	Saturates (wt%)	Aromatics (wt%)	Resins (wt%)	n-Pentane Insoluble Asphaltenes (wt%)	n-Heptane Insoluble Asphaltenes (wt%)
Heavy Oil 1	17.12	496	30.03	41.84	15.56	12.57	1.72
Heavy Oil 2	12.19	168000	11.01	44.89	20.75	23.35	11.15
Heavy Oil 3	18.84	884	22.63	37.57	16.03	23.76	5.71
Heavy Oil 4	12.56	263000	32.02	21.95	7.95	38.08	8.26
Extra-Heavy 1	7.97	251000	12.70	42.11	22.93	22.26	13.4
Extra-Heavy 2	11.56	209000	10.14	38.01	13.09	38.76	21.42
Bitumen 1	12.09	10100	16.51	37.81	17.10	28.58	9.9
Bitumen 2	8.19	53200	23.6	20	21.90	34.30	30.41
Bitumen 3	6.11	12100000	10.68	29.10	20.14	40.08	21.27
Bitumen 4	10.01	19200000	11.05	30.47	16.06	42.41	37.74
Wax 1	27.05	676	24.28	25	5.43	45.30	9.9

Petroleum normally consists of different hydrocarbon fractions such as saturates, aromatics, and heteroatoms constituents such as asphaltenes and resins.

It is worth noting that the composition of each fraction of the petroleum is determined by the separation process. For example, near-neutral molecular locales such as nitrogen, oxygen, and sulphur species can occur in the higher molecular weight fractions, asphaltenes and resins, as well as lighter fractions, saturates and aromatics [9, 11].

The traditional methods to determine the fractions of oil include gravity-driven chromatography separation, High-Pressure Liquid Chromatography (HPLC), and Thin Layer Chromatography (TLC). Gravity-driven chromatography or clay-gel adsorption chromatography is fairly time-consuming and

difficult to automate. It also requires relatively large amounts of oil samples and solvents. Early versions of HPLC techniques were used to separate lighter petroleum fractions, while the new HPLC methods are also capable of separating heavier fractions of oil. In comparison with gravity-driven chromatography separation, HPLC is faster, reproducible, and more automated. The TLC method is the fastest technique in petroleum separation. Thin Layer Chromatography with Flame Ionization Detection (TLC-FID) is considered one of the most popular methods in this category. This technique, in comparison with other methods, requires a relatively smaller amount of samples [55]. Fan et al. (2002) compared the performance/accuracy of the three approaches discussed above using six oil samples. It was concluded that volatile hydrocarbons with a boiling point of less than 250°C (including saturates and aromatics) are considerably lost in TLC-FID [56, 57].

Saturates are nonpolar hydrocarbons, which include normal alkanes (n-paraffins), branched alkanes (iso-paraffins), and cyclo-alkanes (also known as naphthenes) [58, 59]. Paraffin waxes and microcrystalline waxes consist of the n-paraffins and iso-paraffins cluster together. They can be converted to solid form (precipitate) during oil production or processing. In general, paraffin waxes are the main element of most solid deposits from crude oils [58, 59].

Aromatics are hydrocarbons consisting of cycloalkanes and alkyl chains, and aromatic chains. Their structures and chemical and physical properties are significantly different from paraffins and naphtanes. Due to their particular structures, they have also been considered a solvent for paraffin waxes [60]. Resins are made of heteroatoms such as oxygen, sulphur, nitrogen, and nonpolar paraffinic groups. This fraction of oil is soluble in pentane and heptane, which are light alkanes and insoluble in propane. In terms of structure, they are very similar to asphaltene; however, they have a lower molecular weight and a higher hydrogen-to-carbon ratio [61, 62].

In 1837, Boussingault first defined asphaltene as a petroleum residuum, which is soluble in turpentine and insoluble in alcohol [63]. Generally, crude oil is classified into two fractions, including maltene and asphaltene. Maltene consists of saturates, aromatics, and resins in the form of continuous oil, while asphaltene is dispersed or dissolved in crude oil [11]. Asphaltene is a complex molecule which is the heaviest and the most aromatic fraction of crude oil. From the operational point of view, this fraction of crude oil is soluble in aromatic solvents such as benzene and toluene and insoluble in light alkanes such as n-pentane and n-heptane. The precipitants, particularly paraffins, are also used to classify asphaltene, implying that the quantity of precipitated asphaltene is a function of the type of solvent, dilution ratio (solvent/oil), and contact time [11].

2-2-1. Chemical Composition

As asphaltene does not crystallize, a variety of methods can be used to sub-fraction asphaltene to achieve its elemental compositions [1]. Elemental compositions of different asphaltenes have been reported in the literature [64-68]. It has been revealed that typically asphaltenes are composed of carbon, hydrogen, oxygen, nitrogen, and sulphur, as well as small amounts of iron, vanadium, and nickel in ppm levels [2]. It has been shown that the carbon and hydrogen content of asphaltene of different oils vary within a small range of $82\pm3\%$ and $8.1\pm0.7\%$, respectively. It can be concluded that the hydrogen/carbon ratio in different asphaltenes is almost constant at $1.15\pm0.05\%$. In comparison, heteroatoms, including oxygen and sulphur, have various concentrations of 0.3-4.9% and 0.3-10.3%, respectively. However, the nitrogen content shows less variation in the range of 0.6-3.3% [11].

2-2-2. Molecular Structure

The molecular structure of asphaltene has been the subject of many research studies [53, 69-72]. In early works, two dominant structure models were accepted to describe the molecular structure of the asphaltene; namely, the "island" and the "archipelago" models [73, 74]. The nature of these two models is similar. Both consist of a polyaromatic condensed hydrocarbon core, which is stabilized by a shell of alkyl side chains. However, in the archipelago model, the core is composed of multiple aromatic cores connected by alkyl chains. Although the "island" model is believed to be the best model in describing the molecular structure of the asphaltenes, both methods are a matter of debate [75]. The Yen model is one of the early models that has been widely employed to describe the structure of asphaltene. However, the model is not able to overcome uncertainties about molecular weight, architecture, and aggregation of asphaltenes [53]. The modification of the "Yen-Mullins" is considered one of the most acceptable molecular structures of asphaltene (see Figure 3) [10]. The molecular weight of petroleum asphaltene was determined to be 750 g/mole (Da), which is typical for island model structures. Also, the molecular weight of asphaltene was approved by the Nuclear Magnetic Resonance (NMR) relaxation measurements. The Yen-Mullins model can clearly illustrate the hierarchies of cluster formation. The model considered the molecule of asphaltene from light oil as a single and fairly large Poly-Aromatic Hydrocarbon (PAH) with peripheral alkyls [37, 76, 77]. It has been suggested that asphaltene nano-aggregates can disperse in stable black oils. Asphaltene nano-aggregates in stable black oils are composed of six asphaltene molecules, which are formed by a single disordered stack in the interior and peripheral alkyls in the exterior. However, clusters of unstable heavy oils can be composed of up to eight nano-aggregates [10, 69].
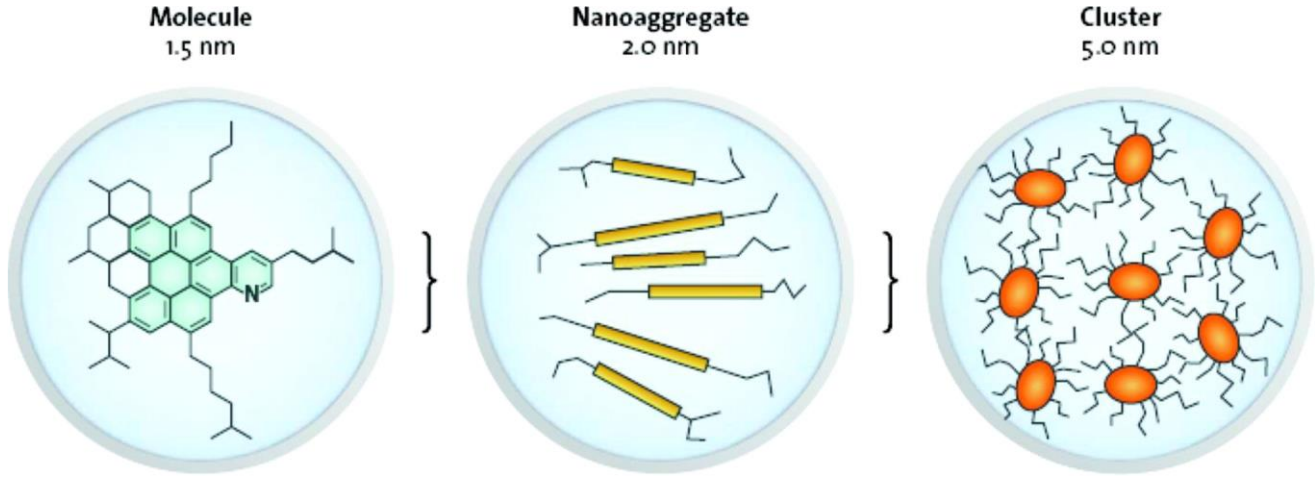
Figure 2-3. The Yen-Mullins model and the "island" structure as dominant architectures where the asphaltene molecular weight is ~750 g/mole [10, 53]

Schuler et al. (2015) presented the first direct measurement of the molecular structure of asphaltenes and applied the technique to more than 100 asphaltene samples from petroleum or coal [12]. They combined atomic resolution and molecular orbital imaging using Atomic Force Microscopy (AFM) and Scanning Tunnelling Microscopy (STM), respectively, as demonstrated in Figure 4. The findings of the research led to a long-standing debate about asphaltene molecular architecture. The research output revealed that coal asphaltenes are smaller than petroleum asphaltenes. The model also endorsed the "Yen-Mullins" model in terms of the molecular weight of asphaltene. Asphaltene molecules are mainly composed of one polycyclic aromatic group formed by almost seven rings to which linear or branched hydrocarbon chains are attached [12].
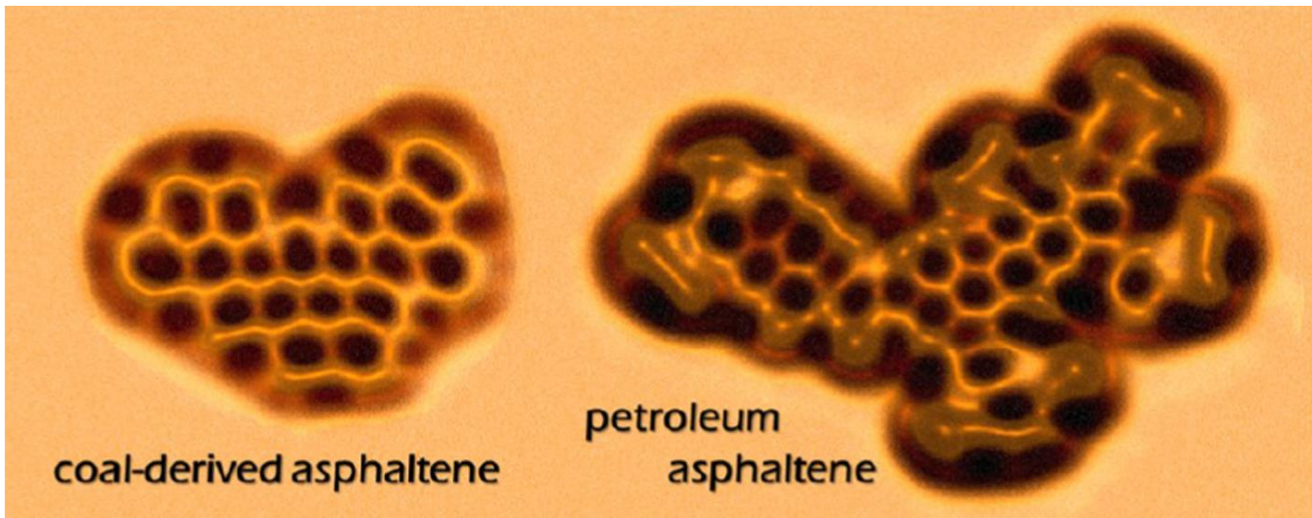
Figure 2-4. STM image of the molecular structure of asphaltene [12]

2-3. Theory of Asphaltene Precipitation/Deposition: Description and Mechanisms

Asphaltene precipitation and deposition is an important issues in petroleum sectors. The self-aggregation tendency of asphaltene is considered the main reason for its "unwanted" fame. Asphaltene precipitation and, consequently deposition are of industrial interest due to deposition on rocks, transportation equipment, and facilities of refineries, leading to a considerable reduction in the performance of the corresponding operations [11].

Prior to the discussion on the mechanisms of precipitation and deposition, a few terms in the context of asphaltene precipitation, including destabilization, aggregation, and precipitation, need to be introduced. Asphaltene destabilization refers to the nanoscale asphaltene that is able to grow. Following this event is the aggregation, which represents the asphaltene particles in microscale. The final stage is the precipitation process that involves the transition from stable nanoscale particles to unstable microscale [30].

2-3-1. Mechanism of Asphaltene Precipitation

The state of asphaltene and its flocculation in crude oil has been the subject of many research efforts; however, there are still no comprehensive mechanisms to describe the state of asphaltene. Four mechanisms and effects have been recognized for the flocculation of asphaltene, including polydispersity, steric colloidal, aggregation, and electrokinetic [52, 78]. The state of flocculated asphaltene in oil can be described by one or more of these mechanisms. The stability of asphaltene

21

depends on the nature and amount of the species in the oil mixture. A summary of the mechanisms of asphaltene precipitation is provided in the supplementary information (Appendix A).

2-3-2. Kinetics of Asphaltene Precipitation

Different aspects of asphaltene precipitation and deposition, such as the kinetics of asphaltene destabilization and aggregation, and precipitation, are reviewed/discussed in this review paper. In most of the research studies presented so far, asphaltene precipitation induced by adding a paraffinic solvent was investigated by waiting 24 hours to collect equilibrium data. The kinetics of asphaltene precipitation can be explained by the kinetics of nucleation and growth, which are generally dominant in particle formation. Nucleation is the creation of molecular embryos (critical nuclei) from the supersaturated fluid during the transformation of vapour to liquid and liquid to solid, which has the minimum Gibbs free energy [79]. Consequently, the nuclei turn to nanoscale particles that are able to coagulate with other particles [79]. The formation of asphaltene nuclei requires several hours before equilibrium data is collected; since the growth of the nuclei is limited to adsorption and diffusion from the medium phase to the nuclei [11]. Further information (and/or literature review) on the kinetics of asphaltene precipitation can be found in the supplementary information (Appendix A).

2-3-3. Asphaltene Phase Behaviour and Precipitation

The two approaches widely used to describe the asphaltene phase behaviours and precipitation include thermodynamic solubility and colloidal theory-based models. These two models differ in their basic concept, which is the state of asphaltene in crude oil. The solubility strategy considers the asphaltene particles dissolved in the oil and defines precipitation as a phenomenon in which the solubility is lower than a threshold level [20-24]. Two main theoretical approaches are the lattice fluid theory and the Equation of State (EoS). In the colloidal approach, resins play the major role in the stabilization of the asphaltene colloidal particles as their adsorption around asphaltene colloids stabilizes asphaltene in the crude oil medium, and asphaltene precipitation is a result of resins desorption. The solubility models and colloidal theory are described in more detail in the open sources [20, 25-29, 80-86].

The solubility model, which is more popular than the other approach, considers asphaltene precipitation as a reversible process and categorizes oil into two components, namely, asphaltenic and non-asphaltenic phases. The solubility method implies that any changes in thermodynamic conditions, including temperature, pressure, and composition lead to solubility alteration of either of the two phases and, consequently asphaltene precipitation [80]. In this category, the Flory-Huggins polymer-solution

theory and the regular-solution theory of Scatchard-Hildebrand have been more common in comparison with the Scott–Magat theory to study the precipitation of asphaltene. In the earlier model, asphaltene is considered to have a monodisperse nature, while the latter takes into account the polydispersity nature of asphaltene [20]. The four different categories of solubility models, including the regular-solution theory, the Flory-Huggins polymer-solution theory, the Scott–Magat theory, and the Equation of State (EoS) are reviewed in this section.

The regular solution theory, based on the lattice fluid theory, is one of the simplest models to describe asphaltene precipitation. It considers a random distribution for molecules and accounts for Gibbs free energy as an additional amount from the enthalpy and entropy of the system (see Figure 5). The different colours in Figure 5 shows two pseudo-components of the mixture, solvent (oil) and solute (asphaltene), which can change their positions in the liquid phase [81].
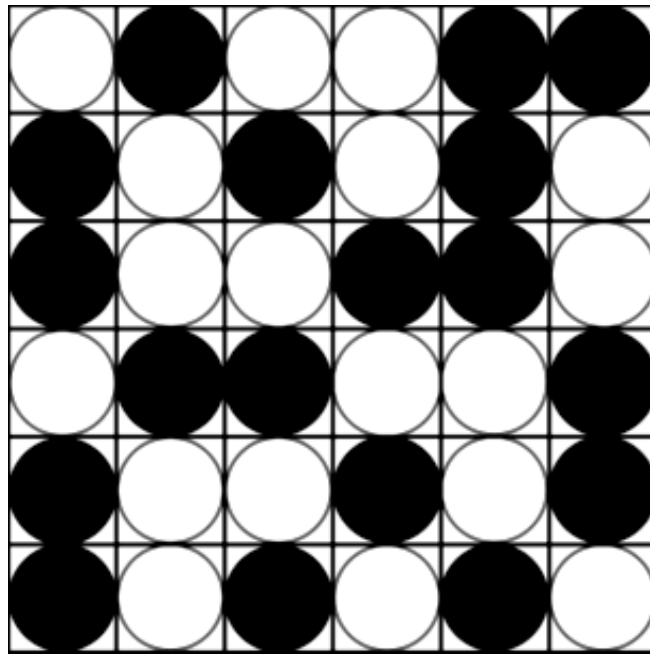
Figure 2-5. Simple cartoon of the lattice theory [81]

The oil mixture is characterized by the solubility parameter and molar volume. The solubility parameter is obtained using the Gibbs free energy as follows [82]:

$$\Delta G_{min} = RT\left[n_s \ln \phi_s + n_a \ln \phi_a + n_a \phi_a \frac{\upsilon_s}{RT}(\delta_a - \delta_s)^2 \right] \tag{2-1}$$

In which G, R, T, n, and Φ stand for the Gibbs free energy of the mixture, gas constant, temperature, number of moles, and volume fraction, respectively. The first term in Equation (1) represents the

23

entropy of the mixture, and the last term introduces the enthalpy. The interactions between the molecules are represented by the cohesive energy density from the heat of vaporization (Hildebrand [82] and Scatchard [87]). The Hildebrand model has shown better performance for non-polar molecules since the polarity, and specific interactions were not taken into account [82].

Many of the assumptions made for the regular solution theory were used by other researchers, leading to the development of the Flory-Huggins polymer solution theory [83, 84]. They considered polymers in the form of a flexible chain of segments, which had the same size as a molecule of solvent. Both regular solution and Flory-Huggins theories did not consider the impact of pressure. Hence, the utilization of various EOSs can tackle the drawback of the lattice theory for vapour-liquid equilibrium. Considering asphaltenes as polydisperse molecules with different chain lengths and molecular weights, the Scott-Magat polymer theory, which was an extension of the Huggins theory, was applied to model asphaltene phase behaviours [85]. For this purpose, the partial molar free energy of the mixture is expressed by the following relationship [85]:

$$\frac{\overline{\Delta F_0}}{RT} = \ln \phi_0 + (1 - \phi_0)(1 - \frac{1}{\overline{m}_N}) + \mu(1 - \phi_0)^2 \tag{2-2}$$

where $\overline{\Delta F_0}$, Φ_0, $\overline{m}_N$, and μ refer to the partial molal free energy of mixing of the solvent, the volume fraction of the solvent, the function of the number of average molecular weight, and a constant parameter for the polymer–solvent mixture, respectively [85].

The simplicity and reliability of the lattice fluid theory imply that it has a popular base for others, such as the regular solution, Flory-Huggins, and Scott-Magat methods, while it has some drawbacks. For instance, the effect of pressure (density or compressibility) is not considered in these techniques unless the pressure variations are calculated by an EOS [86]. In addition, the effect of temperature on the solubility parameters, densities, and mass distribution are taken into account using only empirical correlations [21]. The regular solution theory does not consider the solubility parameters of the components as measured values, so the theory treats the solubility parameters as the tuning variables. This is the main drawback of the model so that the parameters are obtained by fitting with experimental data. Furthermore, the necessity of physiochemical phenomena causes a further challenge [22].

The next group of models in the solubility approach is the EOSs, including the cubic equation of state, the cubic plus association equation of state, and the statistical associating fluid theory. The main advantages of the EOSs are that they can be applied to a wide range of thermodynamic conditions and are not restricted to precipitation boundaries [22].

The cubic EoSs, including Soave–Redlich–Kwong (SRK) and Peng–Robinson (PR), have been widely used due to their simplicity and reasonable accuracy, though they do not take into account the polarity and/or association between particles. The general form of SRK and PR is given as follows [25]:

$$P = \frac{RT}{\upsilon - b} - \frac{a}{\upsilon(\upsilon + b)}$$

(2-3)

$$P = \frac{RT}{\upsilon - b} - \frac{a}{\upsilon(\upsilon + b) + b(\upsilon - b)}$$

(2-4)

In which a and b denote the constants of the EoS (e.g., a is the attractive parameter and b stands for the cross co-volume parameter) and υ, P, T, and R represent the molar volume, pressure, temperature, and gas constant, respectively. The other model in this category is the solid model or the cubic EoS, which has two parts: a solid phase (precipitated asphaltene) and the remaining components (oil and gas phase). The first part is modeled with the solid approach, while the latter is described with a cubic EoS [25]. The Cubic-Plus-Association (CPA) EoS is the extension of the cubic EoS, while the association terms such as hydrogen bonding are incorporated in the model. It consists of two sections: the non-associating molecules section and the polar interactions section on the basis of the perturbation theory. It is important to note that in the absence of polarity section of the CPA EoS, it reduces to the form of SRK or PR EOS [26].

Different versions of the Statistical Associating Fluid Theory (SAFT), including Perturbed-Chain or PC-SAFT have been proven as the most accurate and reliable EoS models to be utilized for modeling of asphaltene precipitation on the basis of the statistical mechanics. The SAFT model was proposed by Chapman et al. using the perturbation theory of Wertheim's theory, considering the non-spherical shape for molecules as well as the association term. The model is presented in terms of the Helmholtz free energy (A) as follows [27]:

$$A = A^{ideal} + A^{mono} + A^{chain} + A^{assoc}$$

(2-5)

In Equation (5), $A^{ideal}, A^{mono}, A^{chain},$ and A^{assoc} denote the ideal free energy, the free energy of monomers, free energy of chain formation, and intermolecular association, respectively [27]. Due to the versatility of the model, different versions, including PC-SAFT, SAFT-HS, and SAFT-VR have been proposed [27].

The colloidal model supposes the asphaltene precipitation as an irreversible phenomenon. Asphaltene particles are regarded as the colloidal or micelle, surrounded by resin molecules as the peptizing agent to stabilize asphaltene particles in the oil mixture [28]. Experimental investigations introduced the

Critical Micelle Concentration (CMC) as an important factor in precipitation occurrence [28,29]. When the concentration of asphaltene is lower than the CMC, the asphaltene is fully dissolved in the medium, while an increase in this critical value leads to the micelles formation [28, 29].

2-4. Experimental Studies: Description and Findings

It has been well understood that variation in the thermodynamic conditions of the oil mixture, including temperature, pressure, and composition results in destabilization, aggregation, precipitation, and consequently, deposition of asphaltene. Experimental studies have been used to properly investigate the effects of different parameters on the asphaltene from the destabilization stage to the deposition stage. In this section, various experimental studies (in terms of methodology and operating conditions) for determining the asphaltene destabilization and onset point are briefly described. Different techniques have been applied to detect asphaltene destabilization, such as De Boer Plot, optical microscopy, viscosity measurement, small angle scattering, ultraviolet–visible spectroscopy, refractive index method, and indirect methodologies [31, 88-92].

2-4-1. De Boer Plot

De Boer et al. (1995) developed a simple screening technique to depict the tendency of asphaltene particles to precipitate. The model is based on the Flory-Huggins theory, and the main parameters are the Hildebrand solubility parameters and molar volumes. De Boer et al. suggested that all the parameters/properties of the oil can be correlated with the in-situ density. It was found that decreasing the pressure leads to the reduction of the solubility up to the bubble point, while the further reduction in the pressure below the bubble point increases the asphaltene solubility [88]. As a result, they introduced three regions within the differential pressure of initial and bubble point versus solubility at the initial density of the oil so that they showed where the possibility of precipitation is highest [88].

2-4-2. Viscometric Approach

The viscometry determination of the asphaltene onset point was developed by taking accurate viscosity measurements of an oil mixture induced with a solvent. The method is applicable when precipitation happens by adding a solvent in the presence of a reference system. The onset point is then shown graphically, indicating the point when a remarkable increase in the oil density is observed in comparison with the reference system, which does not contain the precipitant [89]. The increase in the viscosity was attributed to the aggregation and entanglement of the asphaltene particles. The viscometric

determination has some advantages and disadvantages. For instance, the model can be applied to find the onset point of asphaltene precipitation for either light or heavy oil samples. Moreover, the equipment to measure the viscosity is not expensive. Hence, the model is economically feasible. However, the inevitable clogging of the viscometer is considered to be a serious limitation of the method [89].

2-4-3. Optical Microscopy

Maqbool et al. employed the optical microscopy method to demonstrate the kinetics of asphaltene precipitation under different temperatures and concentrations of the solvent [31, 90]. For this purpose, an optical microscope and a Charge-Coupled Device (CCD) camera were used to observe and record the precipitation. At different time intervals, the sample was withdrawn and observed. Several samples were compared to explore the time needed for precipitation to visually illustrate the onset time. The amount of the precipitated asphaltene was then measured with centrifugation-based separation[31, 90]. This method has some drawbacks. For example, the measurement of onset time is highly dependent on the time of intervals of sampling. In addition, the microscope can only measure particles of 0.5 µm or bigger [31, 90].

2-4-4. Small Angle X-Ray and Neutron Scattering

In order to tackle the limitations of the optical microscopy method, which is only able to measure particle sizes of 0.5 µm or bigger, X-ray and neutron scattering are generally utilized to determine the asphaltene aggregation size. It was shown that the soluble asphaltene is characterized by fractal dimension [91]. The fractal dimension of destabilized insoluble asphaltene is much larger than that of soluble clusters, implying that the fractal clusters are modified [90,91]. The modification and change of the cluster size are due to the changes in the packing organization/sorting of individual asphaltene nanoaggregates. This phenomenon is depicted in Figure 6. This method suggests that an adequate understanding of the microscopic asphaltene destabilization mechanism, asphaltene nanoaggregate size, shape, polydispersity, and steric stabilization can be used to model and treat the asphaltene precipitation [91]. These observations questioned the notion of asphaltene onset point. They also suggested that asphaltene precipitation through the change in temperature, pressure, and composition is a complex phenomenon and cannot be easily measured [91].
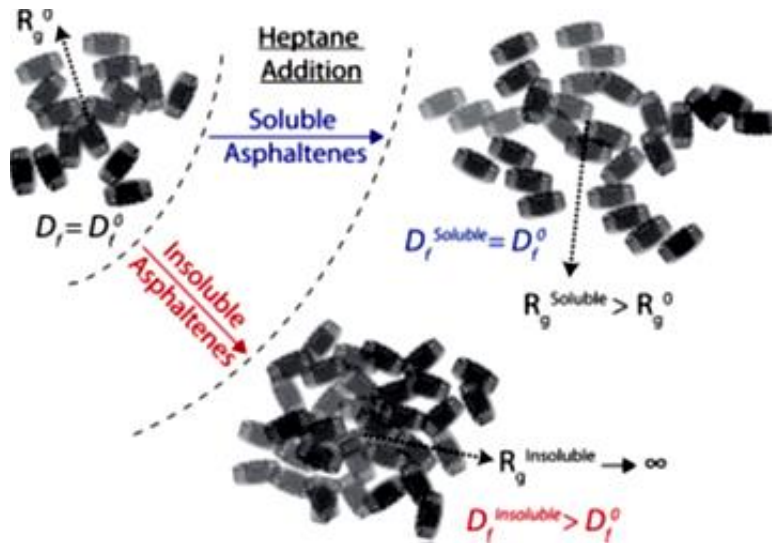
Figure 2-6. Asphaltene clusters by adding solvent; R^0_G and D^0_f represent the radius of gyration and fractal dimension of asphaltene clusters [91]

2-4-5. Indirect Method

Tavakkoli et al. introduced the indirect method and highlighted some advantages of the indirect method in comparison with other industrial techniques, such as light scattering and high-pressure microscopy [92]. For example, this approach is able to determine the asphaltene onset and the amount of precipitation. In addition, it can be used for various oil samples in terms of composition and characteristics, even oils with low asphaltene content. The sensitivity of the method is 100 nm, which is better than available commercial techniques [92]. In the indirect method, the oil sample is diluted with n-heptane and after the aging time and centrifuging, the precipitated onset is detected by plotting the value of absorbance versus volume fraction of n-heptane. However, further investigations on the method are needed to ensure the proper aging time and centrifugal speed [92].

Deposition of asphaltene is a ubiquitous phenomenon that can occur in reservoirs, processing units, and transportation facilities. Asphaltene particles are adsorbed to the surface and form the arterial clogging. The experimental investigation of asphaltene deposition can be conducted in capillary flow and Taylor–Couette (TC) cells [93-99]. The different experimental methods used to investigate asphaltene deposition have their own characteristics. For example, stainless steel capillaries allow for pressure measurements, while glass capillaries have the advantage of allowing for images to be captured for deposition demonstration. The capillary flow experiments can be applied over an extended period, even with a small amount of oil sample. Listing the disadvantages, isothermal experiments cannot be conducted in large tubes, since the temperature of the bulk is different from the wall. TC cells can be

used under reservoir conditions of temperature, pressure, composition, different shear rates, and capillary diameters; however, the model requires a high volume of oil to demonstrate deposition [97]. A brief of the experimental methods, including capillary flow and Taylor−Couette (TC) cells, are provided in the supplementary information (Appendix A).

A summary of the experimental investigations on the kinetics and deposition of asphaltene is presented in Table 2.

Table 2-2. A brief overview of experimental studies on kinetics and deposition of asphaltene

Year	Study's goal	Type of destabilization	Experimental tools	Theoretical concept/analysis	Remarks	Ref
1998	Effect of asphaltene on the permeability of the carbonate rock	Injection of n-heptane	Core test	Gruesbeck and Collins theory	The onset point was determined by viscosity measurement. They suggested three regimes of asphaltene plugging, including monotonous steady state, quasi-steady state, and continuous plugging. The most asphaltene deposition is likely to occur where continuous plugging is dominant, such as near the wellbore.	[100]
1999	Asphaltene deposition on carbonate rock in static and dynamic tests	CO_2 injection and operational pressure	Core test	-	The likelihood of deposition was examined in static and dynamic tests. The X-ray CAT-scanning tests revealed that most asphaltene deposition happens in the inlet of the core. It was shown that the bigger pores are more prone to asphaltene precipitation/ deposition.	[101]
2000	Thickness of deposition	Variation of pressure, temperature, and composition	Stainless steel capillary	Hagen-Poiseuille law	Asphaltene deposition happened when asphaltene was unstable.	[93]
2004	Thickness of deposition	n-alkane injection	Stainless steel capillary	Hagen-Poiseuille law	The higher rate of deposition was noticed with the heavier precipitant.	[94]

2005	Asphaltene adsorption on carbonate rock and reversibility of asphaltene deposition under dynamic flow	Ageing	Core test	-	Two series of experiments, static and dynamic, were conducted. They found that 40% and 80% of the initial asphaltene content are deposited in static adsorption and dynamic deposition, respectively. It was concluded that asphaltene deposition and permeability impairment under dynamic flow condition are reversible.	[102]
2006	Asphaltene deposition	Hydrodynamic of flow and temperature	Taylor-Couette cell	-	Under-measuring deposition tests by Organic Solid Deposition and Control (OSDC) device were performed.	[98]
2007	Asphaltene deposition and its effect on permeability	Gas injection	Core test	-	Dead and live oil samples, as well as cores with different permeability and pore structures, were used. The setup could work at high temperatures (~200˚C) and high pressures (~400 bar). It was observed that the inlet and outlet sections of the core are more affected by asphaltene deposition and smaller pores are more affected by asphaltene deposition. The main mechanism of deposition was suggested to be the formation of filtration cake.	[103]
2008	Asphaltene deposition	n-alkane injection	Capillary experiment and optical microscopy	Stochastic Rotation Dynamics (SRD) simulations	Pressure drop was increased over time with increasing asphaltene deposition and flow rate.	[95]
2009	Kinetics of asphaltene precipitation	n-alkane injection	Optical microscopy and centrifugal separation	-	Varying onset time for long span experiments, the solubility of asphaltenes can be established as a function of the amount of precipitation.	[31]

Year	Topic	Method	Apparatus	Model	Findings	Ref
2011	Asphaltene deposition in a pipeline	Pressure reduction	Taylor-Couette cell	A population balance model and Brownian motion	The model was proposed for turbulent pipe flow and the parameters of the model were tuned by TC cell. Two mechanisms were considered for deposition on the outer wall of the device, including the evolution of particle size and transportation of the particles to the wall. The concept of critical particle size was introduced	[104]
2011	Rate and amount of deposition	Shear rate	Modified Taylor-Couette cell	Eskin model	The shear rate was dominant in the deposition rate; more deposition was observed at the bubble point pressure of the reservoir.	[99]
2013	Kinetics of asphaltene precipitation	n-alkane injection	Atmospheric titration	Smoluchowski's aggregation model	They suggested a universal trend for the kinetics of asphaltene onset point.	[32]
2016	Measuring the thickness of asphaltene deposition in the microchannel	Injection of n-heptane	Vertical transparent micro-channel	3-D reconstructed image	A 3-D digital microscopy was used to visualize asphaltene deposition in the microchannel. An increase in the thickness of the asphaltene deposited layer was observed by increasing the total injection volume of dead oil and n-heptane.	[105]
2016	Kinetics of asphaltene precipitation and deposition	n-alkane injection	Harvard apparatus	A geometric population balance model	The higher carbon number of the solvent, the slower equilibrium for asphaltene precipitation; deposition by precipitant was faster for the cases with higher concentration and lower carbon number.	[30]
2017	Asphaltene deposition and its effect on permeability	Pressure reduction	Slimtube which was packed with silica sands	NIR light intensity scan during depressurization	Using a live oil sample of the Gulf of Mexico with asphaltene related problems, 32% permeability impairment was observed to be in the middle and latter section of the slimtube.	[36]

| 2017 | Asphaltene deposition in a turbulent and laminar oil flow | n-alkane injection | Capillary experiment | Scaling equation and colloidal approach | Asphaltene deposition under laminar and turbulent oil flow conditions with Re ≈ 7500 was studied. The flow rate and asphaltene concentration were introduced as dominant factors in the rate of asphaltene deposition. The higher flow rate, the lower deposition was observed. The more amount of precipitant agent, the more deposition occurred. | [35] |

2-5. Modeling Studies: Description and Findings

Modeling strategies are categorized into asphaltene precipitation modeling and deposition methods. A brief description of the deposition modeling investigations is provided in this section. A systematic review of the asphaltene precipitation modeling studies on the basis of different theories (solubility and/or colloidal approach) is also presented in the supplementary information (Appendix A).

Asphaltene Deposition Modeling. Some mathematical techniques have been proposed to model asphaltene deposition, porosity reduction, and permeability impairment [106-109]. Three principal mathematical modeling mechanisms have been introduced for the permeability reduction of porous media. The first mechanism refers to the deposition of asphaltene on the capillary channel surfaces, which is known as the adsorption mechanism. The second mechanism is entrainment, and the third mechanism introduces plugging, which blocks the pore throat with bigger asphaltene aggregations. The model developed by Gruesbeck and Collins was regarded as the basis for many of the reservoir impairment modeling strategies [106]. They considered three mechanisms for asphaltene deposition, including surface deposition, entrainment, and pore-throat plugging [107]. They assumed that the plug throat occurs due to the fluid passing through small pores, while the surface deposition happens in pores with larger sizes, as demonstrated in Figure 7 [106].

The most popular asphaltene impairment model for core tests was proposed by Wang [49], followed by Wang and Civan [50]. They regarded the asphaltene impairment through surface adsorption, entrainment, and plugging of pore throat. They assumed that the liquid mixture is a single-phase system, which flows in a horizontal well, and the effect of gravity is negligible. They used the mass balance equations for the oil phase and asphaltene, the model of asphaltene deposition rate, the momentum balance equation of Darcy's law, and the permeability and porosity models to represent the asphaltene deposition. The mass balance equation for the liquid phase is as follows [49, 50]:

$$\frac{\partial}{\partial t}(\phi \rho_L w_{OL}) + \frac{\partial}{\partial x}(\rho_L u_L w_{OL}) = 0 \tag{2-6}$$

Where subscripts O and L represent the oil and liquid phase, respectively, $\emptyset$ stands for the porosity; ρ_L denotes the liquid density; u_L introduces the liquid velocity; and w_{OL} represents the mass fraction of the oil phase in the liquid mixture. The mass balance equation for asphaltene (component A) in the 1-D coordinate is as follows [49, 50]:

$$\frac{\partial}{\partial t}(\phi C_A \rho_A + \phi \rho_L w_{AL}) + \frac{\partial}{\partial x}(\rho_L u_L w_{SAL} + \rho_L u_L w_{AL}) = -\rho_A \frac{\partial E_A}{\partial t} \qquad (2\text{-}7)$$

In Equation (7), the subscript A refers to the asphaltene; C_A is the volume fraction of the suspended asphaltene in the liquid phase; w_{AL} and w_{SAL} stand for the mass fraction of dissolved and suspended asphaltene in the liquid phase, respectively; and E_A denotes the volume fraction of asphaltene deposited in porous media. The model of Wang and Civan that represents the net rate of asphaltene deposition is given below [49, 50]:

$$\frac{\partial E_A}{\partial t} = \alpha C_A \phi - \beta E_A (u_L - u_{cr,L}) + \gamma u_L C_A \qquad (2\text{-}8)$$

The rate of surface deposition of asphaltene is represented by three terms. The first term on the right-hand side of Equation (8) refers to the surface deposition of small particles. The second term represents the entrainment, and the last term in the equation stands for the plugging of narrow pore throat. In Equation (8), α denotes the empirical surface deposition rates on a solid surface, β introduces a coefficient for the rate of entrainment, and the coefficient of γ represents the rate of plugging. v_L and $v_{cr,L}$ are the interstitial velocity and the critical interstitial velocity of the liquid phase, respectively. The coefficients of β and γ are defined as follows [49, 50]:

$$\beta = \beta i \quad \text{where } u_L > U_{cr,L}; \text{ otherwise } \beta = 0 \qquad (2\text{-}9)$$

$$\gamma = \gamma_i (1 + \sigma E_A) \quad \text{when } D_{pt} \leq D_{ptcr}; \text{ otherwise } \gamma = 0 \qquad (2\text{-}10)$$

where the coefficients β_i and γ_i represent the immediate entrainment rate and plugging deposition rate, respectively; σ denotes a constant which stands for the deposition under the snowball effect; and D_{pt} and D_{ptcr} are the average diameter of the pore throat and the critical diameter of the pore throat, respectively. The momentum balance of Darcy's law is shown below [49, 50]:

$$u_L = -\frac{k}{\mu_L}\frac{\partial P}{\partial x} \qquad (2\text{-}11)$$

In Equation (11), k represents the absolute permeability of the porous medium and μ_L stands for the dynamic fluid viscosity. Other variables/parameters are defined as follows:

$$\phi = \phi_0 - E_A \qquad (2\text{-}12)$$

$$k = f_P k_0 \left(\frac{\phi}{\phi_0} \right)^3 \qquad\qquad (2\text{-}13)$$

In Equations (12) and (13), ϕ is the local porosity; ϕ_0 denotes the initial porosity; f_P stands for the permeability modification constant; and k_0 refers to the initial permeability [49, 50]. Although the performance of the model and its modified versions were evaluated through coreflooding tests, it suffers from being far away from realistic conditions and cannot capture the physics of the permeability impairment process. In addition, it does not consider the effect of particle size on permeability impairment [108]. In addition, the first term in Equation (8), which represents the surface deposition, is based on Gruesbeck and Collins model [106]. It was believed that this is the main drawback of the proposed model since the model was employed and examined using fine mineral particles rather than asphaltene [109].
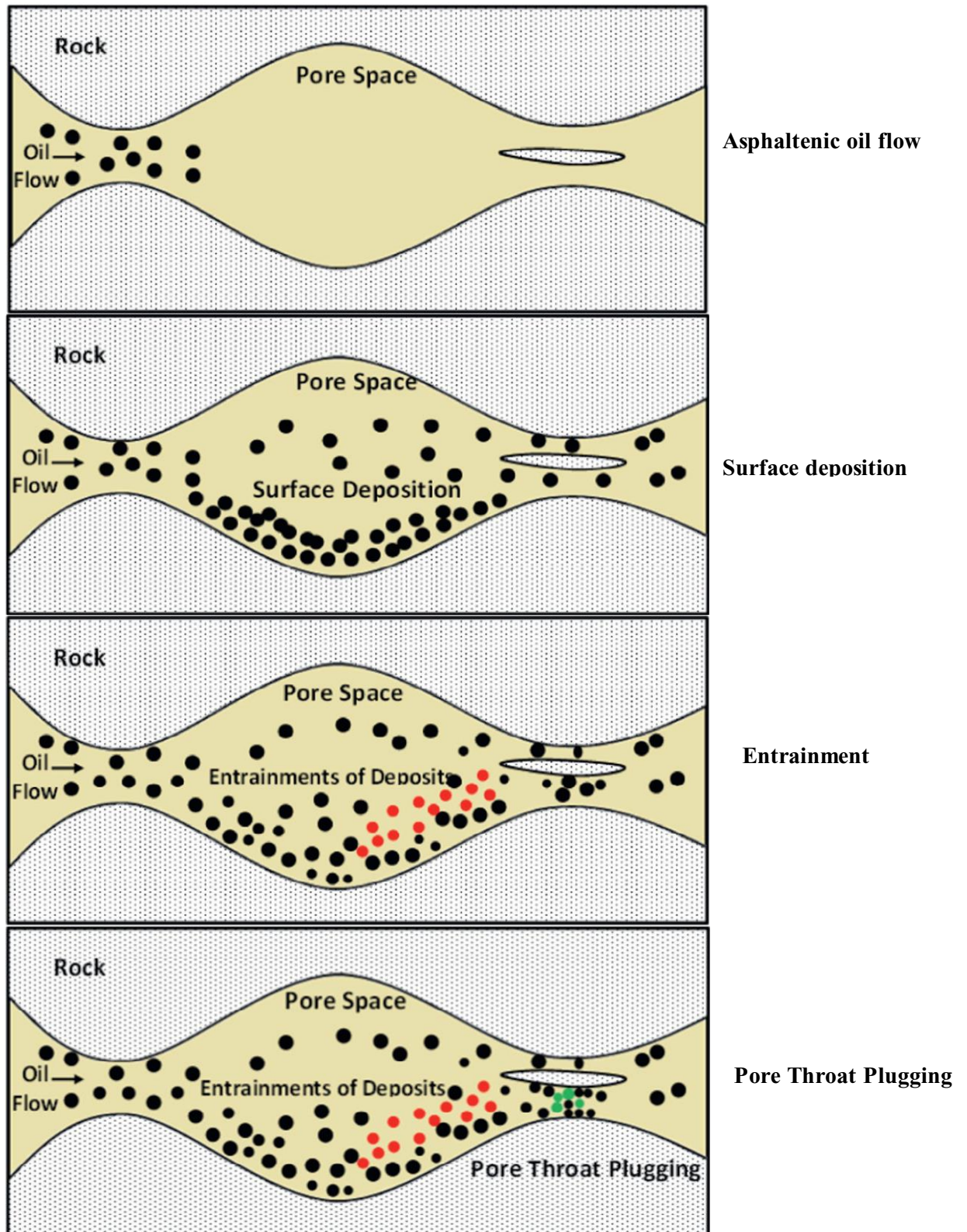
Figure 2-7. Schematic of asphaltene surface deposition and pore throat plugging [110]

Kariznovi et al. (2012) [111] used the Wang and Civan based model [49, 50] and added the dispersion and adsorption terms to offer a more realistic approach (added two terms to Equation (8)). The modified model is shown below [111]:

$$\frac{\partial}{\partial t}(\phi C_A \rho_A + \phi \rho_L w_{AL}) + \frac{\partial}{\partial x}(\rho_L u_L w_{SAL} + \rho_L u_L w_{AL}) - \lambda \frac{\partial^2}{\partial x^2}(\rho_L u_L w_{SAL} + \rho_L u_L w_{AL}) = -\rho_A \frac{\partial E_A}{\partial t} - (1-\phi)\rho_r \frac{\partial n_a^{ea}}{\partial t}$$

(2-14)

The third term on the left side of Equation (14) represents the dispersion effect, and the last term on the right side stands for the adsorption or surface excess. They also applied a proper numerical solution by discretizing the developed model and genetic algorithm
to find the best initial values of parameters [111]. To validate the modified model in core tests with a dead oil sample, the capillary pressure and gravity forces were neglected, and the experiments were carried out at a constant temperature. The pressure was set to be above the bubble point pressure, and there was no connate water in the core. The researchers concluded that surface deposition is the predominant mechanism of asphaltene deposition in the porous media. Their results elucidated that the entrainment and plugging act against each other. It was also found that the flow rate has a significant impact on the asphaltene deposition [111]. Figures 8 and 9 depict permeability and porosity variations along the core when different pore volume injection rates are utilized. It was shown that by injection of one or more pore volume to the core, the permeability/porosity of the inlet section decreased remarkably. However, the permeability/porosity of the outlet section remained almost constant. By increasing the pore volume injection, the permeability/porosity front moved forward within the core, and at seven pore volume injection, the entrainment mechanism started [111].
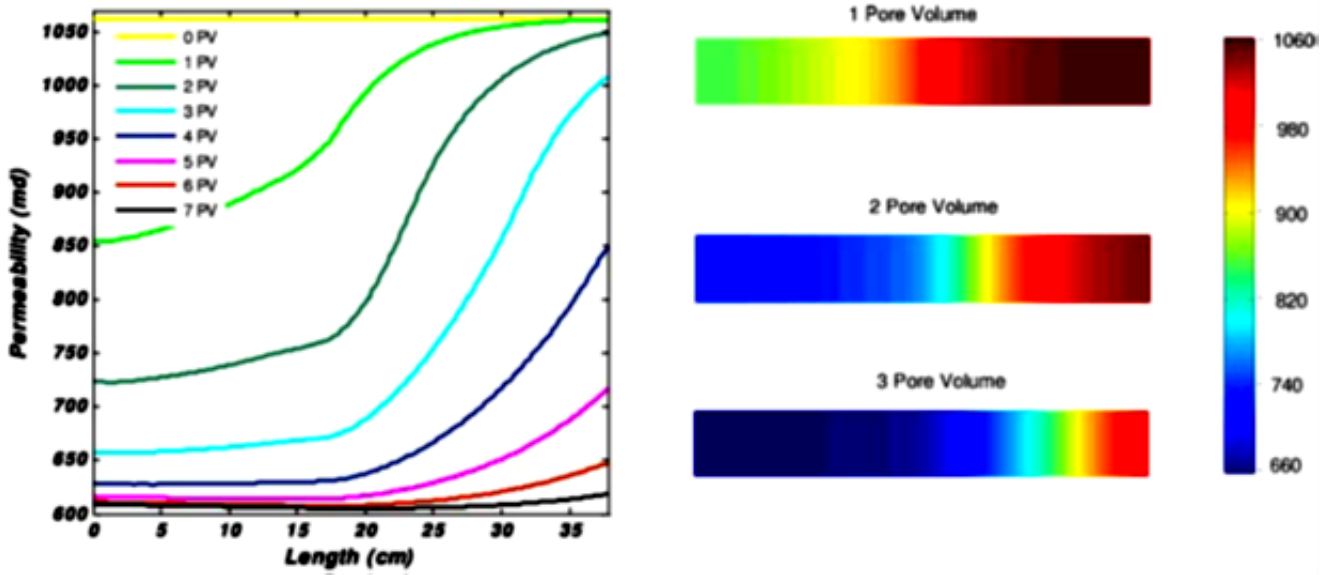
Figure 2-8. Permeability change along the length at different PV injection [111]
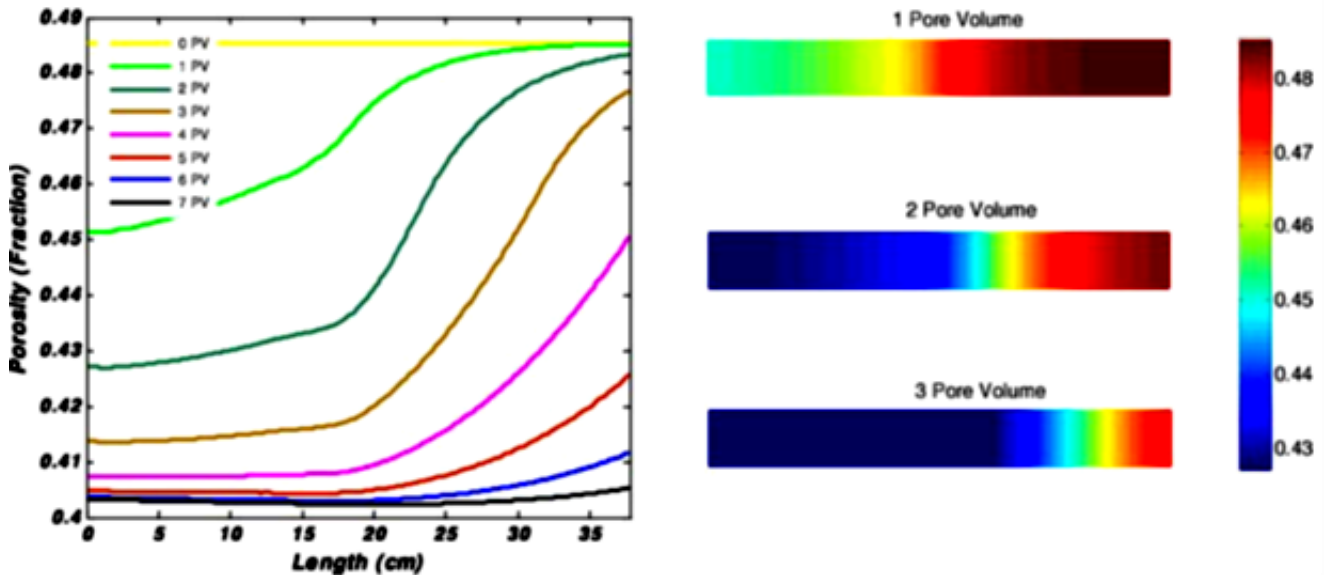
Figure 2-9. Porosity variation along the length at different PV injection [111]

Kord et al. (2014) made a modification to the Wang and Civan model [49, 50] by adjusting the adsorption and pore throat terms. Their equation is given as follows [110]:

$$\frac{\partial E_A}{\partial t} = \alpha e^{-\frac{E_a}{RT}} C_A \phi - \beta E_A (u_L - u_{cr,L}) + \gamma (1 + \sigma E_A)(u_L \phi - u_{cr,L}) C_A \qquad (2\text{-}15)$$

The first term on the right side of Equation (15) is a new mathematical representation of the surface deposition that was previously introduced by Soulgani et al. (2011) on the basis of the Arrhenius kinetic rate; however, they neglected the effect of velocity in their modified equation [109]. The last term of Equation (15) represents the pore throat plugging, which considers the effect of natural depletion in the late lifespan of permeability impairment through incorporating the critical velocity (indicating the partial removal of particles). They concluded that Wang and Civan model [49, 50] is not capable to model the asphaltene deposition at a high number of injected pore volumes. They improved both mechanisms of the impairment; namely, adsorption and pore-plugging. The performance of the modified model was examined and confirmed by the experimental data; however, the main shortcoming of the Wang and Civan model, which is the negligence of the effect of particle size, was not removed [110].

Permeability impairment due to the asphaltene deposition in porous media was modeled by Hematfar et al. (2012), where the mass and momentum balance equations, auxiliary equations, and Genetic Algorithm (GA) tool were employed [112]. In the experimental phase, the asphaltene deposition and permeability reduction at a constant temperature in the presence of water were measured by employing the IP-143 method during core-flooding tests. Providing more information, the mass balance equation of Wang et al. (1999) [113], the momentum equation of Darcy's law, the deposition model of Gruesbeck and Collins (1982) [106], porosity-permeability relation of Chang and Civan (1997) [114], and connate water saturation were optimized by GA [115]. The optimized parameters were the surface deposition rate coefficient, the entrainment rate coefficient, the pore throat plugging rate coefficient, the snowball deposition effect coefficient, critical interstitial velocity, the permeability modification coefficient, and exponent. They found an acceptable agreement between the experimental data and their model results. They concluded that the more pore volume injected, the more permeability reduction, and the more asphaltene saturation in the porous media happens. Although they applied GA to improve the capability of the model, it still suffers from the main drawbacks existing in the original Wang and Civan model [49, 50, 112].

Rezaian et al. (2012) used a mathematical model and an artificial neural network tool to model asphaltene deposition and subsequently permeability damage during dynamic displacement [116]. In their work, the asphaltene precipitation stage was not taken into account, so they assumed that the asphaltene precipitation induced by n-hexane happens at a given thermodynamic condition. In the analytical modeling phase, the mass balance in a vertical direction was applied where the laminar flow regime in porous media, constant temperature, and neglecting capillary pressure were the main

assumptions of the model [116]. In the next step, the porosity of the core sample was given and the porosity-permeability relation of Chang and Civan (1997) [114] was utilized. For the neural network model, a multilayer perceptron network with one hidden layer was trained and validated using an extensive amount of experimental data. The input parameters of the model were the injection velocity, concentration, initial permeability, and injection time, while the output of the model was the permeability reduction of the core [114]. Although both models have some drawbacks, such as neglecting the asphaltene precipitation in the flow, the need for an extensive number of data, and manual tuning of the neural network, they exhibited an acceptable performance to predict the permeability alteration of the core system [117].

In addition to Wang and Civan based model [49, 50], the modeling strategies developed by Ramirez-Jaramillo et al. [118] and Nabzar and Aguiléra [119] appear to be useful. For example, Ramirez-Jaramillo et al. (2005) developed a multiphase model, which has a potential to be applied for multicomponent fluid (oil, gas, asphaltene, and water). The transport phenomena and phase equilibrium concepts were used to model asphaltene deposition in production pipelines [118]. The initial assumptions of the model included: asphaltene aggregation forms at the thermodynamic conditions of the oil flow (temperature and pressure); Second, for both turbulent and laminar flow regimes, asphaltene deposition resulted from the radial diffusion, which is dominated by the molecular diffusion or shear removal mechanism in a competition [118]. The transport model for four-phase interactions was made of three important elements; including thermodynamic model, a rheological equation, and a semi-empirical correlation. To find the temperature profile and heat flux of the well in the turbulent oil flow, a laminar sublayer, a transition zone, and a turbulent region were considered. The temperature profile in the radial direction was neglected in the turbulent flow regime [118]. However, a higher heat conduction and, consequently a more significant temperature drop occurred in the laminar sublayer. The temperature profile on the wall and the inner turbulent core of the pipe was used to explore the asphaltene precipitation phenomenon. The presence of asphaltene precipitation in the oil flow was modeled using the Statistical Association Fluid Theory (SAFT-VR) equation of state. For the rheological model, a modified Casson EOS was chosen because of the yield stresses and time-dependent phenomena of the heavy oil solutions with aggregated asphaltene. In addition, the effects of friction, acceleration, and elevation were considered in a semi-empirical correlation to model the pressure drop in the vertical pipe [118]. It is worth noting that in the vertical pipe, asphaltene deposits in the layer next to the wall, where the heat flux, boundary layer flow, and diffusion in the radial direction are important. The final step to model asphaltene deposition was the utilization of molecular diffusion of

Fick's law for each component in the mixture. Ramirez-Jaramillo et al. applied their model to two samples of crude oils and found that asphaltene deposition is related to the initial stage of development. They did not find the thickness of the deposition layer greater than 15% of the effective inner pipe diameter. No relationship between the growth rate of the deposit and the flow regime was observed. The simulator was able to successfully model the location and rate of the deposition where the profile of temperature and pressure of the multiphase flow is given [118]. However, Ramirez-Jaramillo et al. (2005) did not consider the kinetics of aggregation and de-aggregation, which is a weakness of their model. Furthermore, the thermodynamic equilibrium was attained very fast, which is not realistic [118]. Nabzar and Aguiléra (2008) employed a colloidal approach and an experimental study to model asphaltene deposition kinetics in porous media. Their observations revealed that asphaltene deposits under the general scaling law of colloidal deposition. They suggested the general scaling laws for the deposition kinetics in the form $\propto A\gamma^{-s}$, where η stands for the capture efficiency and γ refers to the shear rate. The exponent s is universal, depending on the deposition regime, and A represents the specific features of the system. They found that at a low flow rate under the first critical shear rate, no asphaltene is deposited (e.g., a small value for exponent s was found under the classical diffusion limit deposition). At the higher shear rates, it was concluded that asphaltene deposition is more sensitive to the shear rate and the power law exponent (s) is higher, compared to the classical diffusion, as illustrated in Figure 10 [119]. Table 3 presents a brief overview of the modeling studies related to asphaltene deposition available in the literature.
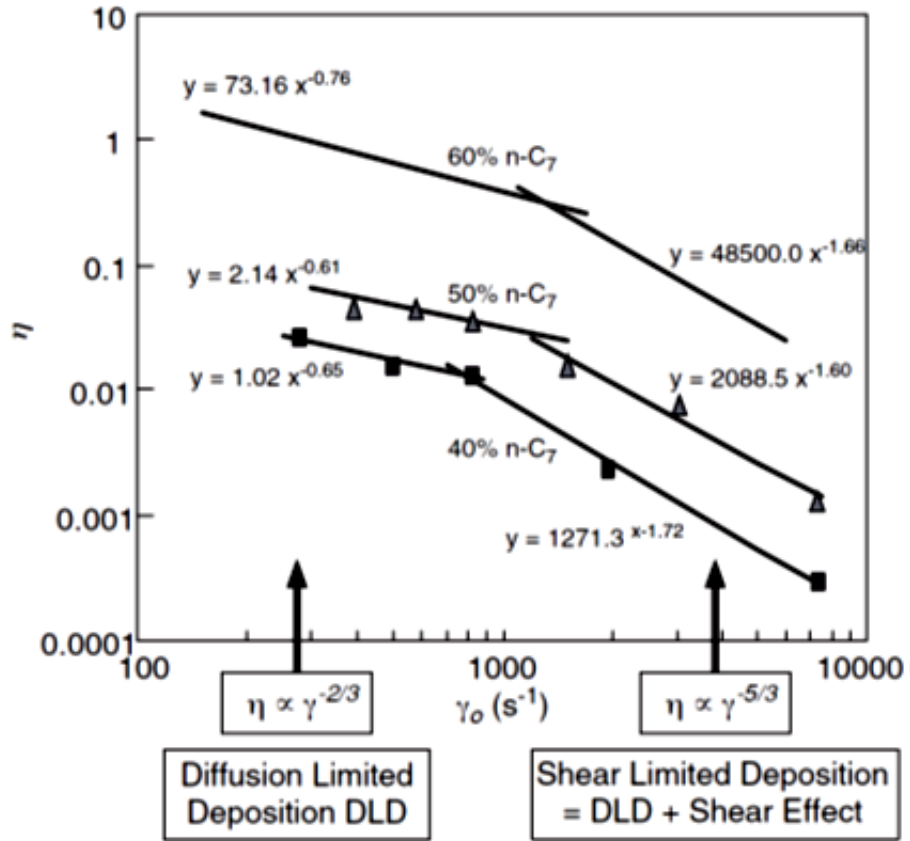
Figure 2-10. Kinetics of asphaltene deposition using a crude oil sample of Weyburn [119]

Table 2-3. Summary of asphaltene deposition modeling works

Year	Researchers	Model	Deposition mechanism	Assumptions	Remark	Drawback	Ref
1997	Ali and Islam	Sarwar and Islam model of surface excess	Adsorption and mechanical entrapment	Three deposition regimes, including monotonous S.S, Quasi S.S, and continuous plugging	Using core flooding experiments, the asphaltene deposition rate was suggested to be a function of flow rate; most deposition was assumed to happen in plugging process near wellbore	Considering suspended asphaltene particles which are ready to deposit	[100]
1998	Leontaritis	Leontaritis model	Surface deposition and plugging of pore throat	Radial diffusion and precipitation at the operational conditions	A relationship between permeability reduction and available area reduction was found	Not considering pressure changes due to deposition, and using a simplified permeability reduction model	[120]
2000/ 2005	Wang and Civan	Wang and Civan model	Surface deposition and plugging of pore throat	Neglecting capillary pressure and gravity; constant temperature	Acceptable accuracy was found	Not considering particle size and kinetics, and oversimplification of the phenomenon	[49, 50]
2004	Almehaideb	Almehaideb model	Surface deposition, pore throat plugging, and entrainment	Oil and suspended asphaltene with the same velocity	Considered a fourth material balance equation in cylindrical coordinate	Need for the experimental parameters to account asphaltene	[121]

					precipitation phenomenon	
2005	Ramirez-Jaramillo et al.	EOS and Casson, Correlation	Diffusion and shear removal	Radial diffusion and precipitation at the operational condition	Employing a thermodynamic model, a rheological equation, and a semi-empirical correlation	Neglecting particle size	[118]
2008	Nabzar and Aguiléra	Scaling law of colloidal approach	Surface deposition, pore throat plugging, and re-entrainment	Multilayer deposition and asphaltene-asphaltene repulsion	Recommending general scaling laws for the deposition kinetics	Neglecting particle size	[119]
2009	Jamialahmadi et. al	Jamialahmadi et. al [122];the Stokes–Einstein equation [123]; Cleaver and Yates [124]; Epstein, Watkinson, and Epstein [122]	Diffusional and inertial mechanisms in pipes	Brownian motion of asphaltene particles toward the surface; considering three modules, including transportation of the particles towards the wall, attachment of the particles to the wall; and gradient of the concentration of the particles in the pipe	Considering asphaltene deposition under forced convective conditions; considering the effects of oil velocity, flocculated asphaltene concentration, and temperature	Considering only steady state deposition; neglecting particle size and kinetics	[122]
2012	Kariznovi et al.	Modified Wang and Civan model	Surface deposition and plugging of pore throat	Neglecting capillary pressure and gravity; constant temperature	Incorporation of the adsorption and dispersion terms	Neglecting particle size and kinetics	[111]

Year	Author	Model	Deposition mechanism	Considerations	Assumptions/Results	Limitations	Ref.
2014	Kord et al.	Modified Wang and Civan model	Surface deposition and plugging of pore throat	Neglecting capillary pressure and gravity; constant temperature	Modified adsorption and pore plugging terms	Neglecting particle size and kinetics	[110]
2015	Hashmi et al.	Scaling model	Convective deposition	Considering convection dominated flow (high Pe number); diffusion dominant near the wall; uniform deposition along the pipe	Laminar oil flow; uniform deposition along the pipe was not a crucial factor. The lower flow rates and the higher asphaltene content, the more asphaltene deposition is observed	Neglecting the interactions between colloidal asphaltene and metal surface	[125]
2016	Favero et al.	Homogeneous first-order reaction	Surface deposition	Considering a first-order reaction (A→D) for asphaltene deposition	Conducted their experiments in a packed bed of stainless-steel beads; asphaltene deposition was considered a function of the concentration of the suspended asphaltene	Effect of surface properties was neglected in the deposition phenomenon.	[126]
2016	Kord and Kharrat	Mukherjee and Brill [127]	Diffusional and inertial mechanisms in pipes	Three modules were considered in the model, including transportation of the particles towards the wall, attachment of the particles to the wall, and gradient of the concentration of the particles in the pipe	Introducing deposition velocity to the model by Jamialahmadi et al. [122]	Considering only steady state deposition; neglecting particle size and kinetics	[128]

2017/2018	Guan et al.	Guan et al.	Arterial deposition in pipes (diffusion, inertial, and impaction)	Considering a single phase, multi component oil flow, no shear removal, and only deposition of precipitated asphaltene	Two modules were considered, including thermodynamic (PR EOS) and a transport module; focused on the CFD of asphaltene deposition for both laminar and turbulent flow regimes	Neglecting particle size	[129, 130]
2018	Davudov et al.	Scaling analysis	Diffusion, inertial, and impaction	Local equilibrium, isothermal, incompressible, and single-phase oil flow; uniform deposition around the well	Four dimensionless groups were generated for asphaltene deposition from momentum and mass balance equations; critical Re was suggested whereby below this point (flow) less deposition occurred. After the critical Re, more deposition was predicted; the larger particles were more prone to deposition	Neglecting kinetics of deposition	[131]
2018	Salimi et al.	Jamialahmadi et al. [122], Hausen equation, and the Chilton and Colburn analogy	Diffusional and inertial mechanisms in pipes	Brownian motion of asphaltene particles toward the surface; considering three modules which are the same as Jamialahmadi et al. [122]	Asphaltene deposition under turbulent flow (Re<5000); the higher the temperature and the more concentration of asphaltene, the higher rate of deposition	Neglecting particle size and kinetics	[132]

				occurred. The higher the oil velocity, the lower the rate of deposition		

2-6. Effects of Process/Operational Condition on Asphaltene Precipitation/Deposition

Temperature. Generally, it has been shown that asphaltene precipitation decreases with increasing temperature. The influence of temperature is qualitatively demonstrated in Figure 11. The outcome/observations from various studies show inconsistency and different trends in terms of temperature impact. The controversy over the effect of temperature was discussed by Andersen et al. (1990) [133]. They found that at a certain temperature, the highest amount of precipitation occurs with n-alkane as a solvent. They claimed that at high temperatures (4°C-100°C), an initial increase of asphaltene precipitation is followed by a decrease in the precipitation. It was also observed that more precipitation occurs using solvents with a lower carbon number. In another research work, Andresen et al. (1994) studied the effect of precipitation temperature on the composition and amount of n-heptane induced asphaltene [134]. They conducted several tests in the temperature range of -2°C to 80°C with n-heptane as a solvent. Similar to their previous observations, a decrease in the asphaltene precipitation was experienced with an increase in the temperature. It was also found that the solubility of asphaltene in crude oil increases at high temperatures (80°C) [80, 133-135].
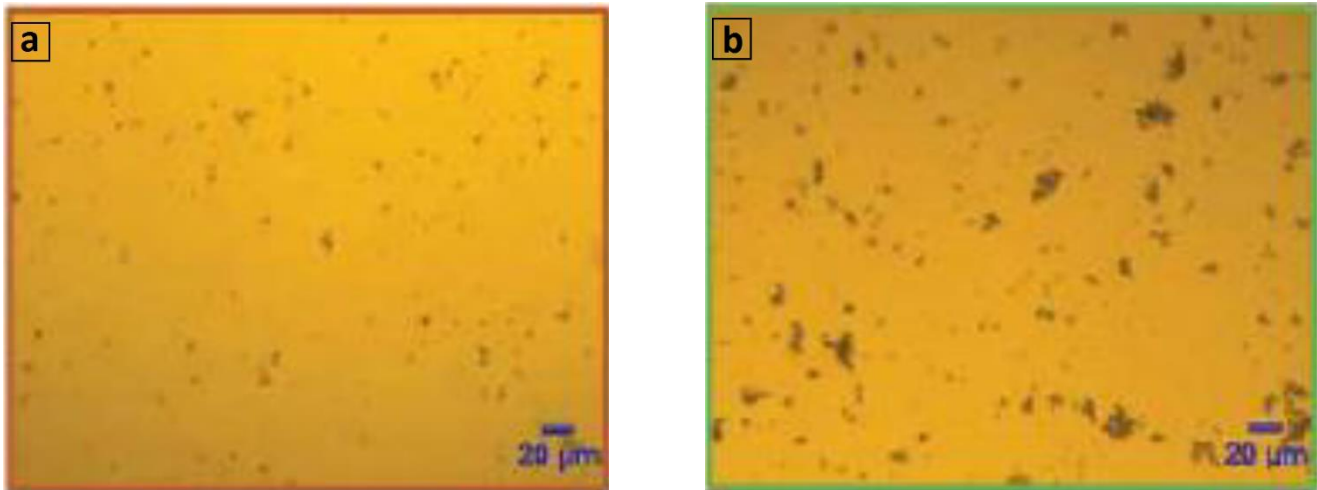
Figure 2-11. Visualization of the effect of temperature on asphaltene destabilization at (a) 364K and (b) 341K and constant pressure 2706 MPa [136]

Leontaritis (1996) showed that the solubility of asphaltene is a function of the temperature of the system. It was concluded that as long as the operating temperature is less than the reservoir temperature, the solubility of asphaltene increases with increasing temperature. In contrast, the solubility of asphaltene

decreases with increasing the temperature if the operating temperature is higher than the reservoir temperature [137]. Maqbool et al. (2011) discussed the effect of temperature on the rate of aggregation from the crude oil mixture. Based on their experimental and theoretical investigations, increasing temperature lowers the asphaltene precipitation onset time. It also decreases the amount of produced asphaltene, while this change increases the solubility of asphaltene [90].

In a research work, Jamialahmadi et al. (2009) used a flow-loop apparatus to observe the effect of oil velocity, bulk and surface temperature, and flocculated asphaltene concentration on the asphaltene deposition. They found that the concentration of flocculated asphaltene is the most vital factor in asphaltene deposition occurrence. It was concluded that the asphaltene deposition rate increases with an increase in the temperature and concentration of flocculated asphaltene (Figure 12). However, the oil viscosity has a reverse effect on the asphaltene deposition so that the deposition decreases with increasing the oil viscosity [122].
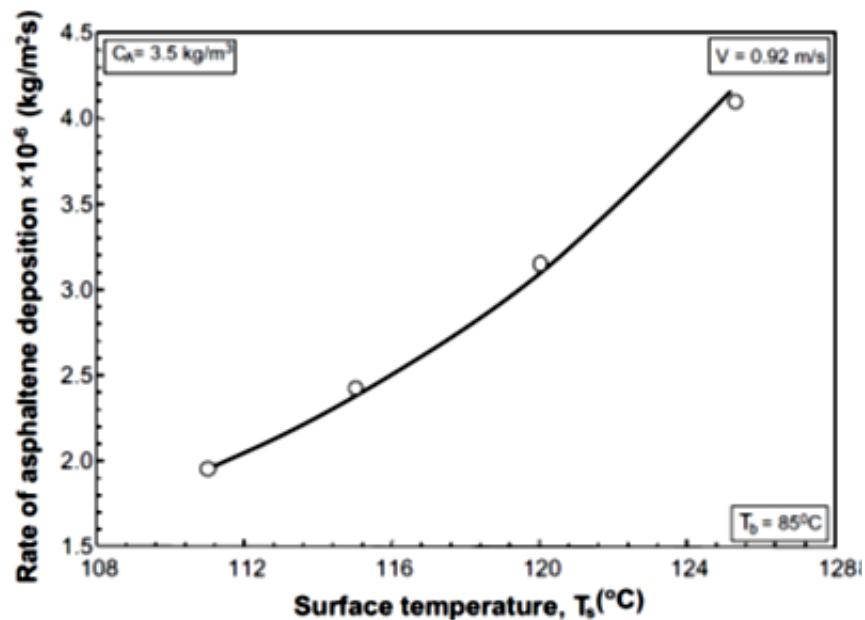
Figure 2-12. The Effect of surface temperature on asphaltene deposition rate [122]

Tavakkoli et al. (2013) investigated the influence of different depositing environments on oil characteristics. They altered the depositing environment by changing the system temperature, asphaltene polydispersity, type of solvent, depositing surface, and flow rate. Asphaltene deposition was observed at two time-scales. At initial times, the asphaltene deposition decreased with increasing temperature due to the lower amount of adsorbed asphaltene. However, asphaltene deposition increased with increasing temperature in longer times as a consequence of a higher diffusion coefficient [138].

Pressure. It has been found that above the bubble point, the solubility of asphaltene decreases as the pressure decreases due to the reduction of oil density until the solubility reaches its minimum at the bubble point pressure. In contrast, by reducing the pressure below the bubble point, the solubility of the oil mixture increases; because the pressure reduction below the bubble point results in evolving the solution gas from the oil and the remnant of the oil would be rich in heavier components (Figure 13) [139]. As the pressure increases, the area of deposition and the amount of deposition are increased, as seen in Figures 14 and 15 [140].
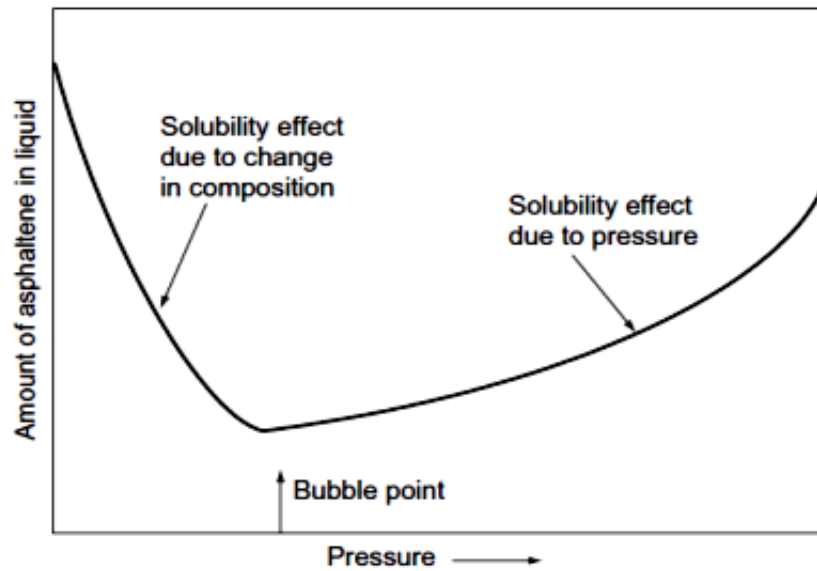
Figure 2-13. Effect of pressure on asphaltene solubility [139]
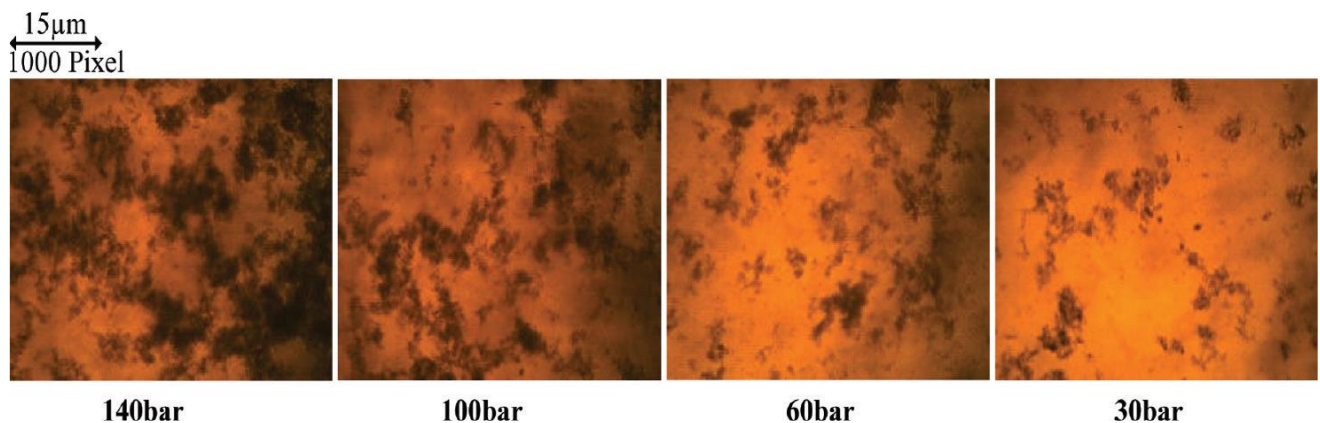
Figure 2-14. Influence of pressure on asphaltene deposition using a heavy oil sample at T=90°C [140]
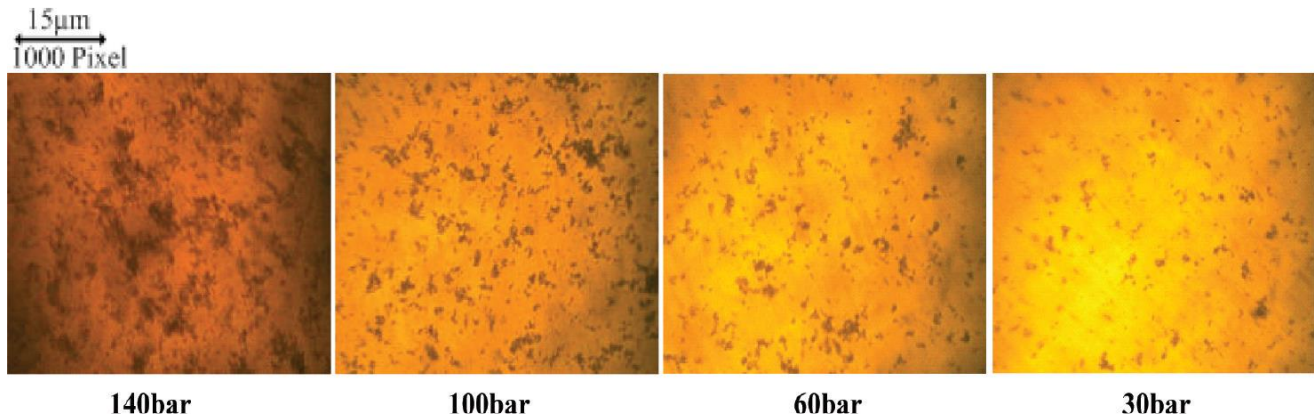
Figure 2-15. Impact of pressure on asphaltene deposition utilizing a light oil sample at T=90°C [140]

Hu et al. (2004) investigated the effect of pressure and CO_2 injection on asphaltene precipitation where they used a Solid Detection System (SDS) to determine the onset point of asphaltene precipitation. They noticed no asphaltene precipitation with pressure depletion. No asphaltene precipitation occurred under CO_2 injection when the pressure is far from the Minimum Miscible Pressure (MMP). However, at a pressure close or higher than MMP, the asphaltene precipitation was detected [141]. Later, Verdier et al. (2006) used a high-pressure cell equipped with a filtration system to measure the amount of asphaltene precipitation under solvent injection. Their observations exhibited a good agreement with the previous works; the asphaltene precipitation decreases at high pressures (50 MPa) where CO_2 as a solvent is injected in the oil phase [142].

Asphaltene deposition usually happens as a result of pressure depletion [143]. Many researchers, including Boresta et al. (2000), observed an increase in the pressure drop within a capillary tube when the asphaltene was deposited on the tube walls and built a deposited layer with time in an irreversible deposition process [93]. Soorghali et al. (2014) studied asphaltene deposition on the slide glasses in a High-Pressure and High-Temperature (HPHT) cell at the reservoir conditions in the presence of resins. The amount and size distribution of asphaltene deposition of two types of crude oils were determined by a high-resolution microscope images that were processed with a software. As depicted in Figure 16, they found that asphaltene deposition increases with increasing pressure [144].
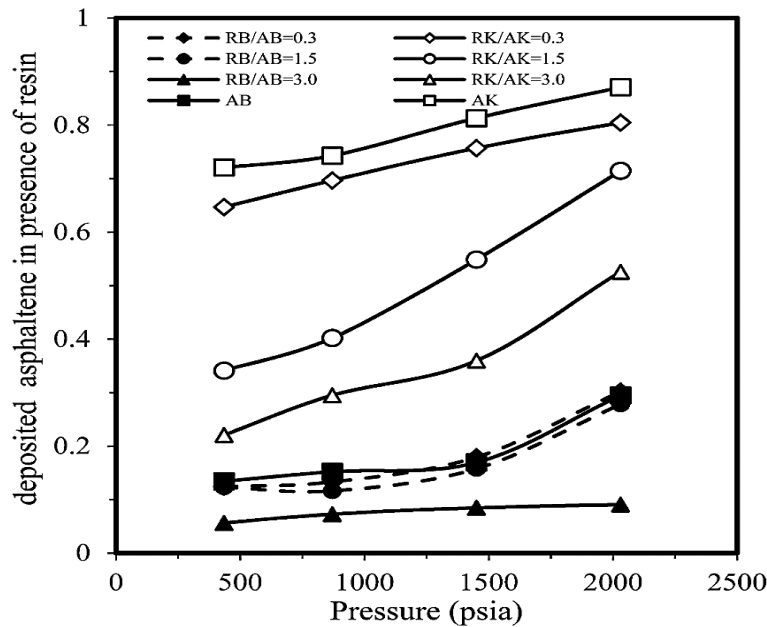
Figure 2-16. Asphaltene deposition at different pressures for various mixtures of oil and resin (RB: resin of Bangestan, AB: asphaltene of Bangestan, RK: resin of Kuh-e-Mond, and AK: asphaltene of Kuh-e-Mond) at a constant temperature of 363.15 K [144]

Flow Rate (Flow Regime). Boek et al. (2008) studied the influence of different flow rates (5 μL/min and 10 μL/min) on the asphaltene deposition in a glass capillary through experiments and a computational method, which is called Stochastic Rotation Dynamics (SRD). They considered pressure drop versus time across the capillary and used optical microscopy to investigate the dynamics of deposition [95]. An increase in the pressure drop with time for both flow rates was experienced as a result of asphaltene deposition. In other words, they observed that asphaltene deposition and pressure drop increase at higher flow rates. In addition, a sharp initial pressure drop was noticed with a flow rate of 10 μL/min, which indicates a faster initial deposition of asphaltene through the capillary walls; however, the flow entrained the deposited asphaltene, afterwards [95]. Later, they repeated the same experiments with an oil sample and found more chaos in comparison with their previous observations, where precipitated asphaltene dissolved in toluene was employed [96].

Asphaltene deposition and particle size evolution in the turbulent flow regime were studied by Eskin et al. (2011) [104]. A Taylor Couette (TC) device was used to perform experiments that showed deposition on the outer wall of the cylinder. They also developed a model to evaluate the particles size distribution by population balance method and the particle movement to the wall of the pipe, driven by the Brownian motion. The parameters of the model were tuned by the experimental results obtained from the Taylor Couette (TC) device [104]. The concept of the critical particle size was introduced in their work. It was confirmed that the particles with a size below this critical size are able to deposit. The maximum initial

deposition of thickness in horizontal transport pipelines was obtained in their work due to the high flow rate and high-pressure drop [104]. Following that, a decrease in the thickness of asphaltene deposition happened because of a decrease in the velocity of particle movement to the wall by the Brownian motion and growth of agglomeration size, as demonstrated in Figure 17. As a conclusion, although asphaltene precipitation rate increases with increasing the velocity, asphaltene deposition rate decreases at higher shear rates [104].
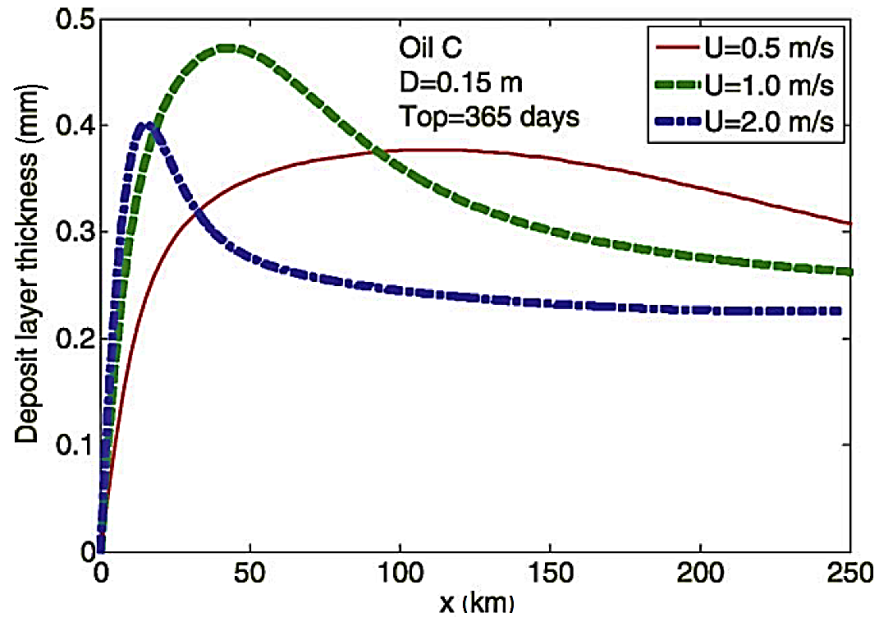
Figure 2-17. Thickness of the deposited asphaltene in a horizontal pipeline [104]

In another research work, Kurup et al. (2011) addressed the shortcoming of the work carried out by Eskin et al., such as application in lab-scale so that they conducted the capillary tube tests and introduced an Asphaltene Deposition Tool (ADEPT) for wellbores [145]. They used a thermodynamic model, Perturbed Chain Statistical Associating Fluid Theory (PC-SAFT), to predict the phase behaviours of oil in conjunction with a mathematical deposition model to monitor/determine the amount of asphaltene deposition for turbulent capillary flow in wellbores. When the oil flows up the wellbore, the temperature and pressure decrease, causing the formation of primary unstable asphaltene precipitation [145]. They proposed an axial dispersion model, knowing that the molecular diffusion in the turbulent axial flow is due to the eddy diffusion. It was observed that the highest amount of deposition happens at the inlet of the axial tube due to the highest concentration of driving force. However, the thickness of asphaltene deposition reduced along the length of the tube due to the reduction in the amount of asphaltene in the oil mixture [145]. Salimi et al. (2013) studied asphaltene deposition in the pipeline under a laminar flow

regime, where the effects of various parameters, such as oil velocity, surface temperature, and asphaltene content, on the magnitude of deposition were considered [146]. It was concluded that increasing oil velocity in the laminar flow leads to the reduction of the thickness of the asphaltene deposition layer [146].

Type of Production Methods. Injection of hydrocarbon and non-hydrocarbon gases in the form of miscible or immiscible gas drive is a practical Enhanced Oil Recovery (EOR) method. Miscible gas flooding, which applies to reduce the viscosity and residual oil saturation, is in favour of permeability impairment [40-45]. Zanganeh et al. (2018) carried out visual experiments to investigate various EOR methods, including gas injection scenarios such as carbon dioxide (CO_2), natural gas (e.g., CH_4), and nitrogen (N_2) to explore the mechanisms and characteristics of asphaltene precipitation and deposition during oil recovery [40]. A high-pressure cell, which was equipped with a high-resolution microscope and an image processing software, was utilized. It was revealed that natural gas and CO_2 have a considerable effect on the asphaltene precipitation, while N_2, as an inert gas, could not alter the asphaltene stability. Injection of both CO_2 and natural gas increased the precipitation of asphaltene; however, the impact of CO_2 was more significant, as depicted in Figure 18 [40].
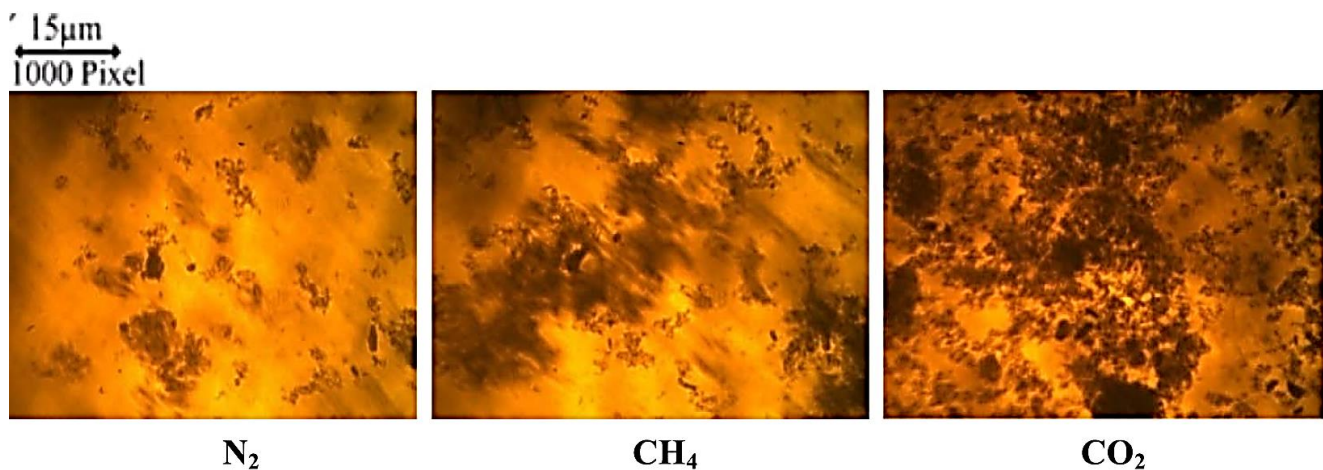
Figure 2-18. Effect of N_2, CH_4, and CO_2 injection on asphaltene deposition at 60 bar, 90 °C and 5% mol gas injection [40]

Mousavi et al. (2007) studied the effect of miscible gas injection on asphaltene deposition during dynamic displacement of oil [147]. The experiments were carried out in two porous media, limestone and sandstone. It was observed that asphaltene deposition increases with increasing the amount (rate) of the injected natural gas. Hence, the asphaltene deposition altered the porosity and permeability of the rock samples [147].

2-7. Effects of Fluid Properties on Asphaltene Precipitation/Deposition

Precipitant Type and Properties. Asphaltene precipitation and deposition may occur by inducing precipitants such as n-alkanes. Wang et al. (2004) studied the effect of the amount of n-alkane on asphaltene deposition from stock tank oil flowing in a stainless-steel capillary [94]. They observed that asphaltene deposition happens step by step by mixing precipitant and oil close to the onset point. In addition, asphaltene deposition increased by adding a higher amount of precipitant [94]. The solubility parameter of the oil was measured with a refractive index to ensure asphaltene destabilization by n-alkanes such as $n-C_5$, $n-C_7$, $n-C_{10}$, $n-C_{11}$, and n-C15. A thicker layer of asphaltene deposition was obtained for the cases with heavier n-alkanes [94]. For example, the deposition induced by normal pentadecane was greater than that by normal heptane. It was also concluded that the more molar volume of precipitant leads to the higher rate of asphaltene deposition when other process conditions remained unchanged [94].

Lawal et al. (2012) carried out an experimental work, and a simple material balance was used to investigate asphaltene induced by n-alkanes in a capillary tube [148]. They used a glass microcapillary pipet, where the asphaltene deposition was measured by imaging and calculation of pressure drop. To investigate the effect of precipitant agents on the heavy crude oil, three n-alkenes, including n-pentane, n-heptane, and n-octane, were used and the design of the experiments was in a manner to have capillary flow without dispersion, insignificant interfacial force, and negligible gravity force. A gravimetric analysis was conducted to ensure about the asphaltene onset point [148]. Their observations revealed that the effect of the type of precipitant on asphaltene deposition is significant. It was found that the rate of asphaltene deposition is higher while using precipitants with a higher carbon number. This finding is illustrated in Figure 19. However, they were not able to propose any relationship between the concentration of precipitant and the deposition rate. It was observed that only at high precipitant/solvent ratios, the deposition rate increases by increasing the concentration of the precipitant agent. Although a minimum threshold for the precipitant/solvent ratio of 1.08 was detected by the gravimetric analysis, no considerable deposition with a ratio of 1.22 was noticed [148].
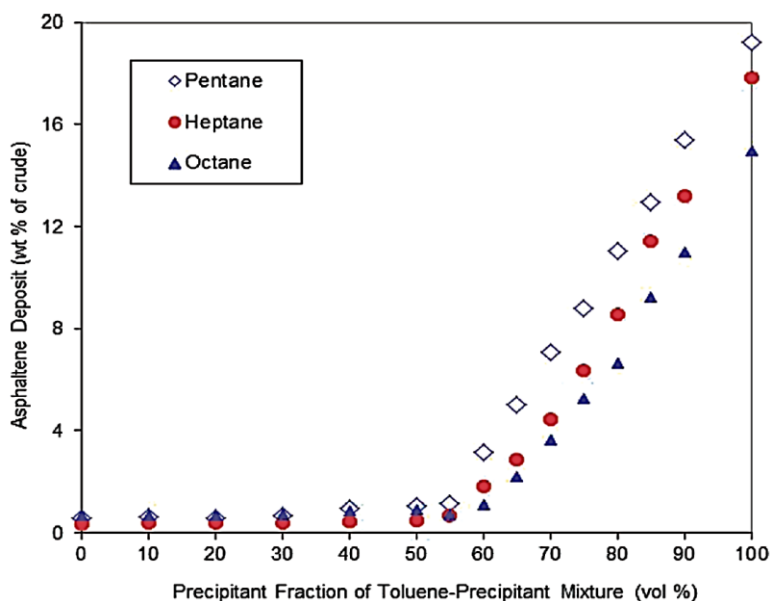
Figure 2-19. Asphaltene Precipitation Onset (APO) as a function of precipitant/solvent ratio [148]

In another research study, Hoepfner et al. (2013) conducted asphaltene deposition in a metal capillary by adding n-heptane as the precipitant agent. It was observed that there is no critical concentration of the precipitant agent, so that deposition was a function of the heptane concentration [143].

Oil Density. A screening method was introduced to show the tendency of different crude oils for precipitation on the basis of the Flory-Huggins solubility model by de Boer et al. (1995). They examined ten crude oil samples to investigate the effect of in-situ density of oil on the asphaltene stability by using the solubility parameter. For this purpose, the Hildebrand solubility parameters as a function of density were correlated for both oil and asphaltene available in the mixture. In general, the asphaltene solubility decreases with depressurization above the bubble point, while below the bubble point, the trend/behaviour is reverse and further depressurization increases the solubility [88]. It was concluded that for light oils containing a small amount of asphaltene, the solubility of asphaltene changes to a higher degree with increasing pressure in comparison with the heavier oils. Therefore, the probability of asphaltene precipitation is higher for the light oil samples, despite the fact that they predominantly have a smaller amount of asphaltene. Decreasing pressure below the bubble point changes the liquid phase composition and consequently increases the solubility of asphaltene. In spite of the fact that heavy crude oils have a high asphaltene content, they experience less asphaltene precipitation occurrence around the bubble point pressure [88]. In conclusion, three detrimental parameters including the density of crude oil, degree of gas saturation, and degree of asphaltene saturation were introduced to show the tendency of asphaltene for precipitation [88].

Oil Viscosity. In general, oil with a higher viscosity usually shows less asphaltene precipitation due to the presence of lighter hydrocarbons to stabilize asphaltene particles. Maqbool et al. (2011) used optical microscopy to investigate the effect of viscosity (due to temperature changes) on the asphaltene aggregation and kinetics of precipitation [90]. It was argued that viscosity decreases with increasing the temperature so that viscosity reduction is the reason to shorten the onset time for precipitation. They also validated their findings with Smoluchowski type aggregation process. The liquid medium was considered as the oil-precipitant mixture in which the asphaltene particles were aggregated [90]. A reduction in the viscosity will lead to an increase in the effective diffusivity of the particles, and consequently a faster aggregation. Hence, the viscosity of the oil controls the collision frequency of asphaltene nanoaggregates [90].

Lawal et al. (2012) investigated the influences of viscosity and the precipitant on the asphaltene deposition rate from a heavy crude oil in a capillary [148]. In spite of previous observations, they concluded that the deposition rate is governed by viscosity, not solubility. It was claimed that the higher carbon number leads to a higher viscosity that prevents the aggregation of asphaltene particles and consequently the deposition rate decreases. It was also found that asphaltene flocculation and deposition are controlled by particle transportation and viscosity [148].

It is known that variation in crude oil composition may lead to the asphaltene precipitation. Burke et al. (1990) showed that the asphaltene solubility decreases with increasing the amount of dissolved gas in a crude oil [139]. Pan and Firoozabadi (1997) employed a thermodynamic micellization model and the Peng-Robinson EOS to describe the asphaltene precipitation. They considered a liquid-liquid equilibrium system in which the precipitated heavy phase consists of asphaltenes and resins [149]. They examined the proposed model with three different reservoir crudes to study the effect of various parameters, including the composition of oil on the asphaltene precipitation. It was observed that, in two of the crudes, an increase in the resin content can prevent asphaltene precipitation, while decreasing resin concentration deteriorates the precipitation [149].

Rogel et al. (2001) applied compositional model and structural characterization of resin and asphaltene to study the stability of asphaltene [150]. It was suggested that the stability of asphaltene in crudes is dominated by asphaltene and resin characteristics more than oil composition. They observed that unstable asphaltene is highly aromatic with low H/C ratio and high condensation of aromatic rings, while crudes with stable asphaltenes show low aromaticity and condensation of aromatic rings and high hydrogen content. It was also claimed that asphaltene and resin (peptizing agent) should be chemically and structurally compatible to stabilize asphaltene [150].

Soorghali et al. (2014) found that an increase in the resin/asphaltene ratio results in stabilization of asphaltene (see Figure 20). They used a PVT cell to recognize the effect of pressure and temperature on asphaltene deposition and validated their findings with the contact angle measurements and the results of the AFM technique [144]. Moreover, it was observed that the effect of resins on the stability of asphaltenes is more dominant in crudes with lower asphaltene precipitation. They claimed that increasing pressure decreases the stability of resins, especially at higher ratios of resin/asphaltene [144]. In general, asphaltene structures and resin content were introduced as important factors that affect the stability of asphaltene in crudes [144]. Then, they investigated the effect of native and non-native resins and their mixture on the asphaltene deposition. Less asphaltene deposition was observed when a mixture of resins from different crudes was added, compared to the native resins. However, they were not able to explore any specific effect of resins on asphaltene deposition, since the various behaviors of resin mixtures were noticed [151].
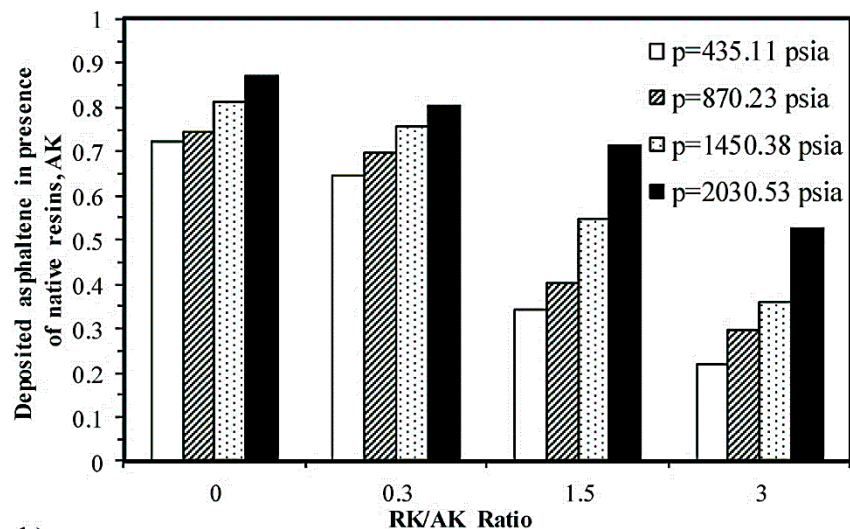
Figure 2-20. Asphaltene deposition in the presence of resin at a constant temperature (T=363.15 K), (MR/AK: a mixture of resin/asphaltene of Kuh-e-Mond) [144]

2-8. Effects of Reservoir Properties on Asphaltene Precipitation/Deposition

Stability of asphaltene clusters can be altered by changes in thermodynamic conditions, oil composition, and presence of clay and ions in the reservoirs [152-154]. The effect of two former parameters on asphaltene stability was reviewed earlier in this paper. The impacts of reservoir properties such as porosity, permeability, and impurities are presented in this section.

Minerals and impurities in reservoirs such as clay and rock minerals (originated from reservoir surfaces or from heavy oil sands) and salt carry the electrical charges that can associate with oil components (e.g., asphaltene) and convey an electrical charge on the asphaltene surface [155]. The electrical charge between the asphaltene and minerals/impurities, whether attractive or repulsive, can strongly influence the stability of asphaltene [155]. In Table 4, the adsorption capacity of different minerals is summarized.

Table 2-4. Adsorption capacity of some minerals

Adsorption capacity ($\frac{mg}{m^2}$)	Ref
kaolin=1.4, alumina=1.3, silica=1.1, and low amount of adsorption capacity for MgO, ZnO, and TiO₂	[156]
chlorite=1.85, Fisher kaolinite=1.55, Berea sandstone=1.43, Ward's kaolinite=1.1, and Illite=1.08	[157]
Limestone=2.77, sandstone=2.6, silica=0.638, and alumina=0.538	[158]
calcite=2.74, quartz=1.64-1.69, and dolomite=1.65	[159]
kaolinite=3.36, Indian limestone=1.82, Baker dolomite=1.46, and Berea sandstone=0.9	[160]

Punase et al. (2017) studied the role of reservoir rock-asphaltene interaction on the stability of asphaltene, in the presence of inorganic impurities such as clay in the reservoir [161]. Eleven samples of asphaltenes were visualized by Scanning Electron Microscopy (SEM) to obtain their surface morphology in the presence of inorganic contents [161]. In addition, the Energy Dispersive Spectroscopy (EDS) analysis was applied to validate the findings of SEM. The high tendency of precipitation in the asphaltene samples due to excessive amounts of negatively charged particles were found in their research. The bigger the size of the asphaltene particles, the higher the chance of precipitation. It was also concluded that asphaltene stability is enhanced by increasing the electrostatic repulsion between the asphaltene particles [161].

Behbahani et al. (2015) used different core samples to investigate the effects of the interfacial interaction of the asphaltene and rock minerals on the asphaltene adsorption and deposition. For this purpose, four rock samples of carbonate, dolomite, and sandstone with different porosities (26%, 22.5%, and 13.15%) and permeabilities (2.7, 106.6, and 22.8 mD) were selected. The SEM micrographs, X-ray, and elemental analysis were employed to understand the impact of surface morphology and mineral composition on asphaltene deposition in porous media [162, 163]. Comparing SEM images of the surfaces, it was concluded that carbonate core experiences severe particle plugging of asphaltene deposition due to the formation of large clusters, which form multilayer adsorption. A higher iron content in the core was found to be in the favour of maintaining the permeability of the core, while a

high calcium content was detected to facilitate the permeability reduction due to the asphaltene deposition, as seen in Figure 21. Hence, the difference in deposition mechanisms in the rock samples was related to the core structure, mineral composition, and interaction of asphaltene particles with the inner surface of porous media. As asphaltene is highly polar, it was concluded that the polar groups in the carbonate core exist. Considering the influence of initial permeability of core samples on the asphaltene deposition, a continuous severe formation damage in low permeability core sample was detected that spread over the core. However, for a high permeability core, a slow plugging in the inlet region was noticed [162, 163].
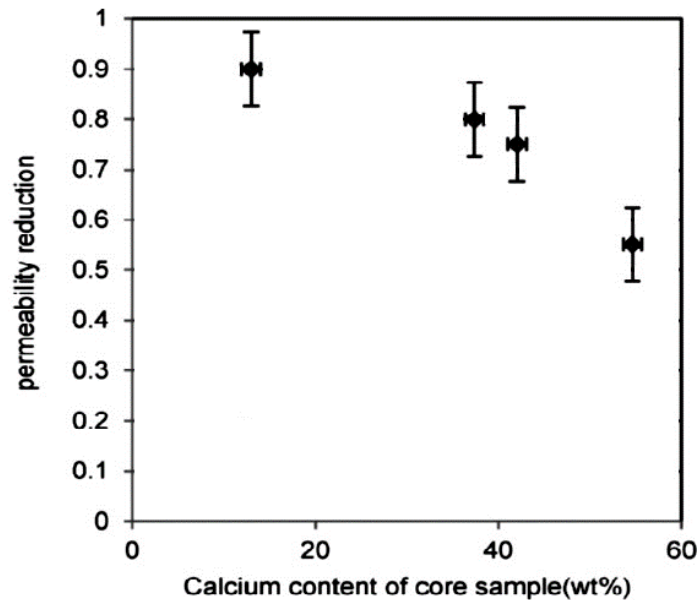
Figure 2-21. Permeability reduction of the core sample with different Calcium content [162, 163]

Kord et al. (2012) performed several dynamic and static asphaltene deposition tests to elucidate important aspects of this unfavourable event including the effect of porous medium characteristics [164]. They used four different core samples from an Iranian oil reservoir (Bangestan) with a permeability ranged from 1.23 mD to 18 mD and different pore sizes (the average size of pores is less than 1 μm). They concluded that all rock samples experience a rapid reduction in the permeability due to the surface deposition, however, the core samples with a higher permeability and porosity impose lower damage. In addition, the core sample with a smaller average pore size (0.008-0.012 μm) was fully plugged due to the size of asphaltene particles (0.15-0.35 μm) [164].

Bolouri et al. (2012) conducted CO_2 miscible core flood tests to perform a parametric sensitivity analysis for further understanding of mechanisms involved in the asphaltene deposition [165]. For this purpose, one sandstone sample and two carbonate rocks were utilized where their characteristics are

presented in Table 5. They also developed a mathematical mass and permeability variation model to simulate the vital mechanisms of asphaltene deposition in various core samples [165]. They observed that 70% of the initial permeability of sandstone was lost as a result of asphaltene deposition, while only a 30% loss happened in the permeability of the carbonate rock. Based on their observations, it was concluded that the cake formation and adsorption are the dominant deposition mechanisms in the sandstone with a higher initial permeability and porosity. However, the gradual pore blocking and pore sweeping were found as the main deposition mechanisms in the carbonate samples with a lower permeability and porosity [165].

Table 2-5. Characteristics of the core samples used in a research study [165]

Core type	CO_2 concentration (mol%)	Length (cm)	Diameter (cm)	Initial permeability (md)	Initial porosity (%)	Irreducible water saturation (%)
Sandstone	30	10.2	3.8	28.9	13.97	25
Carbonate (1)	40	14.9	3.8	0.261	10.37	35
Carbonate (2)	30	8.6	3.8	0.21	8.2	30

After that, Bolouri et al. (2013) conducted experimental and modeling studies of asphaltene deposition in sandstone and carbonate core samples under CO_2 miscible gas injection [166]. It was observed that the degree of damage formation due to CO_2 miscible injection is dominated by core specifications and concentration of the injected gas. Hence, severe permeability damage was observed at the beginning of injection in the carbonate core sample. The deposition within the sandstone core was dominated by the formation of the filter cake, while pore plugging and the formation of filter cake were the main mechanisms in the carbonate rock [166].

Mirzabozorg et al. (2009) analyzed the asphaltene deposition impairment in an oil fractured reservoir [167]. It was revealed that asphaltene deposition has a significant impact on the production performance of the reservoir. It was also observed that asphaltene deposition across the fractures is greater in comparison with the matrix system due to major flow rates in the fractures [167]. According to the simulation sensitivity analysis, it was concluded that increasing the fracture spacing will lead to increasing the asphaltene deposition due to a lower production rate and a higher pressure drop. It was revealed that the properties of the fractures have a significant influence, which needs to be considered in the modeling/simulation of the asphaltene behaviours and field performance [167].

Solaimany-Nazar et al. (2011) proposed a model based on two reservoir case studies to investigate the effects of production rate and reservoir permeability on the asphaltene deposition [168]. The Flory-Huggins model was employed to simulate asphaltene precipitation. It was found that the reservoir initial permeability has a significant effect on asphaltene deposition during production. It was observed that at a fixed production rate, an increase in the initial permeability will result in less formation damage due to the availability of more channels for flow. However, it was concluded that the production rate is considerably affected by deposition of asphaltene, while at a fixed initial permeability, an increase in the production rate causes severe deposition problems. Their findings are summarized in Table 6 [168].

Table 2-6. Effects of initial reservoir permeability and production flow rate on the permeability and porosity due to asphaltene deposition [168]

Oil	Oil initial permeability, md	Flow rate, STB/day	Permeability reduction, %	Porosity reduction, %
	25	500	0.5907	0.2
	25	2000	10.7	3.71
	25	5000	18.84	6.72
	100	500	0	0
No. 1	100	2000	2.15	0.8
	100	5000	16.27	5.75
	1000	500	3.18	1.07
	1000	2000	6.16	2.22
	1000	5000	16.64	5.88
	25	500	2.7	0.91
	25	2000	12.67	4.41
	25	5000	22.53	8.17
	100	500	0	0
No. 2	100	2000	6.68	-
	100	5000	16.7	5.95
	1000	500	7.12	2.43
	1000	2000	9.47	3.26
	1000	5000	18.86	6.73

2-9. Simulation and Optimization Tools/Packages for Asphaltene Precipitation/Deposition

Equations of State (EOSs), correlations, and deposition models have traditionally been used as the main methods to characterize the asphaltene precipitation and deposition. However, some important aspects of the asphaltene behaviours including molecular-level, time dependency, and realistic mechanisms cannot be easily addressed by the conventional techniques. Advanced simulation tools such as Molecular Dynamic (MD) simulation, intelligent tools, Computational Fluid Dynamics (CFD), and

Lattice Boltzmann Method (LBM) are able to provide more detailed information from the molecular scale to the larger scales.

Hu et al. (2011) used the Molecular Dynamic (MD) simulator (LAMMPS MD simulator software) to model the interactions of the asphaltene aggregations with different solvents (such as CO_2) at a constant temperature and pressure [169]. As the oil mixture is considered as a complex system to model, methane or ethane, and octane represented the light and heavy components of the crude, respectively. They assumed that asphaltenes are surrounded by methane, ethane, and octane before CO_2 injection, while after the injection, CO_2 extracted light hydrocarbons from surrounding of asphaltenes [169]. They used an average model structure for asphaltene. It was found that asphaltene deposition by injection of pure CO_2 would be greater at the constant temperature. As CO_2 is a nonpolar component, it boosts hydrogen bonds as well as the dipolar interaction of asphaltene aggregates. CO_2 injection will lead to an increase in the $\pi - \pi$ charge-transfer interaction. To sum up, the more aromatic clusters and heteroatoms of asphaltene presented, the greater the deposition of asphaltene is experienced by CO_2 injection [169].

Yaseen at al. (2017) applied MD simulations to model/simulate the molecular interactions between asphaltene and solvent at different temperatures and pressures [170]. Two solvents including ortho-xylene and water were chosen so that the first solvent is the best asphaltene solvent and the second option is the worst solvent of asphaltene. Similar to Hu et al. (2011) [169], they assumed an average structure for asphaltene consisting of three types with different structures and molecular weights (see Figure 22). The properties of the asphaltene models are presented in Table 7 [169].
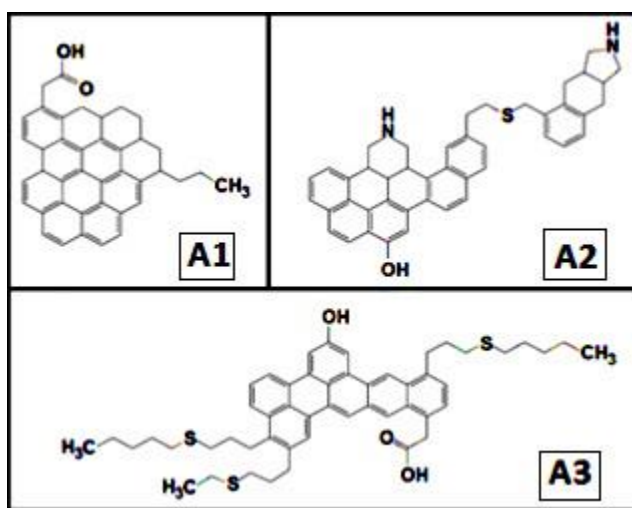
Figure 2-22. Structure of asphaltene models named A1, A2, and A3 [170]

The MD simulations were performed by employing the GROMACS software while a potential model of hydrocarbons and water was simulated in the all-atom optimized potentials for the liquid simulations (OPLS-AA) and the extended Simple Point Charge model (SPC/E), respectively. It was found that interaction energies are dominant in the asphaltene and ortho-xylene mixture, whereas, for the asphaltene and water mixture, the electrostatic interaction energies have a higher impact. It was shown that increasing the temperature and decreasing the pressure reduces the interaction energies. For both solvent mixtures, increasing pressure slightly increased the potential energies [170].

Table 2-7. The properties of model asphaltenes used by Yaseen at al. [170]

Physical specifications	A1	A2	A3
Chemical formula	$C_{40}H_{30}O_2$	$C_{44}H_{40}SN_2O$	$C_{51}H_{60}S_3O_3$
Molecular weight (g/gmol)	542.66	644.86	817.21
No. of aromatic rings	8	7	7
No. of cycloalkanes rings	3	3	0
No. of side chains	2	1	4
Aromaticity	0.7	0.68	0.55
Nitrogen	-	Two secondary amine groups	-
Oxygen	One carboxyl group	One hydroxyl group	One carboxyl group and one hydroxyl group
Sulfur	-	One sulfide group	Three sulfide group

Fang et al. (2018) used an MD simulation to gain more molecular information on asphaltene micelles and precipitation under CO_2 injection and increased pressure. The micelle structure was suggested to be made of eight asphaltene molecules that formed four dimers due to the π-π electron interactions, as illustrated by panel a of Figure 23. The micelle profile revealed that the asphaltene is surrounded by lighter components, resins, and hydrocarbons, as shown in panel b of Figure 23. Figure 23c depicts the Radial Distribution Functions (RDFs) of different components in the micelle [171].
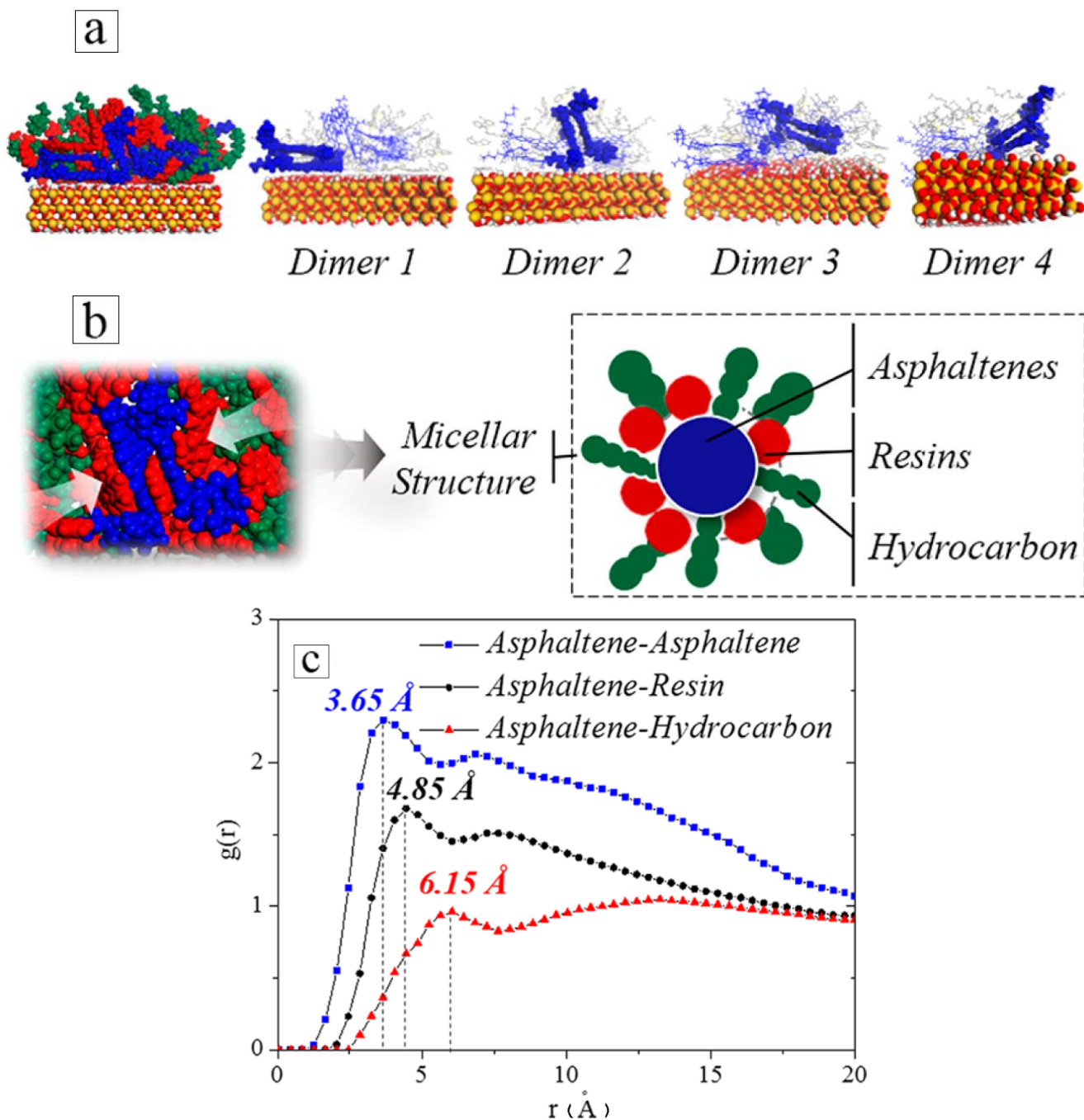
Figure 2-23. (a) Asphaltene equilibrium based on MD simulation, (b) simple schematic of micelles, and (c) RDFs of different components in micelle [171]

The impact of CO_2 injection on the asphaltene aggregation and precipitation is illustrated in Figure 24. It was found that CO_2 stepwise dissolves hydrocarbons and resins, respectively (Figure 24a) and the density distribution also confirms this phenomenon (Figure 24b). The density of hydrocarbons and resins decreased in the surroundings of the asphaltene aggregations at 2.5 and 5.5 ns, according to the

MD simulations [171]. Asphaltene precipitation can be described in panels c, d, and e of Figure 24, in which the RDF peak of asphaltene-asphaltene increases, while the RDFs of asphaltene-resin and asphaltene-hydrocarbon decrease. The former case confirms the closeness of asphaltene molecules and the latter indicates that resins and hydrocarbons are dissolved into CO_2. Under high pressure and CO_2 injection, the interactions between asphaltene aggregations gradually decrease, implying that the high-pressure condition is not in favour of asphaltene precipitation (see Figure 25) [171].
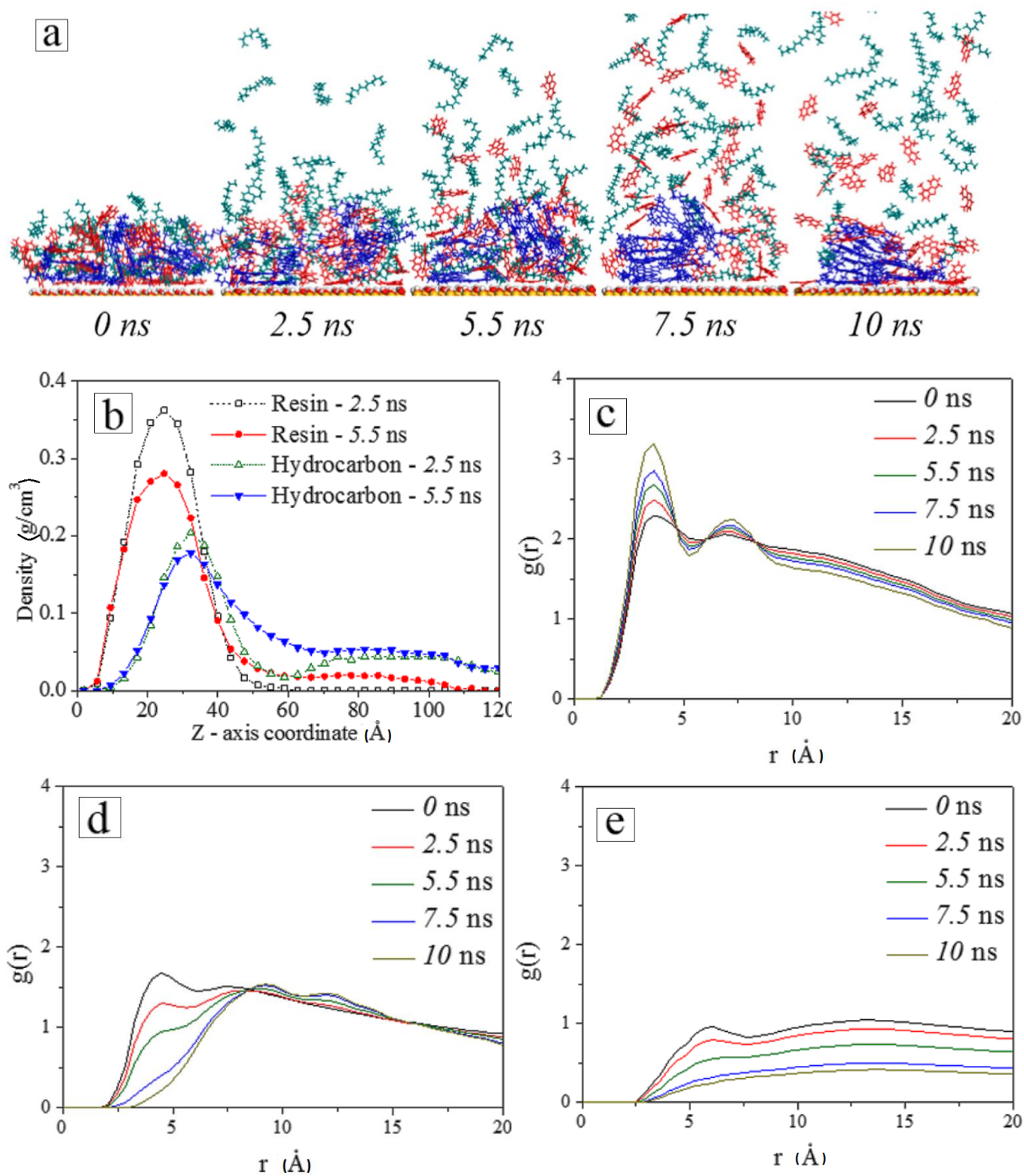
Figure 2-24. (a) Extraction of light hydrocarbons by CO_2, (b) Density distribution of resin and hydrocarbon, (c) Radial Distribution Functions (RDFs) for asphaltene-asphaltene, (d) Radial Distribution Functions (RDFs) for asphaltene-resin, and (e) Radial Distribution Functions (RDFs) for asphaltene-hydrocarbon [171]
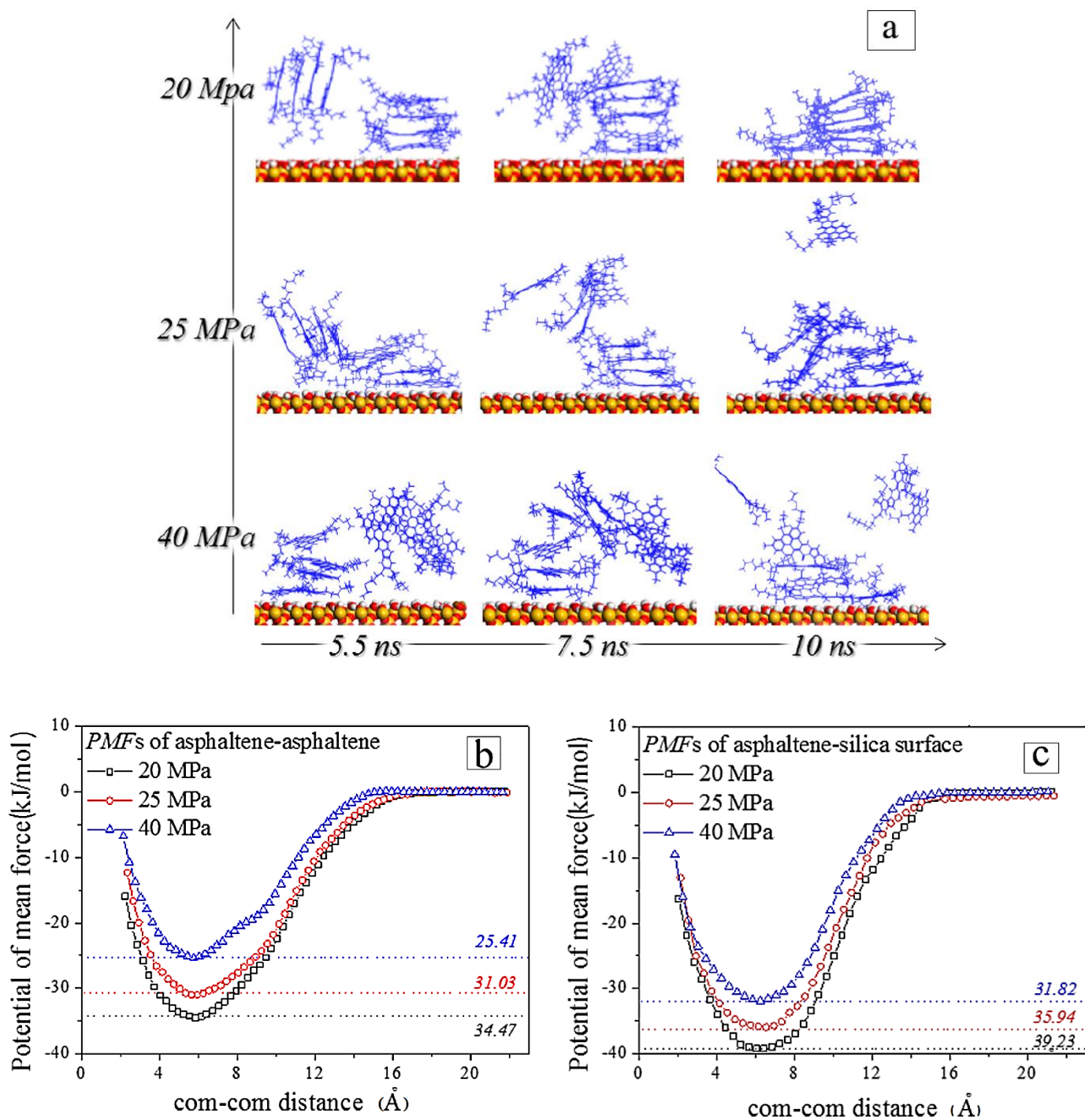
Figure 2-25. (a) Effect of pressure on asphaltene precipitation, (b) Potential of mean force between asphaltene-asphaltene, and (c) Potential of mean force between asphaltene-silica surface [171]

Application of the MD simulations in the research area of reservoir engineering particularly asphaltenes has been limited to the simple representation of asphaltene/fluid and rocks. Hence, further advances in MD simulations need to be conducted.

To address the drawbacks of the conventional methods in modeling of asphaltene precipitation and deposition, connectionist methods have been considered as powerful and reliable techniques in terms of time, cost, and accuracy. Zendehboudi et al. (2014) conducted static and dynamic experiments to study asphaltene precipitation through a systematic parametric sensitivity analysis [16]. Then, intelligent models including Artificial Neural Network (ANN) linked with evolutionary techniques such as Imperialist Competitive Algorithm (ICA) and Particle Swarm Optimization (PSO) were applied to simulate the process and study the effects of different parameters, including temperature, pressure, pressure drop, dilution ratio, and mixture composition on the asphaltene precipitation and deposition. It was found that ICA-ANN, PSO-ANN, and BP-ANN exhibit better performance in modeling of asphaltene precipitation and deposition, in comparison to the conventional deterministic strategies such as correlations. The research results revealed that that pressure and temperature are two key parameters in the static tests. However, pressure drop and temperature were the most important factors in asphaltene deposition in the dynamic experiments [16]. Alimohammadi et al. (2017) developed a comprehensive ANN model for prediction of asphaltene precipitation in three oil types; light, medium, and heavy crude samples [172]. They utilized an extensive data bank within a wide range of operational conditions, including pressure (100-5100 psia), dilution ratio (0.1-20 cm^3/g oil), solvents (n-pentane, n-hexane, and n-heptane), API of crudes (31, 23.8, and 12.8), and resin to asphaltene content (1.1428, 1.6037, and 3.632). Promising results based on their proposed ANN model were attained, compared to Flory-Huggins, modified Flory-Huggins, and scaling correlations [172]. Although the intelligent tools such as ANN and Bayesian Belief Network (BBN) are relatively fast and cost savers, they are black boxes that do not take into account the actual physics and thermodynamics of parameters and their interactions. Hence, no understandable relationships according to the properties of the components are provided. In another research work, Tahami et al. (2014) used the Winprop software and the computational simulator (GEM) to model the asphaltene precipitation and deposition during CO_2 flooding in the reservoir [173]. Employing the Winprop software and Peng-Robinson EOS, oil characterization was conducted. To obtain the Minimum Miscible Pressure (MMP), the IFT changes with pressure were modeled through using CMG. The asphaltene precipitation might be favourable for oil production due to a decrease in the oil viscosity and density, while at the same time it might be unfavourable for oil recovery as the asphaltene deposition impairs the permeability and porosity of the core [173]. Hence, it

is important to consider both scenarios/situations in oil reservoirs. In Saskatchewan reservoir that was studied by Tahami et al. (2014), the advantages and disadvantages of the asphaltene precipitation and deposition seem to negate each other [173]. Haghshenasfard and Hooman (2015) used the Computational Fluid Dynamics (CFD) to model asphaltene deposition, thermal resistance, and the heat transfer coefficient from oil flow under operational conditions [174]. A good agreement between the CFD model results and data/results available in the literature was noticed. In terms of operational conditions, a higher asphaltene deposition rate with the smoother tube indicates that higher roughness does not favour the deposition process. In addition, it was concluded that the higher oil velocity, the lower the asphaltene deposition, while a greater temperature and asphaltene concentration result in a higher asphaltene deposition rate [174]. A review of possible simulation software for investigation of asphaltene phase behaviors is provided in Table 8.

Table 2-8. Summary of asphaltene phase behavior modeling simulators

Simulation Tool	Description	Attributes	Advantages	Disadvantages
MD	• A computer simulation technique for prediction of the time evolution of interacting particles (atoms and molecules) of a system	• No assumption is made • May result in computational findings • Nano to micro scale of application	• Requires one input, which is interatomic/intermolecular interactions • Provides molecular-level information	• Very limited industrial applications • Lack of explicit velocity term

	Year	Type of simulator	Application	Remarks	ref
	2011	LAMMPS	Interactions of the asphaltene aggregations and different solvents at a constant temperature and pressure	• It was assumed that asphaltenes are surrounded by methane, ethane, and octane before CO_2 injection • After the CO_2 injection, the gas extracted light hydrocarbons from surrounding of asphaltenes • Application of an average of three model structures for asphaltene	[169]
	2011	Culgi	The thermodynamic properties of asphaltene and resin during oxidative ageing	• Fixed number of molecules and a constant pressure • Using asphaltene structure by Groenzin and Mullins model [175] • Two structures for resin were considered • Four input parameters to the input matrix, including a number of asphaltene or resin molecules, pressure, temperature, and oxygen atoms	[176]
	2013	Materials Studio	Sorption, diffusion, and distribution of asphaltene, resin, aromatic, and saturate fractions on the quartz surface	• Considering continental type model for the structure of asphaltene • The structure of asphaltenes included cores composed of stacked aromatic sheets and surrounded by aliphatic chains • The energy of each molecule was minimized by a smart minimizer approach	[177]

		Description	Attributes	Advantages	Disadvantages
2013	GROMACS	Gibbs free energy of associated and non-associated asphaltenes	• Application of an average of eight model structures for asphaltene • The effective interactions of molecules were calculated by umbrella sampling • 36 molecules of asphaltene were used to find how dimerization free energy impacts aggregation of asphaltene		[178]
2015	Materials Studio	Aggregation of asphaltene in water in oil emulsion	• Application of an average of two continental model structures for asphaltene • Toluene was considered to represent the oil • Physical properties (density and diffusion coefficients) of water, toluene, and asphaltene were calculated to validate the model force field		[179]
2017	GROMACS	Interactions of the asphaltene aggregations and various solvents at different temperatures and pressures	• Choosing ortho-xylene and water as solvents, while the former is the best solvent and the latter is the worst asphaltene solvent • Application of an average of three model structures for asphaltene		[170]
2017	GROMACS	Asphaltene aggregation in the presence of toluene and resin at ambient condition	• Application of an average of five model structures for asphaltene • The simulation was carried out at low density condition to reduce the probability of molecular overlap • Constant pressure (1 bar) and temperature (300 K)		[180]
2017	NA	Asphaltene aggregation	• Modeling with three types of asphaltene from different sources, including coal-derived, petroleum asphaltene, and source rock asphaltene • Application of island model structure for asphaltene		[76]
2018	Materials Studio	Interactions of the asphaltene aggregations and CO_2 under increasing pressure	• Application of an average of eight model structures for asphaltene • The less the radial distribution functions, the more stability in solution was taken into account		[171]
	Description	**Attributes**	**Advantages**	**Disadvantages**	

Intelligent model	• Intelligent models mimic the intelligent behaviors • The main objective of the intelligent model is to apply intelligence, for example, pattern recognition, machine translation, and computer vision to human tasks.		• A black box • Pattern recognition • Decision making	• Applicable to a wide variety of phenomena • Fast • Cost savers • Easy to use	• Not considering the physics of the phenomena • No understandable relationships on the basis of the properties of the components are provided
	Year	**Type of model**	**Application**	**Remarks**	**ref**
	2014	ICA-ANN, PSO-ANN, and BP-ANN	Asphaltene precipitation and deposition at various conditions of composition, pressure, injection rate, and temperature	• Input parameters to the precipitation model: temperature, pressure, solvent/oil ratio, concentration of injected gas, and molecular weight for precipitated asphaltene • Input parameters to the deposition model: temperature, pressure, solvent/oil ratio, concentration of injected gas, pressure drop, injection flow rate, and molecular weight for deposited asphaltene	[16]
	2015	SVR-SH	Asphaltene precipitation titration data (precipitation by adding solvent at different temperatures)	• Different solvents including nC_5, nC_6, nC_7, nC_8, nC_9, nC_{10}, and nC_{11} • Dilution ratio of 2.3-20.6 mL/g • Temperature of 293-323 K	[181]
	2017	ANN	Asphaltene precipitation at high pressures (precipitation by adding solvent at different pressures)	• Different solvents such as nC_5, nC_6, and nC_7 • Dilution ratio of 0.1-20 mL/g • Temperature of 293 K • Pressure in the range of 100-5100 psia	[172]
	Description	**Attributes**	**Advantages**	**Disadvantages**	
CMG	• A reservoir simulator for advanced recovery processes	• Optimization and analysis tool • Modeling of reservoir and production systems • Post and pre-process visualization and analysis	• A powerful sensitivity analysis, history matching, optimization, and uncertainty tool • Both research and industrial applications	• No direct measurements of phenomena	

	Year	Type of simulator	Application	Remarks			ref
			• Fluid characterization				
		Type of simulator	**Application**	**Remarks**			**ref**
	2014	Winprop	Asphaltene precipitation and deposition during CO_2 flooding	• Oil characterization by Peng-Robinson EOS • Minimum Miscible Pressure (MMP) through the IFT changes with pressure			[173]
	2016	STARS	Asphaltene precipitation occurrence during oil enhanced recovery through air injection	• Considering low temperature, high temperature, and negative temperature gradient region • Developing a mass transfer and kinetic model • Oxygen transfers to the oil in three steps, including from bulk to surface of bitumen, across the surface, and to the bulk of bitumen			[182]
CFD		**Description**	**Attributes**	**Advantages**		**Disadvantages**	
		• CFD represents application of numerical analysis and algorithms in fluid mechanics/dynamics to simulate flow behaviours • It is based on the Navier-Stokes equations and Newton's second law of motion	• Combines conservation of mass, momentum, and energy • Provides optimal model	• Investigation of flow characteristics that are not easy to measure • Making fast and easy changes to the geometry in the modeling work • Providing detailed information about the fluid flow		• Do not provide accurate results, but it offers good approximations • May face convergence error in every time step	
	Year	**Type of simulator**	**Application**	**Remarks**			**ref**
	2015	ANSYS FLUENT	Asphaltene deposition, thermal resistance, and the heat transfer coefficient for the oil flow case under operational conditions in the pipe	• Asphaltene deposition in a vertical pipe • Oil flow under forced convection • Effects of bulk and surface temperature, Reynolds number, asphaltene concentration, and surface roughness were investigated			[174]

	Year		High inertia asphaltene aggregates deposition in the pipe under turbulent flow regime	• Using Reynolds-Averaged Navier-Stokes equations for turbulence, isothermal, and incompressible flow • Considering six molecules of asphaltene per aggregate • Applying Lagrangian eddy lifetime model for asphaltene trajectory	[183]
	2017	NA			

		Description	Attributes	Advantages	Disadvantages
Eclipse		• ECLIPSE is an implicit, multi-phase, and multi dimentional oil simulator	• Animation over time of scalar properties (pressure and water saturation) • Robust and functionality in beneath	• Both research and industrial applications • Dynamic modeling • Handling fields with complexity • Parallel computing • Advanced gridding techniques	• No direct measurements of phenomena and corresponding parameters
	Year	Type of simulator	Application	Remarks	ref
	2011	Eclipse	Asphaltene deposition in porous media	• Comparing the results of the Eclipse with Deep Bed Filtration simulation model • A horizontal oil flow in the pipe was considered • The surface deposition parameter is dominant for short times • The entertainment rate coefficient and critical interstitial velocity are dominant for long-term	[184]
	2016	ECLIPSE 2009.1	Asphaltene deposition in porous media during miscible gas injection	• Viscosity was considered to be constant • The surface deposition and plugging rate coefficients were considered the desired parameters • The entertainment rate coefficient and critical interstitial velocity were set to match the experimental data	[185]

2-10. Inhibition and Treatment Methods for Asphaltene Deposition

The properties, structures, and behaviours of asphaltenes and various developed models to simulate asphaltene precipitation/deposition were reviewed earlier. However, there are still concerns about inhibition and treatment of asphaltene precipitation and deposition in the wellbore, production facilities, and transportation sections. Generally, two categories of techniques have been developed and applied to manage asphaltene deposition; namely, inhibition and treatment. The inhibition techniques include manipulation of oil production conditions/parameters and using chemical inhibitors. The treatment methods involve mechanical, thermal, chemical, biological, and external strategies. A list of various techniques in asphaltene management is given in Figure 26 [186-188].
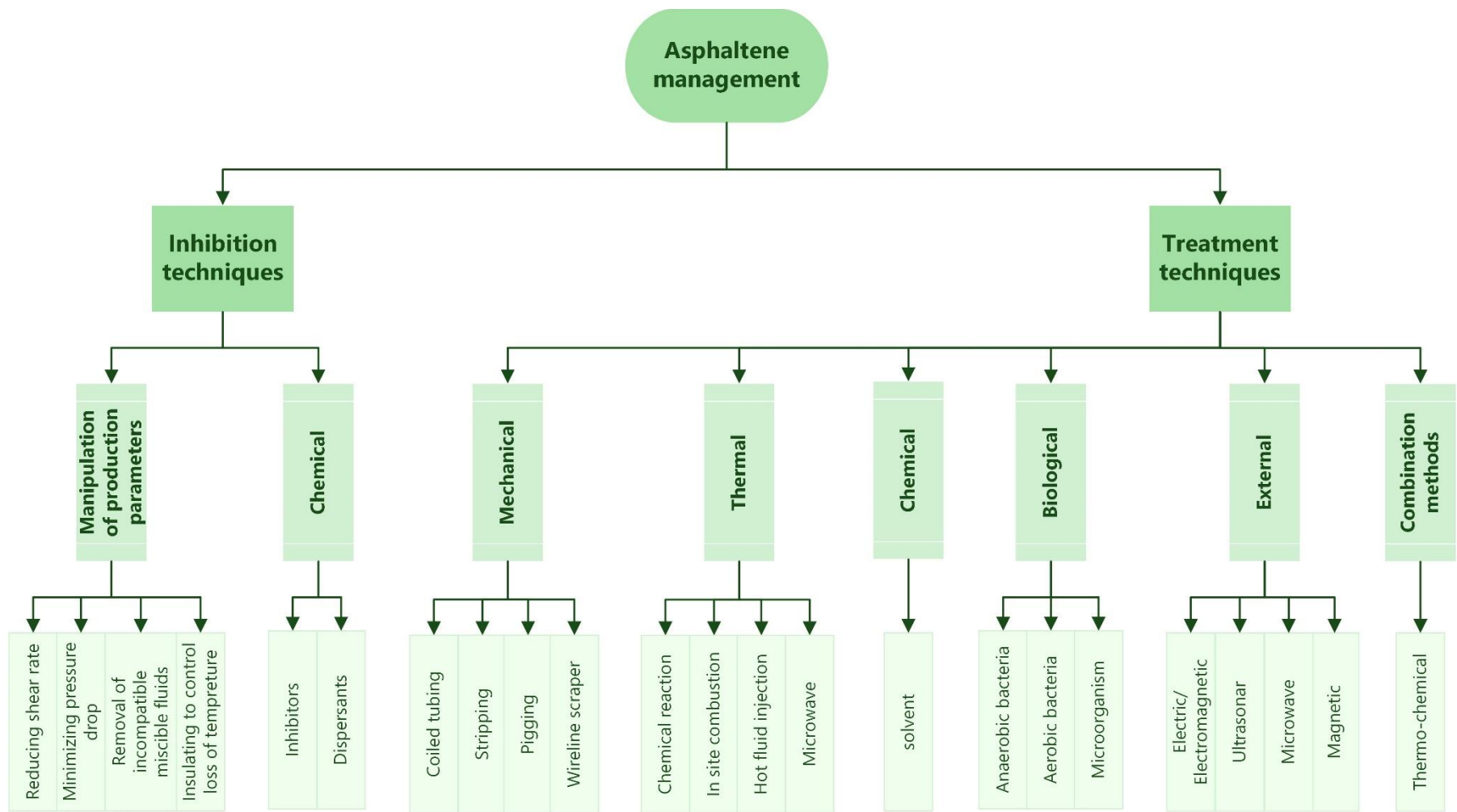
Figure 2-26. Overview of asphaltene management techniques

2-10-1. Inhibition Ways

Manipulation of Oil Production Parameters. One of the methods to inhibit asphaltene deposition is to control asphaltene deposition in oil production facilities by varying the production parameters. This method manages the deposition by reducing the shear rates, minimizing the pressure drop, removing the incompatible miscible fluids, and making insulation to control loss of heat [186, 189].

Chemical Methods. Two kinds of chemical additives can be used to prevent asphaltene deposition, including dispersants and inhibitors. The dispersants accelerate the break-up and dissolution of asphaltene flocculation and keep the asphaltene particles suspended in the oil [190]. The dispersants interact with the aggregated asphaltenes by changing the polarity of the outer layer of aggregates and making them more dispersible in the oil mixture [191]. Kraiwattanawong et al. (2009) studied the effectiveness of three asphaltene dispersants such as 4-dodecyl resorcinol (DR), 4-dodecyl phenol (DP), and 4-dodecyl benzene sulfonic acid (DBSA) in the deposition steps, phase separation, and particle growth [192]. It was observed that using the dispersants delays the onset point of precipitation, which is a result of making asphaltene aggregates stabilized or dispersed to the smaller size. They categorized the asphaltenes in oil solution into three types, including stable, colloidal, and flocculated asphaltenes. It was suggested that the chemical dispersant can stabilize the colloidal asphaltene and also decelerate the asphaltene flocculation [192].

Firoozinia et al. (2016) utilized an experimental method to evaluate the effect of different dispersants on the asphaltene deposition [193]. In their experimental investigation, four dispersants such as rapeseed oil amide (DR), nonylphenol-formaldehyde resin modified by polyamines (DP), polyisobutylene succinimide (DB), and polyisobutylene succinic ester (DF) were chosen. The onset of asphaltene precipitation was studied by employing various tools such as an optical microscope, a viscometer, and a Turbiscan. The influence of the dispersants on the onset pressure of asphaltene was investigated by an SDS setup and a filtration system. It was concluded that DR dispersant has the weakest performance among others, while the DP dispersant, based on nonylphenol-formaldehyde resin modified by polyamines, exhibits the greatest effectiveness to reduce the onset pressure from 4300 to 3600 psi [193].

Higaki et al. (2014) studied the adsorption behaviours, attachment, and detachment of asphaltene deposition on different polymer brushes [194]. The use of organic polymers to the substrate is a practical technique to modify physicochemical properties of the surface. The interface free energy

was used to characterize the efficiency of the polymer brushes. It was found that asphaltene deposition on PHMA and PMAPS brushes is detached when immersed in oil and water, respectively, due to low interface Gibbs free energy. They also concluded that these kinds of antifoulants can be regarded as the new strategy to inhibit asphaltene deposition in the petroleum industry [194].

The other chemicals in this area are inhibitors with the performance similar to natural resins. They encircle asphaltene particles as a peptizing agent to perform steric colloids. They are expected to have an appropriate solubility in the oil mixture to effectively interact with asphaltene and to hinder precipitation and deposition [190]. Mohammadi et al. (2011) [195] and Lu et al. (2016) [196] used nanoparticles to inhibit asphaltene precipitation. Mohammadi et al. (2011) demonstrated that TiO_2 nanoparticles can increase the stability of asphaltene in an acid medium [195]. The second research group also used Al_2O_3 nanoparticles during CO_2 injection and a good performance in hindering asphaltene precipitation was attained [196].

Ovalles et al. (2016) investigated the application of Nonylphenol Formaldehyde Resin (NPFR) as an asphaltene inhibitor. They suggested appropriate process conditions to improve the performance of NPFR. NPFR was used to prevent asphaltene precipitation in Vacuum Residue (VR) where petroleum samples were hydroprocessed through the filtration technique at different temperatures, room temperature (35 °C) to process temperature (195 °C). It was proved that the performance of the chemical depends on the oil sample and process/thermodynamic conditions such as temperature and properties of NPFR [191].

2-10-2. Treatment Ways

Mechanical Methods. One of the treatment ways to remove asphaltene deposition in production facilities is mechanical techniques including stripping, pigging, wireline scraper, and coiled tubing. These techniques have their own advantages and shortcomings. For instance, they are good cleaners and cause minimum formation damage; however, these techniques are expensive, time-consuming, and difficult to operate [197]. Pigging can be considered as the most popular method among the mechanical treatments as it is more suitable for foamy/waxy crudes. Pigging can be used to remove deposition from inside manifolds and pipelines in which the manifolds and pipelines can carry pigs. In terms of asphaltene removal, pigs with disks and cups are more

efficient. The efficiency and performance of pigging removal are dependent on its frequency which is needed to be optimized. Optimization of pigging frequency is conducted by learning the system behaviours [197, 198]. The process of pigging, either too fast or too slow, will lead to the trapping of the pigs and massive asphaltene deposition, respectively. Two types of pigs (e.g., soluble and insoluble) are used to remove asphaltene in arteries [197, 198]. Smart pigs are the new generation of pigs that can be used in remote visualization, control, and local heating. The other two techniques including wireline scraper and coiled tubing can also be used to remove asphaltene from the inner parts of the wellbore and pipelines, respectively. The limitation of the coiled tubing technique is that it cannot be utilized when there is a distance between the coiled tubing deployment point and deposition [198]. In general, mechanical treatments of asphaltene are expensive and difficult in terms of operation [186, 197, 198].

Thermal Methods. Thermal remediation of asphaltene consists of in situ combustions, fluid (steam and hot water/gas/oil) injection, exothermic chemical reactions (such as heat-liberating chemicals), and utilization of microwave. This category of treatment is highly efficient, and a quick response is expected. However, formation damage may occur, implying that a frequent treatment is needed [199]. Injection of hot fluid into the well is performed by circulating fluid to melt deposits. In this method, it is very important to prevent melted deposits from being re-deposited [197-199]. Zekri et al. (2001) applied the heating-liberation chemicals, which involve pumping an equimolar mixture of ammonium chloride, sodium nitrate, and a buffer [200]. The buffer delays the exothermic reaction until the fluid reaches the bottom-hole with a large quantity of nitrogen gas. However, the method is more expensive, compared to conventional thermal techniques [200]. The difference between the microwave treatment and the external force field technique is the location of heating. The thermal treatment applies the central heating [186].

Chemical Methods. The other technique to treat asphaltene deposition is the use of chemical solvents that are mostly aromatic solvents [186]. The solvent breaks asphaltene into the smaller bonds and dissolves bulk deposition. The hydrocarbon solvents (heptane, hexane, ethylbenzene, toluene, and xylenes), methanol, and paraffin have been examined in various research works [201]. In comparison with other solvents, xylene and toluene have been widely used to treat asphaltene deposition. Xylene is more effective due to its lower volatility [201]. Chemical treatments appear to be disadvantageous due to the environmental and personal safety (hazards concerns), and corrosion that may occur [201, 202].

Biological Methods. Utilization of anaerobic/aerobic bacteria or microorganisms such fungus is known as a biological technique for the deposition treatment. One of the biological treatment approaches is biodegradation, which converts asphaltene to lighter hydrocarbons. The process is very slow and can last from months to a year. The bacteria consume the deposited asphaltene to produce carbon, energy, and various components such as H_2O, CO_2, N_2O, and SO_2 [203, 204]. Biological techniques are advantageous because they are non-pathogenic, non-toxic, non-carcinogenic, non-flammable, non-combustible, and environmentally safe. However, they have some drawbacks, including difficulty to control the process, and corrosion or souring. Moreover, the biological methods can only be used in wells producing water [197, 200]. On the other hand, the risks associated with the biological treatment approaches need to be assessed. The risks of marine oil pollution and the impacts of cultivating microorganisms on the local ecological system should be considered [205].

External Methods. Techniques with external forces are employed to treat asphaltene precipitation/deposition, which involve an electrostatic/electrodynamic force field, ultrasound, microwave, and magnetic field. These methods are mostly applicable in small scales [186]. Using the ultrasound technique for asphaltene treatment, Kaushik et al. (2012) upgraded petroleum residue using an ultrasound assisted cavitation to reinforce asphaltene cracking at atmospheric condition [206]. They studied the effect of ultrasound on the composition (upgrading of petroleum residue) and physicochemical properties. It was revealed that the asphaltene content of the residue decreases from 13.5 wt% to 7 wt%. In addition, the viscosity of the residue reduced significantly, indicating that the sonication process can improve the oil upgradation [206]. Disaggregation state in the asphaltenic oil was examined by Jiang et al. (2014). For this purpose, the magnetic technology and Terahertz time-domain spectroscopy (THz-TDS) were used to change characteristics of the petroleum residue and to measure the physical characteristics, respectively [207]. Disaggregation of colloidal particles was proved under a magnetic field. The corresponding absorption coefficient and extinction coefficient are the characteristics of the disaggregation [207].

Combination Methods. Organic deposition removal can be performed by the integration of chemical and thermal treatments (thermo-chemical treatment). The technique melts and dislodges the deposits by heat released from an exothermic reaction. Because of dissolving and dispersing the organic deposits, (which represents an esterification reaction), a mixture of ester and surfactant

is produced. It is also possible to retard the reaction in the damaged reservoir region by using additives [208].

It is important to note that the treatment should be applied before a complete formation of the plug to have access to deposits. If the treatment is accomplished after the formation of deposits, its performance would be limited to the diffusion [209, 210]. The treatment technique has some steps: first, preflushing by an organic chemical solvent to soak the deposits; second, postflushing to generate heat and using a mixture of solvents (including ester and surfactant) to dissolve the organic deposits; and third, production step to remove dissolved and dispersed deposits. Usually, chemical compatibility tests are conducted to avoid formation of emulsions and precipitates during the treatment [209, 210].

2-11. Economic Analysis of Asphaltene Precipitation/Deposition

The steadily increasing demand for energy consumption is projected to double by 2030. In contrast with recent advances in renewable energy resources, fossil fuels still stand for the main source of energy with 80% of the world energy consumption. As almost 50% of all fossil fuels is from oil and gas, its production is becoming more pivotal now and then [211].

The first offshore well was established by Kerr-McGee (1947) in the Gulf of Mexico. Later, in 1970 the concept of subsea field development was introduced [212]. Flow assurance includes maintaining sustainable hydrocarbon production from the reservoir to reception facilities for both onshore and offshore cases. Managing the hydrocarbon flow and preventing the formation of slug or blockage (solids formation, such as waxes, asphaltenes, hydrates, and scales) are the key aspects in terms of flow assurance in the oil and gas energy. Its workflow consists of sampling, lab analysis, and modeling to recognize the system, and also to propose prevention or remediation strategies, optimization, monitoring, and control. Therefore, the flow assurance paradigm currently is shifting from avoidance to the risk management [8, 213-215]. Generally, most projects include two costs, namely capital expenditures (CAPEX) and operating expenditures (OPEX). The first category refers to investment to the project, including initial design, engineering, construction, and installation. While the second category includes the expenses of operation, such as labour, materials, utilities, and other related expenses. It is important to note that flow assurance cost is managed through operating cost (OPEX). In terms of project management and engineering cost, the cost of flow assurance for the subsea field is estimated to be USD 25,000 per month [212].

Organic deposition, especially asphaltenes, is a serious concern with the undeniable impacts on the economy of oil recovery [216]. Asphaltene deposition in wellbore or production facilities reduces the flow of crude which means a reduction of revenue due to remediation. Asphaltene removal can cost differently from $0.5 MM the U.S. for coiled tubing on land to $3 MM the U.S. for shallow water. If the loss of production is considered, asphaltene deposition may cause production loss for $1.2 MM/day [214, 215].

A case study of the reservoir with asphaltene deposition issue was reported in a well of Comalcalco, Mexico [217]. A quick decline in the oil production was reported over six months due to unstable asphaltenic oil. The production of the well decreased from 2,291 BOPD (Barrels of Oil per Day) to 1,483 BOPD (~%35 decline), which is equal to a reduction of revenue for $12,120 per day (considering the price of oil $15 per barrel). A batch treatment of the dispersant and solvent with a cost of $50,000 was applied to mitigate the deposition effect [217].

Asphaltene deposition in the wellbore and near wellbore area cost billions of dollars/year, which includes production reduction, wells shut-in, low production capacity, and implication of the management techniques [218]. For instance, the cost of a well shut-in for ring interventions is approximately $70 million/well for an oil field of the Gulf of Mexico [219]. This amount can increase to $100 million/well if asphaltene deposits in the surface controlled subsurface safety valve. Downtime losses can reach $500,000/day on the basis of 10,000 bbl/day and oil price of $50/bbl [220]. Moreover, asphaltene management costs, including inhibition, treatment, and clean-up are added to the expenses of the economic impacts of asphaltene deposition. The chemical injection to the Gulf of Mexico costs $330,000-$390,000/well per year (on the basis of 10,000 bbl/year). The injection of chemical additives to an oil field in the Middle East is about $31,000-$46,000/well per year [220]. Asphaltene deposition periodic clean-up in severe deposition may require 3 or 4 operations per year, which costs $200,000/operation [221].

Cenegy (2001) reviewed a Venezuelan well that experienced severe asphaltene deposition and a remedy for seven weeks was applied to treat deposition. The process cost was $50,000 with two days shut-in. The production of the well increased to 60,882 bbl that was $1,339,404 of additional revenue at $22/bbl. However, the cost of chemical treatment was reported to be $39,144, which was much lower than additional revenue [222].

2-12. Theoretical and Practical Challenges in Asphaltene Precipitation/Deposition

The phase behaviors and modeling of asphaltene precipitation and deposition comprise reservoir fluid management techniques such as flow assurance and risk assessment. Due to the worldwide dispersion of reservoirs with asphaltene related issues, it is pivotal to know challenges related to asphaltene precipitation and deposition, both theoretical and practical [216].

As explained earlier, several models are reported for the PVT and equilibrium behaviours of asphaltene precipitation. For example, the reversible Liquid-Liquid Equilibrium (LLE) is built on the basis of the solubility model. By contrast, the colloidal model considers asphaltene in the form of a solid component and proposes an equation that relates the solid fugacity to the liquid fugacity of pure asphaltene. Other approaches such as EOSs assume different natures/characters for the asphaltene precipitation (in term of reversibility and phase equilibrium), which lead to controversial thermodynamic behaviours for asphaltene. Hence, the uncertainties about the reversibility or irreversibility of asphaltene precipitation and also the type of precipitation equilibrium (e.g., liquid-liquid and solid-liquid) are considered as the challenges while modeling asphaltene phase equilibrium [20, 25-29, 80-86].

Molecular weight and structure of asphaltene particles are still unsolved matters in this area. The polydispersity of asphaltene makes it hard to determine a specific molecular weight for asphaltene particles. In addition, many researchers have focused on the structure of asphaltene and different architectures have been suggested for asphaltenes [10, 12, 53, 69, 75]. For instance, it was concluded from some studies that asphaltene contains one Polycyclic Aromatic Hydrocarbon (PAH) that is known as the island structure, while others considered multiple PAHs for the asphaltene (called archipelago structure). Obtaining adequate understanding about the molecular weight and structure of asphaltene in the oil mixture appears to be vital to effectively manage the asphaltene issues [10, 12, 53, 69, 75].

Another major challenge in asphaltene studies is attributed to modeling of deposition in porous media and capillaries. The available deposition models have serious drawbacks, which result in oversimplification and non-realistic physics of phenomenon. For instance, the effect of the kinetics of precipitation/ deposition is not considered on the asphaltene impairment. Moreover, the growth of asphaltene particles when passing through a porous medium or capillaries is not taken into account in most of the research studies [49, 50, 108, 109, 111].

Asphaltene related issues occur worldwide, and some regions of Alberta, west Texas and Alaska in the US, southern region of Mexico, and the North Sea, particularly the Norwegian sector, are affected by asphaltenic crudes. Moreover, fields in Venezuela, the Adriatic Sea, the Persian Gulf, and the US Gulf of Mexico have faced serious asphaltene related problems [36, 222]. Hence, asphaltene management techniques are vital to the economy of the oil production. However, asphaltene management techniques, inhibition and treatment have some theoretical and practical drawbacks and finding the best management strategies for an oil field with the asphaltene deposition issue is highly challenging [223].

Using a chemical in either inhibition or treatment techniques, environmental safety, and personal exposure hazards concerns need to be considered [224]. Utilizing a mechanical treatment, there are also some concerns. For instance, mechanical treatment is expensive and only applicable to the production facilities [200]. The application of thermal treatment is also challenging, due to the possibility of formation damage [200]. In addition, the biological methods have some drawbacks such as difficulty of the process control, corrosion or souring, restriction to wells producing water, and environmental impacts [197, 200, 205].

2-13. Conclusions

Asphaltene is linked with numerous flow assurance issues from the production to the destination. Precipitation/deposition has some deleterious effects such as an increase in the viscosity of crudes, stabilization of emulsions, decreasing the distillate yields, and causing unstable phase separation. Therefore, it has been a complicated subject for many researchers and engineers to find various aspects of asphaltene precipitation and deposition. The objective of this review is to delineate the state of asphaltene with respect to precipitation and deposition. Experimental and theoretical investigations have revealed that asphaltene precipitation/deposition is influenced by several parameters/variables, including pressure, temperature, characteristics of the mixture, properties and amount of precipitant, and properties of the porous medium/rock. Although extensive investigations on the experimental and theoretical aspects of precipitation/deposition have been carried out, an updated and systematic review on asphaltene precipitation/deposition seems to be pivotal. In this review paper, the theories and mechanisms of precipitation/deposition, experimental and modeling approaches, the influences of operational/fluid/reservoir parameters, and treatment/inhibition techniques are effectively studied and reviewed. Moreover, the economic

analysis of flow assurance focusing on asphaltene deposition and the most common theoretical and practical challenges in asphaltene precipitation/deposition are discussed. The following key conclusions are drawn based on this review:

- Although several attempts have been made to appropriately understand the molecular weight and structure of asphaltene, its complex nature has not been completely discovered. Within the past decade, many diverse studies had converged on a simple and hierarchical model (Yen-Mullins model) for the molecular weight and structure of asphaltene. Recently, Schuler et al. (2015) developed an exclusive method to provide the first direct measurement of the molecular structure of asphaltenes by the atomic resolution imaging using atomic force microscopy and molecular orbital imaging via scanning tunnelling microscopy. Their observation endorsed the "Yen-Mullins" model in terms of molecular weight of asphaltene. It was revealed that the dominant structures of asphaltene are "Island and Aryl-linked core" structure and the molecular weight of petroleum asphaltene was determined 750 g/mole [12].

- Based on the literature, it was concluded that solubility models are promising, compared to the colloidal approach. In particular, CPA and PC-SAFT EOS in the solubility approach seems to be more accurate due to considering the polarity and association of asphaltene particles. However, the model performance is dependent on the fluid characterization technique and optimization technique.

- Small angle X-ray and neutron scattering were found to be appropriate methods to detect the asphaltene destabilization. The experimental investigation of asphaltene deposition can be conducted in the capillary flow and the Taylor–Couette (TC) cells. Both techniques have some advantages and disadvantages; however, choosing the best experimental technique certainly depends on the purpose of the investigation. For instance, isothermal experiments cannot be conducted in capillaries or TC cells that require a high volume of oil to demonstrate deposition.

- The most popular asphaltene impairment model was proposed by Wang [49], followed by Wang and Civan [50] that considers three deposition mechanisms; namely, surface deposition, entrainment, and plugging of the pore throat. Although the proposed model has exhibited acceptable accuracy, it has serious shortcomings, which lead to oversimplification and non-realistic physics of the phenomenon. The effect of the kinetics

of precipitation and deposition was not considered on the asphaltene impairment. Moreover, the growth of asphaltene particles when passing through a porous medium was not taken into account.

- It was found that increasing pressure and temperature lowers the precipitation. In contrary, the rate of deposition increases at higher pressures and temperatures. Asphaltene deposition is increased by adding a higher amount of a precipitant (particularly heavy precipitants). The higher flow rate of oil, the faster the initial deposition of asphaltene occurs. Gas injection, especially CO_2, leads to more precipitation and deposition.

- Considering the impact of precipitant and fluid properties on asphaltene deposition, it was revealed that more quantity of a precipitant with a higher carbon number causes a thicker layer of deposition. Lighter oil samples with a lower viscosity and crudes with a lower resin content generally experience greater asphaltene precipitation/deposition.

- In general, rocks with higher porosity and lower permeability are more prone to asphaltene deposition and impairment. A higher iron content in the core was reported to be in favour of maintaining the permeability of the core, while a high calcium content was believed to lower the permeability due to asphaltene deposition.

- Two types of techniques are applied to manage asphaltene deposition, including inhibition and treatment. The inhibition techniques include manipulation of oil production parameters/conditions and utilization of chemical inhibitors. The treatment ways involve mechanical, thermal, chemical, biological, and external treatments. It is important to note that the treatment should be applied before a complete formation of the plug in order to have access to deposits.

ACKNOWLEDGEMENTS

NOMENCLATURES

Acronyms

ADEPT	asphaltene deposition tool
APE	asphaltene precipitation envelope
API	American petroleum institute
ASIST	asphaltene instability trend
ASM	asphaltene solubility model
Asp	asphaltene
BP-ANN	backpropagation artificial neural network
BOPD	barrel of oil per day
CAPEX	capital expenditures
CCD	charge-coupled device
CFD	computational fluid dynamics
CMC	critical micelle concentration
CMG	computer modeling group
CPA	cubic plus association
Da	g/mole
DB	polyisobutylene succinimide
DBSA	4-dodecyl benzene sulfonic acid
DF	polyisobutylene succinic ester
DP	4-dodecyl phenol
DR	4-dodecyl resorcinol
EDS	energy dispersive spectroscopy
EoS	equations of state
FID	flame ionization detection
GROMACS	groningen machine for chemical simulations

HPHT	high-pressure and high-temperature
HPLC	high pressure liquid chromatography
ICA	imperialist competitive algorithm
IFT	interfacial tension
LLE	liquid-liquid equilibrium
MD	molecular dynamic
MMP	minimum miscible pressure
NN	neural network
NPFR	nonylphenol formaldehyde resin
OPEX	operating cost
OPLS	optimized potentials for liquid simulations
OSDC	organic solid deposition and control
PAH	poly-aromatic hydrocarbon
PC-SAFT	perturbed-chain statistical associating fluid theory
PHMA	hydrophobic poly (n-hexyl methacrylate)
PMAPS	zwitterionic poly(3-(N-2-methacryloyloxyethylN,N-dimethyl) ammonatopropanesulfonate
PSO	particle swarm optimization
RDF	radial distribution function
SAFT	statistical associating fluid theory
SAFT-HS	statistical associating fluid theory-hard sphere
SAFT-VR	statistical associating fluid theory-variable range
SARA	saturate, aromatic, resin, and asphaltene
SEM	scanning electron microscopy
SPE	simple point charge
SRD	stochastic rotation dynamics
STM	scanning tunnelling microscope
SRK	Soave–Redlich–Kwong
TC	Taylor Couette

THz-TDS	terahertz time-domain spectroscopy
TLC	thin layer chromatography
TLC-FID	thin layer chromatography with flame ionization detection
VLE	vapour-liquid equilibrium
VR	vacuum residue

Variables/Parameters

A	Helmholtz free energy
a	constant of the PR/SRK EoS
b	constant of the PR/SRK EoS
$C_1(0)$	initial concentration of asphaltene nanoparticles
C_k	the concentration of the species/ volume fraction
D	dimension/ diameter
E	volume fraction
e	instantaneous average asphaltene deposition layer hydrodynamic thickness
F	free energy
f_p	permeability modification constant
G	Gibbs free energy
K	collision kernel
k	Initial permeability
L	liquid
$\bar{m}_N$	the function of the number of average molecular weight
n	number of moles
O	oil phase
P	pressure
Pe	Peclet number
PT	pressure-temperature
R	geometric scaling factor/gas constant
r	effective radius

Re	Reynolds
T	temperature
t	time
U	repulsion barrier/internal energy
V	vapour
w	mass fraction
x	horizontal direction

Greek Letters

α	empirical surface deposition rates
β	entrainment rate
γ	plugging deposition rate/ shear rate
Δ	change or difference
δ	solubility
η	capture efficiency
μ	viscosity / a constant parameter
ρ	liquid density
σ	deposition under the snowball effect
υ	liquid velocity/ molar volume
ϕ	porosity
$\underline{\Phi}$	volume fraction

Subscripts and Superscripts

AL	dissolved asphaltene in the liquid phase
asph	asphaltene
assoc	associate
chain	molecule chain
cr,L	critical interstitial property of the liquid phase
E	excess
i	Initial condition

ideal	ideal solution
max	maximum
mono	monomers
pt	pore throat
ptcr	critical property of the pore throat
SAL	suspended asphaltene in the liquid phase
t	condition at time

REFERENCES

1. ExxonMobil, *2018 Outlook for Energy: A View to 2040.* Tech. rep. ExxonMobil Central Europeaing Holding GmbH., 2018.
2. Civan, F., *Reservoir formation damage*. 2015: Gulf Professional Publishing.
3. Olayiwola, S.O. and M. Dejam, *A comprehensive review on interaction of nanoparticles with low salinity water and surfactant for enhanced oil recovery in sandstone and carbonate reservoirs.* Fuel, 2019. **241**: p. 1045-1057.
4. Olayiwola, S.O. and M. Dejam, *Mathematical modelling of surface tension of nanoparticles in electrolyte solutions.* Chemical Engineering Science, 2019. **197**: p. 345-356.
5. Saboorian-Jooybari, H., M. Dejam, and Z. Chen, *Heavy oil polymer flooding from laboratory core floods to pilot tests and field applications: Half-century studies.* Journal of Petroleum Science and Engineering, 2016. **142**: p. 85-100.
6. Mashayekhizadeh, V., S. Kord, and M. Dejam, *EOR potential within Iran.* Special Topics & Reviews in Porous Media: An International Journal, 2014. **5**(4).
7. Gudmundsson, J.S., *Flow assurance solids in oil and gas production*. 2017: CRC Press.
8. Ratulowski, J., et al. *Flow Assurance and subsea Productivity: closing the Loop with Connectivity and Measurements*. in *SPE Annual Technical Conference and Exhibition*. 2004. Society of Petroleum Engineers.
9. Speight, J.G., *The chemical and physical structure of petroleum: effects on recovery operations.* Journal of Petroleum Science and Engineering, 1999. **22**(1): p. 3-15.
10. Mullins, O.C., *The asphaltenes.* Annual Review of Analytical Chemistry, 2011. **4**: p. 393-418.
11. Speight, J.G., *The chemistry and technology of petroleum*. 2014: CRC press.
12. Schuler, B., et al., *Unraveling the molecular structures of asphaltenes by atomic force microscopy.* Journal of the American Chemical Society, 2015. **137**(31): p. 9870-9876.
13. Sayyad Amin, J., S. Alimohammadi, and S. Zendehboudi, *Systematic investigation of asphaltene precipitation by experimental and reliable deterministic tools.* The Canadian Journal of Chemical Engineering, 2017. **95**(7): p. 1388-1398.
14. Agger, C.S. and H. Sørensen, *Algorithm for Constructing Complete Asphaltene PT and Px Phase Diagrams.* Industrial & Engineering Chemistry Research, 2017.

15. Zendehboudi, S., et al., *Thermodynamic investigation of asphaltene precipitation during primary oil production: laboratory and smart technique.* Industrial & Engineering Chemistry Research, 2013. **52**(17): p. 6009-6031.

16. Zendehboudi, S., et al., *Asphaltene precipitation and deposition in oil reservoirs– Technical aspects, experimental and hybrid neural network predictive tools.* Chemical Engineering Research and Design, 2014. **92**(5): p. 857-875.

17. Leontaritis, K., J. Amaefule, and R. Charles, *A systematic approach for the prevention and treatment of formation damage caused by asphaltene deposition.* SPE Production & Facilities, 1994. **9**(03): p. 157-164.

18. Seifried, C.M., J. Crawshaw, and E.S. Boek, *Kinetics of asphaltene aggregation in crude oil studied by confocal laser-scanning microscopy.* Energy & Fuels, 2013. **27**(4): p. 1865-1872.

19. Powers, D., et al., *Regular solution based approach to modeling asphaltene precipitation from native and reacted oils: Part 1, molecular weight, density, and solubility parameter distributions of asphaltenes.* Fuel, 2016. **178**: p. 218-233.

20. Subramanian, S., S. Simon, and J. Sjöblom, *Asphaltene precipitation models: a review.* Journal of Dispersion Science and Technology, 2016. **37**(7): p. 1027-1049.

21. Akbarzadeh, K., et al., *A generalized regular solution model for asphaltene precipitation from n-alkane diluted heavy oils and bitumens.* Fluid Phase Equilibria, 2005. **232**(1-2): p. 159-170.

22. Forte, E. and S.E. Taylor, *Thermodynamic modelling of asphaltene precipitation and related phenomena.* Advances in colloid and interface science, 2015. **217**: p. 1-12.

23. Nikooyeh, K. and J.M. Shaw, *On the applicability of the regular solution theory to asphaltene+ diluent mixtures.* Energy & Fuels, 2012. **26**(1): p. 576-585.

24. Manshad, A.K., et al., *The association thermodynamics modeling of asphaltene precipitation.* Petroleum Science and Technology, 2014. **32**(1): p. 51-60.

25. Li, Z. and A. Firoozabadi, *Cubic-plus-association equation of state for water-containing mixtures: Is "cross association" necessary?* AIChE journal, 2009. **55**(7): p. 1803-1813.

26. Kontogeorgis, G.M., et al., *An equation of state for associating fluids.* Industrial & engineering chemistry research, 1996. **35**(11): p. 4310-4318.

27. Chapman, W.G., et al., *SAFT: Equation-of-state solution model for associating fluids.* Fluid Phase Equilibria, 1989. **52**: p. 31-38.

28. Sheu, E.Y. and O.C. Mullins, *Fundamentals and Applications.* 1995: Springer.

29. Mousavi-Dehghani, S., et al., *An analysis of methods for determination of onsets of asphaltene phase separations.* Journal of Petroleum Science and Engineering, 2004. **42**(2-4): p. 145-156.

30. Chaisoontornyotin, W., et al., *Combined asphaltene aggregation and deposition investigation.* Energy & Fuels, 2016. **30**(3): p. 1979-1986.

31. Maqbool, T., A.T. Balgoa, and H.S. Fogler, *Revisiting asphaltene precipitation from crude oils: A case of neglected kinetic effects.* Energy & Fuels, 2009. **23**(7): p. 3681-3686.

32. Haji-Akbari, N., et al., *A unified model for aggregation of asphaltenes.* Energy & Fuels, 2013. **27**(5): p. 2497-2505.

33. Fávero, C.V.B., et al., *Revisiting the flocculation kinetics of destabilized asphaltenes.* Advances in colloid and interface science, 2017. **244**: p. 267-280.

34.   Guzmán, R., et al., *Methods for determining asphaltene stability in crude oils.* Fuel, 2017. **188**: p. 530-543.

35.   Ghahfarokhi, A.K., et al., *Characterization of asphaltene deposition process in flow loop apparatus; An experimental investigation and modeling approach.* Journal of Petroleum Science and Engineering, 2017. **151**: p. 330-340.

36.   Mohammadzadeh, O., et al. *Experimental Investigation of Asphaltene Induced Formation Damage due to Pressure Depletion of Live Reservoir Fluids in Porous Media*. in *SPE Annual Technical Conference and Exhibition*. 2017. Society of Petroleum Engineers.

37.   Chen, L., et al., *Applicability of simple asphaltene thermodynamics for asphaltene gradients in oilfield reservoirs: The Flory-Huggins-Zuo Equation of State with the Yen-Mullins model.* Fuel, 2018. **221**: p. 216-232.

38.   Davudov, D. and R.G. Moghanloo, *A new model for permeability impairment due to asphaltene deposition.* Fuel, 2019. **235**: p. 239-248.

39.   Rogel, E., et al., *Asphaltene characterization of paraffinic crude oils.* Fuel, 2016. **178**: p. 71-76.

40.   Zanganeh, P., H. Dashti, and S. Ayatollahi, *Comparing the effects of CH 4, CO 2, and N 2 injection on asphaltene precipitation and deposition at reservoir condition: A visual and modeling study.* Fuel, 2018. **217**: p. 633-641.

41.   Prausnitz, J.M., R.N. Lichtenthaler, and E.G. de Azevedo, *Molecular thermodynamics of fluid-phase equilibria*. 1998: Pearson Education.

42.   Kontogeorgis, G.M. and G.K. Folas, *Thermodynamic models for industrial applications: from classical and advanced mixing rules to association theories*. 2009: John Wiley & Sons.

43.   Shirani, B., M. Nikazar, and S.A. Mousavi-Dehghani, *Prediction of asphaltene phase behavior in live oil with CPA equation of state.* Fuel, 2012. **97**: p. 89-96.

44.   Nasrabadi, H., J. Moortgat, and A. Firoozabadi, *New three-phase multicomponent compositional model for asphaltene precipitation during CO2 injection using CPA-EOS.* Energy & Fuels, 2016. **30**(4): p. 3306-3319.

45.   David Ting, P., G.J. Hirasaki, and W.G. Chapman, *Modeling of asphaltene phase behavior with the SAFT equation of state.* Petroleum Science and Technology, 2003. **21**(3-4): p. 647-661.

46.   Panuganti, S.R., et al., *PC-SAFT characterization of crude oils and modeling of asphaltene phase behavior.* Fuel, 2012. **93**: p. 658-669.

47.   Punnapala, S. and F.M. Vargas, *Revisiting the PC-SAFT characterization procedure for an improved asphaltene precipitation prediction.* Fuel, 2013. **108**: p. 417-429.

48.   Mohebbinia, S., et al., *Simulation of asphaltene precipitation during gas injection using PC-SAFT EOS.* Journal of Petroleum Science and Engineering, 2017. **158**: p. 693-706.

49.   Wang, S., *Simulation of asphaltene deposition in petroleum reservoirs during primary oil recovery*. 2000.

50.   Wang, S. and F. Civan, *Modeling formation damage by asphaltene deposition during primary oil recovery.* Journal of energy resources technology, 2005. **127**(4): p. 310-317.

51.   Vazquez, D. and G. Mansoori, *Identification and measurement of petroleum precipitates.* Journal of Petroleum Science and Engineering, 2000. **26**(1-4): p. 49-55.

52.   Mansoori, G.A., D. Vazquez, and M. Shariaty-Niassar, *Polydispersity of heavy organics in crude oils and their role in oil well fouling.* Journal of Petroleum Science and Engineering, 2007. **58**(3): p. 375-390.

53. Mullins, O.C., *The modified Yen model.* Energy & Fuels, 2010. **24**(4): p. 2179-2207.

54. Prakoso, A.A., A.D. Punase, and B. Hascakir, *A Mechanistic Understanding of Asphaltenes Precipitation From Varying-Saturate-Concentration Perspectives.* SPE Production & Operations, 2017. **32**(01): p. 86-98.

55. Bissada, K.A., et al., *Group-type characterization of crude oil and bitumen. Part I: Enhanced separation and quantification of saturates, aromatics, resins and asphaltenes (SARA).* Organic geochemistry, 2016. **95**: p. 21-28.

56. Fan, T. and J.S. Buckley, *Rapid and accurate SARA analysis of medium gravity crude oils.* Energy & Fuels, 2002. **16**(6): p. 1571-1575.

57. Fan, T., J. Wang, and J.S. Buckley. *Evaluating crude oils by SARA analysis.* in *SPE/DOE Improved Oil Recovery Symposium.* 2002. Society of Petroleum Engineers.

58. Leontaritis, K.J. *PARA-based (paraffin-aromatic-resin-asphaltene) reservoir oil characterizations.* in *International Symposium on Oilfield Chemistry.* 1997. Society of Petroleum Engineers.

59. Akmaz, S., et al., *The structural characterization of saturate, aromatic, resin, and asphaltene fractions of batiraman crude oil.* Petroleum Science and Technology, 2011. **29**(2): p. 160-171.

60. Yen, T.F. and G.V. Chilingarian, *Asphaltenes and asphalts, 2.* 2000: Elsevier.

61. Speight, J.G., *Chemical and physical studies of petroleum asphaltenes*, in *Developments in petroleum science.* 1994, Elsevier. p. 7-65.

62. Wu, J., J.M. Prausnitz, and A. Firoozabadi, *Molecular thermodynamics of asphaltene precipitation in reservoir fluids.* AIChE journal, 2000. **46**(1): p. 197-209.

63. Frigerio, F. and D. Molinari, *A multiscale approach to the simulation of asphaltenes.* Computational and Theoretical Chemistry, 2011. **975**(1-3): p. 76-82.

64. Koots, J.A. and J.G. Speight, *Relation of petroleum resins to asphaltenes.* Fuel, 1975. **54**(3): p. 179-184.

65. Waldo, G.S., et al., *Determination of the chemical environment of sulphur in petroleum asphaltenes by X-ray absorption spectroscopy.* Fuel, 1992. **71**(1): p. 53-57.

66. Orr, W.L., *Kerogen/asphaltene/sulfur relationships in sulfur-rich Monterey oils.* Organic geochemistry, 1986. **10**(1-3): p. 499-516.

67. Gaweł, B., M. Eftekhardadkhah, and G. Øye, *Elemental composition and Fourier transform infrared spectroscopy analysis of crude oils and their fractions.* Energy & Fuels, 2014. **28**(2): p. 997-1003.

68. Rogel, E., M. Moir, and M. Witt, *Atmospheric pressure photoionization and laser desorption ionization coupled to fourier transform ion cyclotron resonance mass spectrometry to characterize asphaltene solubility fractions: studying the link between molecular composition and physical behavior.* Energy & Fuels, 2015. **29**(7): p. 4201-4209.

69. Mullins, O.C., et al., *Advances in asphaltene science and the Yen–Mullins model.* Energy & Fuels, 2012. **26**(7): p. 3986-4003.

70. Mullins, O.C. and E.Y. Sheu, *Structures and dynamics of asphaltenes.* 2013: Springer Science & Business Media.

71. McKenna, A.M., et al., *Heavy petroleum composition. 3. Asphaltene aggregation.* Energy & fuels, 2013. **27**(3): p. 1246-1256.

72. Hemmati-Sarapardeh, A., et al., *Toward mechanistic understanding of asphaltene aggregation behavior in toluene: The roles of asphaltene structure, aging time,*

temperature, and ultrasonic radiation. Journal of Molecular Liquids, 2018. **264**: p. 410-424.

73. Chacón-Patiño, M.L., S.M. Rowland, and R.P. Rodgers, *Advances in asphaltene petroleomics. part 1: asphaltenes are composed of abundant island and archipelago structural motifs.* Energy & Fuels, 2017. **31**(12): p. 13509-13518.

74. Chacón-Patiño, M.L., S.M. Rowland, and R.P. Rodgers, *Advances in Asphaltene Petroleomics. Part 2: Selective Separation Method That Reveals Fractions Enriched in Island and Archipelago Structural Motifs by Mass Spectrometry.* Energy & Fuels, 2017. **32**(1): p. 314-328.

75. Hoepfner, M.P., *Investigations into Asphaltene Deposition, Stability, and Structure.* 2013.

76. Wang, W., et al., *Nanoaggregates of Diverse Asphaltenes by Mass Spectrometry and Molecular Dynamics.* Energy & Fuels, 2017. **31**(9): p. 9140-9151.

77. Mullins, O.C., et al. *The Critical Role of Asphaltene Gradients and Data Integration in Reservoir Fluid Geodynamics Analysis.* in *SPE Annual Technical Conference and Exhibition.* 2017. Society of Petroleum Engineers.

78. Mansoori, G.A., *Modeling of asphaltene and other heavy organic depositions.* Journal of petroleum science and engineering, 1997. **17**(1-2): p. 101-111.

79. Zhang, R., et al., *Nucleation and growth of nanoparticles in the atmosphere.* Chemical Reviews, 2011. **112**(3): p. 1957-2011.

80. Andersen, S.I. and J.G. Speight, *Thermodynamic models for asphaltene solubility and precipitation.* Journal of Petroleum Science and Engineering, 1999. **22**(1-3): p. 53-66.

81. Painter, P.C. and M.M. Coleman, *Fundamentals of polymer science: an introductory text.* 1994: Technomic.

82. Hildebrand, J.H. and R.L. Scott, *Regular solutions.* 1962: Prentice-Hall.

83. Huggins, M.L., *Solutions of long chain compounds.* The Journal of chemical physics, 1941. **9**(5): p. 440-440.

84. Flory, P.J., *Thermodynamics of high polymer solutions.* The Journal of chemical physics, 1942. **10**(1): p. 51-61.

85. Scott, R.L. and M. Magat, *The Thermodynamics of High-Polymer Solutions: I. The Free Energy of Mixing of Solvents and Polymers of Heterogeneous Distribution.* The Journal of Chemical Physics, 1945. **13**(5): p. 172-177.

86. Zuo, J.Y., et al., *Advances in the Flory–Huggins–Zuo equation of state for asphaltene gradients and formation evaluation.* Energy & Fuels, 2012. **27**(4): p. 1722-1735.

87. Scatchard, G., *Equilibria in Non-electrolyte Solutions in Relation to the Vapor Pressures and Densities of the Components.* Chemical Reviews, 1931. **8**(2): p. 321-333.

88. De Boer, R., et al., *Screening of crude oils for asphalt precipitation: theory, practice, and the selection of inhibitors.* SPE Production & Facilities, 1995. **10**(01): p. 55-61.

89. Escobedo, J. and G. Mansoori, *Theory of viscosity as a criterion for detection of onset of asphaltene flocculation.* 1994, Society of Petroleum Engineers, Richardson, TX (United States).

90. Maqbool, T., P. Srikiratiwong, and H.S. Fogler, *Effect of temperature on the precipitation kinetics of asphaltenes.* Energy & Fuels, 2011. **25**(2): p. 694-700.

91. Hoepfner, M.P., et al., *The fractal aggregation of asphaltenes.* Langmuir, 2013. **29**(28): p. 8799-8808.

92. Tavakkoli, M., et al., *Indirect method: a novel technique for experimental determination of asphaltene precipitation.* Energy & Fuels, 2015. **29**(5): p. 2890-2900.

93. Broseta, D., et al. *Detection of asphaltene deposition by capillary flow measurements*. in *SPE/DOE Improved Oil Recovery Symposium*. 2000. Society of Petroleum Engineers.

94. Wang, J., J.S. Buckley, and J.L. Creek, *Asphaltene deposition on metallic surfaces.* Journal of dispersion science and technology, 2004. **25**(3): p. 287-298.

95. Boek, E.S., et al., *Deposition of colloidal asphaltene in capillary flow: experiments and mesoscopic simulation.* Energy & fuels, 2008. **22**(2): p. 805-813.

96. Boek, E.S., et al., *Multi-scale simulation and experimental studies of asphaltene aggregation and deposition in capillary flow.* Energy & fuels, 2009. **24**(4): p. 2361-2368.

97. Montesi, A., et al. *Asphaltene Management in GOM DW Subsea Development*. in *Offshore Technology Conference*. 2011. Offshore Technology Conference.

98. Zougari, M., et al., *Novel organic solids deposition and control device for live-oils: design and applications.* Energy & Fuels, 2006. **20**(4): p. 1656-1663.

99. Akbarzadeh, K., et al., *Asphaltene deposition measurement and modeling for flow assurance of tubings and flow lines.* Energy & fuels, 2011. **26**(1): p. 495-510.

100. Ali, M. and M. Islam, *The effect of asphaltene precipitation on carbonate-rock permeability: an experimental and numerical approach.* SPE production & facilities, 1998. **13**(03): p. 178-183.

101. Srivastava, R., S. Huang, and M. Dong, *Asphaltene deposition during CO2 flooding.* SPE production & facilities, 1999. **14**(04): p. 235-245.

102. Shedid, S.A. and E.A.A. Abbas. *An Experimental Approach of the Reversibility of Asphaltene Deposition under Dynamic Flow Conditions*. in *SPE Middle East Oil and Gas Show and Conference*. 2005. Society of Petroleum Engineers.

103. Papadimitriou, N., et al., *Experimental investigation of asphaltene deposition mechanism during oil flow in core samples.* Journal of petroleum science and engineering, 2007. **57**(3-4): p. 281-293.

104. Eskin, D., et al., *Modelling asphaltene deposition in turbulent pipeline flows.* The Canadian Journal of Chemical Engineering, 2011. **89**(3): p. 421-441.

105. Zhuang, Y., et al., *Three dimensional measurements of asphaltene deposition in a transparent micro-channel.* Journal of Petroleum Science and Engineering, 2016. **145**: p. 77-82.

106. Gruesbeck, C. and R. Collins, *Entrainment and deposition of fine particles in porous media.* Society of Petroleum Engineers Journal, 1982. **22**(06): p. 847-856.

107. Danesh, A., et al., *Pore-level visual investigation of miscible and immiscible displacements.* Journal of Petroleum Science and Engineering, 1989. **2**(2-3): p. 167-177.

108. Eskin, D., et al., *Asphaltene deposition in a Taylor-Couette device and a pipe: Theoretically achievable critical deposition regimes.* The Canadian Journal of Chemical Engineering, 2016. **94**(7): p. 1308-1312.

109. Soulgani, B.S., et al., *Modeling formation damage due to asphaltene deposition in the porous media.* Energy & Fuels, 2011. **25**(2): p. 753-761.

110. Kord, S., et al., *Further investigation into the mechanisms of asphaltene deposition and permeability impairment in porous media using a modified analytical model.* Fuel, 2014. **117**: p. 259-268.

111. Kariznovi, M., et al., *Experimental, modelling and optimisation of asphaltene deposition and adsorption in porous media*. The Canadian Journal of Chemical Engineering, 2012. **90**(5): p. 1356-1368.

112. Hematfar, V., et al., *Optimization Assisted Asphaltene Deposition Modeling in Porous Media During a Natural Depletion Scheme.* Petroleum Science and Technology, 2012. **30**(9): p. 958-965.

113. Shaojun, W., F. Civan, and A.R. Strycker. *Simulation of paraffin and asphaltene deposition in porous media*. in *SPE international symposium on oilfield chemistry*. 1999. Society of Petroleum Engineers.

114. Chang, F. and F. Civan, *Practical model for chemically induced formation damage.* Journal of Petroleum Science and Engineering, 1997. **17**(1-2): p. 123-137.

115. Hematfar, V., M.H. Ghazanfari, and M.B. Bagheri. *Modeling and optimization of asphaltene deposition in porous media using genetic algorithm technique*. in *International Oil and Gas Conference and Exhibition in China*. 2010. Society of Petroleum Engineers.

116. Rezaian, A., et al., *Modeling formation damage due to flocculated asphaltene deposition.* Petroleum Science and Technology, 2012. **30**(5): p. 478-488.

117. Rezaian, A., et al. *Modeling formation damage due to flocculated asphaltene deposition through dynamic displacement*. in *International Oil and Gas Conference and Exhibition in China*. 2010. Society of Petroleum Engineers.

118. Ramirez-Jaramillo, E., C. Lira-Galeana, and O. Manero, *Modeling asphaltene deposition in production pipelines.* Energy & fuels, 2006. **20**(3): p. 1184-1196.

119. Nabzar, L. and M. Aguiléra, *The colloidal approach. A promising route for asphaltene deposition modelling.* Oil & Gas Science and Technology-Revue de l'IFP, 2008. **63**(1): p. 21-35.

120. Leontaritis, K.J., *Asphaltene near-well-bore formation damage modeling.* Journal of energy resources technology, 2005. **127**(3): p. 191-200.

121. Almehaideb, R.A., *Asphaltene precipitation and deposition in the near wellbore region: a modeling approach.* Journal of Petroleum Science and Engineering, 2004. **42**(2-4): p. 157-170.

122. Jamialahmadi, M., et al., *Measurement and prediction of the rate of deposition of flocculated asphaltene particles from oil.* International Journal of Heat and Mass Transfer, 2009. **52**(19-20): p. 4624-4634.

123. Bott, T.R., *Fouling of heat exchangers*. 1995: Elsevier.

124. Cleaver, J. and B. Yates, *The effect of re-entrainment on particle deposition.* Chemical Engineering Science, 1976. **31**(2): p. 147-151.

125. Hashmi, S., M. Loewenberg, and A. Firoozabadi, *Colloidal asphaltene deposition in laminar pipe flow: Flow rate and parametric effects.* Physics of Fluids, 2015. **27**(8): p. 083302.

126. Vilas Bôas Fávero, C., et al., *Mechanistic investigation of asphaltene deposition.* Energy & Fuels, 2016. **30**(11): p. 8915-8921.

127. Mukherjee, H. and J. Brill, *Pressure drop correlations for inclined two-phase flow.* Journal of energy resources technology, 1985. **107**(4): p. 549-554.

128. Kor, P. and R. Kharrat, *Prediction of the asphaltene deposition profile along a wellbore during natural production from a reservoir.* Energy Sources, Part A: Recovery, Utilization, and Environmental Effects, 2016. **38**(19): p. 2837-2844.

129. Guan, Q., et al. *Integrated one-dimensional modeling of asphaltene deposition in wellbores/pipelines.* in *Modeling, Simulation, and Applied Optimization (ICMSAO), 2017 7th International Conference on.* 2017. IEEE.

130. Guan, Q., et al., *A unidirectional one-dimensional approach for asphaltene deposition in large length-to-diameter ratios scenarios.* Journal of Petroleum Science and Engineering, 2018. **166**: p. 857-870.

131. Davudov, D., R.G. Moghanloo, and J. Flom, *Scaling Analysis and Its Implication for Asphaltene Deposition in a Wellbore.* SPE Journal, 2018. **23**(02): p. 274-285.

132. Salimi, F., S. Ayatollahi, and M.V. Seftie, *Prediction of asphaltene deposition during turbulent flow using heat transfer approach.* Petroleum Science and Technology, 2018. **36**(9-10): p. 632-639.

133. Andersen, S.I. and K.S. Birdi, *Influence of temperature and solvent on the precipitation of asphaltenes.* Petroleum Science and Technology, 1990. **8**(6): p. 593-615.

134. Andersen, S.I., *Effect of precipitation temperature on the composition of n-heptane asphaltenes.* Fuel science & technology international, 1994. **12**(1): p. 51-74.

135. Hu, Y.-F. and T.-M. Guo, *Effect of temperature and molecular weight of n-alkane precipitants on asphaltene precipitation.* Fluid Phase Equilibria, 2001. **192**(1-2): p. 13-25.

136. Mohammadi, S., et al., *On the effect of temperature on precipitation and aggregation of asphaltenes in light live oils.* The Canadian Journal of Chemical Engineering, 2016. **94**(9): p. 1820-1829.

137. Leontaritis, K.J., *The asphaltene and wax deposition envelopes.* Fuel Science and Technology International, 1996. **14**(1-2): p. 13-39.

138. Tavakkoli, M., et al., *Asphaltene deposition in different depositing environments: Part 2. Real oil.* Energy & Fuels, 2014. **28**(6): p. 3594-3603.

139. Burke, N.E., R.E. Hobbs, and S.F. Kashou, *Measurement and Modeling of Asphaltene Precipitation (includes associated paper 23831).* Journal of Petroleum Technology, 1990. **42**(11): p. 1,440-1,446.

140. Zanganeh, P., et al., *Asphaltene deposition during CO2 injection and pressure depletion: A visual study.* Energy & Fuels, 2012. **26**(2): p. 1412-1419.

141. Hu, Y.-F., et al., *Measurement and corresponding states modeling of asphaltene precipitation in Jilin reservoir oils.* Journal of Petroleum Science and Engineering, 2004. **41**(1-3): p. 169-182.

142. Verdier, S., et al., *Study of pressure and temperature effects on asphaltene stability in presence of CO2.* Energy & fuels, 2006. **20**(4): p. 1584-1590.

143. Hoepfner, M.P., et al., *A fundamental study of asphaltene deposition.* Energy & Fuels, 2013. **27**(2): p. 725-735.

144. Soorghali, F., A. Zolghadr, and S. Ayatollahi, *Effect of resins on asphaltene deposition and the changes of surface properties at different pressures: a microstructure study.* Energy & Fuels, 2014. **28**(4): p. 2415-2421.

145. Kurup, A.S., et al., *Development and application of an asphaltene deposition tool (ADEPT) for well bores.* Energy & fuels, 2011. **25**(10): p. 4506-4516.

146. Salimi, F., M.V. Seftie, and S. Ayatollahia, *Experimental investigation of the effects of different parameters on the rate of asphaltene deposition in laminar flow and its prediction using heat transfer approach.* Journal of Dispersion Science and Technology, 2013. **34**(12): p. 1690-1696.

147. Mousavi Dehghani, S.A., Vafaei, S.M., Mirzaei, B., Fasih, M., *Experimental investigation on asphaltene deposition in porous media during miscible gas injection.* Iranian Journal of Chemistry and Chemical Engineering (IJCCE), 2007. **26**(4): p. 39-48.

148. Lawal, K.A., Crawshaw, J.P., Boek, E.S., Vesovic, V., *Experimental investigation of asphaltene deposition in capillary flow.* Energy & Fuels, 2012. **26**(4): p. 2145-2153.

149. Pan, H. and A. Firoozabadi. *Thermodynamic micellization model for asphaltene precipitation from reservoir crudes at high pressures and temperatures.* in *SPE Annual Technical Conference and Exhibition.* 1997. Society of Petroleum Engineers.

150. Rogel, E., Leon, O., Espidel, Y., Gonzalez, Y., *Asphaltene stability in crude oils.* SPE Production & Facilities, 2001. **16**(02): p. 84-88.

151. Soorghali, F., A. Zolghadr, and S. Ayatollahi, *Effects of native and non-native resins on asphaltene deposition and the change of surface topography at different pressures: An experimental investigation.* Energy & Fuels, 2015. **29**(9): p. 5487-5494.

152. Hirschberg, A., deJong, L.N.J., Schipper, B.A., Meijir, J.G., *Influence of temperature and pressure on asphaltene flocculation.* Society of Petroleum Engineers Journal, 1984. **24**(03): p. 283-293.

153. Mukhametshina, A., T. Kar, and B. Hascakir, *Asphaltene precipitation during bitumen extraction with expanding-solvent steam-assisted gravity drainage: effects on pore-scale displacement.* SPE Journal, 2016. **21**(02): p. 380-392.

154. Demir, A.B., I.H. Bilgesu, and B. Hascakir. *The Effect of Brine Concentration on Asphaltene Stability.* in *SPE Annual Technical Conference and Exhibition.* 2016. Society of Petroleum Engineers.

155. Kar, T., et al., *The effect of clay type on steam-assisted-gravity-drainage performance.* Journal of Canadian Petroleum Technology, 2015. **54**(06): p. 412-423.

156. Fritschy, G. and E. Papirer, *Interactions between a bitumen, its components and model fillers.* Fuel, 1978. **57**(11): p. 701-704.

157. Collins, S. and J. Melrose. *Adsorption of asphaltenes and water on reservoir rock minerals.* in *SPE Oilfield and Geothermal Chemistry Symposium.* 1983. Society of Petroleum Engineers.

158. Curtis, C.W., Y.W. Jeon, and D.J. Clapp, *Adsorption of asphalt functionalities and oxidized asphalts on aggregate surfaces.* Fuel science & technology international, 1989. **7**(9): p. 1225-1268.

159. Saraji, S., L. Goual, and M. Piri, *Adsorption of asphaltenes in porous media under flow conditions.* Energy & Fuels, 2010. **24**(11): p. 6009-6017.

160. Kokal, S., et al., *Electrokinetic and adsorption properties of asphaltenes.* Colloids and Surfaces A: Physicochemical and Engineering Aspects, 1995. **94**(2-3): p. 253-265.

161. Punase, A., et al. *Inorganic Content of Asphaltenes Impacts Asphaltenes Stability.* in *SPE Latin America and Caribbean Petroleum Engineering Conference.* 2017. Society of Petroleum Engineers.

162. Jafari Behbahani, T., et al., *Asphaltene deposition under dynamic conditions in porous media: theoretical and experimental investigation.* Energy & Fuels, 2013. **27**(2): p. 622-639.

163. Behbahani, T.J., et al., *Experimental study and mathematical modeling of asphaltene deposition mechanism in core samples.* Oil & Gas Science and Technology–Revue d'IFP Energies nouvelles, 2015. **70**(6): p. 1051-1074.

164. Kord, S., et al., *Asphaltene deposition in carbonate rocks: experimental investigation and numerical simulation.* Energy & Fuels, 2012. **26**(10): p. 6186-6199.

165. Bolouri, S.H. and E. Ghoodjani, *Permeability impairment study due to asphaltene deposition: experimental and modeling approach.* Transport in porous media, 2012. **91**(3): p. 999-1012.

166. Bolouri, H., et al., *An Experimental and Modeling Study of Asphaltene Deposition Due to CO2 Miscible Injection.* Petroleum Science and Technology, 2013. **31**(2): p. 129-141.

167. Mirzabozorg, A., et al. *Simulation Study of Permeability Impairment Due to Asphaltene Deposition in one of the Iranian Oil Fractured Reservoirs.* in *Canadian International Petroleum Conference.* 2009. Petroleum Society of Canada.

168. Solaimany-Nazar, A.R. and A. Zonnouri, *Modeling of asphaltene deposition in oil reservoirs during primary oil recovery.* Journal of Petroleum Science and Engineering, 2011. **75**(3-4): p. 251-259.

169. Hu, M., et al., *Molecular dynamics simulation of asphaltene deposition during CO2 miscible flooding.* Petroleum Science and Technology, 2011. **29**(12): p. 1274-1284.

170. Yaseen, S. and G.A. Mansoori, *Molecular dynamics studies of interaction between asphaltenes and solvents.* Journal of Petroleum Science and Engineering, 2017. **156**: p. 118-124.

171. Fang, T., et al., *Study on the Asphaltene Precipitation in CO2 Flooding: A Perspective from Molecular Dynamics Simulation.* Industrial & Engineering Chemistry Research, 2018. **57**(3): p. 1071-1077.

172. Alimohammadi, S., J.S. Amin, and E. Nikooee, *Estimation of asphaltene precipitation in light, medium and heavy oils: experimental study and neural network modeling.* Neural Computing and Applications, 2017. **28**(4): p. 679-694.

173. Tahami, S., et al., *Modeling of asphaltene deposition during miscible CO2 flooding.* Petroleum Science and Technology, 2014. **32**(18): p. 2183-2194.

174. Haghshenasfard, M. and K. Hooman, *CFD modeling of asphaltene deposition rate from crude oil.* Journal of Petroleum Science and Engineering, 2015. **128**: p. 24-32.

175. Groenzin, H. and O.C. Mullins, *Molecular size and structure of asphaltenes from various sources.* Energy & Fuels, 2000. **14**(3): p. 677-684.

176. Tarefder, R.A. and I. Arisa, *Molecular dynamic simulations for determining change in thermodynamic properties of asphaltene and resin because of aging.* Energy & Fuels, 2011. **25**(5): p. 2211-2222.

177. Wu, G., L. He, and D. Chen, *Sorption and distribution of asphaltene, resin, aromatic and saturate fractions of heavy crude oil on quartz surface: molecular dynamic simulation.* Chemosphere, 2013. **92**(11): p. 1465-1471.

178. Sedghi, M., et al., *Effect of asphaltene structure on association and aggregation using molecular dynamics.* The Journal of Physical Chemistry B, 2013. **117**(18): p. 5765-5776.

179. Liu, J., Y. Zhao, and S. Ren, *Molecular dynamics simulation of self-aggregation of asphaltenes at an oil/water interface: formation and destruction of the asphaltene protective film.* Energy & Fuels, 2015. **29**(2): p. 1233-1242.

180. Headen, T., et al., *Simulation of asphaltene aggregation through molecular dynamics: Insights and limitations.* Energy & Fuels, 2017. **31**(2): p. 1108-1125.

181. Fattahi, H., et al., *Estimation of asphaltene precipitation from titration data: a hybrid support vector regression with harmony search.* Neural Computing and Applications, 2015. **26**(4): p. 789-798.

182. Bhattacharya, S., et al., *Investigation of Thermal Fingerprint in Accelerating-Rate Calorimetry for Air-Injection Enhanced-Oil-Recovery Processes.* SPE Journal, 2017. **22**(02): p. 548-561.

183. Seyyedbagheri, H. and B. Mirzayi, *CFD modeling of high inertia asphaltene aggregates deposition in 3D turbulent oil production wells.* Journal of Petroleum Science and Engineering, 2017. **150**: p. 257-264.

184. Boek, E.S., et al. *Prediction of asphaltene deposition in porous media by systematic upscaling from a colloidal pore scale model to a deep bed filtration model.* in *SPE Annual Technical Conference and Exhibition*. 2011. Society of Petroleum Engineers.

185. Raz, A., et al., *Prediction of asphaltene deposition parameters in porous media using experimental data during miscible gas injection.* Energy Sources, Part A: Recovery, Utilization, and Environmental Effects, 2016. **38**(11): p. 1620-1627.

186. Mansoori, G.A., *Remediation of asphaltene and other heavy organic deposits in oil wells and in pipelines.* Socar proceedings, 2010. **2010**(4): p. 12-23.

187. Gharbi, K., K. Benyounes, and M. Khodja, *Removal and prevention of asphaltene deposition during oil production: A literature review.* Journal of Petroleum Science and Engineering, 2017. **158**: p. 351-360.

188. Hu, G., J. Li, and G. Zeng, *Recent development in the treatment of oily sludge from petroleum industry: a review.* Journal of hazardous materials, 2013. **261**: p. 470-490.

189. Kokal, S.L. and S.G. Sayegh. *Asphaltenes: The cholesterol of petroleum.* in *Middle East Oil Show*. 1995. Society of Petroleum Engineers.

190. Kelland, M.A., *Production chemicals for the oil and gas industry*. 2014: CRC press.

191. Ovalles, C., et al., *The use of nonylphenol formaldehyde resins for preventing asphaltene precipitation in vacuum residues and hydroprocessed petroleum samples.* Petroleum Science and Technology, 2016. **34**(4): p. 379-385.

192. Kraiwattanawong, K., et al., *Effect of asphaltene dispersants on aggregate size distribution and growth.* Energy & Fuels, 2009. **23**(3): p. 1575-1582.

193. Firoozinia, H., K.F.H. Abad, and A. Varamesh, *A comprehensive experimental evaluation of asphaltene dispersants for injection under reservoir conditions.* Petroleum Science, 2016. **13**(2): p. 280-291.

194. Higaki, Y., et al., *Adsorption and desorption behavior of asphaltene on polymer-brush-immobilized surfaces.* ACS applied materials & interfaces, 2014. **6**(22): p. 20385-20389.

195. Mohammadi, M., et al., *Inhibition of asphaltene precipitation by TiO2, SiO2, and ZrO2 nanofluids.* Energy & Fuels, 2011. **25**(7): p. 3150-3156.

196. Lu, T., et al., *Nanoparticles for inhibition of asphaltenes deposition during CO2 flooding.* Industrial & Engineering Chemistry Research, 2016. **55**(23): p. 6723-6733.

197. Al-Yaari, M. *Paraffin wax deposition: Mitigation and removal techniques.* in *SPE Saudi Arabia section Young Professionals Technical Symposium*. 2011. Society of Petroleum Engineers.

198. Guo, B., S. Song, and A. Ghalambor, *Offshore pipelines: design, installation, and maintenance*. 2013: Gulf Professional Publishing.

199. Bernadiner, M. *Advanced asphaltene and paraffin control technology.* in *SPE International Symposium on Oilfield Chemistry*. 1993. Society of Petroleum Engineers.

200. Zekri, A.Y., S.A. Shedid, and H. Alkashef. *A novel technique for treating asphaltene deposition using laser technology.* in *SPE Permian Basin Oil and Gas Recovery Conference*. 2001. Society of Petroleum Engineers.

201.	Miadonye, A. and L. Evans, *The solubility of asphaltenes in different hydrocarbon liquids.* Petroleum Science and Technology, 2010. **28**(14): p. 1407-1414.

202.	Shedid, S.A., *An ultrasonic irradiation technique for treatment of asphaltene deposition.* Journal of petroleum science and engineering, 2004. **42**(1): p. 57-70.

203.	Niu, Z.-X., et al., *Bio-degradation of resin and asphalt in viscous-oil contaminated soil by actonomyces.* Journal of agro-environment science, 2005. **24**(4): p. 771-774.

204.	YANG, X.-l., et al., *Isolation of Petroleum-degrading Strains and Their Degrading Characteristics [J].* Journal of Agro-Environment Science, 2008. **1**: p. 044.

205.	Xue, J., et al., *Marine oil-degrading microorganisms and biodegradation process of petroleum hydrocarbon in marine environments: a review.* Current microbiology, 2015. **71**(2): p. 220-228.

206.	Kaushik, P., et al., *Ultrasound cavitation technique for up-gradation of vacuum residue.* Fuel processing technology, 2012. **93**(1): p. 73-77.

207.	Jiang, C., et al., *Probing disaggregation of crude oil in a magnetic field with terahertz time-domain spectroscopy.* Energy & Fuels, 2014. **28**(1): p. 483-487.

208.	Alian, S.S., et al. *Organic Deposition: From Detection and Laboratory Analysis to Treatment and Removal.* in *SPE Asia Pacific Oil and Gas Conference and Exhibition.* 2013. Society of Petroleum Engineers.

209.	Civan, F. *Optimal Scheduling of Well Treatment in Commingled Formations Undergoing a Near Wellbore Damage.* in *European Formation Damage Conference.* 2007. Society of Petroleum Engineers.

210.	Al-Ibadi, A. and F. Civan. *Experimental Investigation and Correlation of Thermal Effects on Near-Wellbore Formation Treatment by Gel Particles.* in *SPE International Symposium on Oilfield Chemistry.* 2013. Society of Petroleum Engineers.

211.	EIA, *ANNUAL ENERGY OUTLOOK.* U.S. Energy Information Administration, 2018.

212.	Bai, Y. and Q. Bai, *Subsea engineering handbook.* 2012: Gulf Professional Publishing.

213.	Hammami, A., et al., *Asphaltene precipitation from live oils: An experimental investigation of onset conditions and reversibility.* Energy & Fuels, 2000. **14**(1): p. 14-18.

214.	Creek, J.L., *Freedom of action in the state of asphaltenes: Escape from conventional wisdom.* Energy & fuels, 2005. **19**(4): p. 1212-1224.

215.	Creek, J.L., J. Wang, and J.S. Buckley, *Verification of asphaltene-instability-trend (ASIST) predictions for low-molecular-weight alkanes.* SPE Production & Operations, 2009. **24**(02): p. 360-368.

216.	Leontaritis, K.J., *Challenges and solutions to asphaltene and wax deposition.* Offshore Int., September, 1998. **58**(9): p. 122,124-125,184.

217.	Newberry, M.E. and K. Barker. *Organic formation damage control and remediation.* in *SPE International Symposium on Formation Damage Control.* 2000. Society of Petroleum Engineers.

218.	Atta, A.M. and A.M. Elsaeed, *Use of rosin-based nonionic surfactants as petroleum crude oil sludge dispersants.* Journal of Applied Polymer Science, 2011. **122**(1): p. 183-192.

219.	Gonzalez, F.A., *Personal Communication. Asphaltene deposition economic impact.* Reservoir performance global community of practice Lead BP, 2015.

220.	Vargas, F.M. and M. Tavakkoli, *Asphaltene Deposition: Fundamentals, Prediction, Prevention, and Remediation.* 2018: CRC Press.

221.	Naumov, P. and J. Whelan, *Inhibition of asphaltene.* 2017, Google Patents.

222. Cenegy, L.M. *Survey of successful world-wide asphaltene inhibitor treatments in oil production fields*. in *SPE Annual Technical Conference and Exhibition*. 2001. Society of Petroleum Engineers.
223. Ovalles, C., et al., *Synthesis, characterization, and mechanism of asphaltene inhibition of phosphopropoxylated asphaltenes.* Fuel, 2016. **180**: p. 20-26.
224. Samuelson, M. *Alternatives to aromatics for solvency of organic deposits*. in *SPE Formation Damage Control Symposium*. 1992. Society of Petroleum Engineers.

Chapter 3 : Improved Thermodynamic CPA Modeling of Asphaltene Precipitation

(A Global Optimization Approach for Parameter Estimation of CPA EoS in Asphaltene Modeling; Studying the Temperature, Solvent, and Binary Interactions, (Published)

Preface

A modified version of this manuscript has been published in the Energy Fuels 2022, 36, 21, 13124–13147. I am the primary author of this paper. Along with the co-author, Lesley James, I carried out the literature review, data collection, and discussions on experimental and modeling studies on asphaltene precipitation/deposition process. I prepared the first draft of the manuscript and subsequently revised the manuscript based on the co-authors' feedback as well as the comments received from the peer review process. The co-author, Lesley James, thoroughly reviewed and revised the manuscript, commented on various parts of the manuscript, considerably contributed to entirely correcting the text in terms of technical and editorial aspects, and assisted in reviewing and revising the manuscript.

Abstract

Equation of state (EoS) modeling of complex molecular chain asphaltenes suffers from uncertainty about adjusting the parameters and intermolecular forces. Better accounting of the association of hydrogen bonding and the impact of van der Waals forces could significantly improve our EoS models compared to traditional methods. Our approach is to improve the procedure to estimate parameters (e.g., binary interaction parameters and association energy) and simplify the characterization approach to improve EoS models. In this study, Cubic-Plus-Association (CPA) EoS was employed to calculate asphaltene precipitation yield and onset at different conditions, including temperature, adding n-alkane (nC_5-nC_{12}), and different mixture compositions. A global optimization framework was implemented to estimate the global best fit of the adjustable parameters and skip the local minima. These parameters are the physical and association constants of the CPA EoS and the binary parameters. The oil was treated by the characterization method from Flory-Huggins EoS to simplify the CPA EoS. Besides, new correlations were also developed to calculate the binary parameters and association used in this work. Comparison between the results obtained from the globally optimized CPA EoS and experimental data exhibit acceptable agreement (average deviation of less than 0.067 for correlation and prediction). The relative importance analysis was performed using Pearson's correlation coefficient method to show the importance of the operational conditions studied here on asphaltene precipitation and binary interaction parameters. The analysis revealed that the composition of the mixture (dilution ratio) is the most influential factor contributing to the asphaltene precipitation. Besides, binary interaction parameters are most affected by the carbon number of the n-alkane followed by the temperature. The simplified and accurate CPA EoS can be used by other researchers to increase the efficiency of asphaltene thermodynamic modeling, e.g., industrial application.

Keywords: Asphaltene precipitation, Cubic Plus Association (CPA) EoS, Global Optimization, Systematic Sensitivity Analysis, Data Analysis

3-1. Introduction

Asphaltene precipitation and deposition can cause operational problems in reservoirs, near well region, wells, tie-backs, upstream and downstream processing facilities [1, 2]. Therefore, it is important to understand the asphaltene precipitation and deposition to avoid flow assurance issues during crude oil processing [3]. One of the main challenges of using EoS is the optimization of the adjustable parameters, e.g., BIPs. The EoSs are highly nonlinear and gradient-based optimization methods, e.g., Nelder-Mead (NM) simplex and Least Squares methods, are not capable of performing this complex optimization. Using the gradient-based optimization method has a high chance of getting stuck in local optima and not being able to tune the adjustable parameters best. Therefore, a Global Optimization algorithm was suggested and used to tune the EoS. Moreover, to increase the extrapolation capability of the EoS, the correlations were developed for adjustable parameters, i.e., BIPs and cross-association parameters. Besides, the importance of the operational conditions studied here was determined by relative importance analysis (RI) using Pearson's correlation coefficient method.

Crude oil can be portioned into four solubility classes of multi-component fractions by the SARA analysis, including (saturates, aromatics, resins, and asphaltenes) [4-6]. Saturates and aromatics are nonpolar hydrocarbons (including normal alkanes) and hydrocarbons consisting of cycloalkanes and alkyl chains, respectively [7, 8]. In comparison, asphaltenes and resins are heterogeneous compounds contributing to the polar component of the oil. Asphaltene is not defined based on a specific structure but as the heaviest and most polar fraction of crude oils [9, 10]. It is defined as the solubility class, which is soluble in light aromatics, benzene, toluene, and pyridine, and insoluble in paraffin, typically pentane, hexane, and heptane. From the colloidal point of view, asphaltene particles are suspended in oil by resins. The maltane fraction (saturate, aromatic, resin) cross-associates with asphaltene particles and acts as a peptizing agent for the solubility of asphaltene in oil mixture [11].

A typical asphaltene sample comprises C, H, N, O, and S, with small amounts of iron, vanadium, and nickel [12]. Recently, some findings regarding asphaltene structure can be incorporated into the Yen-Mullins model, which answers typical questions regarding asphaltene structure, nano aggregates, and clusters [13]. A representative asphaltene molecule is composed of a Poly-Aromatic Hydrocarbon (PAH) core that arose from time-resolved fluorescence depletion measurements [4]. The solubility of asphaltene may be altered and result in the precipitation of

asphaltene out of the oil mixture by the influence of some parameters/variables, including pressure, temperature, and composition (adding alkane or gas injection). Alteration of asphaltene solubility and its precipitation/deposition is unfavourable for flow assurance. Therefore, in this work, we are trying to propose a model to investigate the phenomena over a wide range of flow conditions. Unlike most solute-solvent systems, asphaltene shows three stages of solubility. While it is soluble at low concentrations, the higher concentrations of asphaltene will form nano aggregates and asphaltene clusters. At yet higher concentrations, the bulk phase separations will happen. Asphaltene nano-aggregates are composed of six asphaltene molecules formed by a single disordered stack in the interior and peripheral alkyls in the exterior. However, clusters of unstable heavy oils can comprise up to eight nano-aggregates [4, 14, 15].

Due to the importance of investigating asphaltene precipitation/deposition phenomena, having comprehensive knowledge about different aspects of the issue is required. However, conducting experimental investigations has limitations, including the high resource demand and expenses. Besides, we need to predict fluid phase behaviour over the full range of operating conditions to avoid flow assurance issues. Therefore, applying asphaltene modeling approaches is essential to foresee conditions that lead to asphaltene precipitation [16].

The models used for asphaltene phase behaviour can be classified according to whether asphaltene molecules are considered associating or non-associating components (Figure 3-1) [17-33]. The former is focused on the state of asphaltene in crude oil and does not consider association bonding for asphaltene. In contrast, the latter considers the association of asphaltene molecules, such as hydrogen bonding, along with van der Waals forces [34]. The association class of approaches consists of thermodynamic solubility and colloidal theory-based models. In the solubility approach, asphaltene is considered to be dissolved in oil, and precipitation results from decreasing the solubility of asphaltene lower than a threshold level [22-26]. The equation of state modeling includes cubic (Soave-Redlich-Kwong (SRK), Peng Robinson (PR)), and statistical associating fluid theory (PC-SAFT). In this category, asphaltene precipitation is controlled by van der Waals forces. Moreover, asphaltene may be considered as the pre-aggregated molecule. The association energy approach considers van der Waals forces, and the association between asphaltene molecules controls the phenomenon. The advanced EoS, i.e., cubic plus association (CPA) and PC-SAFT, are in this group of models. It should be mentioned that PC-SAFT EoS can be applied

in both categories of models, and association energy can be included ($A=A^{hc}+A^{disp}+A^{assoc}$) or excluded in the EoS ($A=A^{hc}+A^{disp}$).
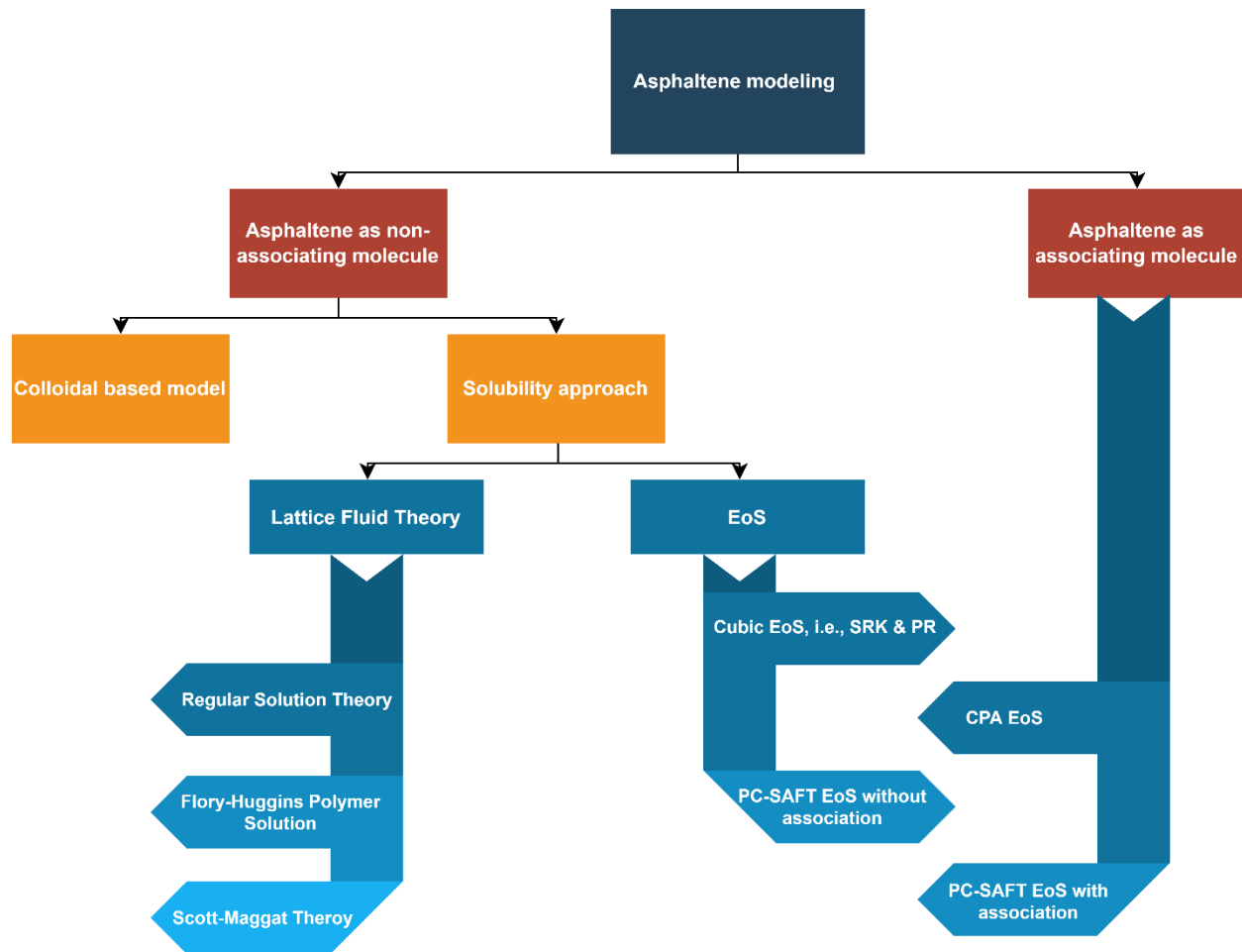
Figure 3-1. Classification of asphaltene modeling approaches

3-1-1. Non-Associating Asphaltene Models

In this category of models, asphaltene is considered pre-aggregated and non-associating molecules that can precipitate by van der Waals forces. Almost all the solubility and colloidal classes can fall under this category; even the PC-SAFT is in this group when the association term is neglected [35, 36]. The solubility approach consists of two categories: the lattice theory and equations of state (EoS) [17, 22-33]. The lattice theory model includes Flory-Huggins polymer solution theory, Scott–Magat theory, and regular solution theory. The regular solution theory is one of the most straightforward approaches in this category. Although the lattice theory modeling approach is

110

reliable and straightforward, it has some drawbacks, such as not considering the effect of the pressure (density or compressibility) and the need to utilize the EoS for vapor-liquid equilibrium (VLE) calculations [18].

Two of the simplest EoS models in this category are SRK and PR; however, their accuracy is questionable. Gupta (1986) used a cubic EoS, i.e., PR EoS, to model the onset of asphaltene [37] and to obtain the critical properties of the solid-liquid equilibrium of the oil mixture. The correlation for fugacity calculation had eight adjustable parameters, which is highly empirical. Sabbagh, Akbarzadeh, Badamchi-Zadeh, Svrcek, & Yarranton, 2006, adapted the PR EoS to model asphaltene precipitation using n-alkane at different temperatures (0-100°C) and pressures (up to 7 MPa). They applied a liquid-liquid equilibrium (LLE) for asphaltene precipitation and the gamma distribution function of different molar masses for asphaltene. Furthermore, the solubility fractions, including saturates, aromatics, resins, and asphaltenes, were used to characterize the oil mixture. Their findings showed that the developed model could not universally correlate/predict asphaltene precipitation, and no superiority was observed compared to the previously developed models [35]. Vargas, Gonzalez, Hirasaki, & Chapman, 2014, compared the prediction capability of the SRK and PC-SAFT EoS to model asphaltene onset point (AOP). It was concluded that both models could fit the experimental data, while the prediction performance of the SRK EoS was inferior [38]. Panuganti, Vargas, Gonzalez, Kurup, & Chapman, 2012, [39] and later Tavakkoli, Panuganti, Taghikhani, Pishvaie, & Chapman, 2014, [40] studied asphaltene phase envelope using the PC-SAFT EoS. They considered asphaltene as polydisperse components. They set part of the binary interaction parameters (BIPs) to zero (asphaltene-paraffin) to correlate the onset and asphaltene yield. Their findings contradicted experimental results, where no sensitivity of the PC-SAFT was observed with the carbon number of precipitants.

3-1-2. Associating Asphaltene Models

Considering the association of asphaltene molecules, e.g., the effect of hydrogen bonding, can result in better performance of the asphaltene modeling approach. However, the performance of thermodynamic models relies on factors such as the quality/accuracy of experimental data and the optimization approach for tuning the EoS., i.e., BIPs and association parameters. The density and precipitation experimental data (asphaltene yield or onset) can improve the EoS model. Yet, the optimization approach for parameter estimation can significantly advance the

correlation/prediction ability of the EoS [41]. The importance of optimization is discussed in the modeling section of the current study.

Li and Firoozabadi, 2010, used PR EoS within a CPA framework to model asphaltene phase behavior [42]. The CPA model was a combination of two parts, including the physical part concerning PR EOS and the association part based on Wertheim's thermodynamic perturbation theory. Oil was assumed to include three pseudo components: saturate, aromatic/resin, and asphaltene. The model had only one adjustable parameter, the association energy parameter, and all BIPs were set to zero. Also, the model exhibited good performance in modeling precipitation occurrence; however, its performance in forecasting the onset point was not acceptable. This shortcoming was attributed to not properly adjusting the association energy parameter and not introducing BIPs to the EoS [42]. Arya, Liang, von Solms, & Kontogeorgis, 2016, applied CPA and PC-SAFT with and without the association contribution to model asphaltene precipitation yield. They compared the results of the PC-SAFT without association (WOA) and CPA EoS (added association term to the SRK EoS). They examined different approaches for oil characterization and used different association parameters for asphaltene. Some of the approaches (CPA EoS while using SARA analysis for oil characterization and different association parameters for asphaltene and PC-SAFT EoS) were unable to accurately model the decrease of asphaltene precipitation when using heavier n-paraffin. Only the CPA EoS could correlate asphaltene precipitation by considering two fractions for oil (heavy fractions and asphaltene) and one association parameter. They did not report the quantity of experimental data they used nor information regarding parameter estimation of the EoS [43]. Recently, there has been some research regarding using CPA EoS for either asphaltene onset or precipitation [63-66]. However, the research does not consider global optimization of CPA EoS (while an advanced optimization technique is required to tune the parameters of the EoS), model both weight percent of precipitation and onset, correlate binary interaction parameters, and consider a wide range of operating conditions. The current research addresses the knowledge gap in applying CPA EoS in asphaltene modeling and presents novel research work. While our research address the knowledge gap in applying CPA EoS in asphaltene precipitation modeling, and incorporate global optimization into the EoS to tune the adjustable parameters and increase the reliability of the EoS, the approach is a prototype that may need further improvements to be applied for more experimental data other than used here.

To the best of our knowledge, we have found very few literature focused on optimizing CPA or PC-SAFT EoS. We believe our implementation of global optimization (GO) to tune association and BI parameters in CPA to be novel. Moreover, a systematic sensitivity analysis of operational conditions and BIPs is missing. The current research uses the CPA approach to study the asphaltene precipitation yield and onset point. The GO approach uses GlobalSearch, MultiStart, and Genetic Algorithms to develop a thorough optimization to find association and BIPs and skip the local minima. The novel developed algorithm and the step-by-step procedure are introduced. A total number of 174 experimental points are employed to validate the proposed EoS and optimization approach [44]. The BIPs are correlated with the temperature and carbon number of the n-alkane. Later, the CPA EoS is further validated by predicting unseen data, is compared with cubic EoSs, i.e., SRK and PR, the existence of the local minima and their impact on the model performance is tested, oil characterization is compared with other approaches, e.g., using SARA analysis, and then an analogy is drawn between the CPA EoS and the scaling equation. Finally, the relative importance analysis is performed to explain the role of each independent variable, i.e., temperature, the carbon number of solvent, and quantity of solvent, on asphaltene yield and BIPs. Section 3-9 summarizes the relative deviations using the CPA EoS and GO approach and shows the reliability and accuracy of this research. The findings of this research can be used by other researchers to increase the efficiency of asphaltene thermodynamic modeling, e.g., industrial software.

3-2. Modeling Approach and Theory

The overall workflow of this article can be divided into six sections, including data and oil characterization, the CPA coding and debugging, optimization and parameter tuning, testing, validation, and relative importance analysis (Figure 3-2). In the first section, a literature review is conducted to study the impact of van der Waals and association forces on asphaltene agglomeration and to find the literature gap regarding EoS optimization. Proper experimental data in a wide range of operating conditions are chosen from Hu and Gue [44]. The oil characterization, the molecular weight of asphaltene, and the critical properties of the oil fractions are determined. The normality of the experimental data is examined using SPSS v27 and doing the Shapiro-Wilk test and boxplot (supplementary information (Appendix B)). In the second step, the equations are extracted from Kontogeorgis and Folas [49], and the coding and debugging are done using Matlab

software. In the third step, adjustable parameters of the CPA EoS, i.e., a_0, b, c_1, ε, β, interaction parameters (three BIPs), and solvation factor (equation 16) are tuned. Genetic Algorithm, GO, and Nelder-Mead (NM) simplex algorithm are used to estimate these parameters. In the fourth step, the model is tested in terms of association schemes (2B, 3B, and 4C), oil characterization approach (SARA analysis and maltene-asphaltene), correlation of the binary parameters (BIPs and cross-association), and correlation of asphaltene yield in operational conditions. The fifth step is the validation of the model, that is the prediction of unseen data of asphaltene yield and onset point in operating conditions, showing the effect of association on model performance by comparing the CPA EoS with EoS containing only the physical term, i.e., SRK and PR EoS, comparing the CPA EoS that is tuned using GO or only local optimization, and validating the CPA EoS with models other than thermodynamics, i.e., the scaling model. The last step is to perform relative importance (RI) analysis to explain the role of each independent variable (operating conditions) on asphaltene precipitation and BIPs.

Data and oil Characterization	CPA Coding and debugging	Optimization and parameter tuning	Testing	Validation	Relative importance analysis
- Literature review - Finding proper experimental data for asphaltene yield and onset point - Temperature: 293 K-338 K - Precipitant: C_5-C_{12} - Dilution ration: 2.3-24.3 (cm^3/g)	- Extract CPA equations from references, physical and association terms - Proper approach to solve equations, i.e., numeric & analytical	- Adjustable parameters, i.e., asphaltene parameter (a_0, b, c_1, ε, β), binary parameters (kij for asphaltene-n-alkane, asphaltene-maltene, and n-alkane-maltene), solvation factor	- Test and valide different schemes (i.e., 2B, 3B, 4C) for asphaltene association sites and compare the correlation abilities using different schemes	- Predict of unseen data of asphaltene yield in different temperatures and dilution rations - Predict onset point of asphaltene precipitation with temperature and using n-alkanes	- Use a relative importance analysis, i.e., the Pearson's correlation coefficient and Pearson's R, to measure the impact of dilution ratio, temperature, and carbon number of n-alkane on asphaltene yield
- Oil Characterization using Maltene and asphaltene - Asphaltene molecular weight (750 g/mol) - Critical properties using correlations	- Use Matlab R2020-b for coding - Debug the code using few data, 5 data points - Test the code using data other than those used for modeling and validation	- Use GA for initialization of parameter bounds (LB and UB) and start point of optimization (X_0) - Global optimization to optimize adjustable parameters - Use Nelder-Mead simplex algorithm to refine the results	- Use different oil characterization approach, i.e., SARA analysis and maltene+asphaltene, and comparing the correlation errors using these approaches	- Compare the CPA including physical and association terms with cubic EoS, i.e., SRK and PR, only include physical term	- Use relative importance analysis to measure the impact of temperature and carbon number on the binary interactions
- Data analysis using SPSS v27, i.e., the Shapiro-Wilk test and boxplot, to study normality of the experimental data, regarding quantity of n-alkane, temperature, and types of n-alkane			- Correlate binary parameters, i.e., binary interactions and solvation factor, with temperatures (293 K-338 K) and using different n-alkane (C_5-C_{12})	- Compare the CPA using global optimization and local optimization to correlate asphaltene yield data	
			- Correlate asphaltene yield in different operational conditions, i.e., dilution ratios (2.3-24.3 cm^3/g), temperature (293, 308, 323, 338 K), n-alkanes (C_5, C_6, C_7, C_8, C_9, C_{10}, C_{12})	- Compare the CPA EoS with model other than thermodynamic models, i.e., scaling model	

Figure 3-2. The overall workflow of the article

3-2-1. CPA EoS

The CPA EoS, which Kontogeorgis and Folas [45] proposed, was used to model asphaltene precipitation under operational conditions, under different temperatures, and with solvents. The compressibility factor of mixtures is represented by physical and association compressibility, which combines the interaction of molecules with cubic EoS as follows [45]:

$$Z = Z^{Physical} + Z^{Assoc} \tag{3-1}$$

$Z^{Physical}$ and Z^{Assoc} represent the physical and chemical interactions in the mixture as follows [45]:

$$Z^{Physical} = \frac{RT}{(v-b)} - \frac{a}{v(v+b)} \tag{3-2}$$

$$Z^{Assoc} = -\frac{1}{2}(1 + \frac{1}{v}\frac{\partial \ln g}{\partial(1/v)}) \sum_i x_i \sum_{A_i}(1 - X_{A_i}) \tag{3-3}$$

The SRK EoS and the conventional mixing rule represent the physical interactions of molecules, e.g., van der Waals forces and a_{ij}, b_i, and k_{ij} stand for the attractive energy, repulsive energy, and BIP, as indicated in equations 3-4 to 3-9. BIP is the physical section's adjustable parameters optimized by experimental data [44]. The mixing rules are necessary to extend an EoS to mixtures successfully. The simple random van der Waals mixing rules (vdW) were applied for the physical term (Eq 3-6). The BIPs are adjusted by minimizing the difference between predicted and experimental data using the optimization approach reviewed in sections 2-5. The inclusion of BIPs in EoS is advantageous for increasing the reliability and flexibility of the EoS. It would be particularly powerful to tune BIPs for reservoir fluid if BIPs are adjusted with the available experimental data. Additional flexibility can also be obtained by making BIP temperature, pressure, and composition-dependent [46].

P, T, R, and v are the pressure, temperature, gas constant, and volume of pure components. Equation 3 defines the association term, which is suitable for describing strongly associating compounds that have the capability of forming hydrogen bonds. The hydrogen bonding formation between molecules of the same kind is called self-association (e.g., in the asphaltene precipitated phase). In contrast, the association of hydrogen bonding complexes between two different molecules is called cross-association (e.g., asphaltene-maltene). In equation 3-3, g denotes the

distribution function, x_i is the mole fraction of the pure component, and X_i represents the association between two molecules.

$$a_{mix} = \sum_i \sum_j x_i x_j a_{ij} \tag{3-4}$$

$$b_{mix} = \sum_i x_i b_i \tag{3-5}$$

$$a_{ij} = \sqrt{a_i a_j}(1 - k_{ij}) \tag{3-6}$$

$$a_i(T) = 0.42747 \, \alpha_{ij}(T) \frac{(RT_c)^2}{P_c} \tag{3-7}$$

$$\alpha_{ij}(T) = [1 + (0.48 + 1.574 \, \omega - 0.176 \, \omega^2)(1 - \sqrt{T_r})]^2 \tag{3-8}$$

$$b_i = 0.08664 \frac{RT_c}{P_c} \tag{3-9}$$

Equations 3-4 to 3-9 represent the physical SRK EoS term describing the attractive parameter of the mixture, cross co-volume of the mixture, binary attractive parameter, pure attractive parameter, and pure volume parameter, respectively. T_r, P_r, and ω are reduced temperature, reduced pressure, and acentric factor of pure components. It is worth noting that the attractive parameter is temperature dependent, whereas cross-co volume is temperature independent [1, 45].

For a compound with the association of two sites (e.g., maltene is shown in Figure 3-4), A and B, the mole fraction of the active site is as follows:

$$X_{A_i} = \frac{1}{1 + \rho \sum_j x_j \sum_{Bj} X_{Bj} \Delta^{A_i B_j}} \tag{3-10}$$

where ρ is the density of the compound, x_j is the mole fraction of molecule j, and $\Delta^{A_i B_j}$ represents the association strength.

$$\Delta^{A_i B_j} = g(v) \left[\exp \left(\frac{\varepsilon^{A_i B_j}}{RT} \right) - 1 \right] b_{ij} \beta^{A_i B_j} \tag{3-11}$$

The radial distribution function is:

$$g(v) = \frac{1}{1-1.9n}, \ n = \frac{1}{4}b\rho \qquad (3\text{-}12)$$

The association energy ($\varepsilon^{A_iB_i}$) and the volume interaction ($\beta^{A_iB_i}$) are two adjustable parameters of the CPA EoS tuned to match the experimental data of the compounds [45]. The following rules have been used to combine the association energy, volume interaction, and association strength of the mixture components. These rules are used to find binary energy, volume, and strength of association between two components. The association energy and volume are named CR-1 mixing rule (equations 3-13 and 3-14), and the association strength is called Elliott CR (equation 3-15).

$$\varepsilon^{A_iB_j} = \frac{\varepsilon^{A_iB_i} + \varepsilon^{A_jB_j}}{2} \qquad (3\text{-}13)$$

$$\beta^{A_iB_j} = \sqrt{\beta^{A_iB_i}\beta^{A_jB_j}} \qquad (3\text{-}14)$$

$$\Delta^{A_iB_j} = \sqrt{\Delta^{A_iB_i}\Delta^{A_jB_j}} \qquad (3\text{-}15)$$

The following form is used for the extension of the CPA EoS for a mixture containing one associating compound (self-associate and cross-associate) and a compound that only cross-associates (i.e., solvates or HC). The cross-association strength in the mixture can be found by multiplying the self-association (associating strength of the associating compound) by a factor that will be referred to as the 'solvation factor' (s_{ij}) [47]:

$$\Delta^{A_iB_j} = \Delta^{A_i} \times S_{ij} \qquad (3\text{-}16)$$

Where i and j denote the associating (asphaltene) and the solvating component (HC), respectively, more information about the equations used in this work is presented in the supplementary information (Appendix B).

3-2-2. Experimental Data and Operational Conditions

In this research, asphaltene precipitation was studied using data from degassed oil in different operational conditions by Hu and Guo [44]. The composition and properties of the crudes are presented in Table 1. For the current research, a total of 174 experimental data points were used. Considering the asphaltene content of the oil mixture, it appears to be a medium gravity oil sample; however, information regarding the API gravity of the oil sample used in the experimental work was not reported. Hu and Guo [44] reported that a series of experiments were carried out to determine the amount of asphaltene precipitation using different precipitants and at different temperatures. The quantity of asphaltene precipitation was determined using the filtration method. The experiments were conducted at four different temperatures, 293, 308, 323, and 338 K, using precipitants, including normal pentane (nC_5), normal hexane (nC_6), normal heptane (nC_7), normal octane (nC_8), normal nonane (nC_9), normal decane (nC_{10}), and normal dodecane (nC_{12}). The ranges of the experimental data are reported in Table 2.

To apply the CPA EOS, oil samples need to be characterized, and each group of components is introduced to the model by their critical properties. Different characterizations have been used for oil with asphaltene, which has pros and cons. In this research, the aforementioned characterization method was used to reduce the degree of freedom (number of adjustable parameters) and solve the issue related to the unavailability of the molecular weights of the oil fractions (C_7^+) and the maltane fraction of oil (saturates, aromatics, and resins, which are lumped into heavy components).

The modeling approach uses the n-heptane plus (C7+) fraction, and stock tank oil (STO) contains a negligible amount of lighter components than n-heptane. The reason for this assumption is; first, the degassed oil was used to determine the asphaltene precipitation in the experiments (hence, lighter hydrocarbons; C_1, C_2, C_3, C_4; are not available in the equilibrium). Second, the insignificant amount of C_5 and C_6 (less than 2%, 0.0001 mol) will not affect the equilibrium in comparison with the amount of C7+ fraction. Third, the diluents with a high dilution ratio (2.3-24.3 ml/g, 0.1-0.95 mol) were added to precipitate asphaltene.

Table 3-1. Compositions (mol%) and properties of the degassed Caoqiao crude oil and separator gas [44]

Component	Degassed oil	Separator gas
CO_2	0.0	2.96
N_2	0.0	1.18
C_1	0.0	89.37
C_2	0.0	3.34
C_3	0.0	2.10
i-C_4	0.0	0.32
n-C_4	0.0	0.26
i-C_5	0.16	0.22
n-C_5	0.58	0.15
n-C_6	1.2	0.12
$C7^+$	98.06	
$C11^+$	87.16	
C_7^+ molecular weight (g/mol)	503.6	
C_7^+ density (at 293 K)	0.9526	
Reservoir temperature (K)	343	
Bubble point pressure at 343 K (MPa)	9.8	
Gas oil ratio (GOR, m^3/m^3)	30.2	
Saturates (wt.%)	38.0	
Aromatics (wt.%)	47.6	
n-C_5 asphaltenes (wt.%)	7.26	
Resins (wt.%)	18.6	

Table 3-2. Ranges of the experimental data [44]

Parameters	Ranges
T (K)	293 - 338
R (mL/g)	2.3 – 24.3
Precipitant	$nC_5 – nC_{12}$
Wt% (g/g)	0.22 – 6.12

3-2-3. Oil Characterization and Liquid-Liquid Equilibrium (LLE)

One of the critical steps in EoS modeling is the characterization of the multi-component oil mixture. Once working with crude oil, finding the best way to characterize the mixture to reduce the number of adjustable parameters of the pseudo components and interaction parameters is crucial. Different approaches have been introduced for oil characterization with asphaltene, e.g., SARA analysis [35, 36, 38, 48]. There are two issues with using SARA analysis for oil characterization. First, the molecular weight of SARA fractions is needed. While SARA analysis provides the mass percent of the fractions, the molecular weights of these fractions are required to convert the titration data to the molar fractions. The molecular weight of fractions is not usually measured/reported in the articles, while it is required for thermodynamic calculations. Second, there are many adjustable parameters or a high degree of freedom. Asphaltene tends to self-associate and cross-associate with maltenes (saturate, aromatic, and resin), which needs optimization of eight adjustable parameters for association energy and volume. To address these, the maltane fraction of oil, including saturates, aromatics, and resins, is lumped into heavy components in the current work [49]. The oil characterization approach is shown in Figure 3-3. This characterization approach is used from Flory-Huggins (FHZ) EoS, which is the first industrial EoS. The characterization method by FHZ is simple and treats oil as a mixture with two or more pseudo-components; the solvent (non-asphaltene component or maltene fractions) and a solute (asphaltene).

We also used C_{7+} as the stock tank oil (STO), and the lighter hydrocarbons were neglected since those amounts in the degassed oil were insignificant. Further, the C_{7+} was categorized into heavy components (HC) and asphaltene. Asphaltene was considered to be a monomer with a molecular weight of 750 g/mol (Dalton, Da) as proposed by "Yen-Mullin", considering a typical island structure with a single and relatively large PAH with peripheral alkyls [50]. Later, Schuler et al., 2015, presented the first direct measurement of the molecular structure applied for more than 100 asphaltene samples and endorsed the "Yen-Mullin" model for asphaltene molecular weight [3, 13].
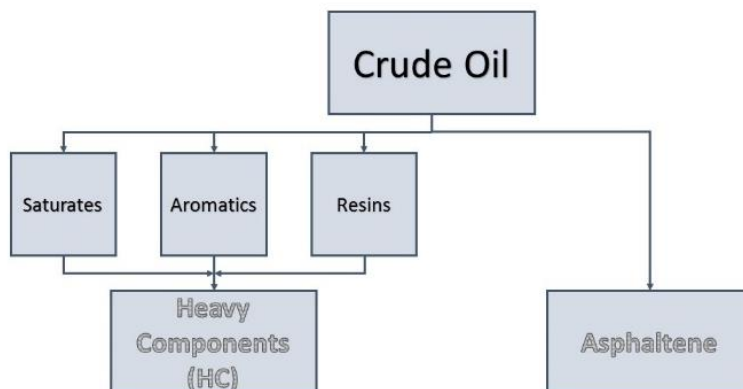
Figure 3-3. Degassed crude oil (C_{7+}) characterization into HC and asphaltene (adapted from [43, 49])

The nonpolar van der Waals and association of hydrogen bonding forces govern asphaltene precipitation. The van der Waals force is a non-bonding interaction resulting from the geometry and polarizability of the large molecule, e.g., asphaltene. The association of hydrogen bonding is a robust interaction and occurs when an electropositive atom/electron donor, e.g., hydrogen, is attached to an electron acceptor, e.g., oxygen. The van der Waals force can be interaction or dispersion forces, while the association of hydrogen bonding is an attractive interaction. A liquid-liquid equilibrium (LLE) was considered for the oil and precipitated phases. Self-association between asphaltene particles and cross-association between heavy components (HC) and asphaltene was assumed in the oil phase. At the same time, the precipitated phase is controlled by the association between asphaltene particles, which leads to aggregation and phase separation of asphaltene. Figure 3-4 represents the assumptions used for the modeling approach. In the oil phase, self-association and cross-association are considered between asphaltene-asphaltene and asphaltene-maltene, respectively. The self-association of asphaltene is an attractive interaction, and the cross-association of asphaltene and maltene is the interaction that suspends asphaltene in the oil mixture. The resultant of these interactions prevents asphaltene from accumulating in the oil phase. However, the precipitated phase is governed by the self-association of asphaltene particles, which results in precipitation.
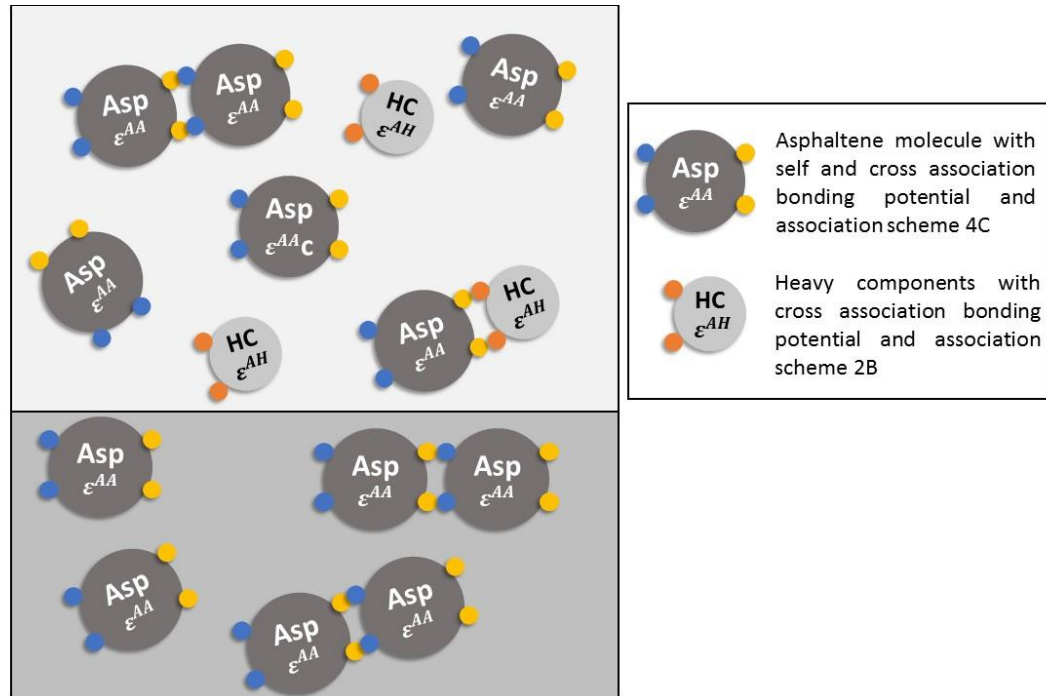
Figure 3-4. Representation of associations considered in this work. The upper section of the figure is the oil phase, considering self-association between asphaltene (ε^{AA}) and cross-association between asphaltene and heavy components (ε^{AH}). The lower part shows the precipitated phase considering self-association between asphaltene (ε^{AA})

3-2-4. Optimization

One of the main challenges of working with advanced thermodynamic EoSs is tuning the adjustable parameters. The advanced EoSs are nonlinear and complex and have no analytical solutions. Moreover, the other impediments to its optimization are the existence of local minima, the continuity of the objective function, and the relative importance of the model parameters on the objective function. Therefore, a multi-variable global optimization method is required in working with advanced EoSs. dos Santos, Abunahman, Tavares, Ahón, & Kontogeorgis, 2015 [51] examined the parameters of the CPA EoS and showed that the five parameters of the pure component (a_0, b, c_1, ε, and β) could present local minima while minimizing the objective function (Figure 3-5).
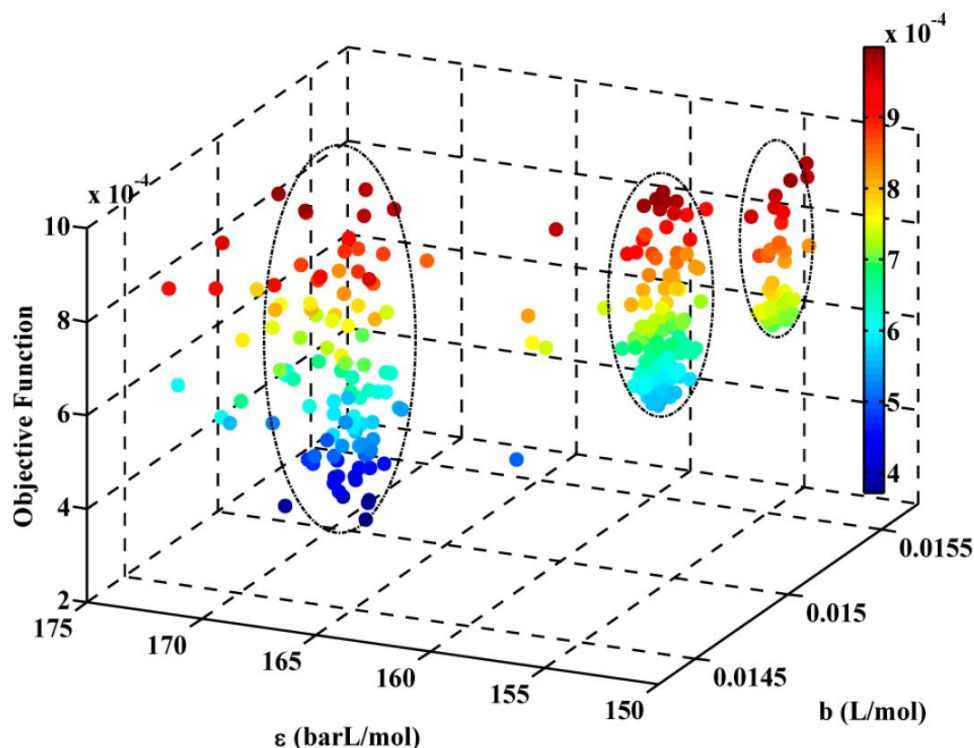
Figure 3-5. Existence of local minima when optimizing parameters of the advanced CPA EoS using a global optimization approach, e.g., Particle Swarm Optimization [51]. Reproduced with permission from ref 51. Copyright 2014, American Chemical Society.

The complexity of the thermodynamic calculations, on the one hand, and the multi-variable and multi-objective nature of the problem, on the other hand, encouraged the current research with a focus on optimization strategies, especially "global optimization (GO)". The approach adopted here has two stages:

- Global Optima: A GO approach is used to find the global optimum of the thermodynamic calculations. For this purpose, two approaches, GlobalSearch and MultiStart, are adopted to find the best optimum. These methods have been widely applied in complex optimization problems to find global or multiple minima. [52, 53]. To the best of our knowledge, we have not found any literature using these GO methods in the thermodynamic area. Each method has advantages and disadvantages. The user should decide which solver to use based on optimization criteria, such as sample size and computational cost.

- Local optima: In addition to the robust GO approach, local and simple optimization is also implemented to assist the other approaches. Once the global optima were found from the above procedure, the Nelder-Mead (NM) simplex algorithm [54] was employed to refine the global optimum within each basin of the optimization. The method is a simple and fast algorithm that does not require additional computations of the derivatives of the objective functions. However, the accuracy of the optimization is highly dependent on the initial guess of the adjustable parameters, e.g., BIPs.

The arbitrated algorithm used by Abunahman, dos Santos, Tavares, & Kontogeorgis, 2020, uses PSO results as the initial estimation of the method. In contrast, the PSO method is not robust enough to locate the global optima of the problem [41]. So, the current research mainly focused on selecting the initial guess of the adjustable variables within the predefined regions of the optimization basins. The NM simplex algorithm should not be used independently due to the complexity of the optimization of the thermodynamic calculations. The two approaches mentioned above were implemented sequentially, and the results of the GO were refined by the NM simplex approach.

The general framework of the proposed optimization technique and algorithm for flash calculation is adapted from Abunahman et al., 2020, [41] and Sabbagh (2005) [55], respectively. The process starts with having the composition and molecular weights of the different fractions/components of the mixture (Figure 3-6). Then, the critical properties of the oil fractions will be calculated using different correlations. Here, these correlations are proposed by Riazi and Al-Sahhaf (1996) [56] and optimized parameters used by Akbarzadeh, Alboudwarej, Svrcek, & Yarranton, 2005 [18].

To start the GO, the upper bound (LB), lower bound (UB), and start points (X_0) should be defined. The nature of the parameters determines the optimization bounds. For instance, we know that the BIPs can be in [-1, +1], so the lower and upper bound for optimization would be -1 and +1, respectively. The rate of optimization convergence is dependent on the X_0. Hence, the X0 vector is determined from the genetic algorithm (GA) to decrease the computational cost. GA is a stochastic algorithm, and its results change with every run. Therefore, it is only used to set the initial X_0 vector. GO starts by designing the optimization problem (objective function, Eq 18), input data, design variables (BIPs, ε, and β), UB, LB, X_0, and optimization options (e.g., population size and parallel computing) (Figure 3-7). Afterward, the start points are analyzed, and those with

the highest $F(X_0)$ are neglected. Then, the (NM) simplex method runs using best start points considering objective function and constraints (i.e., cross association, s_{ij}, increases with decreasing temperature). In each iteration, the objective function and constraints are checked, and whether satisfied (the predicted data is with error < 5% of the experimental data), the optimization ends; if not, the design variables are re-initiated.

The GO runs the NM simplex method in several points to find multiple local minima of the OF. The NM starts with generating a new simplex using initial values. The initial simplex is important, while a poor choice of initial values can stick the NM in local minima. Then, in the reflection step, a new guess (x_{new}) is found while the $F(x_{new})$ decreases. If the condition is satisfied, x_{new} is replaced; if not, the shrink step happens. Shrink handles the case when OF increases in one iteration. For each optimization iteration, the flash calculations are conducted to determine the parameters of the physical term (i.e., a_0, b, and c_1 of the asphaltene component, which is set using an optimization), the volume, compressibility factor (Eq 2 and 3), fugacity, and fugacity coefficients of each phase. The fugacity of the two phases is compared. If the condition is met (error < 10^{-12}), the mole fractions are determined; otherwise, the K values are updated using the fugacity rate. The mole fraction is reported if the calculated mole fractions meet the criteria (error < 5%). Otherwise, the values for BIPs, ε, and β are updated.

It is worth mentioning that the starred sections in Figure 6 are the novelty of this research work, which uses GO, i.e., GlobalSearch and MultiStart, and GA to determine initial values.

The K value is initialized using the Wilson equation.

$$K_i = (P_{ci}/P)exp\left[5.37(1+\omega_i)(1 - T_{ci}/T)\right] \tag{3-17}$$

Start

Start

Input data: LB, UB

Genetic algorithm

Optimize X_0

Input data: z_i and M_{wi}

Calculate of Tc, Pc, ω

Start of Global Optimization, LB, UB, X0

Initialize the start points

BIPs, ε, β

Initialize K-value (Eq 17)

Flash calculations

Calculate the SRK parameters (a_0, b, c_1)

Calculate volume of each phases

Calculate Z of each phase (Eq 2 & 3)

Calculate fugacity and fugacity coefficient

New set of initial guess

Update the K-value
$K_{i_{new}} = K_{i_{new}} \left(f_i^{l_1} / f_i^{l_2} \right)$

$f_i^{l_1} = f_i^{l_2}$
$error < 10^{-12}$

No

Yes

$x_i^{exp} = x_i^{model}$

No

Yes

Calculate mass of dense phase

End

Figure 3-6. Asphaltene precipitation model using CPA EoS

127
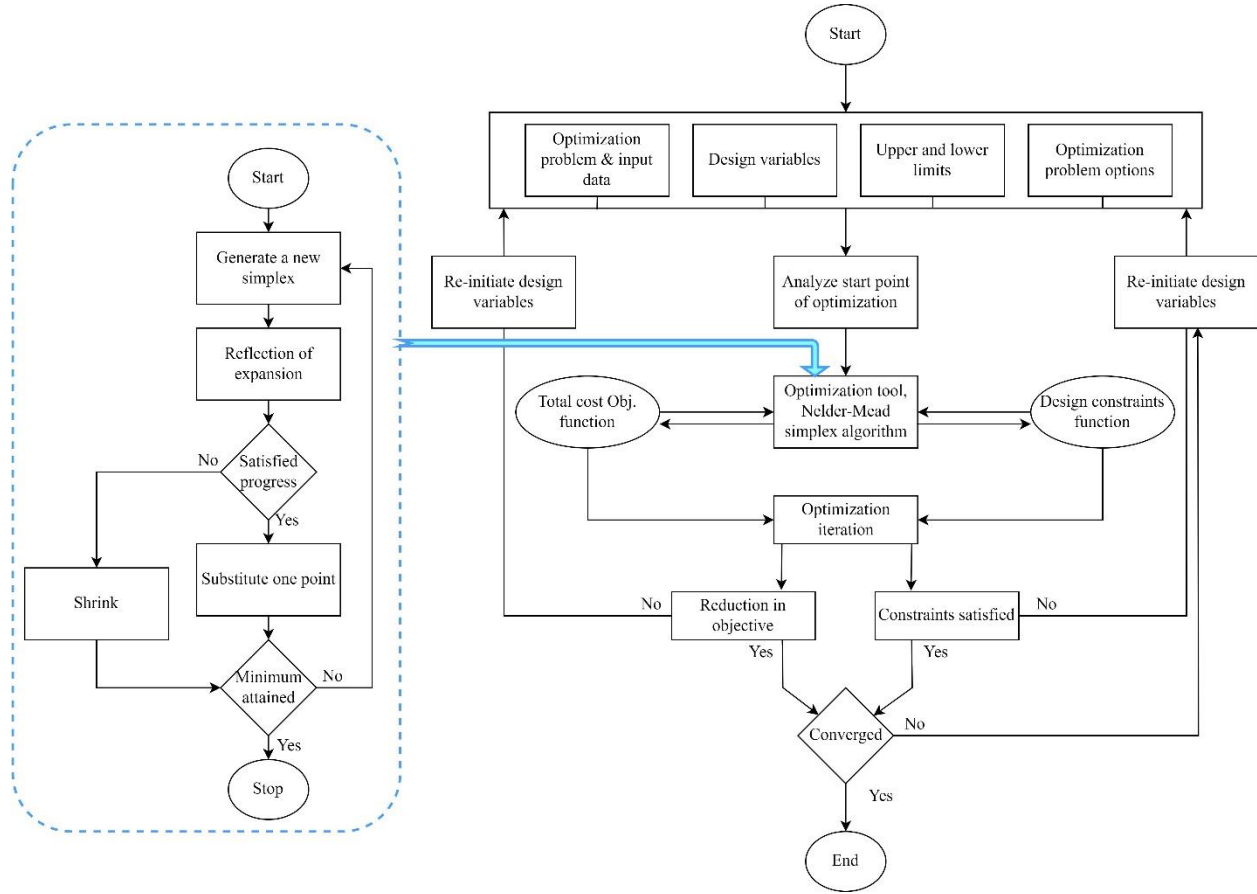
Figure 3-7. Global optimization (GO) algorithm flowchart

3-2-5. Parameter Estimation

To tune the parameters of the thermodynamic model, the optimization approach was used in a procedure in which the error variance is minimized. Therefore, the objective function/functions (F(X)), defined here from the thermodynamic model, are minimized, subject to the restrictions h(X). It is worth mentioning that the accuracy of the tuning procedure is highly dependent on the choice of the objective function and optimization approach [41]. For this purpose

$$F(X) = \sum_{k}^{n_p} \left[\frac{1}{n_e} \sum_{i}^{n_e} \frac{(y_{k,i}^e - y_{k,i}^p)^2}{\sigma_{k,i}^2} \right] \qquad (3\text{-}18)$$

Where y, n, and σ represent the variable, the number of variables, and the variance of the experimental variables, respectively. The superscripts e and p stand for experimental and model variables. The experimental variables can replace the variance value due to the unavailability of this parameter with experimental data used for thermodynamic modeling. Since the experimental data might be limited or difficult to reproduce [41].

While adjusting the thermodynamic model, a wide variety of possible solutions may result in similar deviations. However, the restrictions can be applied along with the objective functions to estimate the parameters of the EoS, as well as projected trends for the parameters. The global estimation method was used to adjust the model with the five parameters for the pure components (three from the physical part a_0, b, c_1, and two from the association part, ε, and β) [45].

In this research, the calculated variable is the weight percent (wt%) of asphaltene precipitation, and only one type of experimental data was available. Therefore, the equation (above) takes the form:

$$F(X) = \frac{1}{n_e} \left[\sum_1^{n_e} \frac{(n_i^e - n_i^p)^2}{\sigma_i^2} + \sum_1^{n_e} \frac{(n_i^e - n_i^p)^2}{\sigma_i^2} \right] \qquad (3\text{-}19)$$

Where vector X contains a_0, b, c_1, ε, and β; hence, critical properties (T_c, P_c, ω), operational conditions (P and T), and experimental values of phase separation ($wt\%$) are needed. When the variance is absent, it can be assumed that it is equal to the respective experimental data of phase separation. The binary parameters, including BIPs and cross associations, are estimated by GO using critical properties, the pure components variables, and the composition data.

The BIPs are usually used in systems, including heavy fractions, such as asphaltene and n-alkane, to calculate the phase behavior of the system using EoS. In the present research, three types of binary interactions are considered, interactions between n-alkane and heavy component (nC$_n$-HC), interactions between n-alkane and asphaltene (nC$_n$-Asp), and interactions between heavy component and asphaltene (HC-Asp). While the BIPs between nC$_n$-HC and nC$_n$-Asp vary with the type of the n-alkane and temperature, the BIPs of HC-Asp only vary with temperature. The BIPs for each composition was optimized using GO techniques and minimizing equation (3-19).

3-3. Results and Discussion

3-3-1. Binary Interactions

Binary interaction parameters (BIPs), dependent on the physical properties of different mixtures, are presented in the literature [57] and have been used to model asphaltene phase behavior in the presence of n-alkane [36]. In this research, the dependency of binary parameters upon carbon number and temperature was studied, and the corresponding correlations are developed by the GO and presented in Table 3-3 and Figures 4-9. The table summarizes adjusted BIPs in different temperatures and solvents. The other binary parameter, cross association, is also optimized and presented in Table 3-3. The optimized BIPs (K_{ij}) are also illustrated in Figure 3-8 - Figure 3-12.

Figure 3-8 and Figure 3-9 demonstrate the behaviour of the BIPs between n-alkane and heavy fraction, and n-alkane and asphaltene as a function of the carbon number of the n-alkane, in different temperatures (293, 308, 323, 338 K). All the BIPs show the same trend using heavier n-alkanes. As the temperature increased, the K_{ij} decreased with increasing the carbon number of n-alkane. It is also shown that the behaviour of K_{ij} can be correlated to functions presented in Table 3-3 in the following form:

$$K_{ij} = (a \times CN) + b \tag{3-20}$$

Where K_{ij} is the binary interaction between n-alkane and asphaltene/heavy fraction, CN stands for the carbon number of the n-alkane used in the mixture (nC_5-nC_{12}), and a and b are two constants of the equation. It is worth mentioning that all experiments were done at atmospheric pressure. Increasing the temperature from 293 K to 323 K leads to an increase in the BIPs of HC-asphaltene; however, further increasing the temperature to 338 K shows a slight decrease in the binary interactions, as shown in Figure 3-10. The BIPs of HC-asphaltene and nC_n-HC (Figure 3-11) showed a monotonic trend increasing with temperature. BIPs demonstrated in these two figures are primarily positive and slightly decrease at a higher temperature.

By contrast, the shape of n-alkane and asphaltene BIPs is different from the two previously mentioned groups of BIPs, shown in Figure 3-12. BIPs of nC_n-asphaltene decreased using a variety of n-alkane and increasing temperature. Whereas the BIPs for normal nC_5 and nC_6 are positive,

the BIPs using nC_7-nC_{12} were negative, decreasing with increasing temperature, no matter how the temperature increased. The differences between Figures 10-12 are attributed to the critical region of the mixture and can be considered as evidence proving different precipitated asphaltene structures using a variety of n-alkane as the solvent.

In summary, the K_{ij} (nC_n-HC and HC-asphaltene) decreases with increased CN, no matter how the temperature increases. It also increases monotonically with increasing temperature. Whereas the K_{ij} (nC_n-asphaltene) decreases with increasing temperature, this behaviour can result from the critical region of the mixture. It is worth mentioning that the BIPs depend on the critical region of the mixture. It is recommended to apply critical properties for the determination of BIPs.

All the constants and equations tabulated in Table 3-3 correlate binary parameters, including binary interactions and cross-association as a temperature and carbon number function.

Table 3-3. Binary parameters, binary interaction parameters (K_{ij}), cross-association, and the correlated equations

	Binary parameter correlations	Constants			Range	
		a	b		T (K)	carbon number
nC$_n$-HC	$k_{ij=}a \times CN_{n-alkane} + b$	-0.0156	0.1436		293	
		-0.0283	0.3888		308	
		-0.0259	0.408		323	
		-0.032	0.3977		338	nC$_5$-nC$_{12}$
nC$_n$-asphaltene	$k_{ij=}a \times CN_{n-alkane} + b$	-0.0363	0.3387		293	
		-0.0433	0.349		308	
		-0.0259	0.408		323	
		-0.0332	0.1948		338	

	Binary parameter correlations	a	b	c	T (K)	carbon number
nC$_n$-HC	$k_{ij=}a \times T^2 + b \times T + c$	-0.0003	0.2114	-33.556		5
		-0.0002	0.122	-19.469		6
		-0.0002	0.154	-24.733	293-338	7
		-0.0003	0.164	-26.119		9
		-0.0002	0.1375	-21.811		10
		-0.0002	0.1267	-20.151		12
nC$_n$-asphaltene	$k_{ij=}a \times T^2 + b \times T + c$	-6e-5	0.0353	-4.9742		5
		6e-5	0.039	6.6036		6
		6e-6	-0.0056	1.2197	293-338	7
		8e-6	-0.0071	1.3841		9
		5e-5	-0. 0366	6.1111		10
		7e-5	-0.0462	7.561		12
HC-asphaltene	$k_{ij=}a \times T^2 + b \times T + c$	-0.0002956	0.1961	-32.29	293-338	nC$_5$-nC$_{12}$

$$k_{ij=}a \times T^2 + b \times T + c \times CN_{n-alkane} + d \times T \times CN_{n-alkane} + e$$

	a	b	c	d	e	T (K)	carbon number
nC$_n$-HC	-0.0002	0.147	0.0741	-0.0003	-23.6	293-338	nC$_5$-nC$_{12}$
nC$_n$-asphaltene	2e-5	-0.016	-0.049	3e-5	3.274		

		a	b	Range
S$_{ij}$	$a - b/T$	-2.2029	-1049	293-338

Figure 3-8. The optimized binary interactions between n-alkane and heavy hydrocarbon fractions, at different temperatures (293, 308, 323, 338 K) and using different n-alkanes

133
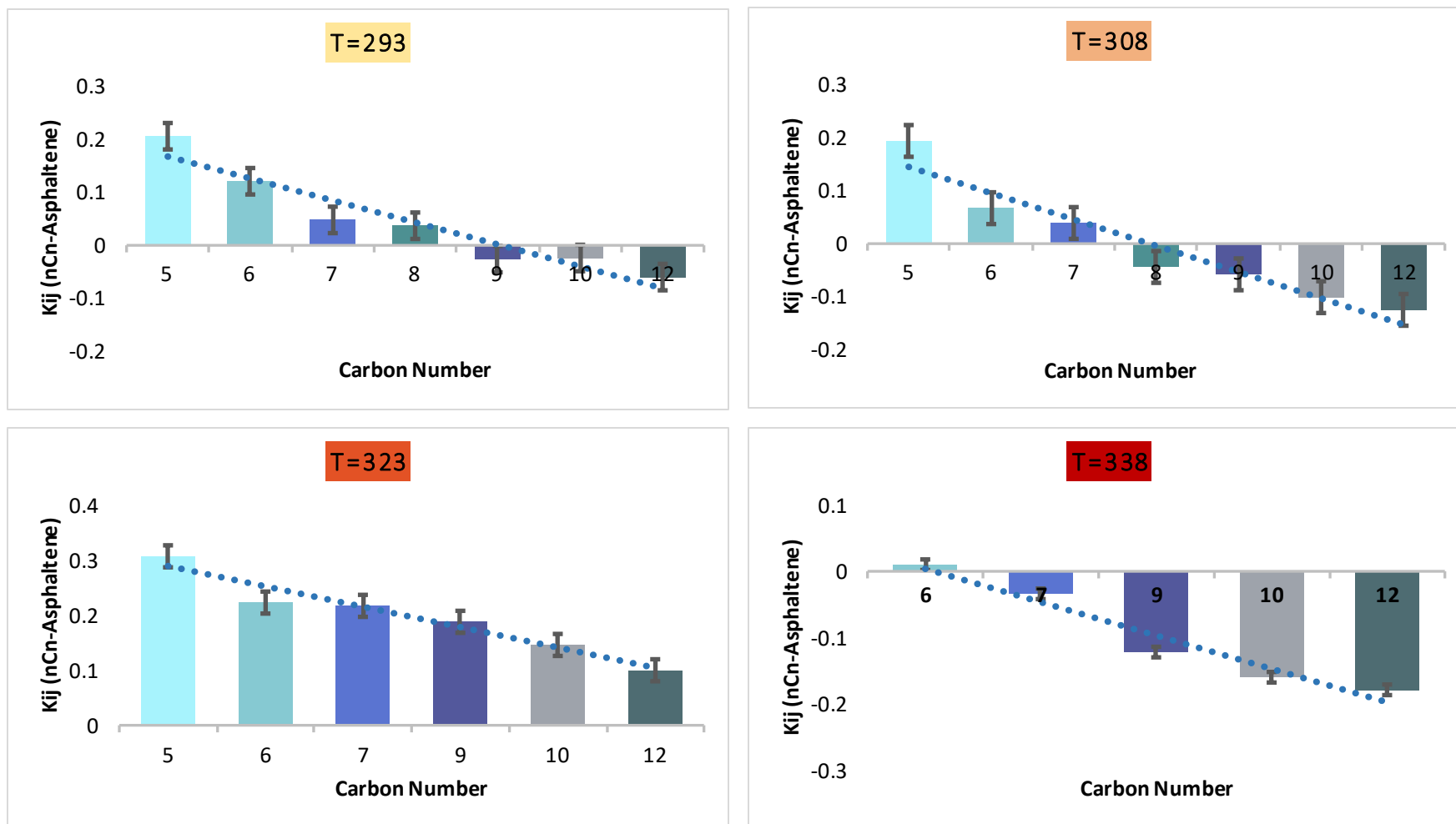
Figure 3-9. The optimized binary interactions between n-alkane and asphaltene, in different temperatures (293, 308, 323, 338 K) and using different n-alkanes
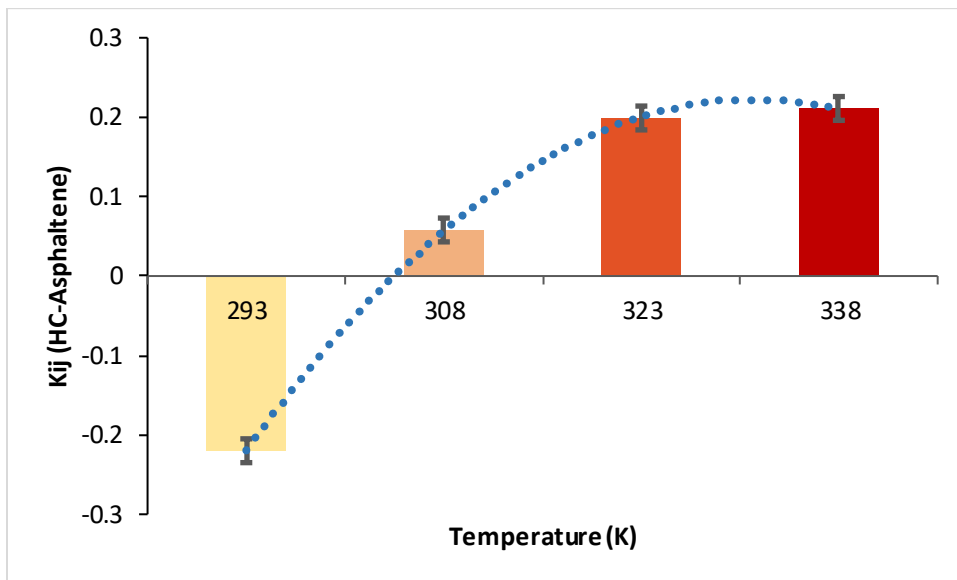
Figure 3-10. The optimized binary interactions between heavy hydrocarbon fractions and asphaltene in different temperatures (293, 308, 323, 338 K)
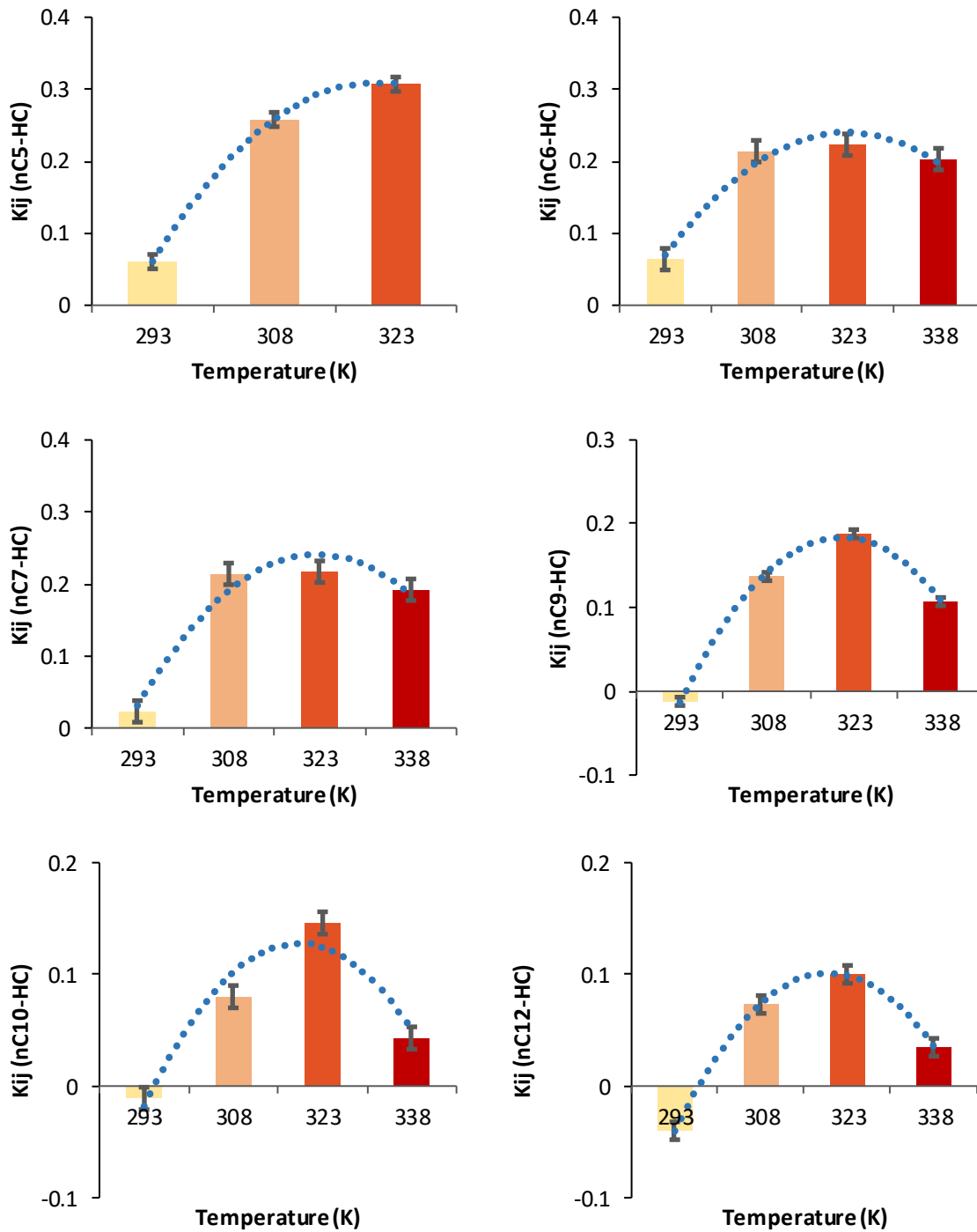
Figure 3-11. The optimized binary interactions between n-alkane and heavy hydrocarbon fraction, in different temperatures (293, 308, 323, 338 K)
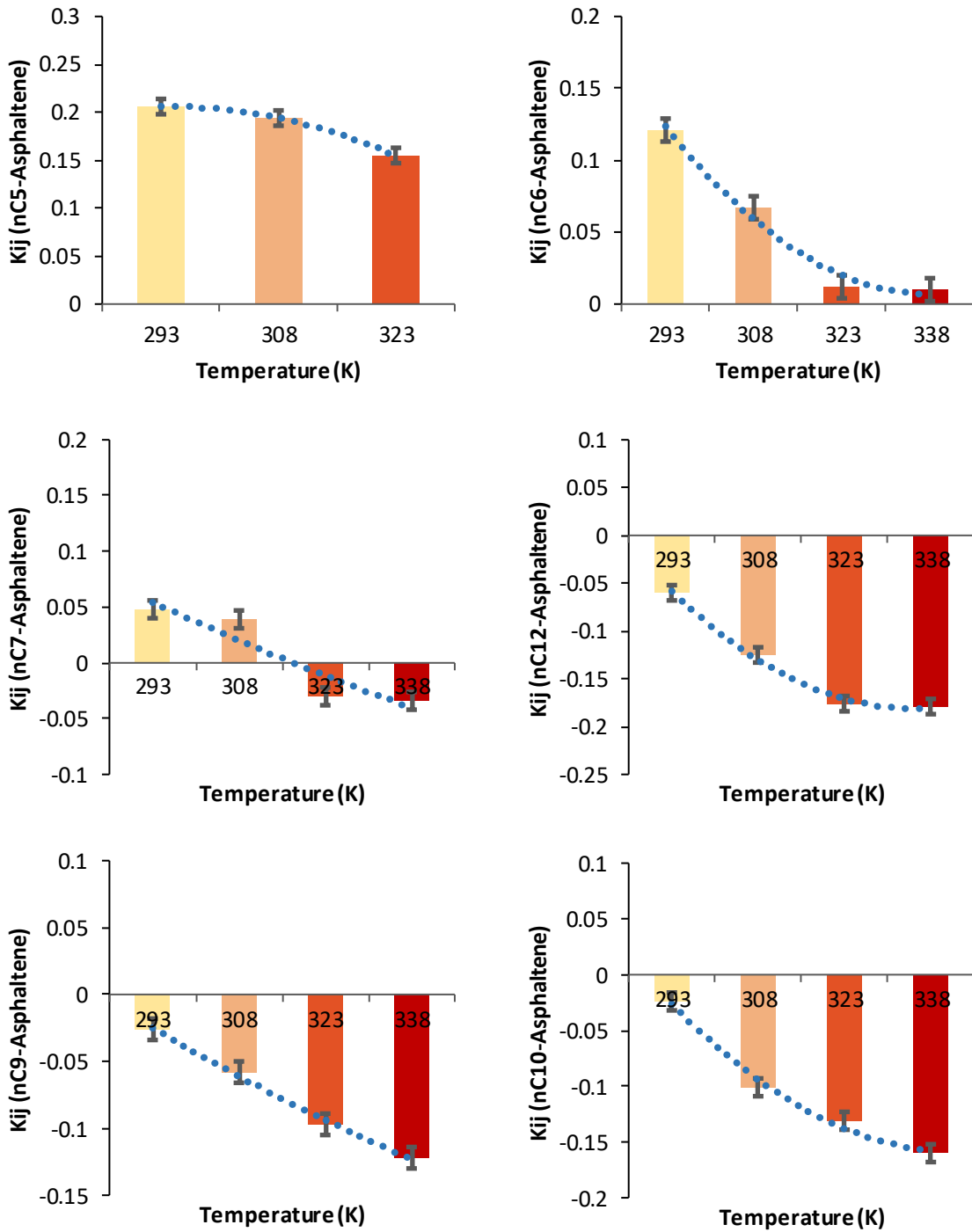
Figure 3-12. The optimized binary interactions between n-alkane and asphaltene, in different temperatures (293, 308, 323, 338 K)
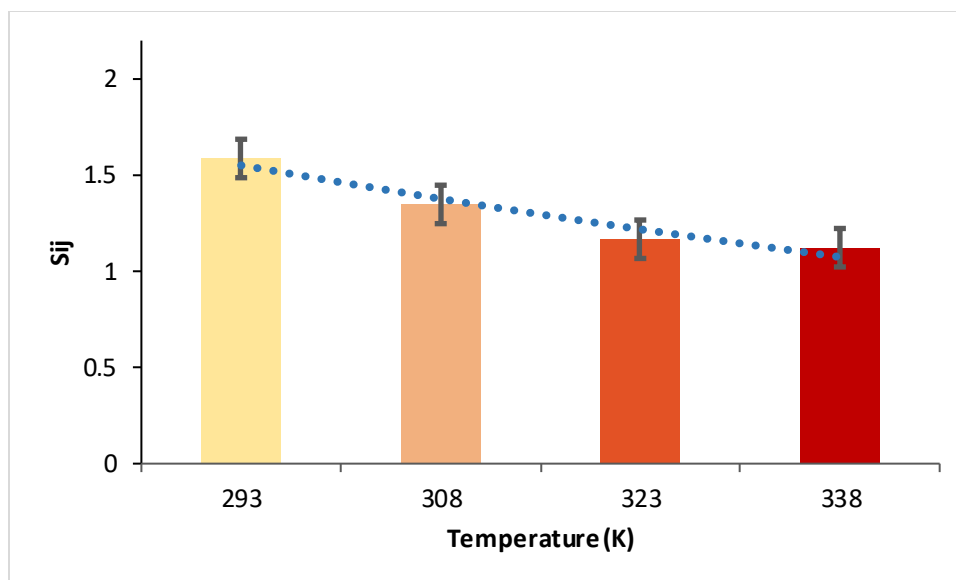
Figure 3-13. Cross association parameter (solvation factor) in different temperatures (293, 308, 323, 338 K), correlated as Sij=a-b/T

3-3-2. Asphaltene and Association Schemes

An examination of different schemes for asphaltene was completed to choose the best scheme for the current research. In the literature, the schemes that have been used most frequently include 2B (one lone pair of electrons and one hydrogen atom), 3B (one site for the two lone pairs of electrons and one site for each hydrogen atom, or one site for the two hydrogen atoms and one for each of the pair of electrons), and 4C (two lone-pairs of electrons and two hydrogen atoms). However, in this research, some data has been used to evaluate the performance of the CPA using Absolute Average Deviation Error (AAD%) as the evaluation criteria. After estimating BIPs, the 4C scheme showed a better performance with a lower error percentage. A summary of the evaluation of different schemes is shown in Table 3-4.

Table 3-4. Examination of different schemes for asphaltene in the CPA model

Association scheme	T (K)	k_{ij}		AAD%[a]
		Asp-C$_5$	Asp-HC	
2B	308	0.2748	-0.7023	0.0505
3B	308	0.6416	0.3357	0.4739
4C	308	0.194	0.058	0.0401

[a] $AAD\% = {100}/{n_p} \times \Sigma \, {|\psi^{cal} - \psi^{exp}|}/{\psi^{exp}}$, ψ is the number of moles

In this work, asphaltene particles were considered molecules with four association sites that cause asphaltene particles to form aggregations. Asphaltene molecules were considered to tend to self-associate within four association sites and also tend to have cross-association with resin to be stabilized. The 2B scheme was suggested for the non-asphaltene fraction and showed good agreement with the modeling results. Therefore, the self-association is dominant, which makes asphaltene particles prone to precipitation and subsequent deposition. Since the heavy fractions do not show a self-association tendency, the solvation factor is considered the criterion for the solubility of the asphaltene in the oil phase. The cross-association independent parameters and correlation are shown in Table 3-3 and Figure 3-13.

3-3-3. Asphaltene Precipitation from n-Alkane Diluted Oil

Figure 3-14 shows the experimental asphaltene yield (weight percent of precipitation) using different precipitants and the corresponding data obtained from the CPA EoS at different temperatures, including 273, 308, 323, and 338 K. All figures show that the model correlations are in good agreement with the corresponding experimental data, which validates the accuracy of assumptions and methods that have been reviewed in Section 2. Increasing the amount of precipitants leads to a higher quantity of precipitation, no matter the carbon number of the precipitants or temperature [34, 58], which agrees with findings from the CPA EoS and is consistent with the results of the literature.

Slightly higher discrepancies were observed in the high quantity of n-alkanes. Sabbagh et al. [55] also noticed the same disagreement. The following reasons can explain this discrepancy. First, it may be due to the precipitation of resin, which is not considered in the precipitated phase. Second, the discrepancy may be due to the trapping of maltene (saturate, aromatic, and resin) at high

magnitudes of precipitants, which is neglected in the dense phase. Third, there is the possibility of the formation of multiple liquids and/or solids, which is not incorporated in the modeling approach [55]. Lastly, there might also be an error while measuring the experimental data, as this type of error is inevitable. In addition to the above, we performed data analysis using SPSS software and used the Shapiro-Wilk test. The test showed interesting results, proving that the data reported for the higher amount of precipitants, specifically for dilution ratios over 20 cm^3/g of oil, is not normally distributed, confirming the discrepancies in the higher amount of precipitants. In addition, the boxplot analysis revealed some outlier data in the lower amount of precipitant. Please see supplementary information (Appendix B) for more information regarding the data analysis.

The error margin for their measurement was not reported in the reference article for experimental data [44]. However, an acceptable error margin was reported in the literature as approximately 0.02 wt% [59].
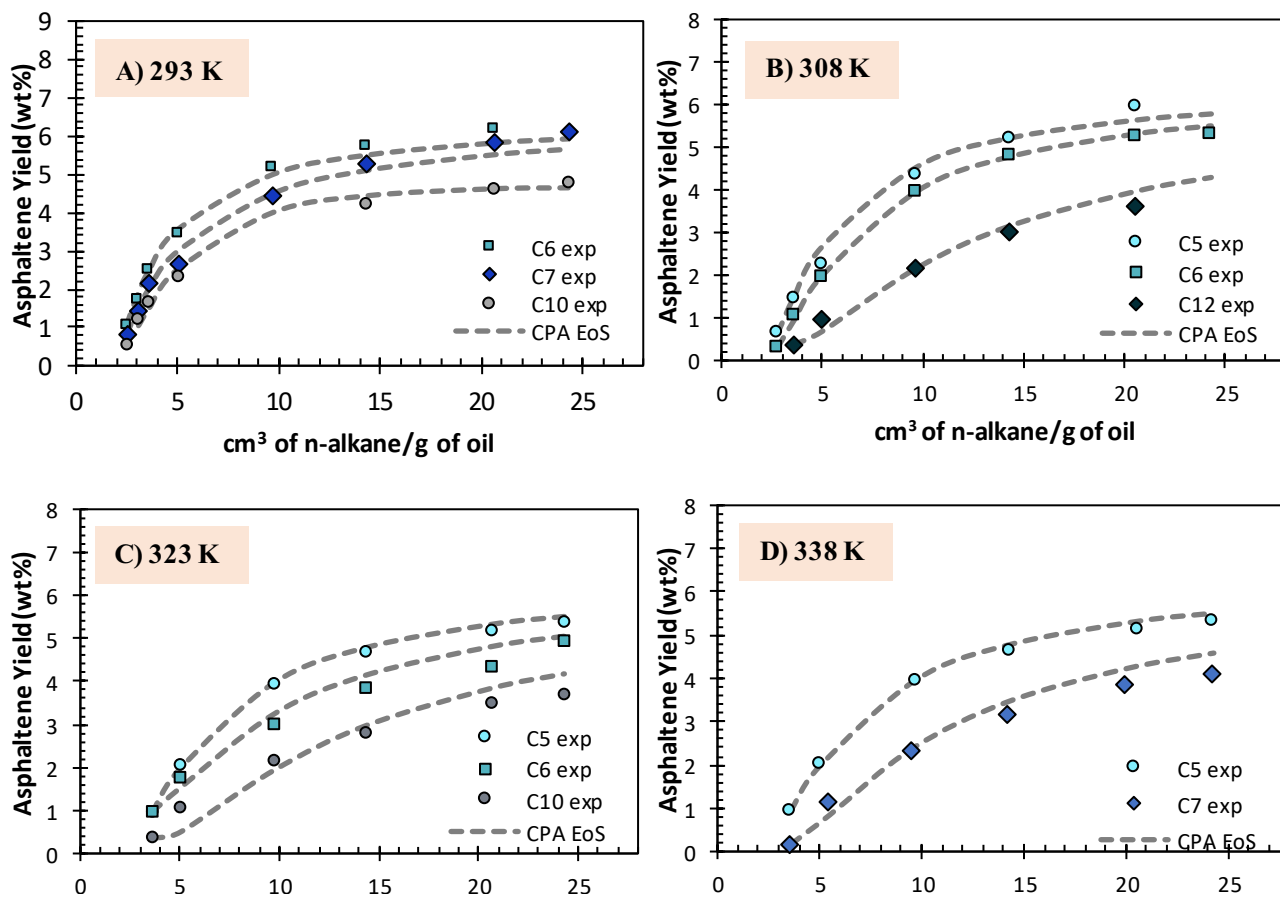
Figure 3-14. Experimental data and CPA model of asphaltene yield (wt%) with n-alkanes, A) Temperature=293 K, B) Temperature=308 K, C) Temperature=323 K, Temperature=338 K

pressure. These figures demonstrate that the results of the approach are in good agreement with the corresponding experimental data, representing the accuracy of the methods used in this research in the application of the CPA EoS, including characterization, optimization, and algorithm. Generally, the solubility of asphaltene in crude oil increases at high temperatures and causes less precipitation. The CPA EoS accurately showed this phenomenon.

However, comparing the results of the four temperatures (293, 308, 323, 338 K), one might notice a slight deviation working at the higher temperatures. This discrepancy might be attributed to the fact that measuring the amount of asphaltene precipitation is difficult at higher temperature due to the difficulties in the consistency of data gathering [55]. Moreover, the analysis of the experimental data, including temperature (independent variable) and asphaltene yield (dependent variable), also revealed the relatively poor normality of data at the higher temperature. It is worth mentioning that the non-normal distribution of data might lead to difficulties in optimization and, consequently, discrepancies in correlations/predictions at the higher temperature.

In addition, adjusting the binary interactions while using constraints to limit them with the specific correlations/trends may cause inconsistencies. The suggested correlations for BIPs ($K_{ij}=f(T)$, $K_{ij}=f(CN)$, & $K_{ij}=f(T, CN)$) are proposed considering simple mixtures [57], while the correlation/trends might be more complex for non-binary asphaltene mixtures. For instance, a second-degree polynomial equation was suggested to correlate K_{ij} with temperature. The absolute amount of K_{ij} has been shown to decrease at higher temperatures while maintaining a linear trend with the carbon number of the precipitant. Although the BIPs calculated from the suggested correlations could accurately model asphaltene precipitation, a slight divergence was observed at the higher temperature, showing less normality of the data (supplementary information (Appendix B)). Table B-2 of this information shows the experimental data's normality test results (Shapiro Wilk test) measured in different temperatures, i.e., 293, 308, 323, 338 K. The null hypothesis of this test examines if a variable is normally distributed in some populations. Thus, the null hypothesis is rejected if the p-value (significant indicator) is less than the chosen alpha level (5% of confidence level). The test results (Table B-2) show that the experimental data is not normally distributed at the higher temperature, i.e., 323 and 338 K. Hence, the hypothesis is not confirmed at a 5% confidence level for higher temperatures. Using this data (not normally distributed) for higher temperature increases the chance of not finding the best fit for the binary parameters, e.g.,

binary interaction parameters and cross-association. To remedy the non-normal distribution problem, one may suggest adding population. Non-normal data means data is either skewed or contains a small number of highly unusual observations, known as 'outliers,' which decreases the chance of optimizing the best fit to the adjustable parameters. All in all, the strong impact of BIPs on the accuracy of the thermodynamic models was evidenced. Besides, the data analysis also revealed that the accuracy of the correlation and prediction ability of the CPA EoS approach is highly dependent on the normal distribution of the experimental data used to adjust the model.
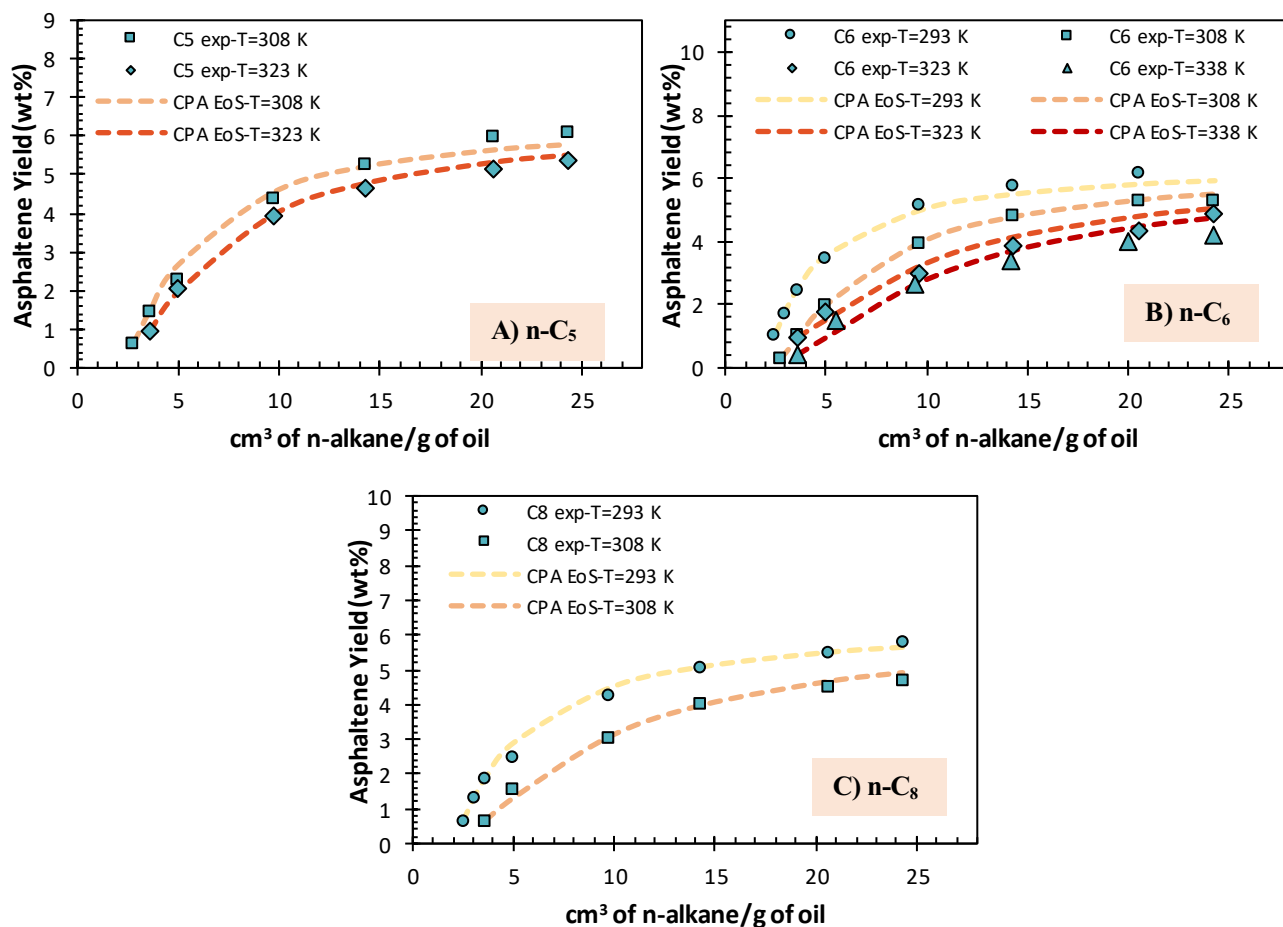
Figure 3-15. Experimental data and CPA model of asphaltene yield (wt%), A) n-C_5 at different temperatures (T=308 & 323 K), B) n-C_6 at different temperature (T=293, 308, 323, 338 K), C) n-C_8 at different temperature (T=293 & 308 K)

3-3-5. Asphaltene Precipitation from n-Alkane Diluted Oil and Carbon Number

Figure 3-16 demonstrates asphaltene yield in different carbon numbers of precipitants, diverse temperatures, and two different quantities of n-alkane (R=3 & 14.3 cm³/g of oil). It has been stated that hydrocarbon with a lower carbon number leads to a higher amount of asphaltene precipitation due to lower density and dielectric constant [43]. The lower density precipitant results in the higher attractive energy parameters between solvent and asphaltene, and consequently, the amount of precipitation increases, as shown in the figures. In these figures, the horizontal axis was assigned to the carbon number of the diluents, and the vertical axis represents the asphaltene yield. The findings of the CPA EoS are in good agreement with the corresponding experimental data. The slight discrepancies observed at the higher carbon number can be attributed to the non-normal distribution of data (supplementary information (Appendix B)) or error engaging in measuring the experimental data. Furthermore, precipitants with higher carbon numbers may trap maltane (saturate, aromatic, and resin) in the dense phase.
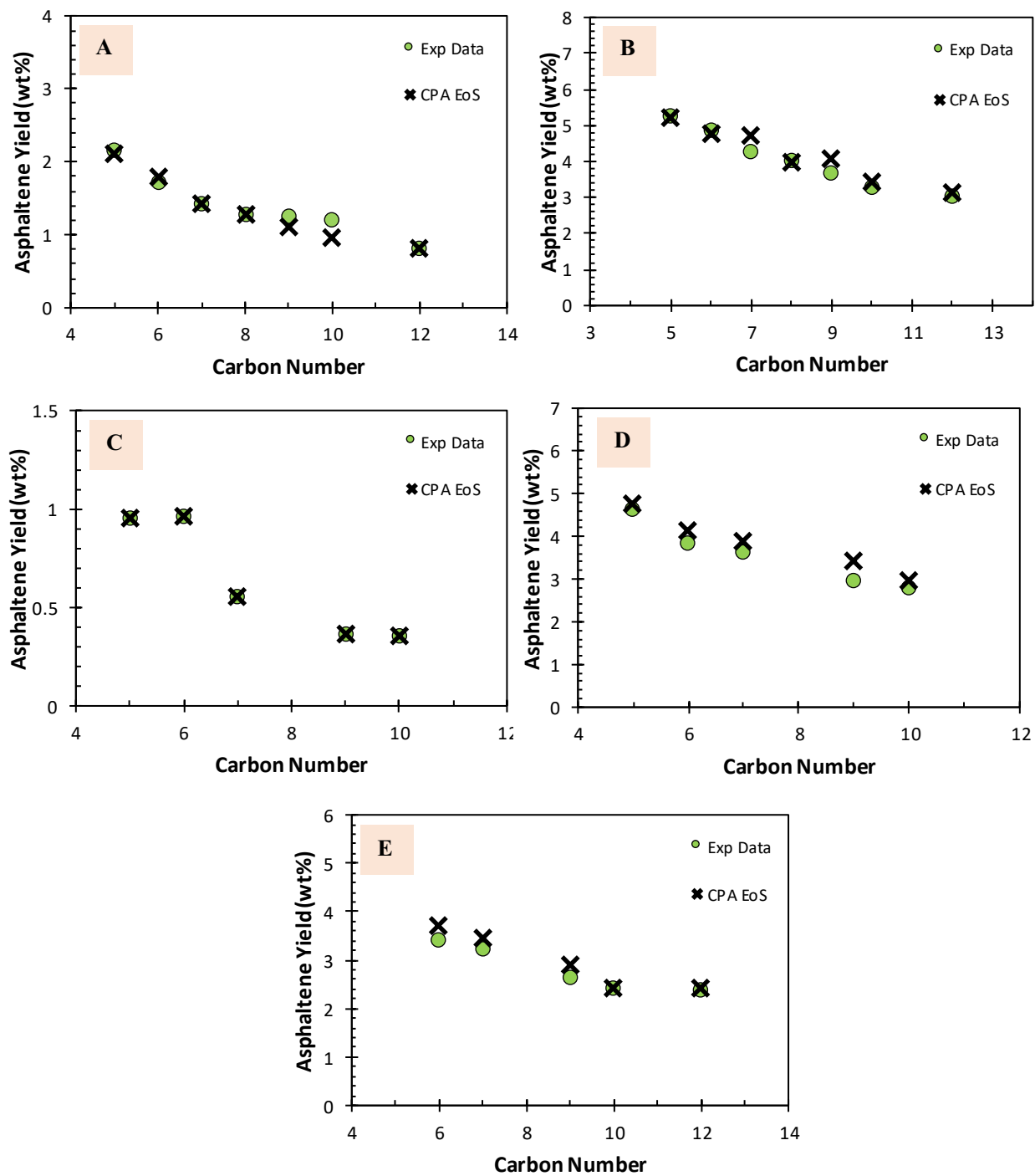
Figure 3-16. Experimental data and CPA model of asphaltene yield (wt%) using different n-alkane (C5-C12). A) R= 3 cm3/g of oil and constant temperature= 293 K, B) R= 14.3 cm3/g of oil and constant temperature= 308 K, C) R= 3.6 cm3/g of oil and constant temperature= 323 K, D) R= 14.3 cm3/g of oil and constant temperature= 323 K, E) R= 14.2 cm3/g of oil and constant temperature= 338 K

3-3-6. Validation of the Approach

In section 3-3-6, the CPA EoS model is validated by evaluating the prediction capabilities of this model for unseen data and onset point of asphaltene precipitation, comparing the results of the CPA EoS with cubic EoS, i.e., SRK and PR, demonstrating the CPA EoS tuned with GO, GA, and NM simplex methods, showing the results from using different oil characterization methods, and finally compares the CPA EoS with scaling model.

3-3-6-1. Prediction Capability of the CPA EoS

Figure 3-17 and Figure 3-18 show the predictions of asphaltene precipitation when diluted with n-pentane and n-heptane, respectively. The effects of temperature and amount of n-alkane on the phenomena are examined. As the experimental data was not available in those conditions, only the predictions of the CPA model are presented.

As demonstrated in the figures, the model responded to increasing temperature and amount of the diluents as expected from theories of asphaltene precipitation. The solubility of asphaltene increases with increased temperature, and increasing the amount of n-alkane alters the solubility of asphaltene and will lead to more precipitation. It should be noted that conducting the test at various temperatures and diluents consume resources; hence the prediction capability of the CPA approach in different temperature and quantity of n-alkane is highly valued. The same behaviour and response of the CPA approach using different n-alkane were observed, but the results are not included here.
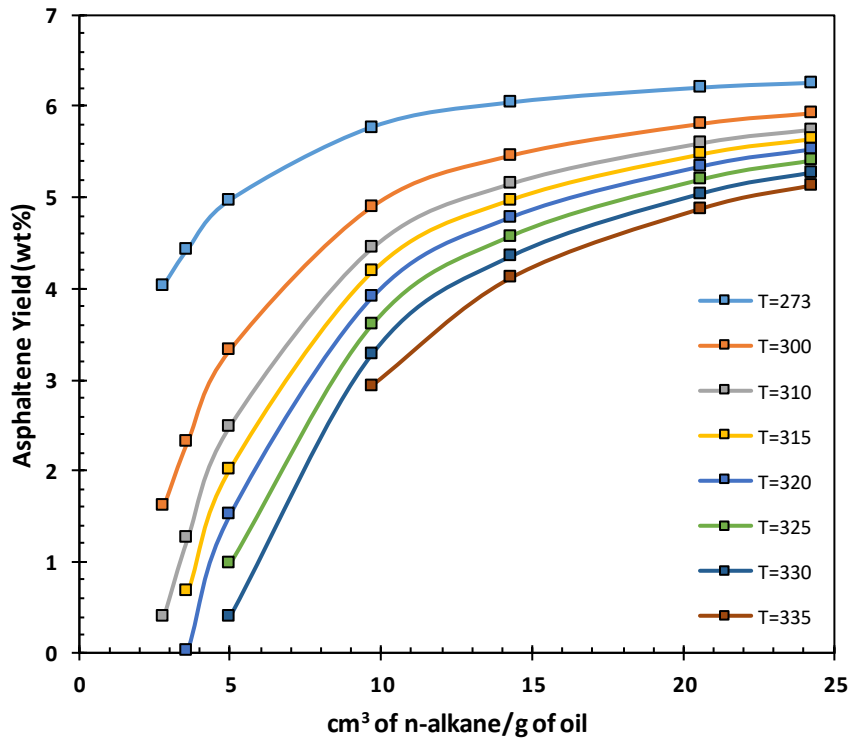
Figure 3-17. Asphaltene precipitation predicted by CPA EoS approach using normal pentane at T=273, 300, 310, 315, 320, 330, 335 K
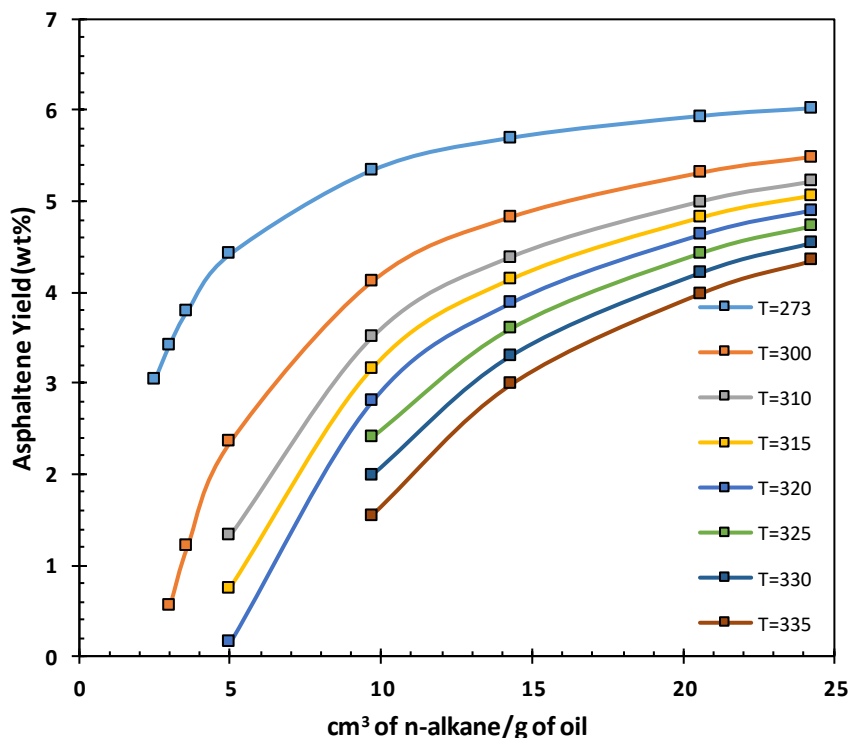
Figure 3-18. Asphaltene precipitation predicted by CPA EoS approach using normal heptane at T=273, 300, 310, 315, 320, 330, 335 K

One can see that the CPA approach was not able to predict the amount of precipitation at higher temperatures and low amounts of precipitant. First, this can be attributed to the fact that the data that was used to adjust the model was not normally distributed at the higher temperature. Second, it might be due to the fact that the onset point of asphaltene increases at a higher temperature.

Figure 3-19 depicts asphaltene onset conditions at different temperatures and using n-alkanes (nC_5-nC_{12}). The experimental data of the onset point was measured using the light scattering method [44] and a three-step approach. First, asphaltene is precipitated by adding n-alkane step-wise with a 1 mL increment. Second, the onset point was repeated using smaller increments (0.2 mL) to achieve higher accuracy. Third, step 2 was repeated using smaller increments, ±0.1 mL, to determine a more precise onset point. Although the process seems to be repeated more than once with higher accuracy, the relative standard deviation of the measurements was not reported. Since the onset point of asphaltene using the optical method is sensitive, having the measurement error is helpful in evaluating the modeling approach capabilities. Tharanivasan et al., 2009 [60] reported the repeatability of the measured yields was between ±5 and ±14, depending on the n-alkane used.

Considering these values of repeatability and onset prediction of asphaltene shown in Figure 15, the CPA approach is reasonably capable of predicting the onset condition of the asphaltene precipitation.
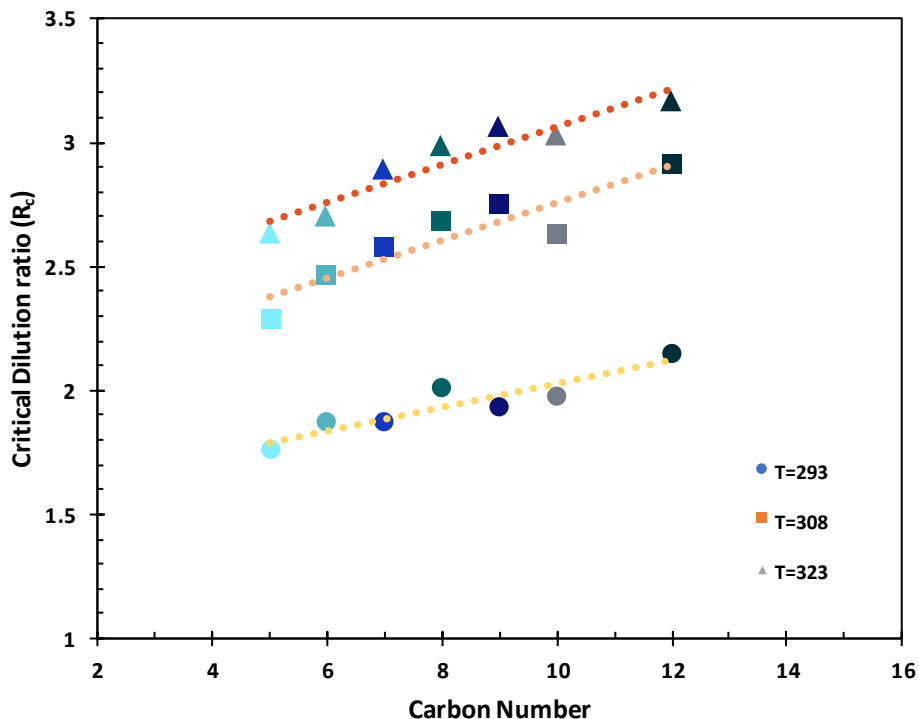
Figure 3-19. Predictions of the CPA EoS approach of the onset point using different n-alkanes (nC$_5$-nC$_{12}$). The circle symbol is determined by the optical method [44]

3-3-6-2. CPA EoS Versus Cubic EoS, i.e., SRK and PR

CPA EoS is an extension of the cubic EoS, adding an association part representing chemical interactions of the particles, e.g., hydrogen bonding. In the current research, the SRK EoS represents the physical term, and the association part is added to consider self and cross-association of the oil fractions. Adding this extension to the cubic EoSs is expected to increase their reliability and capability. Hence, the CPA model is compared against the cubic EoS, i.e., SRK and PR, to validate one of the assumptions used in this study which is the importance of self and cross association between asphaltene-asphaltene particles (in both phases in the equilibrium) and asphaltene-maltene fractions (in the oil phase of equilibrium), respectively.

Figure 3-20 depicts the CPA, SRK, and PR EoSs to compare the modeling capabilities of these methods. It is demonstrated that CPA EoS has a much better ability to predict/correlate asphaltene precipitation yield and approve the early assumption that association energy, i.e., hydrogen bonding, along with van der Waals forces, play a significant role in aggregation and precipitation of asphaltene particles and considering association parts in the cubic EoSs can increase their reliability significantly.
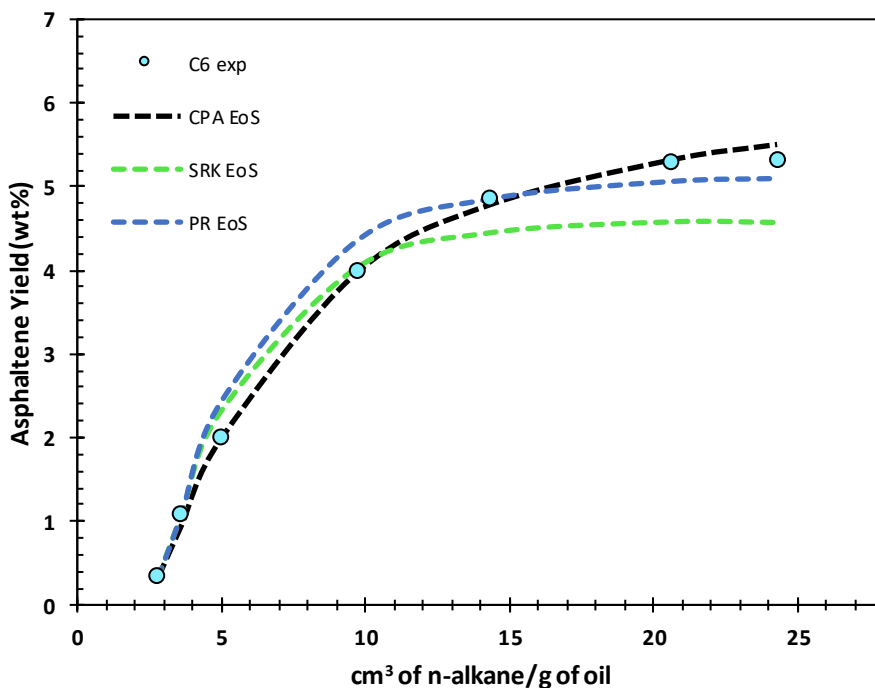
Figure 3-20. Asphaltene yield during adding normal hexane (nC6) as precipitants and T=293 K. The lines represent the EoSs, and the symbols represent the experimental data, R^2 (CPA)= 0.99, R^2 (SRK)= 0.97, R^2 (PR)= 0.98

3-3-6-3. Comparison of Using Global Optimization (GO), Genetic Algorithm (GA), and Local Optimization of NM Simplex Method to Tune CPA EoS

Equation of states, e.g., CPA EoS, are mathematical models consisting of algebraic and differential equations representing the relationship between thermodynamic variables, i.e., dependent and independent thermodynamic properties. Some parameters of the EoS are not measurable and need to be estimated from experimental data using objective functions. The EoSs are nonlinear models and require an iterative procedure to estimate those non-measurable parameters of the EoS and

minimize the objective function. Besides, the minimization of the objective function/functions is challenging due to the existence of the local minima. Hence, there is a need to use a global and robust optimization method to find the global minima and reduce the computational cost.

In this research, global optimization (GO) was adopted to estimate the parameters of the CPA EoS. While the need for using a GO and the possibility of the existence of the local minima have been shown in section 2-4, the performance of the CPA EoS using GO, GA, and NM Simplex is demonstrated in Figure 3-21. This figure shows the asphaltene yield experimental data using normal nonane as a precipitant and the modeling results of the CPA EoS using optimization methods. It is evident that using GO to estimate parameters of the CPA EoS, i.e., binary interactions, decreases the deviation of CPA EoS from the experimental data to about 5%, while using the GA and NM Simplex methods have deviations of 7.5% and 21%, respectively.
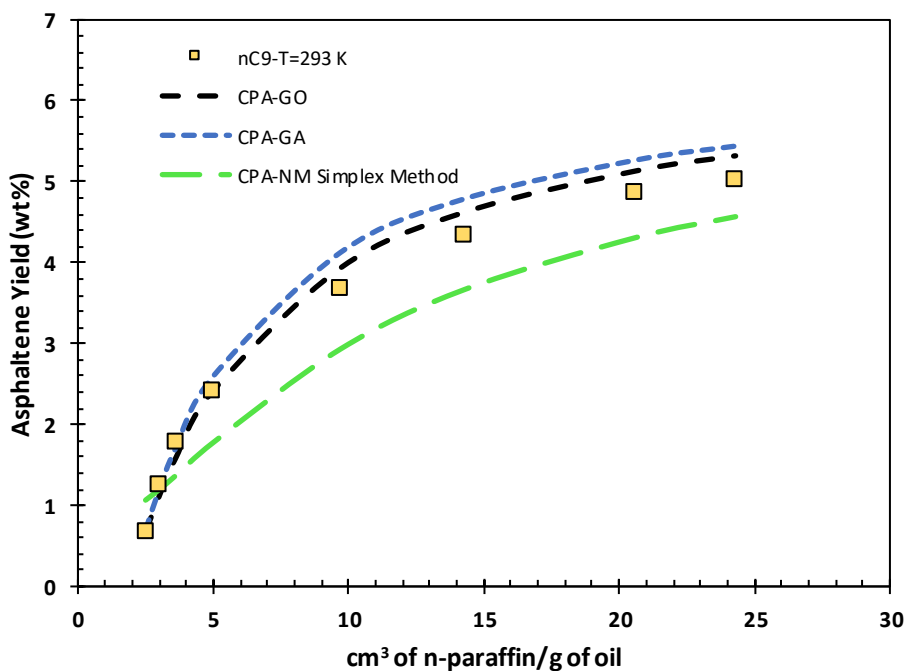
Figure 3-21. Asphaltene yield during adding normal nonane (nC9) as precipitants and T=293 K. The lines represent the EoS using different optimization methods, and the symbols represent the experimental data, R^2 (CPA-GO)= 0.98, R^2 (CPA-GA)= 0.97, R^2 (CPA-NM Simplex)=0.92

3-3-6-4. Oil Characterization Validation, SARA Analysis and HC-Asphaltene

Characterization of the oil sample is one of the critical steps for using an EoS. The oil blend can be defined as a mixture of similar components/fractions to reduce the computational cost due to decreasing the number of adjustable parameters, e.g., binary interaction parameters. In this research, we adapted the characterization method by Arya et al., 2016 & 2017 [43, 49], and the oil sample is divided into two categories, asphaltenic and non-asphaltenic fractions. The non-asphaltenic fraction includes maltane (saturates, aromatics, and resins), which are lumped and introduced as heavy component (HC). Self-association and cross-association are considered in both the oil and precipitated phases. While the oil phase is controlled by the self-association of asphaltene particles and cross-association between HC and asphaltene to stabilize asphaltene particles, the precipitated phase is dominated by self-association between asphaltene particles.

Figure 3-22 demonstrates how using the oil characterization method impacts the EoS and accuracy of the model. Using the characterization method of this research (HC-Asphaltene) increases the accuracy of the modeling by 3% in comparison with using SARA analysis as the characterization method. It is worth mentioning that using SARA analysis for oil characterization increases the computational time due to a significant number of adjustable parameters, i. e., binary interaction parameters. The characterization method used in this research only needs three binary interactions to be tuned, while using the SARA analysis increases the number of tuning parameters to at least seven, in the condition of disregarding the interactions between saturate-aromatic, saturate-resin, and aromatic-resin.
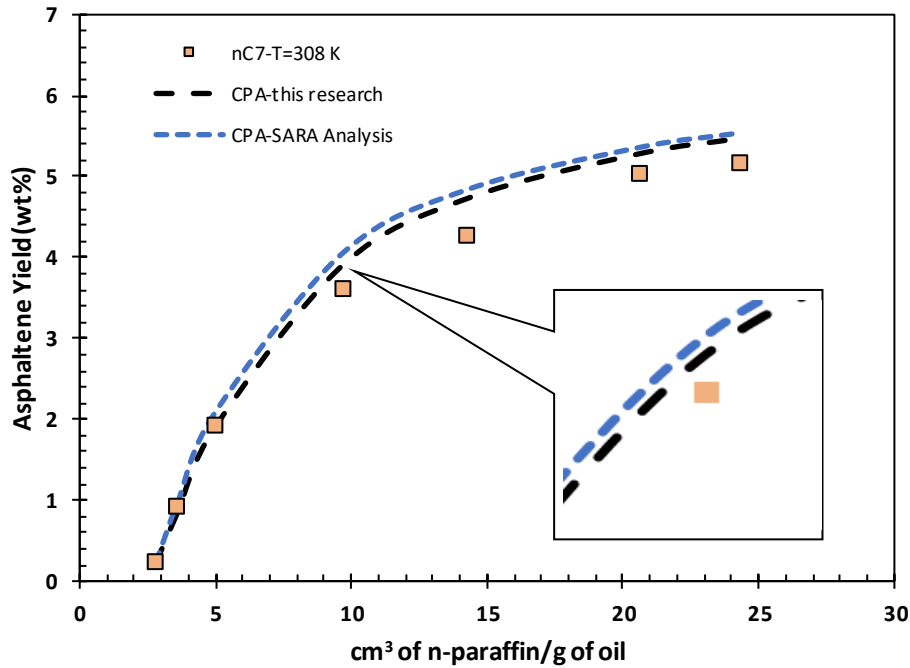
Figure 3-22. Asphaltene yield during adding normal heptane (nC7) as precipitants and T=308 K. The lines represent the EoS using different characterization methods, and the symbols represent the experimental data, R^2 (CPA-this research) = 0.98, R^2 (CPA-SARA Analysis) = 0.97

3-3-6-5. CPA EoS and Scaling Model

To analyze the robustness of the CPA EoS, the model is validated against the scaling model proposed for asphaltene precipitation phase behavior. The scaling model is a simple three-parameter equation that relates the weight percent of asphaltene precipitation (*wt%, g/g*) to the dilution ratio (*R, cm3 of n-alkane/g of oil*) and the molecular weight of precipitant (*Mw, g/mol*). The model follows the analogy between the cluster-size distribution of asphaltene aggregates and precipitation. The scaling model defines a universal trend for $Y \left(= {wt\%}/{R^{\acute{z}}}\right)$ versus $X \left(= {R}/{Mw^z}\right)$. In these equations, Z and $\acute{Z}$ are constants; while the former is an adjustable parameter, the latter is universal and equal to -2. The other operating conditions, i.e., pressure and temperature, were later included in the equation; nevertheless, the equations can only consider one of these operating conditions simultaneously.

Figure 3-23 demonstrates the modeling capabilities of the CPA EoS and scaling model in different compositions and temperatures (e.g., 308 and 323 K). Comparing the experimental data and these models, it is shown that the CPA EoS is superior to the scaling model and provides insight into the interaction of particles, PVT properties, and predicts unseen data. It is also more reliable in the correlation of the experimental data.
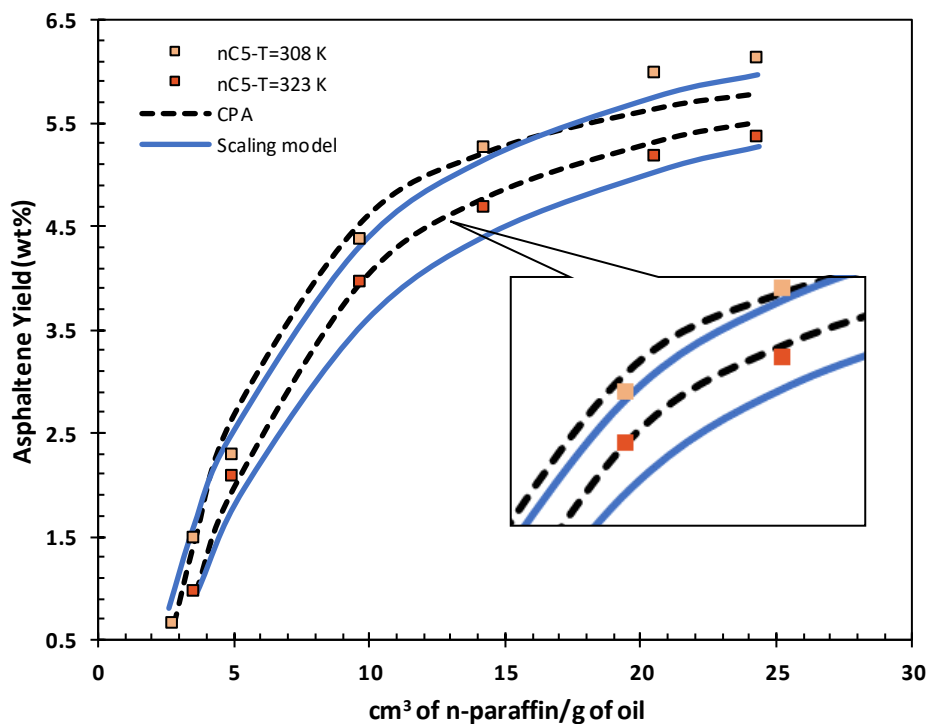
Figure 3-23. Asphaltene yield during adding normal pentane (nC5) as precipitants and T=308 and 323 K. The dashed lines represent the EoS, and blue line represents the scaling model, and the symbols represent the experimental data, R^2 (CPA)= 0.99, R^2 (Scaling model)= 0.95

3-3-7. Relative Importance (RI) Analysis

The relative importance analysis is used to indicate a supplement to the thermodynamic model for dividing variance among multiple independent variables and explaining the role of each independent variable. For this purpose, a two-relative importance analysis (Pearson's correlation coefficient or Pearson's R) is used to measure the strength of the association between two continuous variables. This coefficient is commonly used in linear regression. It provides information about the magnitude of the association, or correlation, and the direction of the relationship between two continuous variables. However, it cannot differentiate between dependent and independent variables, and this is the user's responsibility to define these

parameters. Pearson's coefficient represents the covariance ratio of two desired variables to the product of their respective standard deviations. It is worth mentioning that there are limitations while applying the relative importance for the prediction of the dependent variable. However, it can accurately be used to show the impact of each independent variable on the outcome [61].

This coefficient can have a value of [-1, +1], where 1 and -1 indicate a strong positive and negative monotonic relationship. The smaller absolute amount of this coefficient means a weaker relationship between the two variables. A zero coefficient will indicate no association between the two variables [61].

Figure 3-24 shows the impact of the dilution ratio, temperature, and carbon number of the diluents (n-alkane) on the quantity of precipitation using the CPA EoS. The test reveals that the amount of the n-alkane significantly impacts the asphaltene precipitation with RI= +0.719, which is experimentally sensible. The type of n-alkane (carbon number) has the second most substantial impact on the phenomenon negatively. The RI value for the carbon number of the n-alkane is -0.247, showing that using heavier n-alkane leads to a decrease in the quantity of precipitation. The last decisive parameter of the phenomenon is the temperature with RI= -0.195 and a negative impact.
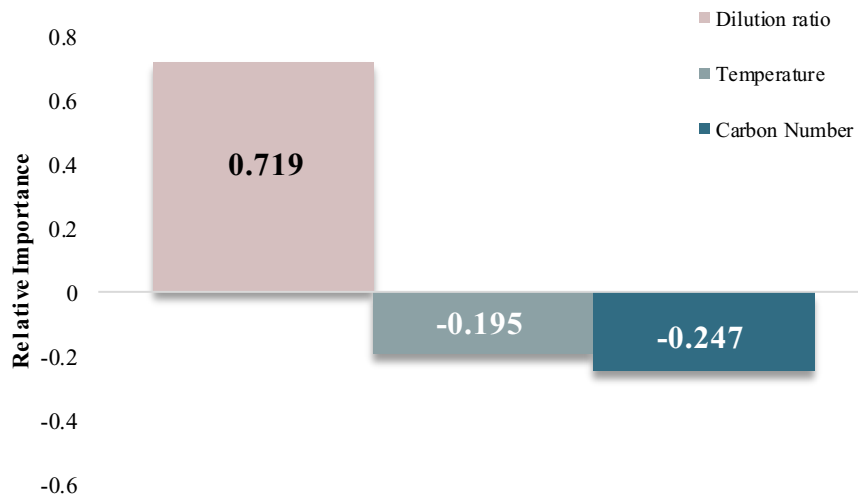
Figure 3-24. The relative importance of independent variables on the amount of precipitation using CPA EoS

Figure 3-25 depicts the RI values for the input parameters on the binary interactions for two systems of n-alkane-heavy fraction (nC$_n$-HC) and n-alkane-asphaltene (nC$_n$-Asp). It has been shown that the type of n-alkane (carbon number of the diluent) has the most decisive impact on the binary interactions of the systems in a negative direction. The temperature impact was ranked second for the two systems, nC$_n$-HC and nC$_n$-Asp. While the effect of temperature on the former is positive, it negatively affects the latter. This dual behaviour can be attributed to the critical region of the system and, accordingly, reduced property of asphaltene.
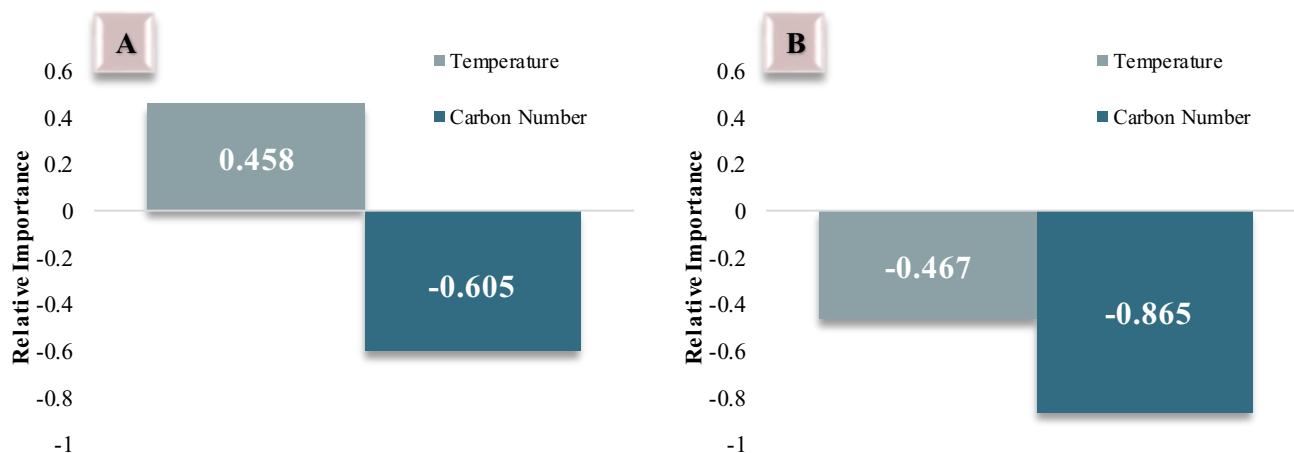
Figure 3-25. Relative importance of independent variables (temperature and carbon number of the n-alkane) on the binary interaction parameters, A) K$_{ij}$ of n-alkane and heavy fractions (K$_{ij}$(nC$_n$-HC)), B) K$_{ij}$ of n-alkane and asphaltene (K$_{ij}$(nC$_n$-asp))

3-3-8. Relative Deviations between Experimental Data and Modeling Results of the CPA Approach

Table 5 presents the average relative deviation in calculating the asphaltene yield and onset conditions for all data studied in this work. The average relative deviation is a good indicator to show the reliability and accuracy of the CPA approach [62]. The results of asphaltene yield are categorized considering two criteria, temperature and n-alkane.

First, the deviation related to modeling asphaltene yield using different n-alkane is reported. Using normal pentane showed the lowest deviation and best modeling results obtained. This can be justified by the data analysis results and normal distribution of the experimental data used in this section. One can see that normal octane also had a low error because there were only a few experimental data to compare the modeling results (data to higher temperatures were not

available); hence, a low deviation is reported. Slightly higher discrepancies are observed while using dodecane at the precipitant. This discrepancy can be explained by the precipitation of resin, trapping of maltene (saturate, aromatic, and resin), the possibility of forming multiple liquids and/or solids, and an error while measuring the experimental data. Besides, applying the Shapiro-Wilk test revealed that the data using dodecane was the least significant data used in this research. By contrast, the data used for normal pentane as precipitants were highly significant (supplementary information (Appendix B)).

In addition, the relative deviations were studied at different temperatures. As expected from the Shapiro-Wilk distribution test, the temperature=273 K showed the lowest deviation because it has the best significant parameters for normal distribution (the lower the significant indicator is, the better normally distributed the data are).

The deviations in predicting the onset condition (the critical dilution ratio (R_c)) are also presented in Table 5. The approach was reasonably capable of predicting the onset of asphaltene. Considering the relative deviations reported in Table 5, the proposed CPA approach was reasonably capable of modeling and predicting asphaltene precipitation in different temperatures and n-alkane.

While the application of the current research increases the reliability of the CPA EoS by incorporating GO, it is a prototype that may need further improvements to be applied for more experimental data other than those used here.

Table 3-5. Average Relative Deviation of the CPA approach for different temperatures and n-paraffin

<table>
<tr><td colspan="9" align="center">**Average Relative Deviation**</td></tr>
<tr><td rowspan="4">**Asphaltene Yield**</td><td>Mixture</td><td>nC_5+Oil</td><td>nC_6+Oil</td><td>nC_7+Oil</td><td>nC_8+Oil</td><td>nC_9+Oil</td><td>nC_{10}+Oil</td><td>nC_{12}+Oil</td><td>Temperature</td></tr>
<tr><td>Error</td><td>0.03</td><td>0.05</td><td>0.065</td><td>0.035</td><td>0.077</td><td>0.085</td><td>0.145</td><td>293-338 K</td></tr>
<tr><td>Temperature</td><td colspan="2">293 K</td><td colspan="2">308 K</td><td colspan="2">323 K</td><td colspan="2">338 K</td></tr>
<tr><td>Error</td><td colspan="2">0.065</td><td colspan="2">0.057</td><td colspan="2">0.093</td><td colspan="2">0.086</td></tr>
<tr><td rowspan="2">**Onset Predic**</td><td>Mixture</td><td>nC_5+Oil</td><td>nC_6+Oil</td><td>nC_7+Oil</td><td>nC_8+Oil</td><td>nC_9+Oil</td><td>nC_{10}+Oil</td><td>nC_{12}+Oil</td><td>Temperature</td></tr>
<tr><td>Error</td><td>0.02</td><td>0.02</td><td>0.04</td><td>0.09</td><td>0.06</td><td>0.07</td><td>0.07</td><td>293-338 K</td></tr>
</table>

3-4. Theoretical and Practical Challenges in Asphaltene Precipitation Modeling Using CPA-GO Approach

Understanding the occurrence of asphaltene precipitation is crucial for managing reservoir fluids, including flow assurance and risk assessment. Due to the worldwide dispersion of reservoirs with asphaltene related issues, it is pivotal to know the challenges related to asphaltene precipitation modeling, both theoretical and practical. Asphaltene modeling is a complex process that involves understanding the behavior of asphaltenes in crude oil.

One of the theoretical challenges in asphaltene modeling using EoS is understanding the molecular structure of asphaltenes and determining the molecular weight of this fraction. Asphaltenes are composed of a complex mixture of molecules, and their molecular structure varies with the origin of the oil sample. The successful application of EoS to model asphaltene phase separation requires a comprehensive understanding of the molecular weight and structure of asphaltenes in the oil mixture.

Another major challenge in asphaltene modeling using EoS is the proper characterization of the fluid sample. Once working with crude oil, finding the best way to characterize the mixture to reduce the number of adjustable parameters is crucial. While a simplified characterization method with few adjustable parameters is time and cost-efficient, the characterization method should be able to accurately represent the fluid sample's characteristics.

In addition, the accuracy of a model is reliant on the consistency of the experimental data used to tune the model. Inaccurate or incomplete experimental data may lead to incorrect model predictions, as the model is only as reliable as the data on which it is based. Therefore, selecting appropriate experimental data is critical to ensure the accuracy and reliability of the model. However, the measurement of asphaltene precipitation experimentally can be challenging since the other fractions, e.g., resins, may also precipitate out of oil and impact the amount of precipitation measurement. Besides, maltene can trap in the dense phase and affect the precipitated phase measurements. In addition, there is the possibility of the formation of multiple liquids and/or solids [55]. Also, there might be an error while measuring the experimental data, as this type of error is inevitable. Lastly, the presence of impurities or other non-asphaltene materials in the crude oil can interfere with the measurement process, leading to inaccurate results.

Optimizing the adjustable parameters is one of the primary challenges of using an EoS, e.g., BIPs. The EoSs are highly nonlinear and gradient-based optimization methods, e.g., Nelder-Mead (NM)

simplex and Least Squares methods, are not capable of performing this complex optimization. Using the gradient-based optimization method has a high chance of entrapment in local optima and not being able to tune the adjustable parameters best. Therefore, it is suggested to use a global optimization technique to adjust the EoS; however, applying the global optimization technique is also challenging. This technique is dependent on the start point of the optimization; moreover, to ensure the model's accuracy, it is essential to meticulously establish its constraints.

3-5. Summary and Conclusions

In this research, asphaltene precipitation was studied through a systematic sensitivity analysis of the operating conditions and using a CPA approach, considering the association of hydrogen bonding and van der Waals interactions. A total of 174 experimental data were studied, and it was shown that the suggested approach could correlate with asphaltene precipitation conditions and predict the onset condition of asphaltene precipitation.

The oil was treated by the characterization method from Flory-Huggins EoS (the first EoS with application in the industry) to simplify the CPA EoS. A "global optimization (GO)" framework was employed to conduct the multi-variable optimization of the thermodynamic approach and improve the optimization of the EoS by decreasing the chance of getting stuck in the local optima. This multi-step process contains two main steps: global optima and local optima. These two steps are implemented sequentially to find the unique best optimum of the thermodynamic model. The former consists of the GlobalSearch, MultiStart, and Genetic Algorithms, and the latter is the Nelder-Mead simplex algorithm. The binary parameters, especially the binary interaction parameters (BIPs), play a significant role in the correlation and prediction capability of the thermodynamic model. Hence, thorough correlations were suggested and adjusted for finding BIPs and associations in the range of experimental data. The correlations were later examined in a broader range of operating conditions, and an acceptable performance was observed (average deviation of less than 0.067 for correlation and prediction).

It was shown that the asphaltene fraction could be treated as a monodisperse fraction rather than polydisperse to calculate the asphaltene yield and onset point. The 4C association scheme of the asphaltene was optimized by examining different schemes and comparing the error obtained. It was shown that the CPA approach could accurately simulate the asphaltene precipitation and onset

condition with acceptable accuracy. Slightly higher discrepancies were observed with a high quantity of n-alkane and high temperature. After analyzing the experimental data, it was revealed that the experimental data used to adjust the CPA approach are not normally distributed in some ranges, resulting in the discrepancies observed. Finally, the relative importance analysis demonstrated that the composition of the mixture (dilution ratio) is the most influential factor contributing to the asphaltene precipitation, followed by the carbon number of n-alkane and temperature.

ACKNOWLEDGEMENTS

Nomenclature

List of Abbreviations

API	American Petroleum Institute
CN	Carbon Number
CP	Cubic plus association
EoS	Equation of State
GA	Genetic algorithm
GO	Global optimization
HC	Heavy component
LLE	Liquid-Liquid equilibrium
LB	Lower bound
NM	Nelder-Mead
PC-SAFT	Perturbed-chain statistical associating fluid theory
PAH	Poly-Aromatic Hydrocarbon
PR	Peng-Robinson
SARA	Satrurate aromatic resin asphaltene
SRK	Soave–Redlich–Kwong

STO	Stock Tank Oil
TRFD	Time resolved fluorescence depletion
UB	Upper bound
WOA	without association

Variables/Parameters

A_i	Associating site (A) of molecule i
a_{ij}	cross energy
a_0	physical energy parameter of CPA EoS [Pas m^2 mol^{-2}]
B_j	Associating site (B) of molecule j
b	co-volume parameter of CPA EoS [m^3 mol^{-1}]
b_{ij}	cross co-volume
c_1	parameter in the energy term of CPA EoS
Da	g/mole
g	radial distribution function
K_i	equilibrium constants
k_{ij}	Binary interaction parameter
P	pressure [Pascal]
Pc	critical pressure [Pascal]
R	universal gas constant [8.314 J mol^{-1} K^{-1}]
s_{ij}	solvation factor
T	temperature [K]
Tc	critical temperature [K]
V	volume [m^3]
ω	acentric factor
X_{Ai}	fraction of type-A sites in molecule i not bonded at other sites
x	Mole fraction
X_0	Start point
Z	compressibility factor

Greek Letters

β	association volume
α	association energy
Δ	association strength

Subscripts and Superscripts
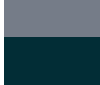
Assoc	association
Physical	physical portion

Color Code

T

293		RGB: 255, 230, 153
308		RGB: 242, 176, 126
323		RGB: 227, 82, 37
338		RGB: 192, 00, 00

Carbon Number

nC_5		RGB: 130, 238, 253
nC_6		RGB: 82, 178, 191
nC_7		RGB: 19, 56, 190
nC_8		RGB: 1, 96, 100
nC_9		RGB: 10, 17, 114
nC_{10}		RGB: 117, 124, 136
nC_{12}		RGB: 2, 45, 54

Supplementary Information (Appendix B and C)

In Appendix B, there are equation derivations for total volume and Helmholtz free energy using pressure of the equilibrium. Besides, the data analysis information is provided. The data analysis was performed using SPSS v27, and methods including the Shapiro-Wilk test and boxplot regarding the amount of solvent, temperature, and carbon number of the solvent (C_5-C_{12}). Appendix C contains the code developed for this research.

REFERENCES

1. Gudmundsson, J.S., Flow assurance solids in oil and gas production. 2017: CRC Press.
2. Ratulowski, J., Amin, A., Hammami, A., Muhammad, M., & Riding, M., Flow Assurance and subsea Productivity: closing the Loop with Connectivity and

Measurements. in SPE Annual Technical Conference and Exhibition. 2004. Society of Petroleum Engineers.

3.   Schuler, B., Zhang, Y., Liu, F., Pomerantz, A. E., Andrews, A. B., Gross, L., Pauchard, V., Banerjee, S., & Mullins, O. C., Overview of asphaltene nanostructures and thermodynamic applications. Energy & Fuels, 2020. 34(12): p. 15082-15105.

4.   Mullins, O.C., The modified Yen model. Energy & Fuels, 2010. 24(4): p. 2179-2207.

5.   Mullins, O.C., The asphaltenes. Annual Review of Analytical Chemistry, 2011. 4: p. 393-418.

6.   Alboudwarej, H., Akbarzadeh, K., Beck, J., Svrcek, W. Y., & Yarranton, H. W., Regular solution model for asphaltene precipitation from bitumens and solvents. AIChE Journal, 2003. 49(11): p. 2948-2956.

7.   Leontaritis, K.J. PARA-based (paraffin-aromatic-resin-asphaltene) reservoir oil characterizations. in International Symposium on Oilfield Chemistry. 1997. Society of Petroleum Engineers.

8.   Akmaz, S., Iscan, O., Gurkaynak, M. A., & Yasar, M., The structural characterization of saturate, aromatic, resin, and asphaltene fractions of batiraman crude oil. Petroleum Science and Technology, 2011. 29(2): p. 160-171.

9.   Speight, J.G., Chemical and physical studies of petroleum asphaltenes, in Developments in petroleum science. 1994, Elsevier. p. 7-65.

10. Wu, J., J.M. Prausnitz, and A. Firoozabadi, Molecular thermodynamics of asphaltene precipitation in reservoir fluids. AIChE journal, 2000. 46(1): p. 197-209.

11. Buenrostro-Gonzalez, E., Lira-Galeana, C., Gil-Villegas, A., & Wu, J., Asphaltene precipitation in crude oils: Theory and experiments. AIChE Journal, 2004. 50(10): p. 2552-2570.

12. Speight, J.G., The chemistry and technology of petroleum. 2014: CRC press.

13. Schuler, B., Meyer, G., Peña, D., Mullins, O. C., & Gross, L., Unraveling the molecular structures of asphaltenes by atomic force microscopy. Journal of the American Chemical Society, 2015. 137(31): p. 9870-9876.

14. Mullins, O., Reservoir fluid geodynamics and reservoir evaluation. Schlumberger, Houston, Texas, 2019.

15. Zhang, L., Chen, P., Pan, S., Liu, F., Pauchard, V., Pomerantz, A. E., Banerjee, S., Yao, N., & Mullins, O. C., Structure–Dynamic Function Relations of Asphaltenes. Energy & Fuels, 2021. 35(17): p. 13610-13632.

16. Theyab, M.A., Fluid flow assurance issues: literature review. SciFed Journal of Petroleum, 2018. 2(1): p. 1-11.

17. Subramanian, S., S. Simon, and J. Sjöblom, Asphaltene precipitation models: a review. Journal of Dispersion Science and Technology, 2016. 37(7): p. 1027-1049.

18. Akbarzadeh, K., Alboudwarej, H., Svrcek, W. Y., & Yarranton, H. W., A generalized regular solution model for asphaltene precipitation from n-alkane diluted heavy oils and bitumens. Fluid Phase Equilibria, 2005. 232(1-2): p. 159-170.

19. Forte, E. and S.E. Taylor, Thermodynamic modelling of asphaltene precipitation and related phenomena. Advances in colloid and interface science, 2015. 217: p. 1-12.

20. Nikooyeh, K. and J.M. Shaw, On the applicability of the regular solution theory to asphaltene+ diluent mixtures. Energy & Fuels, 2012. 26(1): p. 576-585.

21. Manshad, A. K., Manshad, M. K., Rostami, H., Mohseni, S. M., & Vaghefi, M., The association thermodynamics modeling of asphaltene precipitation. Petroleum Science and Technology, 2014. 32(1): p. 51-60.
22. Andersen, S.I. and J.G. Speight, Thermodynamic models for asphaltene solubility and precipitation. Journal of Petroleum Science and Engineering, 1999. 22(1): p. 53-66.
23. Painter, P.C. and M.M. Coleman, Fundamentals of polymer science: an introductory text. 1994: Technomic.
24. Hildebrand, J.H. and R.L. Scott, Regular solutions. 1962: Prentice-Hall.
25. Huggins, M.L., Solutions of long chain compounds. The Journal of chemical physics, 1941. 9(5): p. 440-440.
26. Flory, P.J., Thermodynamics of high polymer solutions. The Journal of chemical physics, 1942. 10(1): p. 51-61.
27. Scott, R.L. and M. Magat, The Thermodynamics of High-Polymer Solutions: I. The Free Energy of Mixing of Solvents and Polymers of Heterogeneous Distribution. The Journal of Chemical Physics, 1945. 13(5): p. 172-177.
28. Zuo, J. Y., Mullins, O. C., Freed, D., Elshahawi, H., Dong, C., & Seifert, D. J., Advances in the Flory–Huggins–Zuo equation of state for asphaltene gradients and formation evaluation. Energy & Fuels, 2012. 27(4): p. 1722-1735.
29. Li, Z. and A. Firoozabadi, Cubic-plus-association equation of state for water-containing mixtures: Is "cross association" necessary? AIChE journal, 2009. 55(7): p. 1803-1813.
30. Kontogeorgis, G. M., Voutsas, E. C., Yakoumis, I. V., & Tassios, D. P., An equation of state for associating fluids. Industrial & engineering chemistry research, 1996. 35(11): p. 4310-4318.
31. Chapman, W. G., Gubbins, K. E., Jackson, G., & Radosz, M., SAFT: Equation-of-state solution model for associating fluids. Fluid Phase Equilibria, 1989. 52: p. 31-38.
32. Sheu, E.Y. and O.C. Mullins, Fundamentals and Applications. 1995: Springer.
33. Mousavi-Dehghani, S. A., Riazi, M. R., Vafaie-Sefti, M., & Mansoori, G. A., An analysis of methods for determination of onsets of asphaltene phase separations. Journal of Petroleum Science and Engineering, 2004. 42(2-4): p. 145-156.
34. Alimohammadi, S., S. Zendehboudi, and L. James, A comprehensive review of asphaltene deposition in petroleum reservoirs: Theory, challenges, and tips. Fuel, 2019. 252: p. 753-791.
35. Sabbagh, O., Akbarzadeh, K., Badamchi-Zadeh, A., Svrcek, W. Y., & Yarranton, H. W., Applying the PR-EoS to asphaltene precipitation from n-alkane diluted heavy oils and bitumens. Energy & fuels, 2006. 20(2): p. 625-634.
36. Zúñiga-Hinojosa, M. A., Justo-García, D. N., Aquino-Olivos, M. A., Román-Ramírez, L. A., & García-Sánchez, F., Modeling of asphaltene precipitation from n-alkane diluted heavy oils and bitumens using the PC-SAFT equation of state. Fluid Phase Equilibria, 2014. 376: p. 210-224.
37. Gupta, A.K., A model for asphaltene flocculation using an equation of state. 1986: Chemical and Petroleum Engineering, University of Calgary.
38. Vargas, F. M., Gonzalez, D. L., Hirasaki, G. J., & Chapman, W. G., Modeling asphaltene phase behavior in crude oil systems using the perturbed chain form of the statistical associating fluid theory (PC-SAFT) equation of state. Energy & fuels, 2009. 23(3): p. 1140-1146.

39. Panuganti, S. R., Vargas, F. M., Gonzalez, D. L., Kurup, A. S., & Chapman, W. G., PC-SAFT characterization of crude oils and modeling of asphaltene phase behavior. Fuel, 2012. 93: p. 658-669.

40. Tavakkoli, M., Panuganti, S. R., Taghikhani, V., Pishvaie, M. R., & Chapman, W. G., Asphaltene deposition in different depositing environments: Part 2. Real oil. Energy & Fuels, 2014. 28(6): p. 3594-3603.

41. Abunahman, S. S., dos Santos, L. C., Tavares, F. W., & Kontogeorgis, G. M., A computational tool for parameter estimation in EoS: New methodologies and natural gas phase equilibria calculations. Chemical Engineering Science, 2020. 215: p. 115437.

42. Li, Z. and A. Firoozabadi, Cubic-plus-association equation of state for asphaltene precipitation in live oils. Energy & fuels, 2010. 24(5): p. 2956-2963.

43. Arya, A., Liang, X., von Solms, N., & Kontogeorgis, G. M., Modeling of asphaltene precipitation from crude oil with the cubic plus association equation of state. Energy & Fuels, 2017. 31(2): p. 2063-2075.

44. Hu, Y.-F. and T.-M. Guo, Effect of temperature and molecular weight of n-alkane precipitants on asphaltene precipitation. Fluid Phase Equilibria, 2001. 192(1-2): p. 13-25.

45. Kontogeorgis, G.M. and G.K. Folas, Thermodynamic models for industrial applications: from classical and advanced mixing rules to association theories. 2009: John Wiley & Sons.

46. Danesh, A., PVT and phase behaviour of petroleum reservoir fluids. 1998: Elsevier.

47. Perakis, C., Voutsas, E., Magoulas, K., & Tassios, D., Thermodynamic modeling of the vapor–liquid equilibrium of the water/ethanol/CO2 system. Fluid Phase Equilibria, 2006. 243(1-2): p. 142-150.

48. Vargas, F.M. and M. Tavakkoli, Asphaltene Deposition: Fundamentals, Prediction, Prevention, and Remediation. 2018: CRC Press.

49. Arya, A., Liang, X., von Solms, N., & Kontogeorgis, G. M., Modeling of asphaltene onset precipitation conditions with cubic plus association (CPA) and perturbed chain statistical associating fluid theory (PC-SAFT) equations of state. Energy & Fuels, 2016. 30(8): p. 6835-6852.

50. Yen, T.F. and G.V. Chilingarian, Asphaltenes and asphalts, 2. 2000: Elsevier.

51. dos Santos, L. C., Abunahman, S. S., Tavares, F. W., Ahón, V. R. R., & Kontogeorgis, G. M., Modeling Water Saturation Points in Natural Gas Streams Containing CO2 and H2S-Comparisons with Different Equations of State. Industrial & Engineering Chemistry Research, 2015. 54(2): p. 743-757.

52. Podlaski, M., Vanfretti, L., Bogodorova, T., Rabuzin, T., & Baudette, M., RaPId-A Parameter Estimation Toolbox for Modelica/FMI-Based Models Exploiting Global Optimization Methods. IFAC-PapersOnLine, 2021. 54(7): p. 391-396.

53. Stripinis, L., Žilinskas, J., Casado, L. G., & Paulavičius, R., On MATLAB experience in accelerating DIRECT-GLce algorithm for constrained global optimization through dynamic data structures and parallelization. Applied Mathematics and Computation, 2021. 390: p. 125596.

54. Nelder, J.A. and R. Mead, A simplex method for function minimization. The computer journal, 1965. 7(4): p. 308-313.

55. Sabbagh, O., An EoS approach for modeling asphaltene precipitation. (Thesis), 2005.

56. Riazi, M.R. and T.A. Al-Sahhaf, Physical properties of heavy petroleum fractions and crude oils. Fluid Phase Equilibria, 1996. 117(1-2): p. 217-224.

57. Xu, X., Chen, H., Liu, C., & Dang, C., Prediction of the Binary Interaction Parameter of Carbon Dioxide/Alkanes Mixtures in the Pseudocritical Region. ACS omega, 2019. 4(8): p. 13279-13294.

58. Lawal, K. A., Crawshaw, J. P., Boek, E. S., & Vesovic, V., Experimental investigation of asphaltene deposition in capillary flow. Energy & Fuels, 2012. 26(4): p. 2145-2153.

59. Wang, J. and J. Buckley, Effect of dilution ratio on amount of asphaltenes separated from stock tank oil. Journal of dispersion science and technology, 2007. 28(3): p. 425-430.

60. Tharanivasan, A. K., Svrcek, W. Y., Yarranton, H. W., Taylor, S. D., Merino-Garcia, D., & Rahimi, P. M., Measurement and modeling of asphaltene precipitation from crude oil blends. Energy & Fuels, 2009. 23(8): p. 3971-3980.

61. Chok, N.S., Pearson's versus Spearman's and Kendall's correlation coefficients for continuous data. 2010, University of Pittsburgh.

62. Nahmias, S. and T.L. Olsen, Production and operations analysis. 2015: Waveland Press.

63. Shirani, B., Nikazar, M., Naseri, A., Mousavi-Dehghani, S.A., Modeling of asphaltene precipitation utilizing Association Equation of State. Fuel, 2012. 93: p. 59-66.

64. Behnous, D., Palma, A., Zeraibi, N., & Coutinho, J. A., Modeling asphaltene precipitation in Algerian oilfields with the CPA Eos. Journal of Petroleum Science and Engineering, 2020. 190, 107115.

65. Nazemi, R., Daryasafar, A., Bazyari, A., Shafiee Najafi, S. A., & Ashoori, S., Modeling Asphaltene Precipitation in live crude oil using cubic plus association (CPA) equation of State. Petroleum Science and Technology, 2019, 38(3), 257-265.

66. Zare Talavaki, M., Afsharpour, A., & Taherian, Z., Determination of asphaltene precipitation using a CPA equation of State. Petroleum Science and Technology, 2017, 35(9), 839-844.
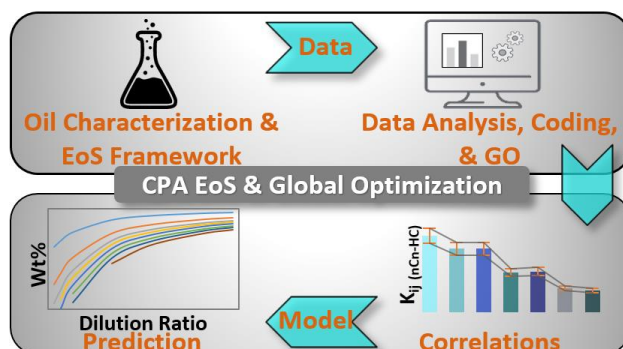
"Graphical Abstract"

Chapter 4 : Improved CPP EoS and MD to Model

Asphaltene Precipitation

(A CPP Model to Asphaltene Precipitation; Mapping π-π Interactions onto an Equation of State, (Published)

Preface

A modified version of this manuscript has been presented at the SPE Canadian Energy Technology Conference, Calgary, Alberta, Canada, in March 2022. I am the primary author of this paper. Along with the co-authors Lesley James and Sohrab Zendehboudi, I carried out the literature review, data collection, and discussions on modeling studies on the asphaltene precipitation/deposition process. I prepared the first draft of the manuscript and subsequently revised the manuscript based on the co-authors' feedback as well as the comments received from the peer review process. The co-author, Lesley James, thoroughly reviewed and revised the manuscript, commented on various parts of the manuscript, considerably contributed to entirely correcting the text in terms of technical and editorial aspects, and assisted in reviewing and revising the manuscript. The co-author, Sohrab Zendehboudi, contributed by providing comments on various parts of the manuscript.

Abstract

Asphaltene may destabilize during the oil recovery, transportation, and processing and cause significant flow assurance problems that negatively affect operational expenditures (OPEX). Modeling investigation of asphaltene precipitation and deposition is a vital research component in flow assurance requiring the accurate description of the phenomena under various operational conditions. The structure of asphaltene molecules and the presence of heteroatoms play a significant role in the intermolecular forces and the mechanism of asphaltene aggregation. Nevertheless, the intermolecular forces, e.g., polar forces, and their addition to thermodynamic modeling of asphaltene phase behavior still need investigation. While the traditional equation of state (EoS), e.g., cubic EoS, does not provide any special treatment to polar energy, the π-π interaction and polar effect can be mapped into the EoS using a separate polar term. In this research, we use cubic EoS, cubic plus polar (CPP) EoS, and molecular dynamics (MD) (three different modeling approaches) to analyze the effect of asphaltene structure and operational conditions on the precipitation phenomenon. Comparing the error associated with correlation and prediction results of the models, we show that the CPP approach using optimization to tune parameters of the EoS is the most reliable approach, followed by CPP EoS using MD to find dipole moment for the aryl-linked core asphaltene structure. The CPP EoS and MD optimizing island structure for asphaltene is the third-best model, and SRK EoS is a less efficient approach. Considering the values for dipole moment and molecular weight of asphaltene, along with the correlation and prediction ability of the techniques, it is revealed that polar forces can be considered in a separate term in addition to van der Waals force to increase the model efficiency. Moreover, the aryl structure with a 750 g/mol molecular weight and one/two thiophene/pyridine group is the most proper asphaltene structure.

Keywords: Asphaltene modeling, Equation of State, van der Waals forces, Polar forces, Thermodynamics

4-1. Introduction

Asphaltene molecules, known as the heaviest and most polar fraction of crude oil [2], may cause operational problems in reservoir, upstream, and downstream production and processing facilities. These problems are not limited to blocking pore throats, altering the wettability of the reservoir,

stabilizing the water-in-oil emulsion, solid formation in storage tanks, fouling of safety valves, and deactivation of catalysts. Due to the flow assurance issues that asphaltene may cause, it is important to understand asphaltene precipitation and deposition phenomena thoroughly. Equation of States (EoSs) have been used to model asphaltene phase behavior and have shown promising performance in these applications. Advanced EoS, e.g., Cubic Plus Association (CPA) and Perturbed Chain Statistical Associating Fluid Theory (PC-SAFT), have been used to model asphaltene phase behavior by incorporating association energy into EoS. While to the best of our knowledge, polar energy and the impact of π-π interactions in EoS (Cubic Plus Polar, CPP) have not been used in this area.

One of the main challenges of using EoS is tuning the adjustable parameters of the model, e.g., Binary Interaction Parameters (BIPs). Moreover, EoS needs a number of physical properties, e.g., dipole moment, and experimental test results, e.g., PVT test, to be tuned and used, while these tests are not often feasible economically and operationally. Therefore, there is a necessity to reduce the amount of resources needed to conduct experimental tests and optimization of the adjustable parameters. Besides, it is insightful to link the macroscale properties (e.g., temperature and pressure) to microscale properties (e.g., molecular structure) to be used in the EoS. Hence, a robust non-gradient-based optimization approach (global optimization) and Molecular Dynamic (MD) can be sued to optimize the best fit of the adjustable parameters and to determine the physical properties needed for EoS modeling (dipole moment).

The complex structure of asphaltene is the reason to define it by solubility and polarity characteristics. It is operationally categorized as a soluble class of components in aromatic solvents, such as toluene and benzene. Nonetheless, it is insoluble in light paraffinic solvents, including n-heptane and n-hexane [3]. Experimental results show that the lighter n-paraffin solvents cause more insoluble asphaltene. Moreover, the characteristics of precipitated asphaltene change when using different n-paraffin solvents [4].

A representative asphaltene molecule has a Poly-Aromatic Hydrocarbon (PAH) core with aliphatic chains. It also consists of heteroatoms, including N, O, S, Fe, V, and Ni, imparting polarity. Polar interactions contribute to asphaltene aggregation and precipitation due to anisotropic π-π interactions of asphaltene particles [5, 6].

While asphaltene precipitation and deposition are considered unfavourable to the profitability of upstream or downstream sections of oil production, it is essential that we strive to transport oil safely and sustainably [7-9]. The solubility of asphaltene in the oil mixture can be altered upon the oil composition, pressure, temperature, and properties of asphaltene. Therefore, a thorough understanding of the effect of these operational conditions on asphaltene precipitation is indispensable [1, 10-14].

Two types of approaches have been used to model asphaltene precipitation from a thermodynamics perspective: solubility and colloidal theory-based models [7]. The state of asphaltene in these two models is different. In the first modeling category approach, asphaltene is dissolved in the oil, and precipitation is caused by decreasing the solubility of asphaltene lower than a threshold level. The second hypothesis is based on colloidal theory, where asphaltene is suspended and stabilized by resins [15-19].

The solubility approach is divided into the equation of state (EoS) and the lattice fluid theory. Considering these two categories, it can be said that, generally, the EoS approach has more advantages than the lattice fluid theory. The shortcomings of the latter approach include, but are not limited to, the effect of pressure in combining with EoS, investigating mass distribution by only the empirical correlations, and considering the solubility parameters of the components as tuning parameters. Hence, it does not have much industry application [16, 17, 20, 21].

The EoS mainly includes cubic, CPA, and PC-SAFT. The cubic EoSs (e.g., Soave-Redlich-Kwong (SRK) and Peng Robinson (PR)) are simple models with acceptable accuracy which have wide industry applications [17]. The intermolecular forces are collectively represented in one attractive and one repulsive term ($a/_{v^2}$ and b), lead to a relatively large pure fluid attraction energy [22]. The cross van der Waals attraction is calculated using a geometric mean of the pure fluid attraction energies in the form of $\sqrt{a_1 a_2}(1 - k_{ij})$. The relatively large attractive energy needs a higher amount for k_{ij}, that might be composition-dependent, to compensate for neglecting the multipolar interactions. Thus, the prediction ability of the EoS would be reduced [23].

Sabbagh et al. (2006) adapted the PR EoS to model asphaltene precipitation in the presence of toluene and n-alkane at different temperatures (0-100°C) and pressures (up to 7 MPa) [30]. A liquid-liquid equilibrium was considered between the liquid oil phase and the asphaltene phase.

Furthermore, the solubility fractions, including saturates, aromatics, resins, and asphaltenes, were used to characterize the oil mixture. Their findings showed that the developed model could not universally correlate/predict asphaltene precipitation, and no superiority was observed compared to the previously developed models. Hustad et al. (2013) modeled the lower and upper onset and bubble point pressures of asphaltene with SRK and PC-SAFT EoS where the injection of nitrogen gas at 94 MPa (13634 psia) and 94°C (201.2 F) was conducted. They found both models with acceptable performance in forecasting the upper onset pressure. However, a better performance was reported at the thermodynamic conditions with high concentrations of nitrogen (15% mole of N2 in the mixture) while using the PC-SAFT [52]. Vargas et al. (2014) compared the prediction capability of the SRK and PC-SAFT EoS. They showed that although both models can fit the asphaltene precipitation and the bubble point (asphaltene onset point or AOP) experimental data, the prediction performance of the SRK EoS is questioned [53].

The association of hydrogen bonding can be included in CPA and PC-SAFT EoS and has been previously used to represent asphaltene systems. The correlation and prediction abilities of these EoSs are significantly improved by including a separate association term. However, they have some disadvantages, including more adjustable parameters (in compassion to cubic EoS), higher computational costs, and the need for a robust optimization algorithm. Although these two EoSs have been used to consider the effect of the hydrogen bonding association in asphaltene precipitation, the polar force is not reflected in those models [24].

Arya et al. (2016) applied CPA and PC-SAFT with and without the association contribution to model asphaltene precipitation yield. They compared the results of the PC-SAFT without association (WOA) and CPA EoS (added association term to the SRK EoS). They examined different approaches for oil characterization and used different association parameters for asphaltene. Some of the approaches (CPA EoS while using SARA analysis for oil characterization and different association parameters for asphaltene and PC-SAFT EoS) were unable to accurately model the decrease of asphaltene precipitation when using heavier n-paraffin. Only the CPA EoS could correlate asphaltene precipitation by considering two fractions for oil (heavy fractions and asphaltene) and one association parameter. They did not report the quantity of experimental data they used nor information regarding parameter estimation of the EoS. Besides, the polarity effect due to the presence of heteroatoms (π-π interactions) was not included in the EoS [25-28].

To the best of our knowledge, we have not found any literature focused on polar heteroatom forces in asphaltene phase behavior. We believe our implementation of polar energy in the asphaltene system and the approach used here will be novel (cubic plus polar, CPP EoS). CPP EoS applies asphaltene structure and intermolecular forces, and relates these characteristics to macro-level properties and quantity of precipitation. Adding the extension of polar forces into the cubic EoS provides an understanding of the asphaltene structure, polarity of the asphaltene molecules, and impact of polarity and van der Waals forces on asphaltene phase separation. Accounting for polar interactions in asphaltene separation will be shown to improve the reliability of the EoS since asphaltene molecules are highly polar due to heteroatoms, e.g., N or S. However, the modeling capability of the EoS depends on the adjustable parameters, e.g., binary interaction parameter, the polar term of the CPP EoS, e.g., the dipole moment of the asphaltene molecule, and reliability of the experimental data used to tune the EoS.

In this work, we demonstrate how a single term can be added to the SRK EoS to account for polar interactions and effectively be applied to calculate asphaltene precipitation when considering asphaltene phase behaviour as a liquid-liquid equilibrium (LLE). Besides, we make the model less complex using an oil characterization adopted from Li and Firoozabadi [25, 26] and Arya et al. [25-28]. Therefore, the number of adjustable parameters (binary interactions) and the need for experimental measurements have been reduced using the characterization method. A global optimization approach and molecular dynamic (MD) simulation have also been used to increase the reliability of the optimization and reduce the number of adjustable parameters for polar forces. Our findings can help improve the reliability of asphaltene modeling approaches and be used in industry.

4-2. Methodology

4-2-1. Workflow of the Research

This study develops a workflow process to analyze asphaltene precipitation and suggests the best strategy/method for modeling the phenomenon. Figure 4-1 shows the workflow which enables modeling approaches to consider different intermolecular forces for asphaltene precipitation. The workflow and practices presented here are essential in determining asphaltene phase separation and related issues to ensure proper oil management and flow assurance risks.

The overall workflow can be divided into four main sections: data and model preparation, SRK EoS modeling, CPP EoS and global optimization, and CPP EoS and MD. The last section consists of two sub-sections using two different molecular structures in the MD calculations.

Collecting pertinent data and preparing the models are the first steps of the workflow on which all subsequent steps depend. Representative samples/data points are required to understand the effect of operational conditions and asphaltene characterization. For this purpose, a literature review was done, and the proper experimental data was selected. See section 3-3 for more information. Following that, the mass balance, phase calculations (initial oil and the separated phase), and critical property analysis were conducted to prepare the inputs to the EoS. Next, the proper equations were extracted from Kontogeorgis and Folas [24], and equations for the mixture were derived accordingly. The flash phases and liquid-liquid equilibrium (LLE) algorithm determined the phase separation (section 3-3). Dominant forces, including van der Waals and polar forces, were coded using Matlab and an algorithm adapted from Abunahman et al. [29] and Sabbagh et al. [30] (section 3-3). The debugging and testing of the developed codes were done using a limited portion of the experimental data different from those selected for testing and validating the model (steps 1-10 of the workflow).

When codes and input parameters were ready, the first approach was conducted to analyze the effect of van der Waals forces on the asphaltene precipitation using SRK EoS. The binary interaction parameters were first optimized using a genetic algorithm and initial values in this section. Second, the compressibility factors, volume, and fugacity were calculated using SRK EoS. Third, the equilibrium criteria are conducted by comparing the fugacity coefficients of fractions in two available phases. Fourth, the model's outcomes are calculated once the equilibrium criteria are met, including K values ($K=y_i/x_i$) (steps 11-14 of the workflow).

Approach-2 is based on including polar forces into the SRK EoS and using a global optimization approach to optimize the adjustable parameters of the model, including binary interactions and polar energy parameters. This approach consisted of five main steps: first, using the genetic algorithm to estimate the lower bound, upper bound, and start points of optimization. Second, a global optimization approach was conducted using the GlobalSearch method to determine the adjustable parameters. Third, the tuned parameters are used to calculate van der Waals and polar forces, compressibility factors, volume, and fugacity. The fourth and fifth steps are conducting equilibrium criteria and final results calculations (steps 15-18 of the workflow).

172

Approach-3 is based on reducing the number of adjustable parameters of approach-2 by including MD calculations. Hence, approach-3 comprises two molecular structures for asphaltene particles, *island* (steps 19-23 of the workflow) and *aryl* (steps 24-28 of the workflow) structures. First, molecules of asphaltene were built using Gaussview software. Second, the Gaussian09 software was employed to optimize the molecular structure and find proper atoms and partial charges calculations. Third, a global optimization approach was used to tune the adjustable parameters of the model. The fourth and fifth steps are the calculation of van der Waals and polar forces, compressibility factors, volume, fugacity, and conducting equilibrium criteria.
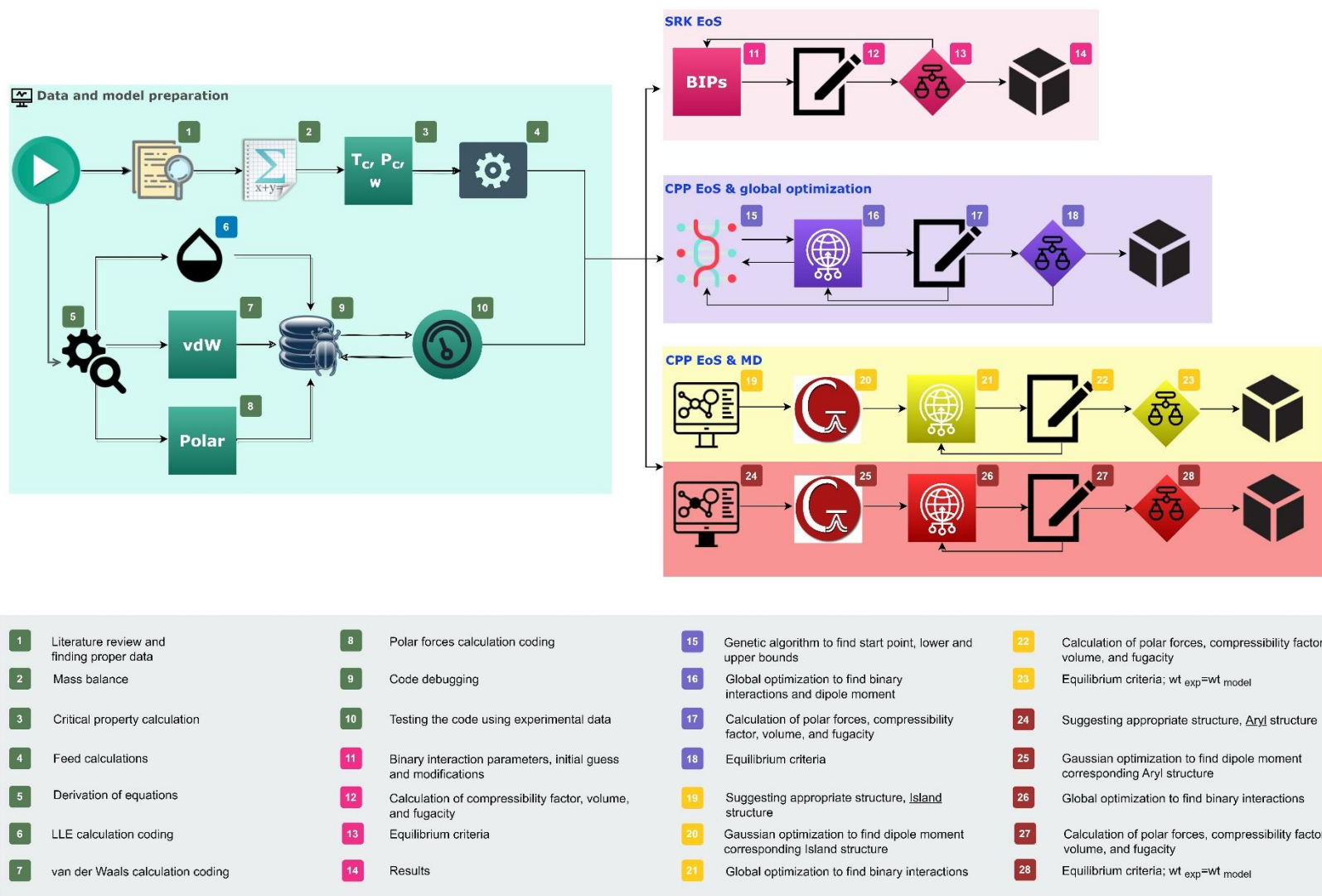
Figure 4-1. Workflow showing all steps used in this research

1	Literature review and finding proper data	8	Polar forces calculation coding	15	Genetic algorithm to find start point, lower and upper bounds	22	Calculation of polar forces, compressibility factor, volume, and fugacity
2	Mass balance	9	Code debugging	16	Global optimization to find binary interactions and dipole moment	23	Equilibrium criteria; $wt_{exp}=wt_{model}$
3	Critical property calculation	10	Testing the code using experimental data	17	Calculation of polar forces, compressibility factor, volume, and fugacity	24	Suggesting appropriate structure, Aryl structure
4	Feed calculations	11	Binary interaction parameters, initial guess and modifications	18	Equilibrium criteria	25	Gaussian optimization to find dipole moment corresponding Aryl structure
5	Derivation of equations	12	Calculation of compressibility factor, volume, and fugacity	19	Suggesting appropriate structure, Island structure	26	Global optimization to find binary interactions
6	LLE calculation coding	13	Equilibrium criteria	20	Gaussian optimization to find dipole moment corresponding Island structure	27	Calculation of polar forces, compressibility factor, volume, and fugacity
7	van der Waals calculation coding	14	Results	21	Global optimization to find binary interactions	28	Equilibrium criteria; $wt_{exp}=wt_{model}$

4-2-2. Theory of the EoS and Polar Contribution

The CPP model is developed to incorporate the polar interactions into the cubic EoS. In this approach, the van der Waals forces are represented by SRK EoS, and the extension of the polar energy is added. The overall Helmholtz free energy for a mixture is given as [23, 31-34]

$$A = \frac{A}{Nk_BT} = A^{van\,der\,Waals} + A^{polar} = A^{repulsive} + A^{atractive} + A^{polar} \tag{4-1}$$

Where N is the total number of molecules, T is the temperature, and k_B is the Boltzmann constant. $A^{van\,der\,Waals}$ is the van der Waals free energy that can be evaluated by SRK EoS as [22]

$$A^{SRK} = nRT \ln(\frac{v}{v-b}) + \frac{an}{b}\ln(\frac{v}{v+b}) \tag{4-2}$$

In the above equation, R, T, n, b, and v are universal gas constant (8.314 J/(K.mol)), temperature, the total number of moles, co-volume parameter (m³/mol), and molar volume (m³/mol), respectively. a is the attractive parameter (Pa.m⁶/mol) and is defined as [22]

$$a = a_0\left[1 + c(1 - \sqrt{\frac{T}{T_c}})\right]^2 \tag{4-3}$$

Where a_0, b, and c are parameters of the cubic EoS for pure components, and T_c stands for the critical temperature of the component. The dipolar contribution is calculated using the Jog and Chapman dipolar energy using the perturbation theory [31]

$$A^{polar} = \frac{A_2^{polar}}{1 - A_3^{polar}\Big/A_2^{polar}} \tag{4-4}$$

A_2^{polar} and A_3^{polar} are the second and third-order free energies that are given by [31]

$$\frac{A_2^{polar}}{nRT} = -\frac{2\pi}{9}\frac{\rho}{(k_bT)^2}\sum_i\sum_j x_ix_j\frac{\alpha_{pi}\alpha_{pj}}{d_{ij}^3}I_{2,ij} \tag{4-5}$$

$$\frac{A_3^{polar}}{nRT} = \frac{5\pi^2}{162}\frac{\rho^2}{(k_bT)^3}\sum_i\sum_j\sum_k x_ix_jx_k\frac{\alpha_{pi}\alpha_{pj}\alpha_{pk}}{d_{ij}d_{jk}d_{ik}}I_{3,ijk} \tag{4-6}$$

In equations (5) and (6), x is the mole fraction, ρ is the number density, α is the polar strength, d is the segment diameter, and I is the constant by Larsen et al. [31]. For the flash calculation, the fugacity coefficient of the components is needed.

$$\ln \phi_{i=} \ln \left(\frac{f_i}{x_i P}\right) = \frac{\mu_i}{RT} - \ln Z = \frac{1}{RT}\left(\frac{\partial A}{\partial n_i}\right)_{T,v,n_j} - \ln Z \tag{4-7}$$

Where f_i and μ_i are the fugacity and chemical potential of the pure component. The compressibility factor is given by [22]

$$Z = \frac{1}{nRT}\rho\left(\frac{\partial A}{\partial \rho}\right)_{T,n} \tag{4-8}$$

$$Z = Z^{SRK} + Z^{polar} = \frac{1}{nRT}\rho\left[\left(\frac{\partial A^{SRK}}{\partial \rho}\right)_{T,n} + \left(\frac{\partial A^{polar}}{\partial \rho}\right)_{T,n}\right] \tag{4-9}$$

Detailed calculations and derivation are presented in the literature [22, 31, 34, 35].

4-2-3. Oil Characterization

The experimental data used here were collected from literature, Hu et al. [1]. They studied the Caoqiao crude oil sampled from Shengli Oil Field. Titration experiments were conducted to determine asphaltene precipitation amounts in tank oil samples using several n-alkanes. Asphaltene precipitation under operational conditions was investigated at four different temperatures, 293, 308, 323, and 338 K, using different precipitants, including normal hexane (nC_6), normal nonane (nC_9), and normal dodecane (nC_{12}). Moreover, a three-step optical (light scattering) method was used to determine the onset point of asphaltene at 293 K. Asphaltene was precipitated out of the oil sample by adding n-alkane step-wise with 1 mL 0.2 mL, and ±0.1 mL increments to achieve higher accuracy. Although the process seems to be repeated more than once to increase measurement precision, the relative standard deviation of the measurements was not reported. Since the onset point of asphaltene using the optical method is sensitive, having the measurement error is helpful in evaluating the modeling approach capabilities.

The composition of the crude oil is reported in Table 4-1.

Table 4-1. Compositions (mol%) and properties of the degassed Caoqiao crude oil and separator gas [1]

Component	Degassed oil
C_5-C_6	< 2
$C7^+$	98.06
C_{11}^+	87.16
C_7^+ molecular weight (g/mol)	503.6
C_7^+ density (at 293 K)	0.9526
Reservoir temperature (K)	343
Bubble point pressure at 343 K (MPa)	9.8
Saturates (wt.%)	38.0
Aromatics (wt.%)	47.6
n-C_5 asphaltenes (wt.%)	7.26
Resins (wt.%)	18.6

Characterization of the oil sample is crucial while using the EoS to model fluid phase equilibria due to the lack of experimental data and reduce the number of adjustable parameters (e.g., binary interactions). The previous characterization methodologies of the EoS assumed the molecular weight of asphaltene was an adjustable parameter [36] or used a gamma distribution function and defined a wide range of amounts for this parameter [16]. Some others also considered the molecular weight of the asphaltene pseudo-component to be a fixed amount (500-1700 g/mol) [25, 26]. However, considering the uncertainty about the molecular weight of asphaltene, this parameter needs to be treated carefully. Moreover, having too many adjustable parameters (a high degree of freedom) is not favourable. Thus, as an improvement to the previous approaches, we adopted an approach with lower uncertainty about the molecular weight of the asphaltene fraction and the use of fewer adjustable parameters. The following assumptions and implications are made in this work:

  i. Asphaltene is dissolved in crude oil (solubility method).

 ii. Asphaltene precipitation is reversible under liquid-liquid equilibrium (LLE) [36, 37].

iii. The precipitated phase is pure asphaltene as a pseudo-liquid phase. The amount of other non-asphaltenic materials is insignificant [37].

iv. Asphaltene associates with solvents to form pre-aggregates, and van der Waals and polar interactions are dominant.

 v. Asphaltene was considered in monomer form with a molecular weight of 750 g/mol (Da) [2].

vi. C7+ of the stock tank oil (STO) was categorized into heavy components (HC) and asphaltene (figure 4-2).

vii. Interaction parameters of asphaltene and HC available in the equilibrium are considered adjustable parameters to be tuned regarding experimental data

viii. Interaction parameters are considered temperature-dependent
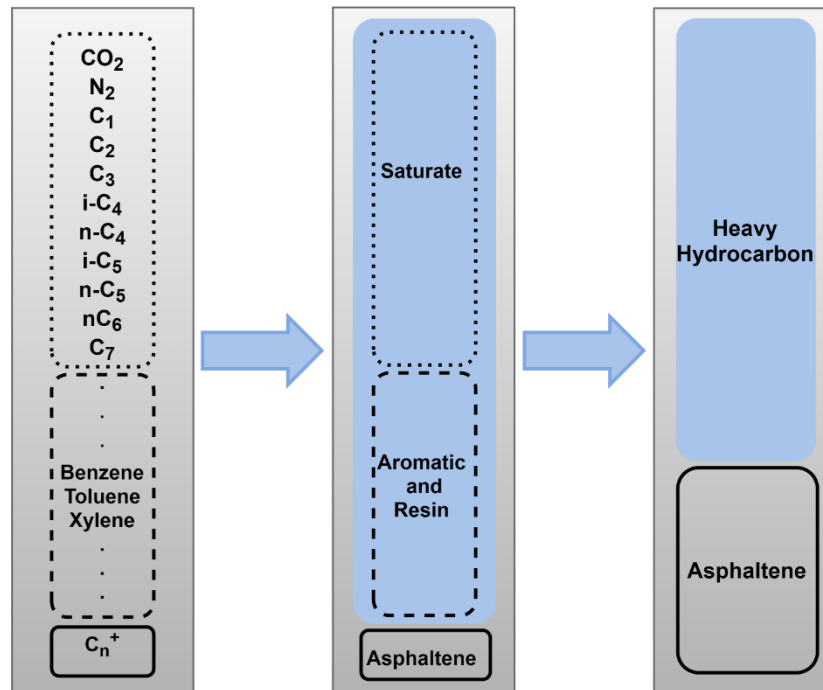
Figure 4-2. Characterization approach for the oil sample, adopted from Arya et al. [27, 28, 36]

The general approach for flash calculation is adapted from Abunahman et al. [29] and Sabbagh et al. [30]. Using the molecular weights of the different fractions/components of the mixture, the critical properties of the oil fractions were calculated using correlations (i.e., Riazi and Al-Sahhaf (1996) [38]). The parameters of the model, including binary interactions, are tuned using global optimization. Having the composition and critical properties of the oil mixture, the global optimization algorithm starts by using the constraints of optimization, including lower bound (LB), upper bound (UB), and start points (X0). These parameters can be found through rapid and reliable optimization using a Genetic Algorithm (GA). The K values ($K=y_i/x_i$) and the flash calculations of the phase separation are conducted to find the volume, Z factor, and fugacity coefficients of the fractions. Fugacity calculations help the modification of the K value. Once the criteria are met

($error < 10^{-12}$), the model results are compared to those from the experiments (mole percent, x_i) to adjust the initial guesses and adjustable parameters.

4-2-4. Objective Function, Model Parameters, and Optimization Approach

Tuning the thermodynamic EoS indicates setting the model parameters so that the predicted values match the reference model within an acceptable error range ($error < 10\%$). In this context, there is a need to define a suitable objective function, know/analyze the model parameters, and choose a proper optimization approach.

The objective function is the metric to map the variable/variables onto experimental data. The following assumptions are made here to define the objective functions:

- The experimental data are considered random variables
- The error of the model is normally distributed
- The independent data and variables are reliable

Therefore, the least square function is used as the objective function. More information can be found in the literature [39, 40] about the probability distribution function and how minimizing the least square function equals maximizing the probability function. So the objective function used is given by the following equation [39]:

$$F(X) = \frac{1}{n_e} \left[\sum_1^{n_e} \frac{(n_i^e - n_i^p)^2}{\sigma_i^2} \right] \tag{4-10}$$

Where vector X contains constants of the EoS, n_e is the number of data points, n_i^e and n_i^p are experimental data and corresponding calculated values, respectively, and σ represents the variance of the experimental variables.

There is a need to adjust the parameters of EoS, i.e., parameters of the physical and the polar sections. The only adjustable parameter of the polar section of the model is the number of segments with dipolar moments. The dipole moment of the molecule is also needed in polar force calculations. Typically, this parameter is measured from the experimental data for pure components. However, as here we are considering fractions, there is a need to adjust this parameter. We calculated the dipole moment by optimization and MD calculations in the current research.

To tune the model parameters of the EoS, an objective function must be optimized considering the experimental data and calculated values. Since the model parameters cannot be measured experimentally/theoretically (e.g., number of segments with dipolar moments) and the EoS is also nonlinear, a proper optimization method is needed to find the best answer for the tuning parameters and minimize the objective function. Moreover, the optimization process of the EoS (non-linear problem) has other difficulties, such as the range of the parameters, the possibility of local minima, the continuity of the objective function, and the effect of each model parameter on the objective function. Hence, we cannot use simple optimization approaches (such as derivative-based approaches, Newton method), a global optimization method is also needed to find the global optima iteratively [40, 41].

In this study, a multi-variable optimization method is used to tune the model parameter of the EoS. We adapted the approach from Santos et al. [40, 41] and modified the optimization algorithm using the global optimization method. The technique used here has two main sections, including finding global and local optima.

GlobalSearch toolbox was acquired to find the best optimal. This method has been widely applied in complex optimization problems to find global or multiple minima. [54, 55]. To the best of our knowledge, these algorithms have not been used in this area of research. Details of the global approach can be found at the Matlab help center.

In addition to the global approach, local and simple optimization is also implemented. Once the global optimum was found from the above approach, the Nelder-Mead simplex algorithm [42] was employed to increase the possibility of finding the global optimum within each basin of the optimization. The method is a simple and fast algorithm that does not require additional computations of the derivatives of the objective functions. However, the accuracy of the optimization is highly dependent on the initial guess of the adjustable parameters.

The two approaches mentioned above were implemented sequentially, and the global optimization results were considered the initial estimation for the simplex approach. Consequently, the global method is refined by the results of the simplex method. The current research mainly focused on selecting the initial guess of the adjustable variables within the predefined regions of the optimization basins. The Nelder-Mead simplex algorithm should not be used independently due to the complexity of optimizing the thermodynamic calculations.

4-2-5. Approach-1

Approach-1 is based on representing the van der Waals forces in asphaltene precipitation. For this purpose, the SRK EoS was used and tuned. The van der Waals forces are the primary molecular interaction that causes phase behaviour and asphaltene precipitation compared to polar and association interactions. Hence, it is widely applied in many phase behaviour calculations, especially industrial simulations. Many industrial PVT simulation software and reservoir packages, including CMG, use van der Waals forces in their analyses by SRK or PR EoS.
As shown in Figure 4-2, the modeling approach has a single component for saturate, aromatic, and resin fractions (maltene fraction) and the rest of the components are known as asphaltene. The critical properties and acentric factors of oil solubility fractions are obtained using the equations provided by Riazi and Al-Sahhaf [38], and the modified constants of the equations are used from Akbarzadeh et al. [43]. The only adjustable parameter of the model is the binary interactions between normal paraffin-maltene, normal paraffin-asphaltene, and maltene-asphaltene.

4-2-6. Approach-2

This approach is based on SRK EoS, and the polar forces are incorporated into the model. While the traditional EoS, e.g., SRK, only consider standard dispersion attraction in one single attractive energy parameter, the polar energy is also lumped into the EoS to include both energy scales separately. The derivation of the equations for polar forces are extracted from Jog et al. [23], Perfetti et al. [44], Villiers et al. [45], Marshall et al. [35], and is presented in section 3-2.
The polar energy has two adjustable parameters: the number of dipolar moments per molecule, n_p, and dipole moment, μ. The former parameter would be equal to one when a single polar site is considered. However, for real fluids, n_p is an adjustable parameter (Larsen et al. [31]). The latter parameter is the dipole moment and is the indicator of the molecule's polarity, e.g., asphaltene, and can be evaluated by experiments. We do not have access to this parameter experimentally, so it has been considered an adjustable parameter that fits experimental data of the asphaltene precipitation.

4-2-7. Approach-3

This approach is based on incorporating the polar forces into the EoS, and the same coding algorithm is used as approach-2. This section aims to reduce the number of adjustable parameters of approach-2. While there are two adjustable parameters for polar forces in the previous section, including n_p (number of dipolar moments per molecule) and μ (dipole moment), in this approach, it has been reduced to one adjustable parameter, i.e., n_p. The other parameter of the polar forces, dipole moment, is determined using MD.

For determining the dipole moment of a molecule in MD, it is essential to define a precise and realistic molecular structure. As there is uncertainty regarding the molecular weight and structure of the asphaltene molecules, two more acceptable structures for asphaltene have been suggested in the literature [2]. The island and aryl-linked core structures seem to be the most accepted characteristic of the asphaltene molecules. The island model supports small molecules with predominantly a single PAH core. In contrast, the aryl structure possesses a core with all aromatic carbon of the molecule and one or more aryl linkages between aromatic moieties [2]. In this research, we adopted two different hypothetical asphaltene structures, as shown in Figure 4-3, to represent asphaltene molecules from Headen et al. [46], Goual et al. [47], and Ghamartale et al. [48]. The red circles show the section of the molecules that is prone to polar forces due to heteroatoms, e.g., N or S. The optimized molecule is used to determine the dipole moment using Gaussian09 software. Information regarding MD calculations is presented in Appendix D.
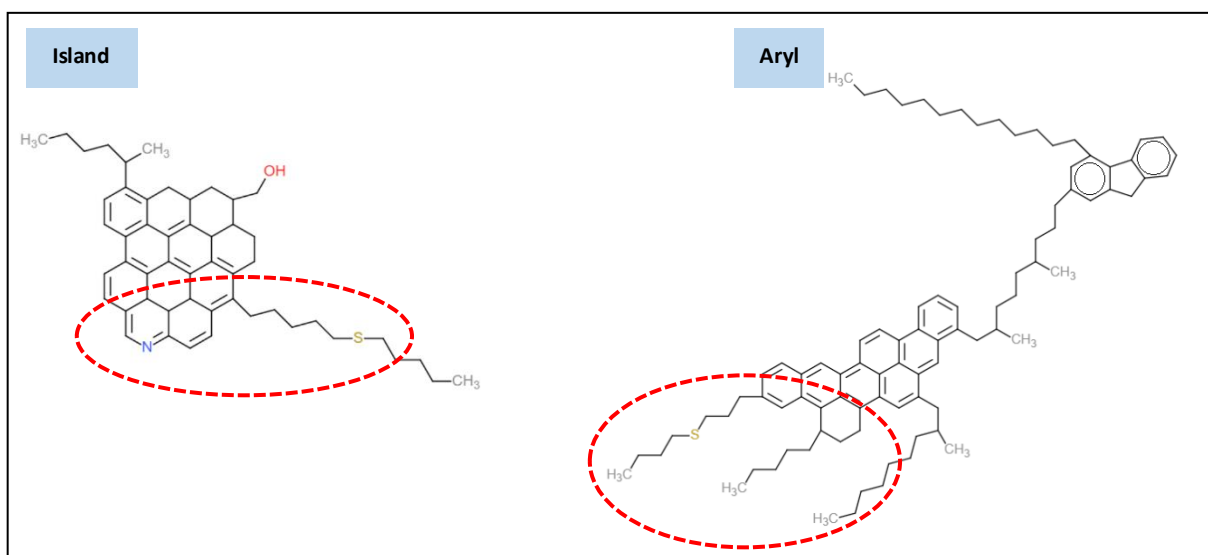
Figure 4-3. Asphlatene structures used in this research, the red circles show the part of the molecules impart polarity

4-3. Results and Discussion

In this research, a total of 78 experimental data from a crude oil sample are studied [1]. Three approaches were suggested to model asphaltene precipitation under different operational conditions. The effect of the quantity of n-paraffin, type of n-paraffin, and temperature have been studied using the proposed approaches. Approach-1 is an SRK EoS, considering a single term for attraction and repulsive forces. The binary interaction parameters (k_{ij}) used here are modified using experimental data. Approach-2 and Approach-3 are advanced EoS, and the polar forces are considered in a separate term. The main difference between these two approaches is reducing the number of adjustable parameters in the latter approach using MD calculations. Moreover, the approaches are validated by predicting the onset of asphaltene precipitation and comparing it with other asphaltene precipitation models, e.g., the scaling model.

4-3-1. Asphaltene Precipitation Using Cubic EoS (Approach-1)

This section discusses the modeling approach to calculate the asphaltene precipitation using the SRK EoS. The model correlates the extent of asphaltene precipitation at different operational conditions. The binary interactions are introduced as adjustable parameters and tuned with experimental data. Here we use the weight percent of asphaltene precipitation to adjust binary interactions, and no other data regarding density/volume is available. Hence, to reduce the degree of freedom of the model, a few parameters can be adjusted. The characterization method helped decrease the number of adjustable parameters (k_{ij}), by incorporating non-asphaltenic fractions in the heavy hydrocarbon fraction. Generally, resins play a major role in stabilizing the asphaltene particles as their adsorption around asphaltene colloids stabilizes asphaltene in the crude oil medium (as the peptizing agent), and asphaltene precipitation is a result of resins desorption. Asphaltene aggregation and phase separation generally occur due to the disconnection of resins from the asphaltene by adding light hydrocarbon.

Using this characterization strategy, the correlation ability of SRK EoS is demonstrated in Figure 4-4. As shown in Figure 4-a, the model accurately correlated the asphaltene precipitation by adding different quantities of n-paraffins (nC_6, nC_9, and nC_{12}). However, slightly higher discrepancies are observed at the high amount of n-alkanes. Adding n-alkane as precipitant, Figure 4-b shows the asphaltene yield versus the carbon number of the n-paraffin. Adding n-alkane with lower carbon

number decreases the solubility of asphaltene in the oil phase with a higher degree and causes more precipitation. Also, it seems that the accuracy of the model decreases while using heavier n-paraffin. Figures 4-a and 4-b show that approach-1 can correlate the data, while the model's prediction ability is under question.

Figure 4-4. (a) Asphaltene yield by addition of different quantities of n- paraffins (dilution ratio of n-paraffin). (b) Asphaltene yield by using nC_6, nC_9, and nC_{12} at constant temperature 293 K. Symbols represent experimental data [1] and the line is approach-1

4-3-2. Asphaltene Precipitation Using CPP EoS and Global Optimization (Approach-2)

This approach considers asphaltene as mono-aggregate particles that tend to have polar interactions. Hence, a term for polar forces are included in the volume, compressibility factor, and Helmholtz free energy calculations. The experimental data were used to tune the parameters of the EoS. In this research, we use the optimization method presented in section 3-4 to adjust the model based on global estimation with five parameters for the pure components, i.e., three parameters of the physical part a_0, b, and c_1, and two parameters for the polar forces, n_p, μ [24]. To reduce the

184

number of adjustable parameters of the physical part from three to two parameters (i.e., a and b), the energy factor (Eq 4-3) is regarded as an adjustable parameter.

The experimental data has been divided into three sets (10%-80%-10%). The first 10% of the data was used to tune the parameters of the EoS for physical and polar parts, and 80% of unseen data was utilized to adjust binary interactions and examine the correlation capability of the model. The last 10% of unseen data was deployed to check the model's prediction ability. It is worth mentioning that the last data sets are not in the range of the other data sets; hence, the extrapolation capability of the EoS also is examined.

The mixing rules are necessary to extend an EoS to mixtures successfully. The simple van der Waals one fluid mixing rules (vdW1f) were applied in the cubic part. Since the optimization is based on using the weight percent of asphaltene precipitation, and data for density or volume of fractions is not available, adjusting the co-volume parameter (i.e., b) is challenging. Therefore, the mixing rules were extended to the co-volume calculations.

Figure 4-5 compares the measured asphaltene precipitation data with those obtained from approach-2 with different quantities of n-alkanes (nC6, nC9, and nC12) at constant pressure (14.7 psi) and temperature (293 K). Figure 5-a depicts how increasing the quantity of n-paraffin (1.9 – 24.3 cm3 of n-paraffin per gram of oil) causes higher asphaltene yields. Using this approach, we were able to accurately model asphaltene precipitation in a wide range of quantities of precipitant. Figure 4-5-b shows the effect of using different n-paraffins and the impact of the carbon number of n-alkane on the precipitation. It has been shown that using light hydrocarbons causes a higher asphaltene yield due to changing the solubility of asphaltene to a higher degree. Approach-2 can accurately correlate the asphaltene precipitation data using three different n-alkane and dilution ratios.
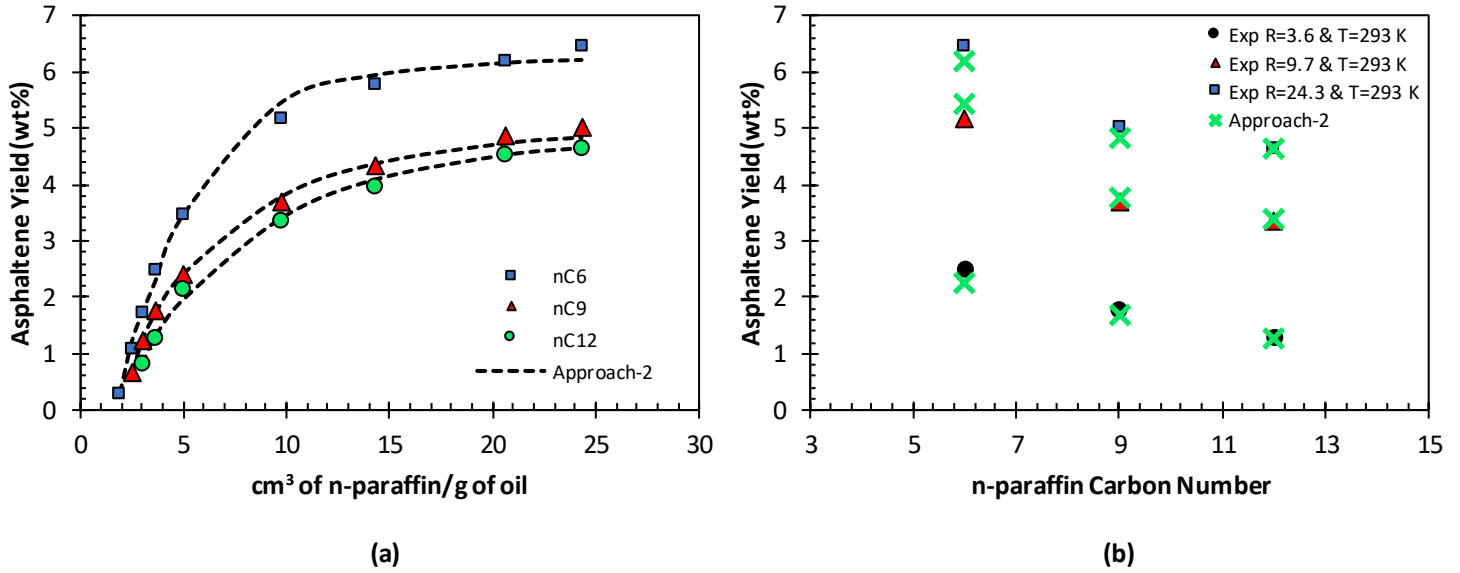
Figure 4-5. (a)Asphaltene yield by addition of different quantities of n‑ paraffins (dilution ratio of n-paraffin). (b) Asphaltene yield by using nC_6, nC_9, and nC_{12} at constant temperature 293 K. Symbols represent experimental data [1] and the line is approach-2

4-3-3. Asphaltene Precipitation Using CPP EoS and Molecular Dynamics (Approach-3)

The number of adjustable parameters has been reduced in this approach by substituting the dipole moment (μ) with those obtained from the MD. Hence, the number of adjustable parameters of the approach was reduced to three parameters, i.e., a, b, n_p. Two of the most common structures for asphaltene were optimized to find μ. The other steps to tune this approach are similar to approach-2, while the BIPs were not optimized again, and those from approach-2 were utilized here.

Figure 4-6 shows the correlation results of approach-3A and approach-3B of the experimental data using n-paraffins. Figure 4-6-a depicts the impact of adding the different quantities of n-alkane on precipitate asphaltene using nC_6, nC_9, and nC_{12}. The results from both experiments and CPP EoS show an increase in the amount of precipitation with increasing the quantity of n-alkane. Both approaches in using CPP EoS are capable of modeling asphaltene precipitation. Figure 4-6-b shows the amount of precipitation with the carbon number of n-alkane. It is shown that using a lighter n-alkane leads to more precipitation, and the findings are in agreement with the theoretical expectations. Approach-3A uses the island structure for asphaltene with a higher dipole moment

186

implying more polarity of the molecule. This structure suggests a higher aggregation degree for asphaltene than approach-3B using *the* aryl structure. Aryl structure is less polar with a lower dipole moment. Both approaches could accurately correlate asphaltene precipitation data, while a slightly better capability was observed in approach-3B. This can be attributed to the polarity of these two asphaltene structures that 3B suggests a molecule with a lower dipole moment. One can conclude that although the asphaltene molecule is polar, less polarity can be considered a more suitable characteristic of the molecule.
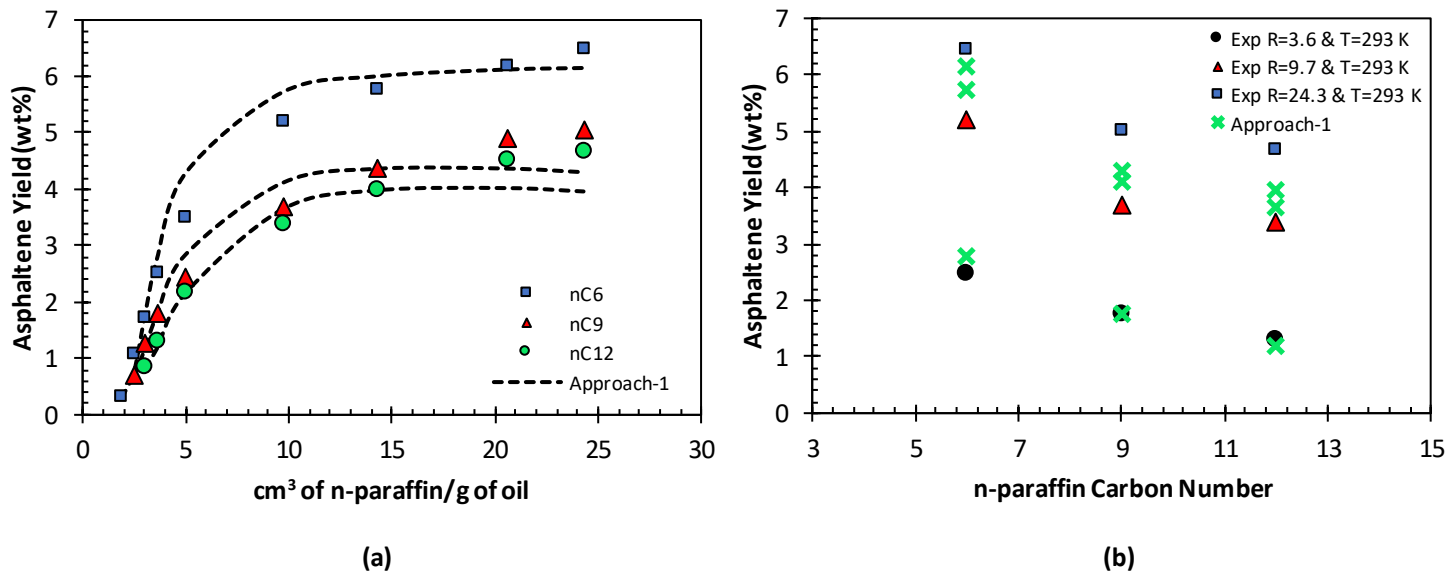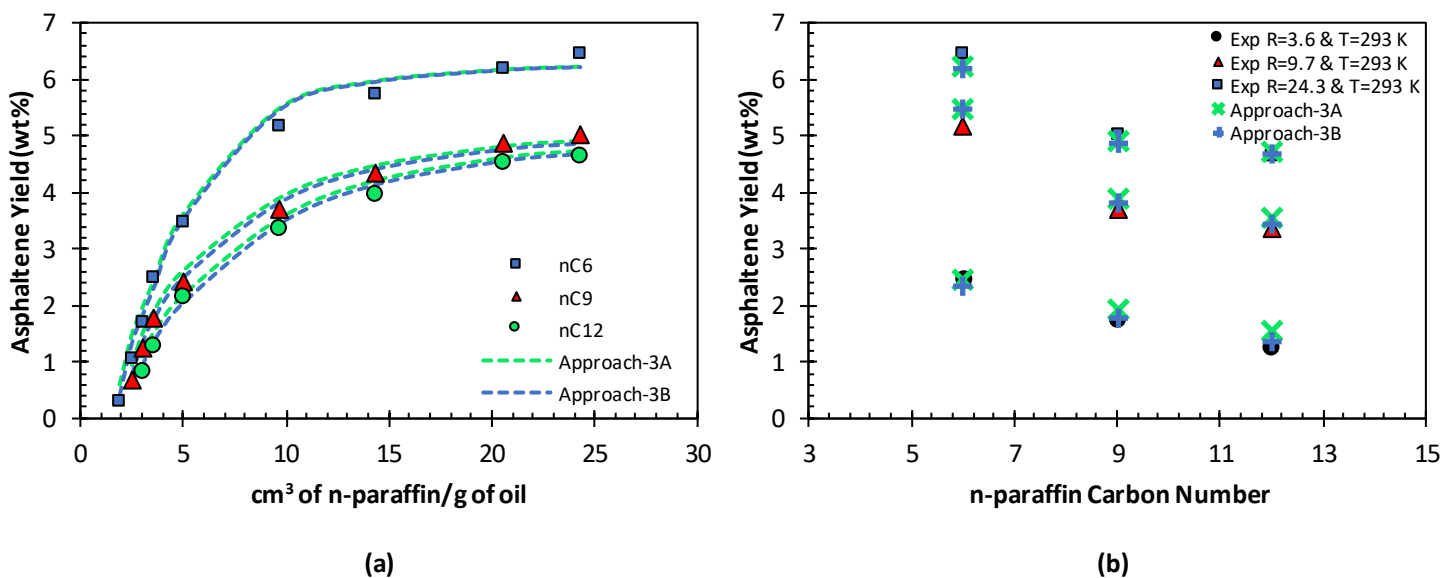

Figure 4-6. (a)Asphaltene yield by addition of different quantities of n- paraffins (dilution ratio of n-paraffin). (b) Asphaltene yield by using nC_6, nC_9, and nC_{12} at constant temperature 293 K. Symbols represent experimental data [1] and the line is approach-3A and 3B

4-3-4. Asphaltene Precipitation and Comparison of Approaches

Asphaltene particles can destabilize and form aggregates during oil production and improve oil recovery/enhanced oil recovery (IOR/EOR) by changes in operational conditions, e.g., pressure, temperature, and mixture composition. Hence, the proposed approaches are evaluated in different operating conditions. Figure 4-7 compares the performance of these approaches in various operational conditions, i.e., temperature (293-338 K), composition (2.8-24.3 cm³/g of oil), and application of different n-paraffins (nC_6, nC_9, and nC_{12}). Figure 4-7-a depicts asphaltene precipitation in different temperatures (293-338 K). It is shown that asphaltene precipitation decreases with increasing temperature due to increased solubility of asphaltene with temperature.

Figure 4-7-b shows asphaltene yield versus the amount of the n-alkane. Adding n-alkane disconnect resins from asphaltene, and more n-alkane contributes to more precipitation. Figure 4-7-c demonstrates the amount of precipitation versus the carbon number of the n-alkane. The lighter n-alkanes cause more precipitation due to changing the solubility of asphaltene to a higher degree. The figure shows that approach-2 best models asphaltene precipitation in various operational conditions considering temperature and composition, followed by approach-3 as the second-best correlation. It is worth mentioning that approach-3A and 3B demonstrate acceptable performance, while approach-3B is slightly more reliable. Approach-1 results are not as accurate as the results of the two other approaches that validate the theory for considering polar forces in asphaltene precipitation modeling.
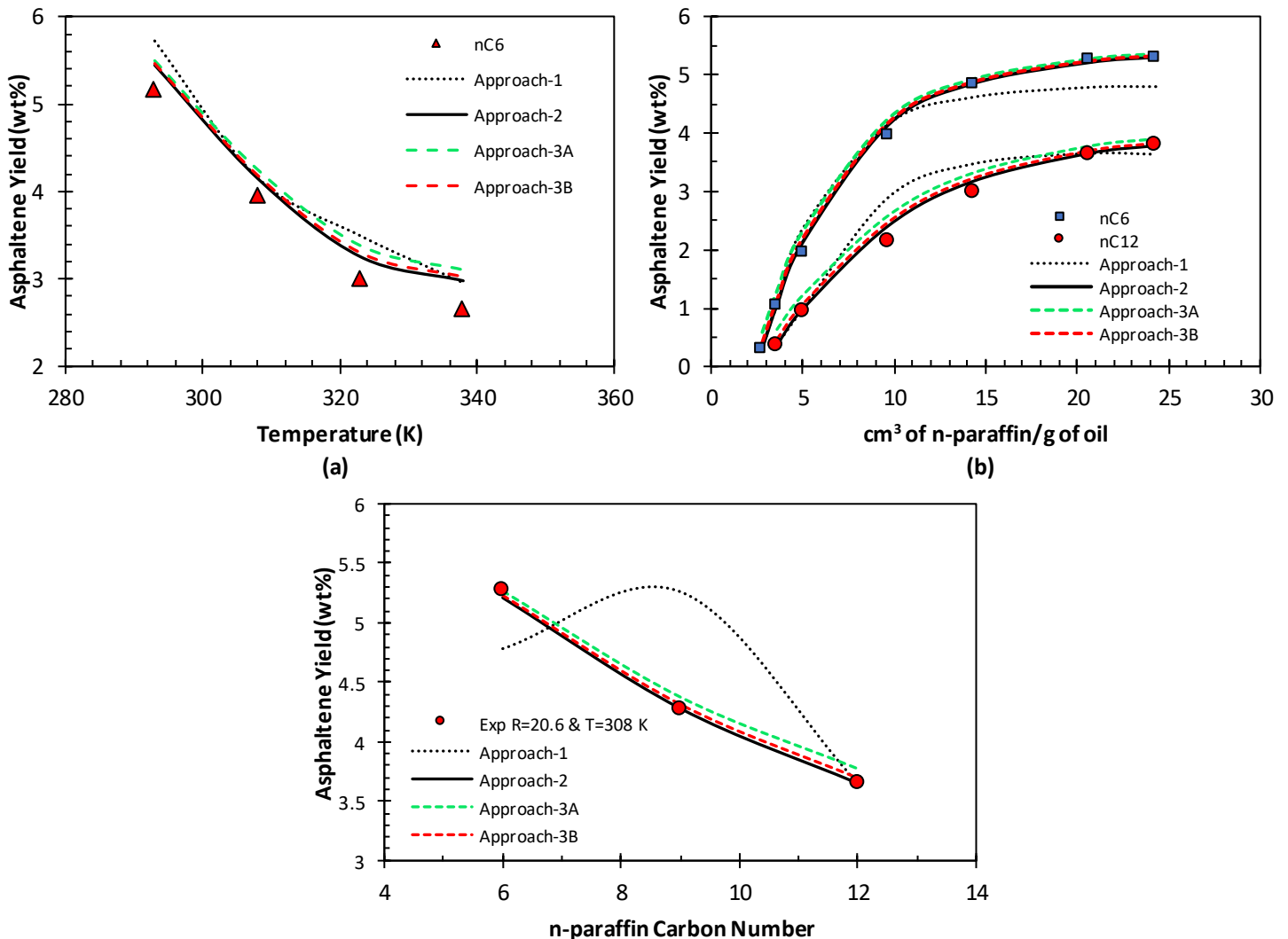
Figure 4-7. (a) Asphaltene yield in different temperature. (b) Addition of different quantities of n- paraffins at T=308 K, (c) Using n-paraffins. Symbols represent experimental data [1].

Slightly higher discrepancies are observed at the high temperature and the higher quantity of n-Sabbagh et al. [30] also noticed the same disagreement. They claimed that it might be due to the precipitation of resin, which is not considered in the precipitated phase. Also, the discrepancy may be due to the trapping of maltene (saturate, aromatic, and resin) at high magnitudes of diluents, which is neglected in the dense phase. Moreover, there is the possibility of the formation of multiple liquids and/or solids, which is not incorporated in the modeling approach [30]. One can also claim that error is possible while measuring the experimental data, as this error is inevitable. The error margin was not reported in the experimental data [1], while Wang and Buckley [49] concluded from their experimental studies that the overall error on asphaltene amount measurement was around ±0.02 wt%. Table 4-2 compares the average relative deviation in calculating the asphaltene yield in different temperatures. The results suggest that the average relative deviation is lower using lighter n-paraffins. Moreover, approach-2, 3A, and 3B are more accurate in lower temperatures.

Table 4-2. Average Relative Deviation of the approaches for different temperature and n-paraffin

error	n-paraffin	293 K				308 K				323 K				338 K			
		Approach-1	Approach-2	Approach-3A	Approach-3B	Approach-1	Approach-2	Approach-3A	Approach-3B	Approach-1	Approach-2	Approach-3A	Approach-3B	Approach-1	Approach-2	Approach-3A	Approach-3B
AARD	nC_6	0.09	0.04	0.1	0.09	0.1	0.01	0.05	0.03	0.09	0.03	0.09	0.06	0.09	0.03	0.05	0.04
	nC_9	0.13	0.01	0.1	0.04	0.3	0.03	0.06	0.06	0.1	0.04	0.06	0.09	0.05	0.01	0.08	0.04
	nC_{12}	0.1	0.01	0.09	0.04	0.08	0.02	0.05	0.03	0.08	0.05	0.05	0.03	0.06	0.01	0.03	0.05
ave error		0.1	0.02	0.09	0.05	0.1	0.02	0.05	0.04	0.09	0.04	0.06	0.06	0.06	0.01	0.05	0.04

Table 4-3 shows the values optimized for approach-2, 3A, and 3B using global optimization and MD for μ and n_p. Comparing the performance of these approaches (approach-2 with the lowest error) and the quantities for these adjustable parameters, one can suggest that asphaltene particles are polar; however, the molecule's dipole moment is more realistic for less than 2 Debye. Therefore, an aryl structure with a molecular weight of 750 g/mol and few alkyl chains (in comparison with structure B used in this study) and one/two thiophene/pyridine groups can be suggested for asphaltene. Schuler et al. [50] also observed the "Aryl-linked core" structure and a

molecular weight of approximately 750 g/mol for asphaltene molecules using atomic force microscopy and molecular orbital imaging using a scanning tunnelling microscope. They also suggested that petroleum asphaltene is less polar than coil-derived asphaltene.

Table 4-3. The parameters of the CPP models

	Apporach-2	Approach-3A	Approach-3B
μ (D)	1.83	4.44	3.64
n_p	0.007	0.01	0.009
M_w (g/mol)	750	730	1250

4-3-5. Predicting the Onset Point for Asphaltene Precipitation

One of the main applications of thermodynamic models is their ability to predict unseen data and provide information other than those measured experimentally. Experimental measurements can not always be feasible due to the cost and operational difficulties, e.g., high temperatures. Hence, the approaches proposed in this study are evaluated by unseen data that are not in the range of the seen data used for tuning the models. So, both the prediction and extrapolation capability of these approaches is examined.

Table 4-4 lists the prediction results of approach-2, 3A, and 3B for the onset point of asphaltene in different temperatures, i.e., 293 K, 308 K, 323 K, and 338 K. The approaches can model variation of onset with temperature and use different n-paraffins. Increasing temperature leads to a higher solubility of asphaltene in the oil mixture, so a higher quantity of n-paraffin is needed for the onset point. Asphaltene yields increase, and the onset point decreases with light n-paraffins since they have higher solubility parameters.

Table 4-4. Prediction of the onset points of asphaltene precipitation for n-paraffins at various temperatures

T (K)	R_c (cm^3 of n-paraffin/g of oil)								
	n-C$_6$			n-C$_9$			n-C$_{12}$		
	Approach-2	Approach-3A	Approach-3B	Approach-2	Approach-3A	Approach-3B	Approach-2	Approach-3A	Approach-3B
293	1.725	1.656	1.748	2.088	1.931	2.031	2.292	2.039	2.195
308	2.456	2.225	2.383	2.712	2.451	2.637	2.872	2.301	2.653
323	2.260	1.938	2.164	3.091	2.719	2.938	3.156	2.794	3.038
338	3.008	2.684	2.871	2.963	2.450	2.770	3.131	2.482	2.873

Table 4-5 compares the prediction results of the approaches with those from experiments in constant temperature 293 K. The average relative errors prove that approach-2, with the lowest error, is the most accurate for predicting the onset point, followed by approach-3B as the second-best model. Approach-3A is placed as the third-best model in this study.

Table 4-5. Average Absolute Relative Deviation of onset prediction of approach-2, 3A, and 3B for different temperature and n-paraffin, experimental data is from Hu et al., [1]

T (K)	n-paraffin	Experimental data (R_c) [1]	Approach-2 (R_c)	AARD	Approach-3A (R_c)	AARD	Approach-3B (R_c)	AARD
	n-C6	1.903	1.725	0.0935	1.656	0.129	1.748	0.0813
293	n-C9	2.188	2.088	0.0454	1.931	0.117	2.031	0.0715
	n-C12	2.312	2.292	0.0083	2.039	0.117	2.195	0.0502

4-3-6. Validation of the Proposed Approaches

To show the robustness of the CPP, further analysis is performed using the scaling model applied by Hu et al. [1] and compared with the experimental data. Scaling models have been developed based on aggregation/gelation phenomena independent of asphaltene structure. The scaling model is a four-parameter equation that expresses the weight percent of asphaltene precipitation in terms of dilution ratio, the molecular weight of solvent, and temperature [51]. However, the model does not provide any further information regarding the asphaltene structure and interaction of particles.

Figure 4-8 depicts asphaltene yield using n-paraffin, e.g., nC_{12}, and compares the approaches used here and the scaling model. The figure shows that the CPP can simulate asphaltene precipitation; even approach-1 seems more accurate than the scaling model. Although the scaling model is simple, it does not provide any insight into the mixture's PVT properties and thermodynamic state.
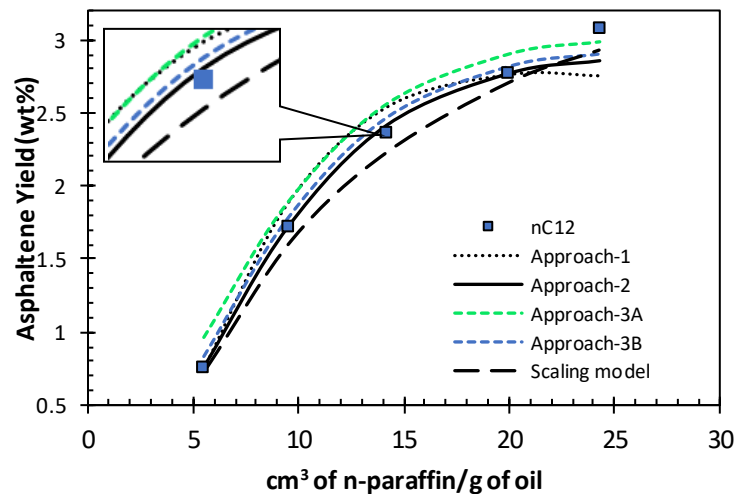
Figure 4-8. Comparing approaches used here with scaling model, symbols represent experimental data [1], T=338 K and R^2 (Approach 2, 3A, 3B)=0.988, R^2 (approach 1)=0.95, R^2 (Scaling model)=0.95

4-4. Conclusion

The need for accurate insight into the asphaltene properties and phase behaviour is crucial due to flow assurance issues caused by asphaltene precipitation and deposition. Hence, asphaltene precipitation under different operational conditions and the impact of intermolecular forces on the phenomenon need careful consideration. Traditional/advanced EoS, e.g., cubic and CPA EoS, and MD, have been used to study asphaltene precipitation. Nevertheless, few research investigations focus on asphaltene structure and intermolecular forces and relate these characteristics to macro-level properties and quantity of precipitation. This work suggests three approaches to study the effect of asphaltene structure and polarity on the precipitation phenomenon. The approaches include SRK EoS (approach-1), CPP EoS and global optimization (approach-2), CPP EoS and MD (island structure: approach-3A, aryl structure: approach-3B). Approach-2 shows promising performance in the correlation of asphaltene yield and prediction of onset point. Approach-3 also demonstrates acceptable efficiency, while slightly less accurate than approach-2. Approach-1 is the less efficient model with a relatively poor prediction capability. It is worth mentioning that all three approaches have more reliable results than the scaling model. Considering the values for dipole moment and molecular weight of asphaltene, along with the correlation and prediction

ability of the techniques, it is revealed that adding the polar term to cubic EoS increases its efficiency considerably. Moreover, the aryl structure with a 750 g/mol molecular weight and one/two thiophene/pyridine group is the most proper asphaltene structure.

Nomenclature

List of Abbreviations

AOP	Asphaltene onset point
BIP	Binary interaction parameter
CPA	Cubic plus association
CPP	Cubic plus polar
EoS	Equation of State
Fe	Iron
GA	Genetic algorithm
GO	Global optimization
HC	Heavy component
LB	Lower bound
LLE	Liquid-Liquid equilibrium
MD	Molecular dynamics
N	Nitrogen
NM	Nelder-Mead
O	Oxygen
OPEX	Operational expenditures
PC-SAFT	Perturbed-chain statistical associating fluid theory
PAH	Poly-Aromatic Hydrocarbon
PR	Peng-Robinson
S	Sulfur
SRK	Soave–Redlich–Kwong
STO	Stock tank oil
UB	Upper bound
V	Vanadium
WOA	Without association

Variables/Parameters

A	Helmholtz free energy
a	attractive energy parameter
a_0	physical energy parameter [Pas m^2 mol^{-2}]
b	co-volume parameter [m^3 mol^{-1}]
c	parameter in the energy term of SRK
d	segment diameter
Da	g/mole
f	fugacity
F	objective function
I	constants by Larsen et al. [31]
K	equilibrium constants
k_B	Boltzmann constant
k_{ij}	binary interaction parameter
N	number of moles
n_e	number of data points
n_i	data point
n_p	fraction of molecule in polar interaction
P	pressure [Pascal]
Pc	critical pressure [Pascal]
R	universal gas constant [8.314 J mol^{-1} K^{-1}]
T	temperature [K]
Tc	critical temperature [K]
V or ν	Volume or molar volume
x	mole fraction
y	mole fraction
Z	Compressibility factor

Greek Letters

α	polar strength
π	Pi number
π- π	Pi-pi interaction
ρ	density
Φ	fugacity coefficient

| μ | dipole moment |
| σ | variance |

Subscripts and Superscripts

Atractive	Attractive energy
Physical	physical portion
Polar	Polar energy
Repulsive	Repulsive energy
van der Waals	van der Waals energy

Reference

1. Hu, Y.-F. and T.-M. Guo, Effect of temperature and molecular weight of n-alkane precipitants on asphaltene precipitation. Fluid Phase Equilibria, 2001. 192(1-2): p. 13-25.

2. Schuler, B., Zhang, Y., Liu, F., Pomerantz, A. E., Andrews, A. B., Gross, L., Pauchard, V., Banerjee, S., & Mullins, O. C., Overview of asphaltene nanostructures and thermodynamic applications. Energy & Fuels, 2020. **34**(12): p. 15082-15105.

3. Speight, J.G., The chemical and physical structure of petroleum: effects on recovery operations. Journal of Petroleum Science and Engineering, 1999. **22**(1): p. 3-15.

4. Alboudwarej, H., Akbarzadeh, K., Beck, J., Svrcek, W. Y., & Yarranton, H. W., Regular solution model for asphaltene precipitation from bitumens and solvents. AIChE Journal, 2003. **49**(11): p. 2948-2956.

5. Wattana, P., Wojciechowski, D., Bolaños, G., Fogler, H.S., Study of asphaltene precipitation using refractive index measurement. Petroleum science and technology, 2003. **21**(3-4): p. 591-613.

6. Taheri-Shakib, J., A. Shekarifard, and H. Naderi, Experimental investigation of the asphaltene deposition in porous media: accounting for the microwave and ultrasonic effects. Journal of Petroleum Science and Engineering, 2018. **163**: p. 453-462.

7. Alimohammadi, S., S. Zendehboudi, and L. James, A comprehensive review of asphaltene deposition in petroleum reservoirs: Theory, challenges, and tips. Fuel, 2019. **252**: p. 753-791.

8. Wylde, J. and A. Punase, Asphaltenes: A Complex and Challenging Flow Assurance Issue To Measure and Quantify Risk. Journal of Petroleum Technology, 2020. **72**(05): p. 45-48.

9. Yonebayashi, H., Asphaltene Flow Assurance Risks: How Are Pitfalls Brought into the Open? Journal of the Japan Petroleum Institute, 2021. **64**(2): p. 51-66.

10.   Sayyad Amin, J., S. Alimohammadi, and S. Zendehboudi, Systematic investigation of asphaltene precipitation by experimental and reliable deterministic tools. The Canadian Journal of Chemical Engineering, 2017. **95**(7): p. 1388-1398.

11.   Andersen, S.I. and K.S. Birdi, Influence of temperature and solvent on the precipitation of asphaltenes. Petroleum Science and Technology, 1990. **8**(6): p. 593-615.

12.   Andersen, S.I., Effect of precipitation temperature on the composition of n-heptane asphaltenes. Fuel science & technology international, 1994. **12**(1): p. 51-74.

13.   Andersen, S.I. and J.G. Speight, Thermodynamic models for asphaltene solubility and precipitation. Journal of Petroleum Science and Engineering, 1999. **22**(1): p. 53-66.

14.   Soorghali, F., A. Zolghadr, and S. Ayatollahi, Effect of resins on asphaltene deposition and the changes of surface properties at different pressures: a microstructure study. Energy & Fuels, 2014. **28**(4): p. 2415-2421.

15.   Subramanian, S., S. Simon, and J. Sjöblom, Asphaltene precipitation models: a review. Journal of Dispersion Science and Technology, 2016. **37**(7): p. 1027-1049.

16.   Akbarzadeh, K., et al., A generalized regular solution model for asphaltene precipitation from n-alkane diluted heavy oils and bitumens. Fluid Phase Equilibria, 2005. **232**(1-2): p. 159-170.

17.   Forte, E. and S.E. Taylor, Thermodynamic modelling of asphaltene precipitation and related phenomena. Advances in colloid and interface science, 2015. **217**: p. 1-12.

18.   Nikooyeh, K. and J.M. Shaw, On the applicability of the regular solution theory to asphaltene+ diluent mixtures. Energy & Fuels, 2012. **26**(1): p. 576-585.

19.   Manshad, A.K., Manshad, M., Rostami, H., Mohseni, S. M., Vaghefi, M., The association thermodynamics modeling of asphaltene precipitation. Petroleum Science and Technology, 2014. **32**(1): p. 51-60.

20.   Sheu, E.Y. and O.C. Mullins, Fundamentals and Applications. 1995: Springer.

21.   Mousavi-Dehghani, S., et al., An analysis of methods for determination of onsets of asphaltene phase separations. Journal of Petroleum Science and Engineering, 2004. **42**(2-4): p. 145-156.

22.   Danesh, A., PVT and phase behaviour of petroleum reservoir fluids. 1998: Elsevier.

23.   Jog, P.K., Sauer, S.U., Blaesing, J., Chapman, W., Application of dipolar chain theory to the phase behavior of polar fluids and mixtures. Industrial & engineering chemistry research, 2001. **40**(21): p. 4641-4648.

24.   Kontogeorgis, G.M. and G.K. Folas, Thermodynamic models for industrial applications: from classical and advanced mixing rules to association theories. 2009: John Wiley & Sons.

25.   Li, Z. and A. Firoozabadi, Cubic-plus-association equation of state for water-containing mixtures: Is "cross association" necessary? AIChE journal, 2009. **55**(7): p. 1803-1813.

26.   Li, Z. and A. Firoozabadi, Modeling asphaltene precipitation by n-alkanes from heavy oils and bitumens using cubic-plus-association equation of state. Energy & fuels, 2010. **24**(2): p. 1106-1113.

27.   Arya, A., Liang, X., von Solms, N., & Kontogeorgis, G. M., Modeling of asphaltene onset precipitation conditions with cubic plus association (CPA) and perturbed chain statistical associating fluid theory (PC-SAFT) equations of state. Energy & Fuels, 2016. **30**(8): p. 6835-6852.

28.   Arya, A., Liang, X., von Solms, N., & Kontogeorgis, G. M., Modeling of asphaltene precipitation from crude oil with the cubic plus association equation of state. Energy & Fuels, 2017. **31**(2): p. 2063-2075.

29.   Abunahman, S. S., dos Santos, L. C., Tavares, F. W., & Kontogeorgis, G. M., A computational tool for parameter estimation in EoS: New methodologies and natural gas phase equilibria calculations. Chemical Engineering Science, 2020. **215**: p. 115437.

30.   Sabbagh, O., Akbarzadeh, K., Badamchi-Zadeh, A., Svrcek, W. Y., & Yarranton, H. W., Applying the PR-EoS to asphaltene precipitation from n-alkane diluted heavy oils and bitumens. Energy & fuels, 2006. **20**(2): p. 625-634.31.   Larsen, B., J. Rasaiah, and G. Stell, Thermodynamic perturbation theory for multipolar and ionic liquids. Molecular Physics, 1977. **33**(4): p. 987-1027.

32.   Gross, J., An equation-of-state contribution for polar components: Quadrupolar molecules. AIChE journal, 2005. **51**(9): p. 2556-2568.

33.   Vrabec, J. and J. Gross, Vapor− liquid equilibria simulation and an equation of state contribution for dipole− quadrupole interactions. The Journal of Physical Chemistry B, 2008. **112**(1): p. 51-60.

34.   Shahriari, R., M.R. Dehghani, and B. Behzadi, A modified polar PHSC model for thermodynamic modeling of gas solubility in ionic liquids. Fluid phase equilibria, 2012. **313**: p. 60-72.

35.   Marshall, B.D. and C.P. Bokis, A PC-SAFT model for hydrocarbons I: Mapping aromatic π-π interactions onto a dipolar free energy. Fluid Phase Equilibria, 2019. **489**: p. 83-89.

36.   Arya, A., N. von Solms, and G.M. Kontogeorgis, Determination of asphaltene onset conditions using the cubic plus association equation of state. Fluid Phase Equilibria, 2015. **400**: p. 8-19.

37.   Pan, H. and A. Firoozabadi. Thermodynamic micellization model for asphaltene precipitation from reservoir crudes at high pressures and temperatures. in SPE Annual Technical Conference and Exhibition. 1997. Society of Petroleum Engineers.

38.   Riazi, M.R. and T.A. Al-Sahhaf, Physical properties of heavy petroleum fractions and crude oils. Fluid phase equilibria, 1996. **117**(1-2): p. 217-224.

39.   Schwaab, M., Biscaia, E.C., Monteiro, J. J. L., Pinto, J. C., Nonlinear parameter estimation through particle swarm optimization. Chemical Engineering Science, 2008. **63**(6): p. 1542-1552.

40.   dos Santos, L. C., Abunahman, S. S., Tavares, F. W., Ahón, V. R. R., & Kontogeorgis, G. M., Modeling Water Saturation Points in Natural Gas Streams Containing CO2 and H2S-Comparisons with Different Equations of State. Industrial & Engineering Chemistry Research, 2015. 54(2): p. 743-757.

41.   dos Santos, L.C., Tavares, F. W., Ahón, V. R. R., & Kontogeorgis, G. M., Modeling MEA with the CPA equation of state: A parameter estimation study adding local search to PSO algorithm. Fluid Phase Equilibria, 2015. **400**: p. 76-86.

42.   Nelder, J.A. and R. Mead, A simplex method for function minimization. The computer journal, 1965. **7**(4): p. 308-313.

43.   Akbarzadeh, K. and M. Moshfeghian, Application of the polymer chain-of-rotator (PCOR) equation of state and its extension to polymer blends. Fluid phase equilibria, 2001. **187**: p. 347-361.

44.   Perfetti, E., R. Thiery, and J. Dubessy, Equation of state taking into account dipolar interactions and association by hydrogen bonding. I: Application to pure water and hydrogen sulfide. Chemical Geology, 2008. **251**(1-4): p. 58-66.

45.   De Villiers, A., C. Schwarz, and A. Burger, Improving vapour–liquid-equilibria predictions for mixtures with non-associating polar components using sPC-SAFT extended with two dipolar terms. Fluid phase equilibria, 2011. **305**(2): p. 174-184.

46.   Headen, T.F. and M.P. Hoepfner, Predicting Asphaltene Aggregate Structure from Molecular Dynamics Simulation: Comparison to Neutron Total Scattering Data. Energy & Fuels, 2019. **33**(5): p. 3787-3795.

47.   Goual, L., Sedghi, M., Wang, X., Zhu, Z., Asphaltene aggregation and impact of alkylphenols. Langmuir, 2014. **30**(19): p. 5394-5403.

48.   Ghamartale, A., S. Zendehboudi, and N. Rezaei, New Molecular Insights into Aggregation of Pure and Mixed Asphaltenes in the Presence of n-Octylphenol Inhibitor. Energy & Fuels, 2020. **34**(10): p. 13186-13207.

49.   Wang, J. and J. Buckley, Effect of dilution ratio on amount of asphaltenes separated from stock tank oil. Journal of dispersion science and technology, 2007. **28**(3): p. 425-430.

50.   Schuler, B., Meyer, G., Peña, D., Mullins, O. C., & Gross, L., Unraveling the molecular structures of asphaltenes by atomic force microscopy. Journal of the American Chemical Society, 2015. 137(31): p. 9870-9876.

51.   Alimohammadi, S., Sayyad Amin, J., Nikkhah, S., Soroush, M., Zendehboudi, S., Development of a new scaling model for asphaltene precipitation in light, medium, and heavy crude oils. Journal of Molecular Liquids, 2020. **312**: p. 112974.

52.   Hustad, Odd Steve, Jia, Na , Pedersen, Karen Schou, Memon, Afzal , and Sukit Leekumjorn. "High-Pressure Data and Modeling Results for Phase Behavior and Asphaltene Onsets of Gulf of Mexico Oil Mixed With Nitrogen." SPE Res Eval & Eng 17 (2014): 384–395.

53.   Vargas, Francisco M., Garcia-Bermudes, Miguel, Boggara, Mohan, Punnapala, Sameer, Abutaqiya, Mohammed, Mathew, Nevin, Prasad, Sudha, Khaleel, Aisha, Al Rashed, Mariam, and Hadel Al Asafen. "On the Development of an Enhanced Method to Predict Asphaltene Precipitation." Paper presented at the Offshore Technology Conference, Houston, Texas, May 2014.

Chapter 5 : Summary and Recommendations for Future Work

This research focuses on improving the accuracy and modeling capability of describing asphaltene precipitation using various equations of state (EoS) including Cubic (Peng Robinson and Soave-Redlich-Kwong), Cubic Plus Association (CPA), and Cubic Plus Polar (CPP) EoSs. In each phase of this study, the impact of different intermolecular forces is studied for asphaltene precipitation. Thermodynamic investigations are applied to investigate the effect of various operating conditions and binary parameters, e.g., binary interaction parameters and cross association, affecting the asphaltene phase separation. This thesis includes five chapters: Introduction and overview (chapter one), literature review (chapter two), asphaltene modeling using CPA EoS and advanced optimization technique (chapter three), and improved CPP EoS and Molecular Dynamics (MD) (chapter four). The current chapter (chapter 5) includes the summary and recommendations.

First, despite the great importance of asphaltene issues, a comprehensive literature review to study asphaltene precipitation and deposition was missing in the literature. Hence, a comprehensive literature review was first conducted to address asphaltene precipitation from different standpoints and to identify research gaps. In the review section, the theories and mechanisms of precipitation/deposition, experimental and modeling approaches, the influences of operational/fluid/reservoir parameters, and treatment/inhibition techniques are effectively studied and reviewed. Moreover, the economic analysis of flow assurance focusing on asphaltene deposition and the most common theoretical and practical challenges in asphaltene precipitation/deposition are discussed.

Second, a global optimization technique was applied to tune the EoS, and to increase the accuracy and prediction capability of the EoS. One of the main challenges of using EoS is the optimization of the adjustable parameters. Instead of using gradient based optimization techniques, e.g., Nelder Mead Simplex, application of our global optimization approach led to an improvement in the modeling capability of the CPA EoS (~$R2=0.95$), skipped the entrapment in the local optima while optimizing the EoS, and increased the reliability of the EoS. A systematic sensitivity analysis of operational conditions/BIPs were added to better understand the interconnection between operating conditions and asphaltene precipitation, and to increase the reliability of the CPA EoS. Correlations were developed for BIPs and associations in the range of experimental data. The correlations were later examined in a broader range of operating conditions, and the globally optimized CPA using binary interaction parameters still showed a very low deviation (average

deviation of less than 0.067 for correlation and prediction). It was shown that the CPA approach can accurately simulate the asphaltene precipitation and onset condition with acceptable accuracy. Slightly higher discrepancies were observed with a high quantity of n-alkane and high temperature. After analyzing the experimental data, it was revealed that the experimental data used to adjust the CPA approach are not normally distributed in some ranges, resulting in the observed error. Finally, the relative importance analysis demonstrated that the composition of the mixture (dilution ratio) is the most influential factor contributing to the asphaltene precipitation (RI= +0.719), followed by the carbon number of n-alkane (RI= -0.247) and temperature (RI= -0.195).

Third, although the presence of heteroatoms (e.g., sulfur) in asphaltene molecules impart polarity, this phenomenon was not previously considered in asphaltene models. Traditional/advanced EoS have been used to study asphaltene precipitation, however no previous research focused on asphaltene structure and intermolecular forces and related these characteristics to macro-level properties and quantity of precipitation. In this novel work, we demonstrate the extension of the cubic EoS can be considered to effectively calculate asphaltene precipitation. A global optimization approach and molecular dynamic (MD) simulation were used to increase the reliability of the optimization and reduce the number of adjustable parameters for polar forces. Three approaches were applied to study the effect of asphaltene structure and polarity on the precipitation phenomenon: SRK EoS; CPP EoS and global optimization; and CPP EoS and MD (island structure and aryl structure). CPP EoS showed promising performance in the correlation of asphaltene yield (AARD%≈0.024) and prediction of onset point. CPP EoS and MD (AARD%≈0.05) also demonstrated acceptable efficiency while slightly less accurate than CPP EoS and global optimization. SRK EoS was the least efficient model with a relatively poor prediction capability. All three approaches have more reliable results compared to the control model, i.e., the scaling model. Considering the values for dipole moment and molecular weight of asphaltene, along with the correlation and prediction ability of the techniques, it was revealed that adding the polar term to the extension of the cubic EoS increases its efficiency considerably. Moreover, the aryl structure with a 750 g/mol molecular weight is the most proper asphaltene structure.

The overall conclusions of this study can be summarized as following:

- The developed CPA EoS using global optimization can accurately model asphaltene precipitation in operating conditions.

- Correlations developed for BIPs can assist the CPA EoS by increasing the prediction capability and accuracy.

- The CPP EoS enhanced by global optimization, and Molecular Dynamics calculations are able to successfully correlate/predict asphaltene precipitation and onset point with the composition.

- The modeling approach, i.e., Soave-Redlich-Kwong (SRK) and Peng Robinson (PR) EoSs, used a simple characterization approach for oil and divided the C7+ fraction into only two components. While the model is able to correlate asphaltene precipitation, some limited prediction capabilities are observed.

- Sensitivity analysis is conducted to understand further the effect of temperature, composition, and diluents on asphaltene precipitation.

- The modeling approach is more accurate when using our suggested characterization technique in comparison with using SARA analysis for oil characterization due to a lower degree of freedom and few optimization parameters. Therefore, it can easily be integrated with PVT simulators.

- The CPA and CPP models are superior to the scaling model for quantifying asphaltene precipitation.

- A MATLAB tool is developed to calculate asphaltene precipitation with temperature, amount of precipitant, and different n-alkane that can be further developed and used.

The following suggestions and recommendations are given for future studies:

- The effect of pressure and composition of injected gas injection on asphaltene precipitation can be studied using the approaches introduced in this research.

- It is believed that the advanced EoS, e.g., CPA and CPP, and global optimization can improve pore-scale simulation of asphaltene precipitation modeling. We suggest trying pore scale thermodynamic modeling.

- The proposed approaches in this research (CPA-GO and CPP-GO-MD) can be incorporated into the asphaltene deposition simulation to increase the accuracy of the model by having a reliable estimation for asphaltene precipitation. However, there might

be a need to tune the parameters of the precipitation model according to the new operating conditions.

- Molecular dynamic calculations and Zeta potential can be applied to understand asphaltene precipitation in different systems, e.g., aqueous solutions, in the presence of water, and foam, and determine the parameters of the EoS, e.g., association. Therefore the number of adjustable parameters would be reduced.

- The modeling approach proposed here could be further used and validated over a wider range of oil types and blended oil mixtures.

Appendix

Appendix A; asphaltene precipitation/deposition review, supplementary information to chapter 2

Section A: *Mechanism of Asphaltene Precipitation.* Polydispersity balance is a factor to determine the stabilization of an oil mixture, which is dependent on the ratio of polar/non-polar and light/heavy components. Process and thermodynamic conditions such as temperature, pressure, or/and adding a solvent change the polydispersity balance and cause the asphaltene deposition. When a solvent is added to an oil mixture, depending on the type of the solvent (aromatic or paraffinic), asphaltene precipitation or deposition may occur. Firstly, adding an aromatic solvent to the oil mixture results in the formation of micelle-type aggregates that do not grow due to the packing constraints resulting from the complicated structure of asphaltene. Secondly, adding a paraffinic solvent to the oil mixture would cause the formation of the solid aggregate phase, flocculation, and deposition of asphaltene [1, 2].

The self-association tendency of asphaltene results in the formation of steric colloids suspended by peptizing agents such as resins. The concentration of the peptizing agent (resin), number of surface sites occupied by the peptizing agent, and equilibrium between the peptizing agent and colloid particles are the vital factors that determine the stability of steric colloids [2].

The effect of aggregation can be explained by the concentration of the peptizing agent. When the concentration of the peptizing agent (resin) decreases so that the solvent cannot fully cover the surface of the heavy particles, the destabilization, aggregation, and precipitation of asphaltene will occur [3].

Investigating the asphaltene flocculation and deposition in a conduit, the electrokinetic effect needs to be considered. This impact is the result of the electrical potential difference in the conduit due to the movement of the colloidal particles in the oil mixture, which causes asphaltene deposition and plugging. Some of the factors that have considerable influences on to this occurrence include the characteristics of the conduit (electrical, thermal, and wettability characteristics), pressure, temperature, flow regime, and properties of the oil mixture [2].

Section B: *Kinetics of Asphaltene Precipitation.* Maqbool et al. (2009) investigated the kinetics of asphaltene precipitation induced by n-alkane in two crude oil samples [31]. They used optical microscopy and centrifugal separation to detect the onset point and quantity of precipitation. It was concluded that the time span for asphaltene precipitation ranges between minutes to months,

depending on the concentration of the precipitant. They observed that the short time span precipitation experiments in some studies can have misleading results because a system, which is stable in a short time frame, might be unstable in a longer time period. In addition, they did not notice any critical concentration of precipitant in asphaltene precipitation induced by n-alkanes [4]. They showed that the kinetics of asphaltene precipitation is very slow before and near the onset point, while above the onset, it reaches a plateau faster. To summarize, it was suggested that for long time experiments, the solubility of asphaltenes can be established as a function of the amount of precipitant; by contrast, for the short time period, the amount of solubility would be over-predicted [4].

Haji-Akbari et al. (2013) showed that asphaltene precipitation is a kinetic phenomenon and it is also universal for some oil samples [32]. They concluded that two dominant factors normally control the asphaltene aggregation; namely, (1) the rate of sub-micrometre-sized particles collisions, and (2) the tendency between aggregations (see Figure B-1). In addition, the repulsion due to the steric effect is dominant in a pure oil sample, causing stabilization of asphaltene [5].
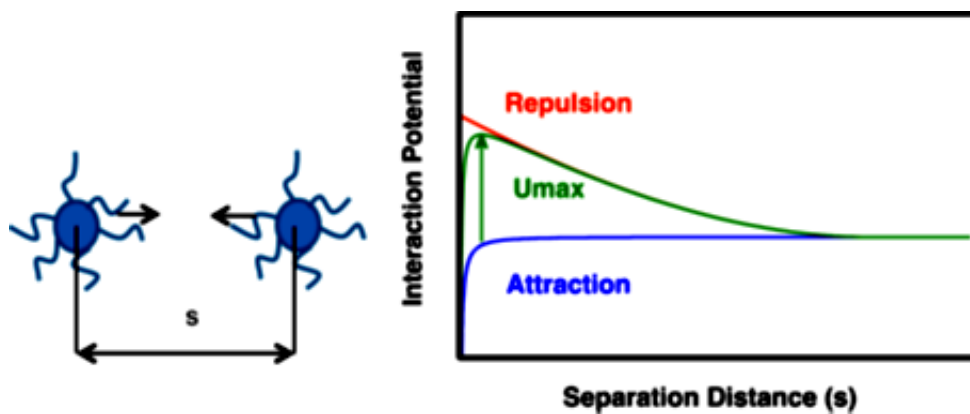
Figure A-1. Interaction of asphaltene particles versus distance [5].

It is important to note that interaction forces (repulsive or/and attractive) between asphaltene aggregations are central for the stability or attachment of asphaltene colloids. When the attractive forces are higher than the repulsive ones, the probability of successful collisions would be higher. As depicted in Figure B-1, the maximum of the potential energy landscape (repulsive barrier) forms at the separation distances at which the steric layers start to overlap [5]. All collisions do not lead to aggregation since enough thermal energy is also required to overcome the repulsive

barrier. Referring to Smoluchowski's aggregation model and steric effect, they found a master universal curve for the asphaltene kinetics. Their new method suggested that the aggregation kinetics of different crude oils are controlled by the viscosity and solubility parameters. It was shown that the difference between the solubility parameter of asphaltene and solution is inversely proportional to the repulsion barrier as follows [5]:

$$U_{max} \propto \left(\frac{1}{(\delta_{asph} - \delta_{solution})^2} \right) \tag{A-1}$$

where δ_{asph} and $\delta_{solution}$ represent the solubility parameters of asphaltene and solution, respectively. They experimentally proved that the measured detection times of aggregation are related to the changes in the solubility parameters at a constant temperature as given below [5]:

$$\ln\left(\frac{t_{detection}\sqrt{C_1(0)}}{\mu} \right) \propto \left(\frac{1}{(\delta_{asph} - \delta_{solution})^2} \right) \tag{A-2}$$

In Equation (B-2), $C_1(0)$ and μ are the initial concentration of asphaltene nanoparticles and viscosity of the solution, respectively. They used ten different oil samples to examine the accuracy of the suggested model as shown in Figure B-2. Although different aggregation behaviours were observed, the model was successfully applied to various crude oils [5].
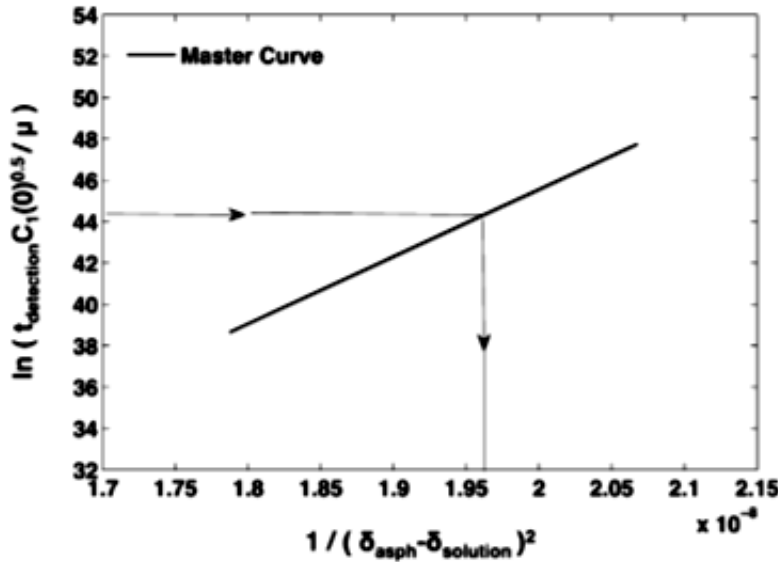
Figure A-2. Master curve for asphaltene aggregation rate [5].

Chaisoontornyotin et al. (2016) studied the effect of the type of the solvent, the carbon number of the solvent, and concentration of the solvent on the asphaltene aggregation and deposition [30]. They used a geometric population balance model to find the efficiency of the asphaltene–asphaltene collision. They showed that in a slow kinetic process, the higher the carbon number of the solvent, the slower equilibrium for asphaltene precipitation (lower collision efficiency) [6]. To shed a light on the issue, they used C_7, C_8, C_9, and C_{10} with a constant concentration. They found that the equilibrium times are 70, 170, 200, and 270 hours for C_7, C_8, C_9, and C_{10}, respectively. This observation was explained by the relationship of viscosity and carbon number. The higher carbon number, the greater viscosity, the slower diffusion of asphaltene colloids, and the fewer collisions, which lead to a slower equilibrium. In addition, decreasing the amount of the precipitant results in a lower collision efficiency [6]. They concluded that the solubility of asphaltene remains constant with slow kinetics and low concentrations of various solvents. Studying the asphaltene tendency to deposit, the capillary flow experiments were conducted under the same conditions. They found a correlation between the time of initial deposition and the difference between asphaltene and solution solubility parameters. They observed that asphaltene is deposited faster using a precipitant with a higher concentration and lower carbon number [6].

Favero et al. (2017) reviewed some recent experimental and modeling studies on the kinetics of asphaltene destabilization and flocculation by adding a precipitant [33]. One of the introduced models is the geometric population balance model as demonstrated in Figure B-3. This model is much simpler than the Smoluchowski kinetics. As Figure B-3 shows, when the geometric scaling factor (R) is equal to 2, the model is presented as follows [7]:

$$\frac{dC_k}{dt} = \sum_{j=1}^{k-2} K_{j,k-1} 2^{j-k+1} C_j C_{k-1} + a\left\{\frac{1}{2} K_{k-1,k-1}(C_{k-1})^2\right\} - b\left\{\sum_{j=1}^{k-1} K_{j,k-1} 2^{j-k} C_j C_k + \sum_{j=k}^{N-1} K_{j,k} C_j C_k\right\} \quad \text{(A-3)}$$

where C_k, K, and t refer to the concentration of the species, collision kernel, and time, respectively. Therefore, the rate of change of particles concentrations is the sum of the formation of the kth species from smaller species and the consumption of the kth species to form larger species. The model was solved numerically to find the kinetics of the asphaltene flocculation [33]. It was found that the asphaltene flocculation is faster for a higher concentration of solvent. They observed a

linear relationship between the heptane volume in a type of semilogarithmic and time [7]. The only parameter of the model that should be tuned is the collision efficiency. It was concluded that the collision efficiency has a linear correlation with the alkane concentration; the more heptane concentration, the more collisions of particles [7].
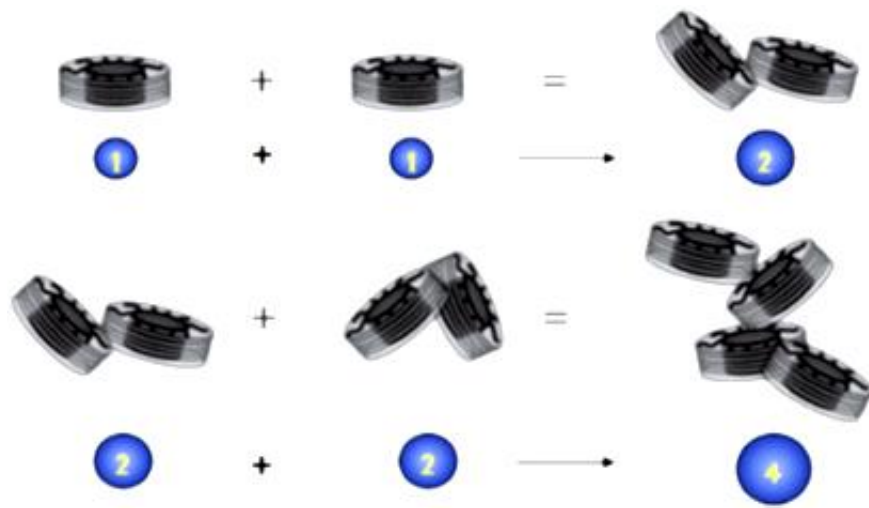
Figure 9. Asphaltene aggregation modeling with the population balance equation [7].

Section C: *Asphaltene Deposition in Capillary Test.* Boresta et al. (2000) conducted the experimental methodology in a stainless-steel capillary and observed the onset point and rate of asphaltene deposition where the changes in the pressure, temperature, and composition were applied [93]. This was accomplished by measuring the pressure drop across the capillary tube that shows the buildup of a deposition layer. They also modified the conventional light transmission method and made it sensitive to test fluids with a small amount of asphaltene content. It was clearly shown that the asphaltene deposition happens when the asphaltene is unstable at the process conditions. This technique was also used to assess the reversibility of asphaltene deposition. They observed that deposition on the walls of the tube can be considered reversible when the fluid condition is far from the onset point state. Considering a homogeneous layer of deposition, they calculated the effective thickness of the deposited layer [8]. Wang et al. (2004) observed that the rate of deposition increases with the heavier precipitant where the asphaltene precipitation is not expected. It was shown that the rate of deposition is higher with a heavier molecular weight solvent (n-pentadecane) in comparison with the lighter one (n-heptane) for two samples of the crude oil [9]. They suggested an optimum for asphaltene phase separation and floc growth to demonstrate

the tendency for arterial deposition. It was found that a part of asphaltene flocculation does not perform arterial deposition so that they just carry through the tube [9]. These two research groups (Boresta et al. (2000) [8] and Wang et al. (2004) [9]) considered a homogeneous arterial deposition and calculated the deposition thickness using the experimental data of the pressure drop by Hagen–Poiseuille equation as follows [9]:

$$\Delta p_i = \frac{128 \mu_i L Q_t}{\pi d_H^4}$$

(A-4)

$$\frac{(\Delta p_t) r_t^4}{\mu_t} = \frac{(\Delta p_i) r_i^4}{\mu_i}$$

(A-5)

In Equations (C-1) and (C-2), i and t refer to the initial condition and condition at time t across the tube; Δp_i and Δp_t represent the pressure drop in the capillary before precipitation and at time t, respectively; μ_i and μ_t denote the viscosity of the oil and average viscosity of the oil at Δp_t; and r_i and r_t are the initial and instantaneous effective radius of the tube, respectively. Assuming that the change of viscosity is negligible and $r_t = r_i - e_t$, the asphaltene deposit hydrodynamic thickness is given below:

$$e_t = r_i \left[1 - (\frac{\Delta p_i}{\Delta p_t})^{1/4} \right]$$

(A-6)

where e_t is the hydrodynamic thickness of the instantaneous average asphaltene deposition layer. Boek et al. (2008) investigated the influence of flow rate on asphaltene deposition rate, induced by n-heptane in a glass capillary [25]. They obtained the deposition rate by measuring the pressure drop along the capillary tube using an optical microscopy to monitor deposition. They noticed that the pressure drop over time is increased due to the asphaltene deposition. It was also increased with an increase in the flow rate. The Stochastic Rotation Dynamics (SRD) simulations were applied to compare the modeling results with the experimental findings. Conducting modeling with SRD, the potential well depth and the flow rate varied to obtain the hydrodynamic interactions dominate (dominant convective heat transfer, $Pe^{flow} \gg 1$) and stocks flow (laminar flow, Re<<1). It was concluded that the asphaltene is more sticky and prone to the buildup blockage in higher

well depths [10]. Later on, they repeated the same tests with the entire crude oils and found that the asphaltene extracted from the oil is more prone to deposit than the entire oil [10, 11].

Asphaltene Deposition in Taylor−Couette (TC) Cell. This is a high-pressure cell, which can be used to generate organic deposition (asphaltene and/ or wax) under the actual conditions of oil fields. The Taylor-Couette cell is schematically illustrated in Figure C-1 [12]. The central part of the cell is made of a rotating spindle, which is capable to simulate the actual pipe flow (Figure C-1, part b). The cell also consists of a cooling/heating bath that controls the temperature by circulating the coolant around the outer cylinder (Figure C-1, part a) [12]. The system can be modified for two types of modes, including batch and flow-through system. However, the batch mode has some limitations, including unreliable measurements for low asphaltene content and deposition under depletion. The drawbacks of the batch mode are overcome in a flow-through system and more realistic measurements can be conducted [13-15]. Zougari et al. (2006) developed an Organic Solid Deposition and Control (OSDC) device [98]. They constructed it based on the Taylor-Couette cell to measure asphaltene deposition in realistic conditions of temperature, pressure, composition, turbulence, shear rate, surface type, and roughness. The effects of hydrodynamics of flow and temperature in the batch mode of the tests were studied. They used the live waxy and asphaltenic oils to perform their experiments at the maximum Reynolds number [12].
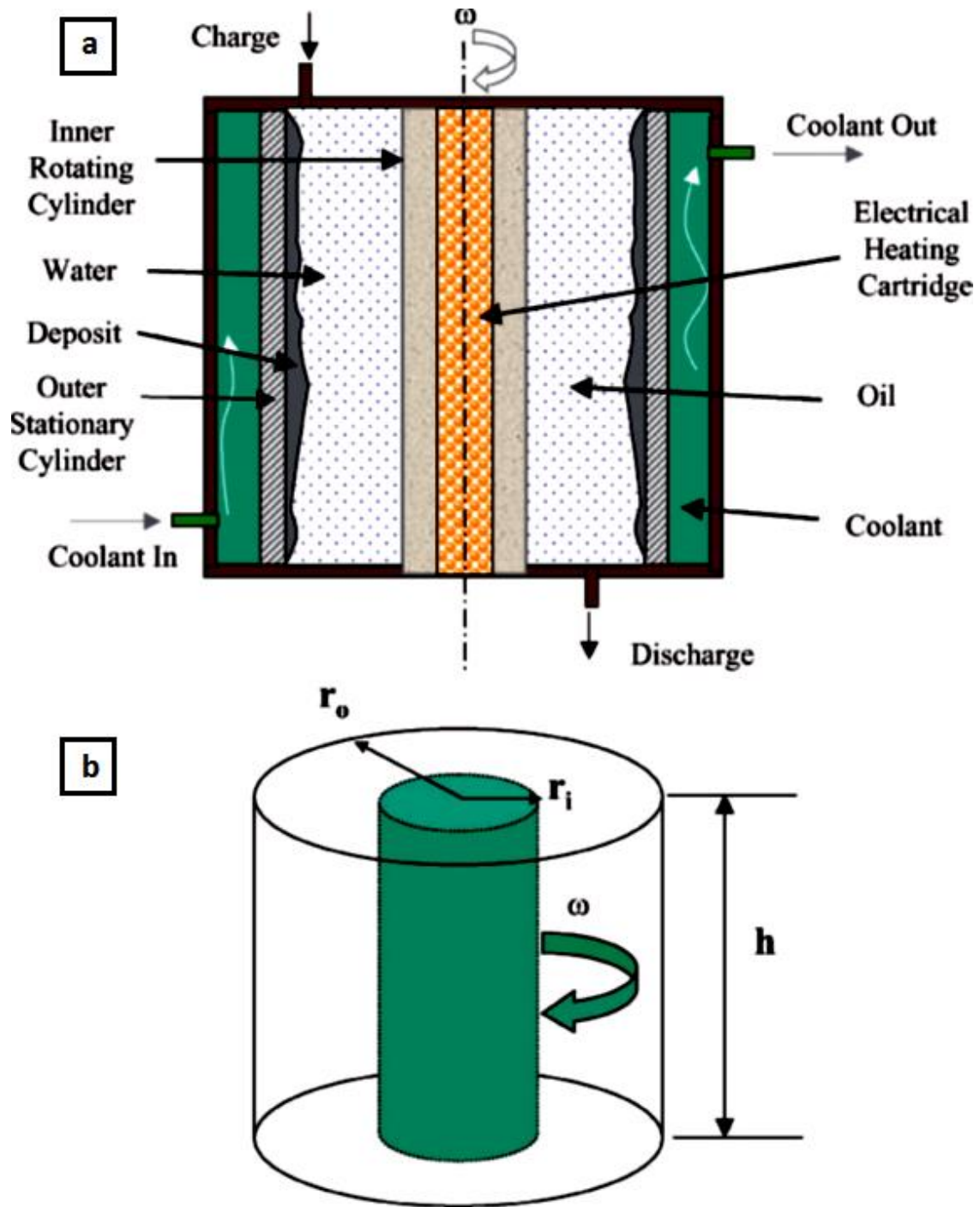
Figure 10. Cylindrical Taylor-Couette (TC) cell [12].

Although the OSDC technique was able to be applied to the small amount of the sample, the amount of the detected deposition was lower than the benchmark pipe flow loop. In addition, the effect of the bulk temperature and wall on the wax deposition was neglected [12, 15]. Akbarzadeh et al. (2011) used the TC cell and made some modifications to overcome the shortcoming of the cell [99]. They used a fresh amount of oil to address the incapability of the cell to be effective with a low amount of asphaltene. It was found that the shear rate is dominant in the deposition rate. They also observed more deposition at the bubble point pressure of the reservoir oil [15].

Section D: *Asphaltene Precipitation Modeling.* Thomas et al. (1992) proposed a regular solution theory for multicomponent systems to describe the asphaltene precipitation behaviours [229]. They used a liquid-solid model for a multicomponent solid phase on the basis of the theory of Prausnitz considering $G_E=U_E$, where G_E stands for the excess internal energy accounting the non-ideality of the system and U_E represents the internal energy [16]. Later, Alboudwarej et al. (2003) developed a regular solution theory of the liquid-liquid equilibrium to model asphaltene precipitation in the Western Canadian bitumens [230]. They studied the effect of different solvents on the precipitation. Since the system pressure was set to be above the bubble point, a liquid-liquid equilibrium was suggested. They divided bitumens into four main pseudo-components on the basis of the SARA fraction; including saturates, aromatics, resins, and asphaltenes, to address the categorizing challenge of the regular solution theory [17]. The main challenge in modeling of asphaltene precipitation through employing the regular solution theory is defining the distribution of molar mass, molar volume, and solubility parameters of asphaltene [17]. The polydispersity of asphaltene, difficulty in lumping asphaltene as a single component, and finding the accurate (and reliable) amount of precipitation are the vital reasons to divide the asphaltene into fractions of variable molar mass on the basis of Schultz-Zimm molar mass distribution [17]. The proposed approach was able to successfully model the onset-point and amount of asphaltene precipitation. However, at the intermediate solvent/bitumen ratios, the model showed underpredicted simulation results [17]. After that, Akbarzadeh et al. (2005) substituted the molar mass distribution function of the model with the gamma function and noticed a better performance [18]. Powers et al. (2016) also considered a liquid-liquid equilibrium to model the asphaltene precipitation with the regular solution theory [19]. It was found that thermal and hydrocracking processes reduce the molar

weight and H/C ratio; however, they increase the density and aromaticity of asphaltene due to the breakage of the aliphatic chains. To take into account the thermal and hydrocracking effect, the self-association model of Terminator/ Propagator was utilized [19]. The association model assumes that asphaltene and resin have the active sites that enable them to form aggregation by linking to the similar molecules. Moreover, saturate and aromatic are regarded as the neutral components. The molecules with one or multi-active sites are called terminators and propagators, respectively. In conclusion, asphaltene and resin consist of a mixture of terminators and propagators [19]. They reported that the thermal and hydrocracking processes alter the distribution function of molar weight, volume, and solubility, which are the key factors in asphaltene precipitation [19].

The Flory-Huggins theory was applied by Hirschberg et al. (1984) to model the amount of asphaltene precipitation [152]. They considered a vapour-liquid equilibrium case and simulated its thermodynamic state by SRK EoS. The liquid phase was assumed to consist of two cuts; namely, solvent (asphaltene free) and asphalt phase (asphaltene and resin). The Flory-Huggins model suffers from a number of shortcomings [20]. First, there is an overestimation in obtaining the asphaltene solubility in the presence of a high amount of solvent. Second, the model is not able to determine the amount of precipitation under pressures higher than 200 bar. Third, asphaltene is assumed to be homogenous [20]. After that, Rassamdana et al. (1996) applied the Hirschberg model to a light oil sample induced by n-alkanes [231]. They noticed no agreement between the model predictions and experimental data. They suggested that the deviation is originated from the assumption of reversibility of precipitation event [21]. Later, a two-component Asphaltene Solubility Model (ASM) was proposed on the basis of the Flory-Huggins theory. In comparison with the previous applications of the theory, the composition of the phases after asphaltene precipitation was not presumed, while the phases were characterized by a correlation between the refractive index and solubility parameters. Although the ASM was successful in predicting the asphaltene onset, it had some drawbacks [22, 23]. For instance, adjusting solubility parameter and molar volume needed an optimization procedure. In addition, the same extent of solubility parameter was considered for different solvents including pentane and pentadecane. The Asphaltene Instability Trend (ASIST) was also proposed with the same theory, while the solubility parameters were plotted against the molar volume for various liquid solvents. Indeed, a linear relationship between the solubility parameter and molar volume at the onset condition was found

that was named ASIST. The validity of the method to determine the instability of asphaltene was examined by some previous studies; however, the model was not able to acceptably predict the amount of precipitation [22-25].

One of the simplest models in the asphaltene precipitation is on the basis of the cubic EoS, which consists of the solid phase fugacity correlation and Peng-Robinson EoS. The main assumption of the model is to consider the asphaltene precipitated phase as a pure solid (asphaltene) phase. Although the model is simple, it is not accurate enough and it also needs modification upon any alteration of the components [16, 26]. Peng-Robinson EoS was also used by Ngheim et al. (1997) to calculate the fugacity of components in a vapour-liquid equilibrium case [236]. In their model, the heavy fraction of crude oil was assumed to be made of two fractions; precipitating and non-precipitating. The former fraction consisted of asphaltene/resin dissociations, while the second fraction was a mixture of heavy paraffins and non-dissociable asphaltene/resins [27]. The proposed model was successful in forecasting the asphaltene phase separation, while it was dependent on the proper division of the heavy fractions and their characteristics. Furthermore, the model was not applicable for asphaltene precipitation with a high amount of solvents [27]. Some other studies also employed PR EoS to investigate the asphaltene phase behaviours induced by n-alkanes and even defined the thirty divisions to imitate the molar mass distribution of asphaltene. However, the effect of resins and aromatics on the stabilization of the asphaltene was neglected [28, 29].

SAFT, as one of the popular models in modeling asphaltene phase behaviours, was developed by Chapman and coworkers on the basis of the perturbation theory of Wertheim to the mixture. Amongst different versions of the SAFT model, PC-SAFT seems to be more appropriate than others for simulation of asphaltene behaviours [30]. Different methods of lumping in an oil mixture were provided in the literature, since the performance of the SAFT model is highly dependent on the lumping and characteristics of segments, including binary interaction parameters [239-241]. SAFT theory divides molecules into a chain of bonded spherical segments. The number of segments per chain, the diameter of the segment, and van der Waals energy of segments are parameters which need to be tuned to vapour pressures and saturated liquid densities. These parameters are correlated by the molecular weight within a segment. Gonzalez et al. [31] and Vargas et al. [32] conducted extensive studies on the modeling of asphaltene phase behaviours using PC-SAFT EoS. They took into account the effect of gas injection on the onset of asphaltene precipitation and bubble point pressure. They studied the influence of methane, ethane, CO_2, and

N_2 gas injection on the asphaltene onset. They divided asphaltene from three to nine subtractions and adjusted the SAFT parameters with regard to the asphaltene polydispersity [32]. However, asphaltene precipitation was overestimated with the proposed model due to considering the polydispersity effect. In addition, a dual effect for CO_2 injection was found which was attributed to artifact error [33]. After that, their model was improved such that more pseudo-components were included and more subtractions were chosen to represent the oil mixture. The new dividing method led to more flexible binary interactions and model accuracy. In addition, the performance of the model was compared with that of cubic EoS (e.g., SRK), showing a better performance in modeling of asphaltene phase behaviours, while the SRK EoS was acceptably accurate in estimating the density of heavy precipitated fractions [34]. Later, Alhammadi et al. compared the prediction performance of the PC-SAFT and CPA where the Peneloux shift parameter was incorporated to its physical part [243]. Although adding the Peneloux shift parameter to the cubic EoSs (SRK, PR, and physical part of CPA) improved the estimation of liquid densities, the PC-SAFT showed better performance in modeling of the thermodynamic properties at the equilibrium condition [35]. Arya et al. employed PC-SAFT EoS with the association contribution to model the upper asphaltene onset precipitation and bubble point pressure with/without gas injection. They compared the results of PC-SAFT with the association (WA) to the results of PC-SAFT EoS without association (WOA) and CPA EoS. They assessed six reservoir fluids through using the models and found promising results so that the onset point of asphaltene precipitation was properly modeled (see Figure D-1). However, the PC-SAFT (WOA) was not able to correlate the upper onset pressure for two of the fluid samples [33].
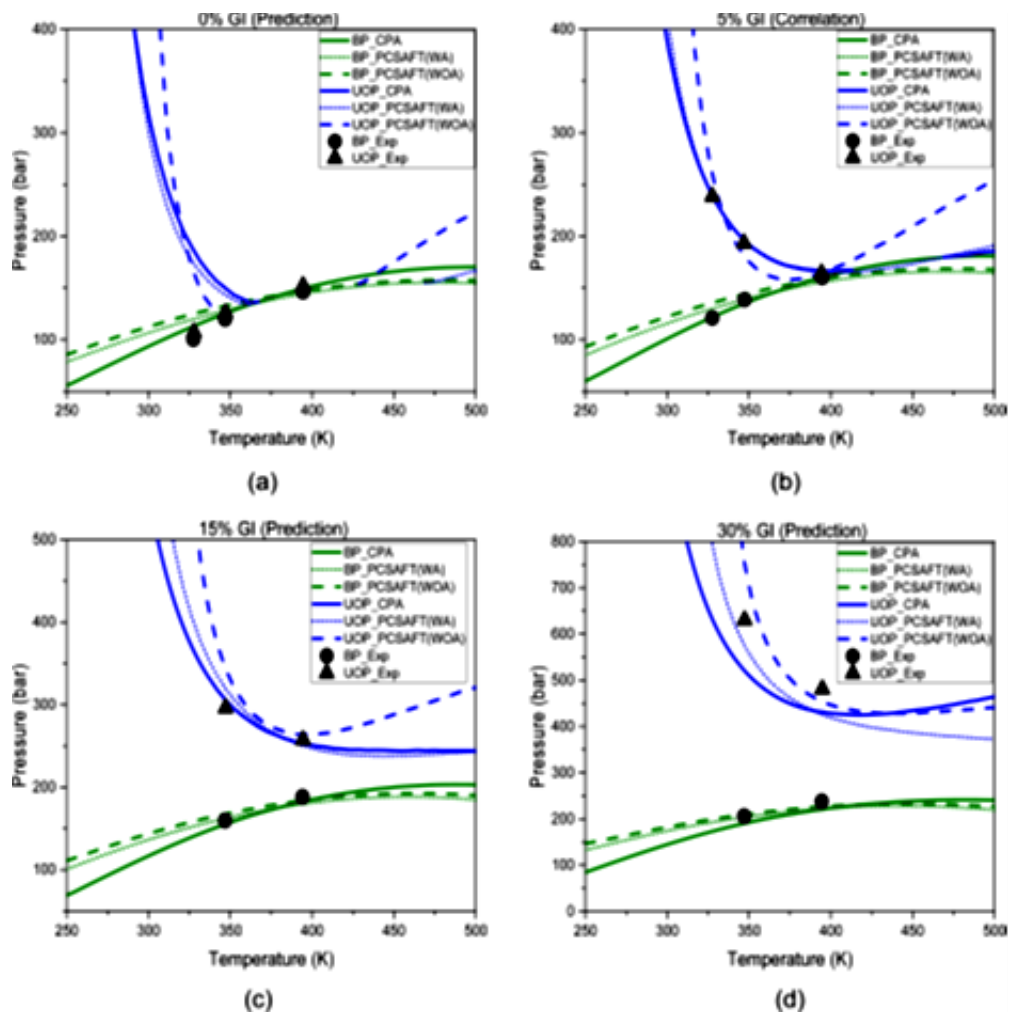
Figure 11. Correlation and prediction of Upper Asphaltene Onset (UOP) and Bubble Point (BP) pressure, (a) without gas injection, (b) 5 mol% of gas injection, (c) 10 mol% of gas injection, and (d) 15 mol% of gas injection [33].

Li and Firoozabad used PR EoS within the CPA framework to model the asphaltene phase behaviours. The CPA model was a combination of two parts; including the physical part with respect to PR EoS and the association part on the basis of Wertheim's thermodynamic perturbation theory [36]. Oil was assumed to include three pseudo components such as saturate, aromatic/resin, and asphaltene. The model has only one adjustable parameter, which is the association energy parameter. Also, the model exhibited a good performance in modeling of precipitation occurrence; however, its performance in forecasting the onset point was not acceptable. This shortcoming is attributed to adjusting the association energy parameter [36]. Shirani et al. used the same framework to be applied on a live oil sample with fifteen pseudo-components, where only self-

association of asphaltene particles was considered and the association of asphaltene with other components was neglected [245]. They examined both SRK and PR EoSs for the physical part of the model and found a better performance with SRK EoS in comparison with PR EoS and colloidal models [37]. In the CPA studies for modeling of asphaltene phase behaviours, it is believed that the chemical reaction of monomers leads to association due to increasing new species. The limitation of the technique is that some temperature dependent parameters were assumed to be constant [36, 37].

Application of colloidal theory to asphaltene precipitation was introduced by Pfeiffer and Saal [38]. They claimed that asphaltene is peptized in the oil mixture by lighter hydrocarbons and asphaltene precipitation is resulted from the resins shortage to surround asphaltene heavy particles [38]. Asphaltene aggregation and precipitation are due to the transfer of peptizing agent (resin) from the asphaltene phase to the oil phase and vice-versa. The outer layer stabilizes the asphaltene as a result of steric repulsion. Therefore, adding a solvent (n-alkane) causes peptizing agents in the outer layer to transform to the oil phase such that it makes the asphaltene phase more polar, while the oil phase would become less polar. At the onset, the polarity of the asphaltene phase reaches a certain amount at which the asphaltene micelles are attached to each other and grow in size. One of the earliest applications of the colloidal approach to model asphaltene precipitation was conducted by Leontaritis and Mansoori [39]. They considered asphaltene particles as a solid phase that is surrounded by resins. Adding a n-alkane solvent to the oil also induced asphaltene to precipitate. The precipitation condition was modeled through a Vapour-Liquid Equilibrium (VLE) calculation procedure. The critical resin concentration was adjusted with the experimental data. However, the model is only applicable to the situation in which asphaltene precipitation is reversible (asphaltene dissociation) [39]. The colloidal framework was applied by other researchers with different modifications [40-42]. For example, Pan and Firoozabadi considered two phases; including a precipitated phase (asphaltene and resin) and a liquid phase [250]. Thermodynamic parameters of the species were calculated by EoS and compositions of the phases were determined by minimizing the Gibbs free energy. The model suffers from disadvantages such as the need of many parameters and the absence of a specific relationship between the parameters and thermodynamic conditions such as pressure, temperature, and composition [42].

NOMENCLATURES

Acronyms

CPA	cubic plus association
EoS	equations of state
OSDC	organic solid deposition and control
Pe	Peclet number
PC-SAFT	perturbed-chain statistical associating fluid theory
PR	Peng Robinson
Re	Reynolds number
SAFT	statistical associating fluid theory
SAFT-HS	statistical associating fluid theory-hard sphere
SAFT-VR	statistical associating fluid theory-variable range
SARA	saturate, aromatic, resin, and asphaltene
SRK	Soave–Redlich–Kwong
VLE	vapour-liquid equilibrium
WA	With association
WOA	Without association

Variables/Parameters

$C_1(0)$	initial concentration of asphaltene nanoparticles
C_k	the concentration of the species/ volume fraction
e	instantaneous average asphaltene deposition layer hydrodynamic thickness
K	collision kernel
P	pressure
Pe	Peclet number
r	effective radius
Re	Reynolds
t	time

U	repulsion barrier/internal energy

Greek Letters

δ	Solubility parameter
μ	viscosity / a constant parameter

Subscripts and Superscripts

i	Initial condition
T	condition at time

References:

1. Kawanaka, S., S. Park, and G. Mansoori, *Organic deposition from reservoir fluids: a thermodynamic predictive technique.* SPE Reservoir Engineering, 1991. **6**(02): p. 185-192.
2. Mansoori, G.A., *Modeling of asphaltene and other heavy organic depositions.* Journal of petroleum science and engineering, 1997. **17**(1-2): p. 101-111.
3. Ashoori, S., *Mechanisms of asphaltene deposition in porous media*. 2005, University of Surrey.
4. Maqbool, T., A.T. Balgoa, and H.S. Fogler, *Revisiting asphaltene precipitation from crude oils: A case of neglected kinetic effects.* Energy & Fuels, 2009. **23**(7): p. 3681-3686.
5. Haji-Akbari, N., Masirisuk, P., Hoepfner, M.P., Fogler, H.S., *A unified model for aggregation of asphaltenes.* Energy & Fuels, 2013. **27**(5): p. 2497-2505.
6. Chaisoontornyotin, W., Haji-Akbari, N., Fogler, H.S., Hoepfner, M.P., *Combined asphaltene aggregation and deposition investigation.* Energy & Fuels, 2016. **30**(3): p. 1979-1986.
7. Fávero, C.V.B., Maqbool, T., Hoepfner, M.P., Haji-Akbari, N., Fogler, H.S., *Revisiting the flocculation kinetics of destabilized asphaltenes.* Advances in colloid and interface science, 2017. **244**: p. 267-280.
8. Broseta, D.,Robin, M., Fejean, C., Durandeau, M., Zhou, H., *Detection of asphaltene deposition by capillary flow measurements*. in *SPE/DOE Improved Oil Recovery Symposium*. 2000. Society of Petroleum Engineers.
9. Wang, J., J.S. Buckley, and J.L. Creek, *Asphaltene deposition on metallic surfaces.* Journal of dispersion science and technology, 2004. **25**(3): p. 287-298.
10. Boek, E.S., Ladva, H.K., Crawshaw, J.P., Padding, J., *Deposition of colloidal asphaltene in capillary flow: experiments and mesoscopic simulation.* Energy & fuels, 2008. **22**(2): p. 805-813.
11. Boek, E.S., Wilson, A., Padding, J., Headen, T.F., Crawshaw, J.P., *Multi-scale simulation and experimental studies of asphaltene aggregation and deposition in capillary flow.* Energy & fuels, 2009. **24**(4): p. 2361-2368.

12.   Zougari, M., Jacobs, S., Ratulowski, J., Hammami, A., BRoze, G., Flannery, M., Stankiewicz, A., Karan, K., *Novel organic solids deposition and control device for live-oils: design and applications.* Energy & Fuels, 2006. **20**(4): p. 1656-1663.

13.   Akbarzadeh, K. and M. Zougari, *Introduction to a novel approach for modeling wax deposition in fluid flows. 1. Taylor− Couette system.* Industrial & Engineering Chemistry Research, 2008. **47**(3): p. 953-963.

14.   Akbarzadeh, K., Ratulowski, J., Lindvig, T., Davis, T., Huo, Z., Broze, G., Howe, R., Lagers, K., *The importance of asphaltene deposition measurements in the design and operation of subsea pipelines.* in *SPE annual technical conference and exhibition.* 2009. Society of Petroleum Engineers.

15.   Akbarzadeh, K., Eskin, D., Ratulowski, J., Taylor, S., *Asphaltene deposition measurement and modeling for flow assurance of tubings and flow lines.* Energy & fuels, 2011. **26**(1): p. 495-510.

16.   Thomas, F., Bennion, D.B., Bennion, D.W., Hunter, B.E., *Experimental and theoretical studies of solids precipitation from reservoir fluid.* Journal of Canadian Petroleum Technology, 1992. **31**(01).

17.   Alboudwarej, H., Akbarzadeh, K., Back, J., Svreck, W.Y., Yarranton, H.W., *Regular solution model for asphaltene precipitation from bitumens and solvents.* AIChE Journal, 2003. **49**(11): p. 2948-2956.

18.   Akbarzadeh, K., Alboudwarej, H., Svreck, W.Y., Yarranton, H.W., *A generalized regular solution model for asphaltene precipitation from n-alkane diluted heavy oils and bitumens.* Fluid Phase Equilibria, 2005. **232**(1-2): p. 159-170.

19.   Powers, D., Sadeghi, H., Yaranton, H.W., van den Berg, F.G.A., *Regular solution based approach to modeling asphaltene precipitation from native and reacted oils: Part 1, molecular weight, density, and solubility parameter distributions of asphaltenes.* Fuel, 2016. **178**: p. 218-233.

20.   Hirschberg, A., deJong, L.N.J., Schipper, B.A., Meijir, J.G., *Influence of temperature and pressure on asphaltene flocculation.* Society of Petroleum Engineers Journal, 1984. **24**(03): p. 283-293.

21.   Rassamdana, H., Dabir, B., Nematy, M., Farhani, M., Sahimi, M., *Asphalt flocculation and deposition: I. The onset of precipitation.* AIChE Journal, 1996. **42**(1): p. 10-22.

22.   Wang, J. and J. Buckley. *An experimental approach to prediction of asphaltene flocculation.* in *SPE International Symposium on Oilfield Chemistry.* 2001. Society of Petroleum Engineers.

23.   Creek, J.L., J. Wang, and J.S. Buckley, *Verification of asphaltene-instability-trend (ASIST) predictions for low-molecular-weight alkanes.* SPE Production & Operations, 2009. **24**(02): p. 360-368.

24.   Wang, J., J.L. Creek, and J.S. Buckley. *Screening for potential asphaltene problems.* in *SPE Annual Technical Conference and Exhibition.* 2006. Society of Petroleum Engineers.

25.   Buckley, J.S., J. Wang, and J.L. Creek, *Solubility of the least-soluble asphaltenes*, in *Asphaltenes, Heavy Oils, and Petroleomics.* 2007, Springer. p. 401-437.

26.   Gupta, A.K., *A model for asphaltene flocculation using an equation of state.* 1986: Chemical and Petroleum Engineering, University of Calgary.

27.   Nghiem, L.X. and D.A. Coombe, *Modelling asphaltene precipitation during primary depletion.* SPE Journal, 1997. **2**(02): p. 170-176.

28. Vafaie-Sefti, M., S.A. Mousavi-Dehghani, and M. Mohammad-Zadeh, *A simple model for asphaltene deposition in petroleum mixtures.* Fluid Phase Equilibria, 2003. **206**(1-2): p. 1-11.

29. Sabbagh, O., Akbarzadeh, K., Badamchi-Zadeh, A., Svrcek, W. Y., & Yarranton, H. W., Applying the PR-EoS to asphaltene precipitation from n-alkane diluted heavy oils and bitumens. Energy & fuels, 2006. 20(2): p. 625-634.

30. Chapman, W.G., et al., *New reference equation of state for associating liquids.* Industrial & Engineering Chemistry Research, 1990. **29**(8): p. 1709-1721.

31. Buenrostro-Gonzalez, E., Lira-Galeana, C., Gil-Villegas, A., Wu, J., *Asphaltene precipitation in crude oils: Theory and experiments.* AIChE Journal, 2004. **50**(10): p. 2552-2570.

32. Vargas, F. M., Gonzalez, D. L., Hirasaki, G. J., & Chapman, W. G., Modeling asphaltene phase behavior in crude oil systems using the perturbed chain form of the statistical associating fluid theory (PC-SAFT) equation of state. Energy & fuels, 2009. 23(3): p. 1140-1146.

33. Arya, A., Liang, X., von Solms, N., & Kontogeorgis, G. M., *Modeling of asphaltene onset precipitation conditions with cubic plus association (CPA) and perturbed chain statistical associating fluid theory (PC-SAFT) equations of state.* Energy & Fuels, 2016. **30**(8): p. 6835-6852.

34. Panuganti, S.R., Vargas, F.M., Gonzalez, D.L., Kurup, F.M., Chapman, W.G., *PC-SAFT characterization of crude oils and modeling of asphaltene phase behavior.* Fuel, 2012. **93**: p. 658-669.

35. AlHammadi, A.A., F.M. Vargas, and W.G. Chapman, *Comparison of cubic-plus-association and perturbed-chain statistical associating fluid theory methods for modeling asphaltene phase behavior and pressure–volume–temperature properties.* Energy & fuels, 2015. **29**(5): p. 2864-2875.

36. Li, Z. and A. Firoozabadi, *Modeling asphaltene precipitation by n-alkanes from heavy oils and bitumens using cubic-plus-association equation of state.* Energy & fuels, 2010. **24**(2): p. 1106-1113.

37. Shirani, B., Nikazar, M., Naseri, A., Mousavi-Dehghani, S.A., *Modeling of asphaltene precipitation utilizing Association Equation of State.* Fuel, 2012. **93**: p. 59-66.

38. Pfeiffer, J.P. and R. Saal, *Asphaltic bitumen as colloid system.* The Journal of Physical Chemistry, 1940. **44**(2): p. 139-149.

39. Leontaritis, K. and G. Mansoori. *Asphaltene flocculation during oil production and processing: A thermodynamic collodial model*. in *SPE International Symposium on Oilfield Chemistry*. 1987. Society of Petroleum Engineers.

40. Leontaritis, K. and G. Mansoori. *Asphaltene flocculation during oil production and processing: A thermodynamic colloidal model*. in *SPE International Symposium on Oilfield Chemistry*. 1987. Society of Petroleum Engineers Richardson, TX, USA.

41. Victorov, A.I. and A. Firoozabadi, *Thermodynamic micellizatin model of asphaltene precipitation from petroleum fluids.* AIChE journal, 1996. **42**(6): p. 1753-1764.

42. Pan, H. and A. Firoozabadi, *Thermodynamic micellization model for asphaltene precipitation inhibition.* AIChE journal, 2000. **46**(2): p. 416-426.

Appendix B; CPA volume calculations used in chapter 3

Calculation of volume

The total volume is required to calculate fugacity coefficient of each component in the mixture using Newton-Raphson method. The equation for total volume can be used from pressure equation presented in Kontogeorgis and Folas [1, 2].

$$P = \frac{nRT}{V} - \left(\frac{\partial A^r}{\partial V}\right)_{T,n} = \frac{nRT}{V} - \left(\frac{\partial A^r_{SRK}}{\partial V}\right)_{T,n} - \left(\frac{\partial A^r_{association}}{\partial V}\right)_{T,n} \tag{B-1}$$

The following equation is solved through the Newton-Raphson variant for total volume calculation.

$$H(V) = P - \left[\frac{nRT}{V} - \left(\frac{\partial A^r_{SRK}}{\partial V}\right)_{T,n} - \left(\frac{\partial A^r_{association}}{\partial V}\right)_{T,n}\right] \tag{B-2}$$

Data Analysis

This section contains information with respect to data analysis using SPSS v27, including the Shapiro-Wilk test and boxplot.

Table B-1. The Shapiro-Wilk test of experimental data [3] regarding the quantity of n-alkane

		Tests of Normality		
		Shapiro-Wilk		
	R(cm^3/g)	Statistic	df	Sig.
	2.5	0.871	6	0.229
	2.8	0.913	3	0.428
	3.0	0.943	7	0.665
	3.6	0.903	23	0.030
	5.0	0.933	21	0.158
	5.5	0.888	5	0.346
Wt%	9.5	0.916	5	0.506
	9.7	0.959	21	0.505
	14.2	0.878	5	0.302
	14.3	0.977	20	0.890
	20.0	0.893	5	0.375
	20.6	0.978	20	0.912
	24.3	0.972	25	0.707
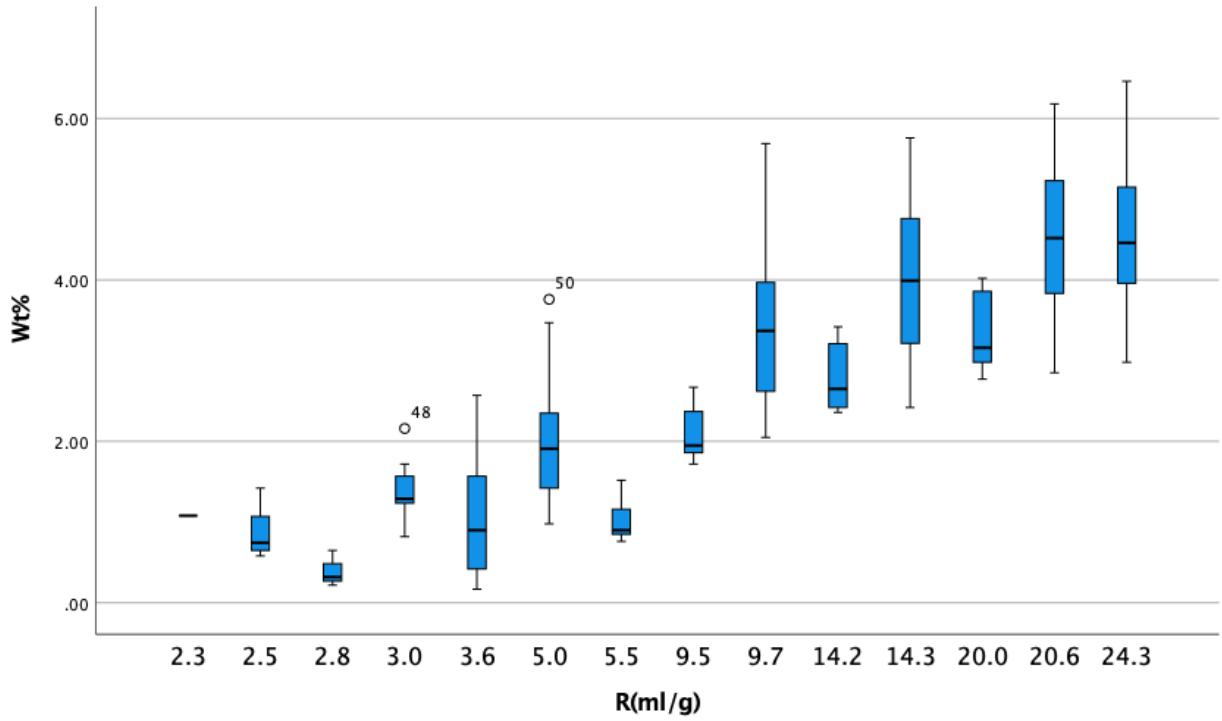
Figure 12. The Boxplot analysis of the experimental data [3] regarding the quantity of n-alkane

Table B-2. The Shapiro-Wilk test of experimental data [3] regarding temperature

<table>
<tr><th colspan="5">Tests of Normality</th></tr>
<tr><td rowspan="2"></td><td rowspan="2">T(k)</td><td colspan="3">Shapiro-Wilk</td></tr>
<tr><td>Statistic</td><td>df</td><td>Sig.</td></tr>
<tr><td rowspan="4">Wt%</td><td>293</td><td>0.932</td><td>53</td><td>0.005</td></tr>
<tr><td>308</td><td>0.945</td><td>45</td><td>0.033</td></tr>
<tr><td>323</td><td>0.955</td><td>42</td><td>0.100</td></tr>
<tr><td>338</td><td>0.957</td><td>27</td><td>0.3164</td></tr>
</table>
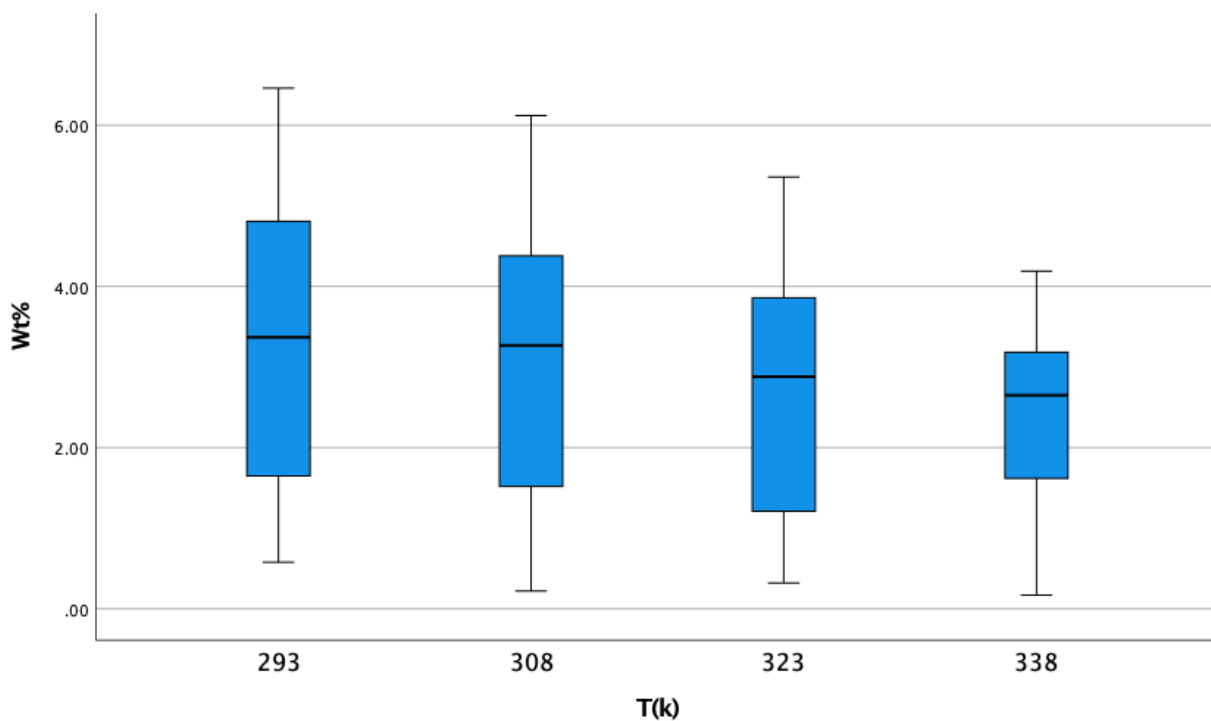
Figure 13 The Boxplot analysis of the experimental data [3] regarding temperature

Table 6 The Shapiro-Wilk test of experimental data [3] regarding the carbon number of the n-alkane

	Tests of Normality				
	nCn	Shapiro-Wilk			
		Statistic	Statistic	df	Sig.
Wt%	5	0.148	0.911	19	0.076
	6	0.103	0.957	27	0.307
	7	0.112	0.956	27	0.298
	8	0.117	0.948	20	0.335
	9	0.116	0.953	25	0.299
	10	0.084	0.963	25	0.481
	12	0.096	0.966	24	0.562
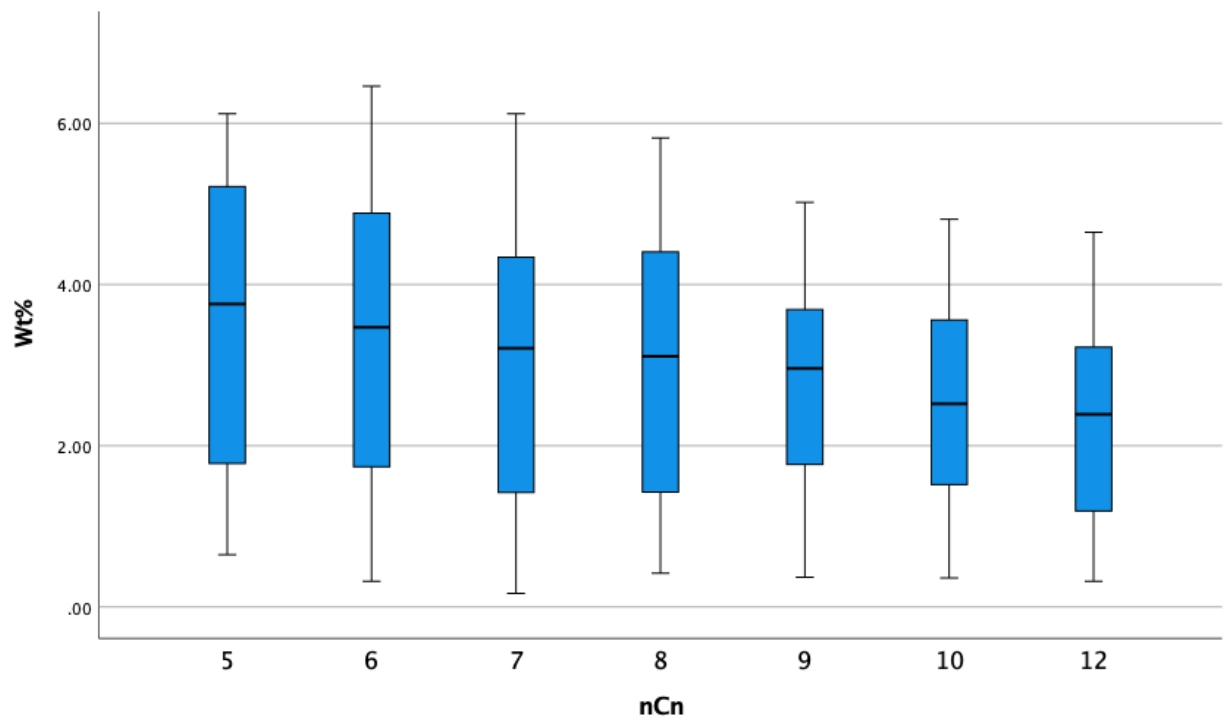
Figure 14 The Boxplot analysis of the experimental data [3] regarding the carbon number of the n-alkane

Acronyms

CPA   cubic plus association

Variables/Parameters

A   Helmholtz free energy

C   carbon number of precipitant

P   pressure

R   gas constant

R (ml/g)   amount of precipitant

T   Temperature

V   molar volume

Subscripts and Superscripts

r   Residual

n   Mole

T   temperature

Reference

1.   Kontogeorgis, G.M. and G.K. Folas, *Thermodynamic models for industrial applications: from classical and advanced mixing rules to association theories*. 2009: John Wiley & Sons.
2.   Perakis, C., Voutsas, E., Magoulas, K., & Tassios, D., *Thermodynamic modeling of the vapor–liquid equilibrium of the water/ethanol/CO2 system.* Fluid Phase Equilibria, 2006. **243**(1-2): p. 142-150.
3.   Hu, Y.-F. and T.-M. Guo, *Effect of temperature and molecular weight of n-alkane precipitants on asphaltene precipitation.* Fluid Phase Equilibria, 2001. **192**(1-2): p. 13-25.

Appendix C; MATLAB code developed in this research

C-1-1; Steps in running the CPA EoS code

There are two flash calculation codes; the first code is C-2-25, a sample code with all the parameters for the asphaltene precipitation using n-C6 as precipitant at temperature 308 K. The run results are shown in figure 3-15, B. The second code in section C-2-12 is a general code for the CPA EoS.

The CPA EoS code follows these steps:

1. C-2-25-1: input parameters are introduced, including critical properties (T_c, P_c, ω), gas constant (R), number of components, and the cubic parameters a_0, b, c_1 are calculated. The correlations were used to determine the critical properties and are proposed by Riazi and Al-Sahhaf (1996) [3] and optimized parameters used by Akbarzadeh, Alboudwarej, Svrcek, & Yarranton, 2005 [4]. For asphaltene fraction, the global estimation method is used [5]. Therefore, the parameters of the pure component are optimized (a_0, b, c_1, ε, β). Sample experimental data is entered to compare the results and calculate the error. The optimized parameters are entered in the code, so there is no need for further optimization.

2. C-2-25-2: calculates mole fractions for sample experimental data

3. C-2-25-3: volume and fugacity calculations for asphaltene rich phase using functions which are Acapital, Bcapital, vcpa, fugacitycoeff.

4. C-2-25-4: first guess and n+1 iteration for flash calculations of the asphaltene mole fraction in asphaltene lean phase.

5. C-2-25-5: volume and fugacity calculations for asphaltene lean phase using functions which are Amix2, Bmix, vcpamixture_ECR, fugacitycoeff_mix, fnonbonded.

6. C-2-25-6: error and output calculations

C-1-2; Steps in running the CPP EoS code

There are two codes; the first code is C-2-26, a sample code with all the parameters for the asphaltene precipitation using n-C6 as precipitant at temperature 308 K. The run results are shown in figure 4-7, B. The second code in section C-2-24 is a general code for the CPP EoS.

The CPP EoS code follows these steps:

1. C-2-26-1: input parameters are introduced, including critical properties (T_c, P_c, ω), gas constant (R), number of components, and the cubic parameters a_0, b, c_1 are calculated. The correlations were used to determine the critical properties and are proposed by Riazi and Al-Sahhaf (1996) [3] and optimized parameters used by Akbarzadeh, Alboudwarej, Svrcek, & Yarranton, 2005 [4]. For asphaltene fraction, the global estimation method is used [5]. Therefore, the parameters of the pure component are optimized (a_0, b, c_1, n_p, miu). Sample experimental data is entered to compare the results and calculate the error. The optimized parameters are entered in the code, so there is no need for further optimization.

2. C-2-26-2: calculates mole fractions for sample experimental data

3. C-2-26-3: volume and fugacity calculations for asphaltene-rich phase using functions which are Acapital, Bcapital, vcpppolar, Z2DD, meannumberdensity, dx3, I6, diameter, A2DD, fugacitycoeff.

4. C-2-26-4: first guess and n+1 iteration for flash calculations of the asphaltene mole fraction

5. C-2-26-5: volume and fugacity calculations for asphaltene lean phase using functions which are Amix2, Bmix2, vcubic, fugacitycoeffmix.

6. C-2-26-6: error and output calculations

The list of scripts and functions used in each EoS is presented in Table C-1.

Table C-7. List of the scripts and functions for CPA and CPP EoS

EoS	Code number	Description
CPA	C-2-1	Attractive energy parameter calculation for asphaltene phase
	C-2-2	Binary attractive energy parameter calculation for oil phase
	C-2-3	Attractive energy parameter calculation for oil phase
	C-2-4	Repulsive energy parameter calculation for asphaltene phase
	C-2-5	Repulsive energy parameter calculation for oil phase
	C-2-6	Fugacity calculations for non-bonded fractions
	C-2-7	Fugacity coefficient calculations of the precipitated phase
	C-2-8	Fugacity coefficient calculations for oil phase
	C-2-9	A sample of Global Optimization method
	C-2-10	Volume calculations using CPA EoS of precipitated phase
	C-2-11	Volume calculations using CPA EoS of oil phase
	C-2-12	CPA flash Calculations (general code)
	C-2-25	Flash Calculations CPA EoS; a sample code with all the parameters for the asphaltene precipitation using n-C6 as precipitant at temperature 308 K
CPP	C-2-13	Polar Helmholtz free energy calculations

	C-2-14	dI6dro; CPP EoS function
	C-2-15	Segment diameter calculation of the component
	C-2-16	CPP EoS function
	C-2-17	Fugacity coefficient of precipitated phase
	C-2-18	Fugacity coefficient for the oil phase
	C-2-19	I6, CPP function; an approximation in the form of an extended virial series
	C-2-20	Mean number density calculation of the CPP EoS
	C-2-21	Volume calculations for asphaltene phase
	C-2-22	Volume calculation for oil phase
	C-2-23	Compressibility factor calculations using CPP EoS
	C-2-24	CPP flash Calculations (general code)
	C-2-26	Flash Calculations CPP EoS; a sample code with all the parameters for the asphaltene precipitation using n-C6 as precipitant at temperature 308 K
	C-2-27	Binary attractive energy parameter calculation for oil phase
	C-2-1	Attractive energy parameter calculation for asphaltene phase
	C-2-3	Attractive energy parameter calculation for oil phase
	C-2-4	Repulsive energy parameter calculation for asphaltene phase
	C-2-5	Repulsive energy parameter calculation for oil phase

C-2; MATLAB code

```
%%%%%%%%%%%%%%%%%%%%%%%%%%%%%%%%%%%%%%%%%%%%%%%%%%%%%%%%%%%%%%%%%%%%%%%%%%
C-2-1
% Attractive energy parameter calculation for asphaltene phase, this parameter
later is used to calculate the cubic parameter of the EoS


% Acapital (D1) = attractive energy parameter for asphaltene
% R (d1) = universal gas constant, J.mol-1.K-1
% a & b (d2 & d3) = cubic EoS parameter
% T (d4)= temperature (K)
% P (d5)= pressure (Pascal)


function D1=Acapital(d1,d2,d3,d4,d5)
D1=(d2.*d5)./((d1*d4).^2);
end


%%%%%%%%%%%%%%%%%%%%%%%%%%%%%%%%%%%%%%%%%%%%%%%%%%%%%%%%%%%%%%%%%%%%%%%%%%
C-2-2
% Binary attractive energy parameter calculation for oil phase, this
parameter later is used to calculate the cubic parameter of the EoS,
Chapter 3, Eq 3-6
```

```
% aij (D2) = binary attractive energy parameter
% BIP (d1)= binary interaction parameter
% ai (d2) = cubic EoS parameter of component i
% n (d3) = number of components


function D2=aij(d1,d2,d3)
kk=0;
for i=1:d3
    for j=1:d3
        kk=kk+1;
        D2(i,j)=(sqrt(d2(i)*d2(j)))*(1-d1(i,j));
    end
end
```

```
%%%%%%%%%%%%%%%%%%%%%%%%%%%%%%%%%%%%%%%%%%%%%%%%%%%%%%%%%%%%%%%%%%%%%%%%%%%%%%
```
C-2-3
```
% Attractive energy parameter calculation for oil phase, this
parameter later is used to calculate the cubic parameter of the EoS,
Chapter 3, Eq 3-4


% Amix2 (D1) = attractive energy parameter for oil mixture
% xi (d1) = mole fractions
% aij (d2) = binary attractive parameter of component i and j
% n (d3) = number of components


function D1=Amix2(d1,d2,d3)
D1=0;
for i=1:1:d3
    for j=1:1:d3
        D1=D1+(d1(i)*d1(j)*d2(i,j));
    end
end
D1;
```

```
%%%%%%%%%%%%%%%%%%%%%%%%%%%%%%%%%%%%%%%%%%%%%%%%%%%%%%%%%%%%%%%%%%%%%%%%%%%%%%
```
C-2-4
```
% Repulsive energy parameter calculation for asphaltene phase, this
parameter later is used to calculate the cubic parameter of the EoS,
Chapter 3


% Bcapital (D2) = repulsive energy parameter for asphaltene phase
% R (d1) = universal gas constant, J.mol-1.K-1
% a & b (d2 & d3) = cubic EoS parameter
% T (d4)= temperature (K)
% P (d5)= pressure (Pascal)


function D2=Bcapital(d1,d2,d3,d4,d5)
```

```
D2=(d3.*d5)./(d1*d4);
end
```

```
%%%%%%%%%%%%%%%%%%%%%%%%%%%%%%%%%%%%%%%%%%%%%%%%%%%%%%%%%%%%%%%%%%%%%%%
C-2-5
% Repulsive energy parameter calculation for oil phase, this
parameter later is used to calculate the cubic parameter of the EoS,
Chapter 3, Eq 3-5
```

```
% Bmix (D1) = repulsive energy parameter for oil phase
% xi (d1) = mole fractions
% bi (d2) = repulsive energy parameter of component i
```

```
function D1=Bmix(d1,d2)
% d1 = mole fractions (xi or yi), % d2 = b ( bi= b1, b2), % D1= bmix
D1=sum(d1.*d2);
```

```
%%%%%%%%%%%%%%%%%%%%%%%%%%%%%%%%%%%%%%%%%%%%%%%%%%%%%%%%%%%%%%%%%%%%%%%
C-2-6
% Fugacity calculations for non-bonded fractions of the asphaltene
mixture in association term of CPA EoS, Eq 3-10
```

```
% X1 & X2 = fraction of the molecule is not engaged in association bonding
% delta2 &delta12 = the association strength
% v = molar volume calculated from CPA EoS
```

```
function F=fnonbonded(xnon)
global X1 X2 v delta12 delta2
F=[xnon(1)+2*(1./v)*X2*xnon(2)*delta12*xnon(1)-1;
    xnon(2)+2*(1./v)*X1*xnon(1)*delta12*xnon(2)+2*(1./v)*X2*xnon(3)*delta2*xnon(2)-1;
    xnon(3)+2*(1./v)*X2*xnon(2)*delta2*xnon(3)-1];
end
```

```
%%%%%%%%%%%%%%%%%%%%%%%%%%%%%%%%%%%%%%%%%%%%%%%%%%%%%%%%%%%%%%%%%%%%%%%
C-2-7
% Fugacity coefficient calculations of the precipitated phase using CPA EoS,
Eq 9-40 & 9-57 of reference [1]
```

```
% z (d1) = compressibility factor for precipitated phase
% xenon (d2) = fraction of the molecule is not engaged in association
% A (d3) = attractive energy parameter for asphaltene
% B (d4) = repulsive energy parameter for asphaltene phase
% NS (d5) = Number of active sites on the associating molecule
% lnphi (D1) = fugacity coefficient of asphaltene
```

```matlab
function D1=fugacitycoeff(d1,d2,d3,d4,d5)
if d5==4||d5==2
    D1=(d1-1)-log(d1-d4)+(d3/d4)*log(d1/(d1+d4))+d5*(log(d2)-(0.5*d2)+0.5);
elseif d5==3
    D1=(d1-1)-log(d1-d4)+(d3/d4)*log(d1/(d1+d4))+d5*(log(d2)-
(0.5*d2)+0.5)+log((2*d2)-1)-0.5*((2*d2)-1)+0.5;
end
```

```
%%%%%%%%%%%%%%%%%%%%%%%%%%%%%%%%%%%%%%%%%%%%%%%%%%%%%%%%%%%%%%%%%%%%%%%%
```

C-2-8

```matlab
% Fugacity coefficient calculations for oil phase using CPA EoS, Eq 9-40 &
9-57 of reference [1]


% xi (d1) = mole fractions
% xenon (d2) = fraction of the molecule is not engaged in association
% v (d3) = molar volume calculated from CPA EoS
% Bmix (d4) = repulsive energy parameter for oil phase
% Amix (d5) = attractive energy parameter for oil mixture
% bi (d6) = repulsive energy parameter of component i
% aij (d7) = binary attractive parameter of component i and j
% R (d8) = universal gas constant, J.mol-1.K-1
% T (d9)= temperature (K)
% z (d10) = compressibility factor for oil phase
% n (d11) = number of components
% lnphi (D1) = fugacity coefficient of oil phase



function D=fugacitycoeff_mix(d1,d2,d3,d4,d5,d6,d7,d8,d9,d10,d11)
for i=1:d11
    for j=1:d11
        sss(j)=d1(j)*d7(i,j);
    end
    h=((d1(2)*2*(1-d2(1)))+(d1(3)*((2*(1-d2(2)))+2*(1-d2(3))))));
    if i==3
        h=((d1(1)*2*(1-d2(1)))+(d1(2)*((2*(1-d2(2)))+2*(1-d2(3))))));
        D(i)=log(d3/(d3-d4))+(d6(i)/(d3-
d4))+(1/(d4*d8*d9))*log(d3/(d3+d4))*((2*sum(sss))-((d5*d6(i))/d4))...
            -((d5*d6(i))/(d8*d9*d4*(d3+d4)))+(2*log(d2(1)))-
((h/2)*((0.475*d6(i))/(d3-0.475*d4)))-log(d10);


    else


        D(i)=log(d3/(d3-d4))+(d6(i)/(d3-
d4))+(1/(d4*d8*d9))*log(d3/(d3+d4))*((2*sum(sss))-((d5*d6(i))/d4))...
            -((d5*d6(i))/(d8*d9*d4*(d3+d4)))+(2*log(d2(2))+2*log(d2(3)))-
((h/2)*((0.475*d6(i))/(d3-0.475*d4)))-log(d10);
    end
end
```

```
%%%%%%%%%%%%%%%%%%%%%%%%%%%%%%%%%%%%%%%%%%%%%%%%%%%%%%%%%%%%%%%%%%%%%%%
C-2-9
% Global Optimization method, available in MATLAB toolbox


% fun = optimization function defined on the basis of the EoS
% opt = optimization function in MATLAB
% problem = creating the optimization basin using the EoS and initial guess generated
by genetic algorithm
% X0 = start point for optimization
% lb = lower bound of the optimization parameters
% ub = upper bound of the optimization parameters


clear
clc
format long
fun = ;
tic;
warning ('off','all')
rng default % For reproducibility
opts = optimoptions(@fmincon,'Algorithm','sqp');
problem = createOptimProblem('fmincon','objective',fun,'x0',[72.77803480255467
        0.003909438929457124        1.823178160267012   6098.567164189547
        9.438624322132323   -0.7216284916395748 0.07182916892932545
        3.120433178986149],...
    'lb',[1e-2 1e-7 1e-3 1000 1e-4 -0.9 -0.9 0.1],'ub',[500 1e-2 20 50000 20 0.9 0.9
5],'options',opts);
ms = MultiStart;
ms.UseParallel='always';
[X,FVAL,EXITFLAG,OUTPUT,solutions] = run(ms,problem,100)
fprintf('x     :%.18f\n',X)
fprintf('fval    :%.18f\n',FVAL)
toc;



%%%%%%%%%%%%%%%%%%%%%%%%%%%%%%%%%%%%%%%%%%%%%%%%%%%%%%%%%%%%%%%%%%%%%%%
C-2-10
% Volume calculations using CPA EoS of precipitated phase, eq B-2 (appendix B)


% v (d1) = molar volume calculated from CPA EoS
% b (d2) = repulsive energy parameter for asphaltene phase
% epsilon (d3) = association energy
% betta (d4) = association volume
% T (d5)= temperature (K)
% P (d6)= pressure (Pascal)
% a (d7) = attractive energy parameter for asphaltene
% R (d8) = universal gas constant, J.mol-1.K-1
% NS (d9) = Number of active sites on the associating molecule


function D=vcpa(d1,d2,d3,d4,d5,d6,d7,d8,d9)
% convergence criteria % considering different ac
```

```matlab
e=1e-12;
error2=1;
m2=0;
k2=1000000;
% error criteria
while (error2>=1e-1)
        for i0=1:1:3
            if i0==2
                d1=d1+e;
            end
            if i0==3
                d1=d1-2*e;
            end
            D1=0.25*(d2/d1);
            D2=1/(1-1.9*D1);
            D3=D2*(exp(d3/(d8*d5))-1)*d2*d4;
% considering different active site on the molecule (NS), fugacity coefficient is
calculated
            if d9==4
                D4=(-1+sqrt(1+8*(D3/d1)))/(4*(D3/d1));

% Volume calculations of the CPA EoS, eq B-2 (Appendix)
fv(i0)=d6-((d8*d5)/(d1-d2))+(d7/(d1*(d1+d2)))+(((d8*d5)/(2*d1))*(1+((0.475*d2)/(d1-
0.475*d2)))*d9*(1-D4));
            elseif d9==2
                D4=(-1+sqrt(1+4*(D3/d1)))/(2*(D3/d1));
                fv(i0)=d6-((d8*d5)/(d1-
d2))+(d7/(d1*(d1+d2)))+(((d8*d5)/(2*d1))*(1+((0.475*d2)/(d1-0.475*d2)))*d9*(1-D4));
            elseif d9==3
                D4=(-(1-D3/d1)+sqrt(((1+D3/d1)^2)+(4*D3/d1)))/(4*D3/d1);
                fv(i0)=d6-((d8*d5)/(d1-
d2))+(d7/(d1*(d1+d2)))+(((d8*d5)/(2*d1))*(1+((0.475*d2)/(d1-0.475*d2)))*(d9+1)*(1-
D4));
            end
        end


% Newton-Raphson algorithm to find volume using CPA EoS
        fpv=(fv(2)-fv(3))/(2*e);
        vnew=(d1+e)-(fv(1)/fpv);
        error2=abs((1/vnew)-(1/d1));
        d1=vnew;
        if m2>100
            k2=50;
            break
        end
        m2=m2+1;
        if isreal(d1)==0
            k2=50;
            break
        end
        if isnan(d1)==1
            k2=50;
            break
        end
```

```matlab
        if isinf(d1)==1
            k2=50;
            break
        end
        if d1<=0
            k2=50;
            break
        end
    end
end
if k2==50
    D=[1000 1000 1000 1000 1000];
else
    D5=d1;
% D1 = etta, reduced density
% D2 = radial distribution function (RDF), eq 3-12
% D3 = delta, the association strength, eq 3-11
% D4 = xnon, non-bonded fraction of the molecule in the association bond, eq 3-10
% D5 = CPA volume, eq B-2
D=[D1 D2 D3 D4 D5];
end
```

C-2-11
```matlab
% Volume calculations using CPA EoS of oil phase, eq B-2 (appendix B)


% v (d1) = molar volume calculated from CPA EoS for oil phase
% b (d2) = repulsive energy parameter for oil components
% epsilon (d3) = association energy
% betta (d4) = association volume
% R (d5) = universal gas constant, J.mol-1.K-1
% T (d6)= temperature (K)
% Bmix (d7) = repulsive energy parameter for oil phase
% Amix (d8) = attractive energy parameter for oil mixture
% P (d9)= pressure (Pascal)
% xi (d10) = mole fractions
% n (d11) = number of components
% sij (d20) = cross association
% etta (D2) = reduced density
% RDF (D3) = radial distribution function, eq 3-12
% delta (D4) = the association strength, eq 3-11


function D=vcpamixture_ECR(d1,d2,d3,d4,d5,d6,d7,d8,d9,d10,d11,d20)
global X1 X2 v delta12 delta1 delta2
% convergence criteria
e=1e-12;
error=1;
v=d1;
m2=0;
k2=1000000;
while (error>=10^-10)
    for i0=1:1:3
```

```matlab
        if i0==2
            d1=d1+e;
        end
        if i0==3
            d1=d1-2*e;
        end
        for i00=1:2;
            if i00==1
                D4(1)=d20;
            else
                D4(i00)=(d1/(d1-(0.475*d8)))*(exp(d3/(d5*d6))-1)*d2(3)*d4;
            end
        end
        delta12=D4(1)*D4(2);
        delta1=D4(1);
        delta2=D4(2);
        X1=d10(2);
        X2=d10(3);
        xnon0=[0.1 0.1 0.1 0.1];
        try
```

```matlab
% Solving eq 3-10 to find non-bonded fraction of the molecule
        options = optimoptions('fsolve','Display','none');
        [xnon_f,fval] = fsolve(@fnonbonded,xnon0,options);
        catch
            k2=50;
            break
        end
% Volume calculations of the CPA EoS, eq B-2 (Appendix)          fv(i0)=d9-
((d5*d6)/(d1-d8))+(d7/(d1*(d1+d8)))+(((d5*d6)/(2*d1))*(1+((0.475*d8)/(d1-
0.475*d8)))*((d10(2)*2*(1-xnon_f(1)))+(d10(3)*((2*(1-xnon_f(2)))+(2*(1-
xnon_f(3)))))))));
    end
    if k2==50
        k2=50;
        break
    end
```

```matlab
% Newton-Raphson algorithm to find volume using CPA EoS
    fpv=(fv(2)-fv(3))/(2*e);
    vnew=(d1+e)-(fv(1)/fpv);
    error=abs(vnew-d1);
    d1=vnew;
    v=d1;
    if m2>100
        k2=50;
        break
    end
    m2=m2+1;
    if isreal(d1)==0
        k2=50;
        break
    end
```

```matlab
        if isnan(d1)==1
            k2=50;
            break
        end
        if isinf(d1)==1
            k2=50;
            break
        end
        if d1<=0
            k2=50;
            break
        end
    end
    if k2==50
        D=[10000 10000];
    else
    D1=d1;
    D2=xnon_f;
    D=[D1 D2 m2 D4];
    end
```

```matlab
%%%%%%%%%%%%%%%%%%%%%%%%%%%%%%%%%%%%%%%%%%%%%%%%%%%%%%%%%%%%%%%%%%%%%%%%%%%%%%%
```

C-2-12
```matlab
% Flash Calculations; main script of the CPA EoS


% R = universal gas constant, J.mol-1.K-1
% TC = critical temperature (K)
% PC = critical pressure (pascal)
% AF = acentric factor
% n = number of components
% epsilon = association energy
% betta = association volume


clear
clc
format long
warning ('off', 'all')



% Input: R, TC, PC, AF, n
R=8.314;
TC=[];
PC=[];
AF=[];
n=[];


% Parameter calculation of the Cubic EoS, Eq 3-4, 3-5, 3-6. 3-7
for i=1:n-1
    a00(i)=0.42748*(((R*TC(i))^2)/PC(i));
    b0(i)=0.08664*((R*TC(i))/PC(i));
```

```matlab
    c0(i)=0.48+1.574*AF(i)-0.176*(AF(i)^2);
end


a0=[a00 a00(asph)];
b=[b0 b0(asph)];
c=[c0 c0(asph)];
epsilon=epsilon;
betta=betta;


T=293;
for i=1:n
    am(i)=a0(i)*((1+c(i)*(1-sqrt(T/TC(i)))).^2);
end


% Binary interaction parameters optimized for the system, available in chapter 3,
Table 3-3
kij=[0          Kij(1)       Kij(2)
     Kij(1)     0            Kij(3)
     Kij(2)     Kij(3)       0 ];



% Precipitated asphaltene (experimental data if available for validation)
% naspre_exp = amount of asphaltene precipitation
% nd = number of experimental data
% PEXP = experimental pressure (pascal)
% nastotal = initial oil asphaltene content
% nmperim = oil component fractions



naspre_exp=[];
nd=numel(naspre_exp);
PEXP=[];
nastotal=[];
nmperim=[];
nm=[nmperim (nastotal-naspre_exp)'];


% Experimental mole fractions in oil phase
xEXP=ones(nd,3);
for j=1:nd
    xEXP(j,:)=nm(j,:)./sum(nm(j,:));
end
xperim=ones(nd,2); % non-asphaltenic oil
for j=1:nd
    xperim(j,:)=nmperim(j,:)./sum(nmperim(j,:));
end


% Flash calculations of the asphaltene phase
```

```matlab
for j=1:nd

    p=PEXP(j);
    kk=1;
    NS=4;
% Volume calculation of the CPA EoS for asphaltene phase
    A=Acapital(R,am(3),b(3),T,p);
    B=Bcapital(R,am(3),b(3),T,p);
    vliqguess=1.1*b(3);
    output=vcpa(vliqguess,b(3),epsilon,betta,T,p,am(3),R,NS);
    if sum(output)==5000
        fugacityas=1e36;
        kk=50;
    else
        xnonliq=output(4);
        vliq=output(5);
        zliq=p*vliq/(R*T);


% Fugacity calculation of the CPA EoS for asphaltene phase
        lnphil=fugacitycoeff(zliq,xnonliq,A,B,NS);
        phias=exp(lnphil);
        fugacityas=phias*p;
        fu(j)=fugacityas;
    end
    error=1;
    k=1;
    m1=1;
    step=0;

    while error>=1e-12



% First guess for flash calculations of the asphaltene mole fraction
    step=step+1;
    if step==1
        kwilson=(PC(3)/p)*exp(5.37*(1+AF(3))*(1-(TC(3)/T)));
        kas=1/(kwilson^(1/3));
        xa=1/kas;
        x=(1-xa)*xperim(j,:);
        x=[x xa];
        nas=(x(3)*sum(nmperim(j,:)))/(1-x(3));


% Modification of the mole fraction calculation, step 2 to step n
    else
        xa=x(3)*(fugacityas/fugacityl(3));
        x=(1-xa)*xperim(j,:);
        x=[x xa];
        nas=(x(3)*sum(nmperim(j,:)))/(1-x(3));
    end
```

```matlab
% Volume calculation of the CPA EoS for oil phase
    bmixliq=Bmix(x,b);
    amixliq=Amix2(x,a,n);
    vliqguess=1.1*bmixliq;
    output=vcpamixture_ECR(vliqguess,b,epsilon,betta,R,T,amixliq,bmixliq,p,x,n,sij);
    m1=m1+1;
    if sum(output)==20000
        fugacityl(3)=fugacityas;
        k=50;
    elseif m1>100
        fugacityl(3)=fugacityas;
        k=50;
    elseif nas>=nastotal(j)
        fugacityl(3)=fugacityas;
        k=50;
    elseif kk==50
        fugacityl(3)=fugacityas;
        k=50;
    else
        vliq=output(1);
        xnonliq=[output(2) output(3) output(4)];


% Fugacity calculation of the CPA EoS for oil phase
        itliq=output(5);
        zliq=p*vliq/(R*T);
        lnphil=fugacitycoeff_mix(x,xnonliq,vliq,bmixliq,amixliq,b,a,R,T,zliq,n);
        phil=exp(lnphil);
        fugacityl=x.*phil*p;



    end
    error=(1-(fugacityas/fugacityl(3)))^2;
    end


% Error calculations
    if k==50
        xasphaltene(j)=1e36;
        naspre_calc(j)=1e36;
    else
        xasphaltene(j)=x(3);
        naspre_calc(j)=nastotal(j)-nas;
    end
end
naspre=[naspre_exp' naspre_calc']


xpre=[xEXP(:,3) xasphaltene'];


AARDn=sum(abs((naspre_exp-naspre_calc)./naspre_exp))/nd
AARDx=sum(abs((xEXP(:,3)'-xasphaltene)./xEXP(:,3)'))/nd
```

```
% Plot the results
subplot(1,2,1)
plot(naspre_exp,naspre_calc,'*');
hold on;
plot(naspre_exp,naspre_exp);
subplot(1,2,2)
plot(nmperim(:,1),naspre_calc)
hold on
plot(nmperim(:,1),naspre_exp,'*')
```

%%

C-2-13
% polar Helmholtz free energy calculations, Eq 4-5 and ref [7]

% epsi0 = vacuum permittivity (C^2/J.m)
% KB = Boltzmann constant
% NA = Avogadro's number
% v (d1) = molar volume calculated from CPP EoS for oil phase
% b (d2) = repulsive energy parameter for components
% R (d5) = universal gas constant, J.mol-1.K-1
% T (d6)= temperature (K)
% xi (d10) = mole fractions
% n (d11) = number of components
% rostar (d20) = mean number density
% np (d21) = number of polar segment per molecule
% Dipole moment (d22)
% I6 (D1) = a function of the CPP EoS
% D2 and D3 = functions of the CPP EoS


```
function D=A2DD(d1,d2,d5,d6,d10,d11,d21,d22)
NA=6.0221e23;
KB=1.38065e-23;
epsi0=8.85419e-12;
d20=meannumberdensity(d1,d2,d10,d11); % function
D1=I6(d20); % function
D4=diameter(d2,d11); % function
D2=-(NA*d5*d6)*D1/(6*d1*((KB*d6)^2)*(4*pi*epsi0)^2);
D3=0;
for i=1:d11
    for j=1:d11
        D3=D3+((d10(i)*d10(j)*d21(i)*d21(j)*(d22(i)^2)*(d22(j)^2))/(D4(i,j)^3));
    end
end
D=D2*D3;
```
%%
C-2-14

% dI6dro; a function in CPP EoS, [7]

```
% rostar (d20) = mean number density
% d23 = dx^3 (diameter function of the CPP EoS [2])
% D = D1 = d(I6)/d(ro)
% J6 = constants of the series [2]


function D=dI6dro(d20,d23)

J6=[4.1888 2.8287 0.8331 0.0317 0.0858 -0.0846]; % Coefficient of the extended virial
series approximation for I^HS_k (ρ*)

D1=0;
for i=1:6;
    D1=D1+(J6(i)*(((i-1)*(d20^(i-2))*(d23))));
end
D=D1;
```

%%%

C-2-15

```
% segment diameter calculation of the component, equations from [2, 7]


% NA = Avogadro's number (1/mol)
% b (d2) = repulsive energy parameter for components
% n (d11) = number of components
% D(i,j) (dij) = segment diameter
% pi = π, approximately equal to 3.14159


function D=diameter(d2,d11)
NA=6.0221e23;
for i=1:d11;
    dia(i)=((3*d2(i))/(2*pi*NA))^(1/3);
end

for i=1:d11;
    for j=1:d11;
        D(i,j)=(dia(i)+dia(j))/2;
    end
end
```

%%%

C-2-16

```
%dx3 [2, 7]
```

```
% NA = Avogadro's number (1/mol)
% v (d1) = molar volume calculated from CPP EoS for oil phase
% b (d2) = repulsive energy parameter for components
% xi (d10) = mole fractions
% n (d11) = number of components
% D (D1) = dx^3 ( a function of the CPP EoS)
% sicma = diameter function


function D=dx3(d2,d10,d11)
NA=6.0221e23;
sicma=diameter(d2,d11);   % function

D1=0;
for i=1:d11;
    for j=1:d11;
        D1=D1+(d10(i)*d10(j)*(sicma(i,j)^3));
    end
end
D=D1;
```

%%

C-2-17

% fugacity coefficient of precipitated phase [2, 6, 7]. Function A2DD (d6) is also used to account for polar section

% z (d1) = compressibility factor
% xenon (d2) = fraction of the molecule is not engaged in polar interactions
% A (d3) = attractive energy parameter for asphaltene
% B (d4) = repulsive energy parameter for asphaltene
% NS (d5) = number of active site on the molecule
% Apolar/RT (d6) = Helmholtz free energy of the component divided by gas constant and temperature
% lnphi (D1) = fugacity coefficient for the precipitated phase


```
function D1=fugacitycoeff(d1,d3,d4,d6)
D1=(d1-1)-log(d1-d4)+(d3/d4)*log(d1/(d1+d4))+d6;
```

%%

C-2-18

% fugacity coefficient for the oil phase [2, 8]

% xi (d1) = mole fraction
% v (d3) = molar volume calculated from CPP EoS for oil phase

```
% bmix (d4) = repulsive energy parameter for oil phase
% amix (d5) = attractive energy parameter for oil phase
% aij (d7) = binary attractive energy parameter
% R (d8) = universal gas constant, J.mol-1.K-1
% T (d9)= temperature (K)
% z (d10) = compressibility factor
% n (d11) = number of components
% bij (d50) = binary repulsive energy parameter
% lnphi ( D) = fugacity coefficient for the precipitated phase



function D=fugacitycoeffmix(d1,d3,d4,d5,d7,d8,d9,d10,d11,d50)
for i=1:d11
    for j=1:d11
        sa(j)=d1(j)*d7(i,j);
        sb(j)=d1(j)*d50(i,j);
    end
        D(i)=log(d3/(d3-d4))+(2*sum(sb)-d4)/(d3-d4)...
        +(1/(d8*d9))*(((d5/d4)*log(d3/(d3+d4)))+(log(d3/(d3+d4))*((2*d4*sum(sa)-
2*d5*sum(sb))/(d4^2)))-((d5/d4)*((2*sum(sb)-d4)/(d3+d4))))...
        -log(d10);
end
```

%%%

C-2-19

```
% I6  An approximation in the form of an extended virial series [2,
7]



% rostar (d20) = mean number density
% D = function of the CPP EoS, I6 [2]
% J6 = constants of I6 function series [2]



function D=I6(d20)

J6=[4.1888 2.8287 0.8331 0.0317 0.0858 -0.0846]; % Coefficient of the extended virial
series approximation for I^HS_k (ρ*)

D1=0;
for i=1:6;
    D1=D1+(J6(i)*(d20^(i-1)));
end
D=D1;
```
%%%

C-2-20

```
% mean number density calculation of the CPP EoS [2, 7]
```

```matlab
% NA = Avogadro's number (1/mol)
% v (d1) = molar volume calculated from CPP EoS for oil phase
% b (d2) = repulsive energy parameter for components
% xi (d10) = mole fractions
% n (d11) = number of components
% D = mean number density
% sicma = diameter function




function D=meannumberdensity(d1,d2,d10,d11)
NA=6.0221e23;
sicma=diameter(d2,d11); %function
D1=0;
for i=1:d11;
    for j=1:d11;
        D1=D1+(d10(i)*d10(j)*(sicma(i,j)^3));
    end
end
D=(NA/d1)*D1;
```

%%

C-2-21

```matlab
% polar volume calculations for asphaltene phase [1, 7]


% v (d1) = molar volume calculated from CPP EoS
% b (d2) = repulsive energy parameter for components
% T (d6) = temperature (K)
% P (d6) = pressure (Pascal)
% ai (d7) = attractive energy parameter
% R (d8) = universal gas constant, J.mol-1.K-1
% np (d10) = fraction of the molecule is engaged in the polar interaction
% miu (d11) = dipole moment




function D=vcpppolar(d1,d2,d5,d6,d7,d8,d10,d11)
% convergence criteria
e=1e-12;
error2=1;
m2=0;
k2=1000000;
% error criteria
while (error2>=1e-1)

        for i0=1:1:3
            if i0==2
                d1=d1+e;
```

```matlab
            end
            if i0==3
                d1=d1-2*e;
            end
% compressibility factor using CPP EoS, function [7]
            z2=Z2DD(d1,d2,d5,1,1,d10,d11);
            zpolar=z2;
% volume calculation and New-Raphson Method [1]
        fv(i0)=d6-((d8*d5)/(d1-d2))+(d7/(d1*(d1+d2)))-(zpolar*d8*d5/d1);
        end
        fpv=(fv(2)-fv(3))/(2*e);
        vnew=(d1+e)-(fv(1)/fpv);
        error2=abs((1/vnew)-(1/d1));
        d1=vnew;
        if m2>100
            k2=50;
            break
        end
        m2=m2+1;
        if isreal(d1)==0
            k2=50;
            break
        end
    end
end


if k2==50
    D=[1000 1000 1000 1000 1000 1000];
else
D5=d1;
a2=A2DD(d1,d2,d8,d5,1,1,d10,d11);
miupolar=a2*(1/(d8*d5));
D6=miupolar;


D=[D5 D6];
end
```

%%%

C-2-22

```matlab
% Volume calculation for oil phase [8]


% v (d1) = molar volume
% b (d2) = repulsive energy parameter for components
% R (d5) = universal gas constant, J.mol-1.K-1
% T (d6) = temperature (K)
% amix (d7) = attractive energy parameter for mixture
% bmix (d8) = repulsive energy parameter for mixture
% P (d9) = pressure (Pascal)
```

```
function D=vcubic(d1,d5,d6,d7,d8,d9)
global v
% convergence criteria
e=1e-15;
error2=1;
v=d1;
m2=0;
k2=1000000;
while (error2>=1e-1)
    for i0=1:1:3
        if i0==2
            d1=d1+e;
        end
        if i0==3
            d1=d1-2*e;
        end
% volume calculation and New-Raphson Method
        fv(i0)=d9-((d5*d6)/(d1-d8))+(d7/(d1*(d1+d8)));
    end
    fpv=(fv(2)-fv(3))/(2*e);
    vnew=(d1+e)-(fv(1)/fpv);
    error2=abs((1/vnew)-(1/d1));
    d1=vnew;
    v=d1;
    if m2>100
        k2=50;
        break
    end
    m2=m2+1;
    if isreal(d1)==0
        k2=50;
        break
    end
    if isnan(d1)==1
        k2=50;
        break
    end
    if isinf(d1)==1
        k2=50;
        break
    end
    if d1<0
        k2=50;
        break
    end
end
if k2==50
    D=[10000 10000];
else
D1=d1;
D=D1;
```

```matlab
end
```

```
%%%%%%%%%%%%%%%%%%%%%%%%%%%%%%%%%%%%%%%%%%%%%%%%%%%%%%%%%%%%%%%%%%%%%%%%%%%%%%
```
C-2-23

```matlab
% Compressibility factor calculations using CPP EoS, Z(CPP) [7]


% epsi0 = vacuum permittivity (C^2/J.m)
% b (d2) = repulsive energy parameter for components
% T (d6)= temperature (K)
% xi (d10) = mole fractions
% n (d11) = number of components
% rostar (d20) = mean number density
% np (d21) = number of polar segment per molecule
% Dipole moment (d22)
% dx^3 (d23) = diameter function of the CPP EoS [2]
% I6 (D1) = a function of the CPP EoS
% Z2DD (D) = compressibility factor of the CPP EoS extension
% D5 = d(I6)/d(ro), derivation of the I6 function with density [2]




function D=Z2DD(d1,d2,d6,d10,d11,d21,d22)
NA=6.0221e23;
KB=1.38065e-23;
epsi0=8.85419e-12;
% mean number density calculation of the CPP EoS [2, 7]
d20=meannumberdensity(d1,d2,d10,d11); % function
d23=dx3(d2,d10,d11); % function
D1=I6(d20); % function
D5=dI6dro(d20,d23); % function
D6=D1+((NA/d1)*D5);
D4=diameter(d2,d11); % function
D2=-(NA*D6)/(6*d1*((KB*d6)^2)*(4*pi*epsi0)^2);
D3=0;
for i=1:d11
    for j=1:d11
        D3=D3+((d10(i)*d10(j)*d21(i)*d21(j)*(d22(i)^2)*(d22(j)^2))/(D4(i,j)^3));
    end
end
D=D2*D3;
```

```
%%%%%%%%%%%%%%%%%%%%%%%%%%%%%%%%%%%%%%%%%%%%%%%%%%%%%%%%%%%%%%%%%%%%%%%%%%%%%%
```
C-2-24

```matlab
% Flash Calculations; main file of the CPP EoS
```

```matlab
% R = universal gas constant, J.mol-1.K-1
% T = temperature (K)
% TC = critical temperature (K)
% PC = critical pressure (pascal)
% AF = acentric factor
% n = number of components
% np = fraction of the molecule engaged in polar intercation
% miu = dipole moment


clear all
clc
warning ('off', 'all')

n=3;
R=8.314;
TC=[];
PC=[];
AF=[];
% attractive and repulsive parameter calculations of the cubic EoS
for i=1:n-1
    a00(i)=0.42748*(((R*TC(i))^2)/PC(i));
    b0(i)=0.08664*((R*TC(i))/PC(i));
    c0(i)=0.48+1.574*AF(i)-0.176*(AF(i)^2);
end


b=[b0 b0(asph)];
np=[];
miu=[]*3.33569e-30;
T=[];
for i=1:n-1
    amm(i)=a00(i)*((1+c0(i)*(1-sqrt(T/TC(i)))).^2);
end


am=[amm amm(asp)];


% binary interaction parameters adjusted for the equilibrium
kij=[0          kij(1)      kil(2)
     kij(1)     0           kij(3)
     kij(2)     kij(3)      0 ];


lij=[0          lij(4)      lij(5)
     lij(4)     0           lij(6)
     lij(5)     lij(6)      0 ];
a=aij(kij,am,n);
bi=bij(lij,b,n);



% Precipitated asphaltene (experimental data if available for validation)
```

```matlab
% naspre_exp = amount of asphaltene precipitation
% nd = number of experimental data
% PEXP = experimental pressure (pascal)
% nastotal = initial oil asphaltene content
% nmperim = oil component fractions


naspre_exp=[];
nd=numel(naspre_exp);
PEXP=(6894.76*800)*ones(1,nd);
nastotal=0.0003908*ones(1,nd);
nmperim=[];  %non asphaltenic oil
nm=[nmperim (nastotal-naspre_exp)'];
% experimental mole fractions in oil phase
xEXP=ones(nd,3);
for j=1:nd
    xEXP(j,:)=nm(j,:)./sum(nm(j,:));
end


xperim=ones(nd,2);
for j=1:nd
    xperim(j,:)=nmperim(j,:)./sum(nmperim(j,:));
end


% Flash calculations of the asphaltene phase


for j=1:nd

    p=PEXP(j);

    kk=1;
    A=Acapital(R,am(3),b(3),T,p);
    B=Bcapital(R,am(3),b(3),T,p);


% volume and fugacity calculations for precipitated phase
    vliqguess=1.1*b(3);
    output=vcpppolar(vliqguess,b(3),T,p,am(3),R,np,miu);
    if sum(output)==6000
        fugacityas=1e36;
        kk=50;
    else

        vliq=output(1);
        miupolarliq=output(2);
        zliq=p*vliq/(R*T);
        lnphil=fugacitycoeff(zliq,A,B,miupolarliq);
        phias=exp(lnphil);
        fugacityas=phias*p;
        fu(j)=fugacityas;
    end
    error=1;
```

```matlab
        k=1;
        m1=1;
        step=0;




% First guess for flash calculations of the asphaltene mole fraction

    while error>=1e-12

    step=step+1;
    if step==1
        kwilson=(PC(3)/p)*exp(5.37*(1+AF(3))*(1-(TC(3)/T)));
        kas=1/(kwilson^(1/3));
        xa=1/kas;
        x=(1-xa)*xperim(j,:);
        x=[x xa];
        nas=(x(3)*sum(nmperim(j,:)))/(1-x(3));

    else
% Modification of the mole fraction calculation, step 2 to step n
        xa=x(3)*(fugacityas/fugacityl(3));
        x=(1-xa)*xperim(j,:);
        x=[x xa];
        nas=(x(3)*sum(nmperim(j,:)))/(1-x(3));
    end


% Volume and fugacity calculation of the CPA EoS for oil phase
        bmixliq=Bmix2(x,bi,n);
        amixliq=Amix2(x,a,n);
        vliqguess=1.1*bmixliq;

        output=vcubic(vliqguess,R,T,amixliq,bmixliq,p);
        m1=m1+1;
        if sum(output)==20000
            fugacityl(3)=fugacityas;
            k=50;
        elseif m1>100
            fugacityl(3)=fugacityas;
            k=50;
        elseif nas>=nastotal(j)
            fugacityl(3)=fugacityas;
            k=50;
        elseif kk==50
            fugacityl(3)=fugacityas;
            k=50;
        else
            vliq=output(1);
            zliq=p*vliq/(R*T);
            lnphil=fugacitycoeffmix(x,vliq,bmixliq,amixliq,a,R,T,zliq,n,bi);
            phil=exp(lnphil);
            fugacityl=x.*phil*p;
```

```matlab
    end
% Error calculations
    error=(1-(fugacityas/fugacityl(3)))^2;
    end
    if k==50
        xasphaltene(j)=1e36;
        naspre_calc(j)=1e36;
    else
        xasphaltene(j)=x(3);
        naspre_calc(j)=nastotal(j)-nas;
    end
end
naspre=[naspre_exp' naspre_calc']
xpre=[xEXP(:,3) xasphaltene'];
AARDn=sum(abs((naspre_exp-naspre_calc)./naspre_exp))/nd
AARDx=sum(abs((xEXP(:,3)'-xasphaltene)./xEXP(:,3)'))/nd
OF=1000*AARDn


% Plot the results
subplot(1,2,1)
plot(naspre_exp,naspre_calc,'*');
hold on;
plot(naspre_exp,naspre_exp);
subplot(1,2,2)
plot(nmperim(1:end,1),naspre_calc)
hold on
plot(nmperim(1:end,1),naspre_exp,'*')
RR=nmperim(1:end,1);



%%%%%%%%%%%%%%%%%%%%%%%%%%%%%%%%%%%%%%%%%%%%%%%%%%%%%%%%%%%%%%%%%%%%%%%%%%%%%
C-2-25
% Flash Calculations CPA EoS; a sample code with all the parameters for the
asphaltene precipitation using n-C6 as precipitant at temperature 308
K


C-2-25-1
% R = universal gas constant, J.mol-1.K-1
% TC = critical temperature (K)
% PC = critical pressure (pascal)
% AF = acentric factor
% n = number of components
% epsilon = association energy
% betta = association volume


clear
clc
format long
warning ('off','all')

n=3;
```

```matlab
% nC6 (Precipitant) is component 1
% HC is component 2
% Asphaltene (A) is component 3
% R is j/mol.k
R=8.314;
%  Temperature unit is kelvin and TC is critical temperature of components [3,4]
TC=[507.5 1426.75836506728 1740.01142509225];
% Pressure unit is pascal and PC is critical pressure of components
PC=1e5*[30.31 13.4878030350856 9.63655994130257];
% AF is acentric factor and is unitless
AF=[0.299 0.873897311316050 1.05223796413750];

% Parameter calculation of the Cubic EoS, Eq 3-4, 3-5, 3-6. 3-7
for i=1:n-1
    a00(i)=0.42748*(((R*TC(i))^2)/PC(i));
    b0(i)=0.08664*((R*TC(i))/PC(i));
    c0(i)=0.48+1.574*AF(i)-0.176*(AF(i)^2);
end


% Adjustable parameters of the CPA EoS, "u" matrix includes a0, b, c1, ε, β, cross
association. "qq" is binary interaction parameters

u=[0.4733760711654037      1.5648931173134083E-4     0.9202235022284841
       19805.0290113222    6.55842541763739  1.3483088796035694];
qq=[0.214268047330068   0.067480195881593];


a00(asph)=u(1);
b0(asph)=u(2);
c0(asph)=u(3);
epsilon=u(4);
betta=u(5);
a=aij(kij,am,n);
sij=u(6);


a0=[a00 a00(asph)];
b=[b0 b0(asph)];
c=[c0 c0(asph)];
epsilon=epsilon;
betta=betta;


T=308;
for i=1:n
    am(i)=a0(i)*((1+c(i)*(1-sqrt(T/TC(i)))).^2);
end


% Binary interaction parameters optimized for the system, available in chapter 3,
Table 3-3
kij=[0              Kij(1)            Kij(2)
     Kij(1)           0               Kij(3)
```

```matlab
    Kij(2)       Kij(3)          0 ];




% Precipitated asphaltene (experimental data if available for validation)
% naspre_exp = amount of asphaltene precipitation
% nd = number of experimental data
% PEXP = experimental pressure (pascal)
% nastotal = initial oil asphaltene content
% nmperim = oil component fractions




naspre_exp=[0.0000192 0.0000636 0.0001194 0.0002382 0.000291 0.0003168 0.0003186];
nd=numel(naspre_exp);
PEXP=(6894.76*14.7)*ones(1,nd);
nastotal=0.0003908*ones(1,nd);
nmperim=[0.0957646790000000,0.00854300000000000;0.123126015000000,0.00854300000000000
;0.171008355000000,0.00854300000000000;0.331756208000000,0.00854300000000000;0.489083
894000000,0.00854300000000000;0.704554421000000,0.00854300000000000;0.831100603000000
,0.00854300000000000];
nm=[nmperim (nastotal-naspre_exp)'];




C-2-25-2
% Experimental mole fractions in oil phase
xEXP=ones(nd,3);
for j=1:nd
    xEXP(j,:)=nm(j,:)./sum(nm(j,:));
end
xperim=ones(nd,2); % non-asphaltenic oil
for j=1:nd
    xperim(j,:)=nmperim(j,:)./sum(nmperim(j,:));
end




C-2-25-3
% Flash calculations of the asphaltene phase
for j=1:nd

    p=PEXP(j);
    kk=1;
    NS=4;
% Volume calculation of the CPA EoS for asphaltene phase
    A=Acapital(R,am(3),b(3),T,p);
    B=Bcapital(R,am(3),b(3),T,p);
    vliqguess=1.1*b(3);
    output=vcpa(vliqguess,b(3),epsilon,betta,T,p,am(3),R,NS);
    if sum(output)==5000
        fugacityas=1e36;
        kk=50;
    else
        xnonliq=output(4);
```

```matlab
        vliq=output(5);
        zliq=p*vliq/(R*T);


% Fugacity calculation of the CPA EoS for asphaltene phase
        lnphil=fugacitycoeff(zliq,xnonliq,A,B,NS);
        phias=exp(lnphil);
        fugacityas=phias*p;
        fu(j)=fugacityas;
    end
    error=1;
    k=1;
    m1=1;
    step=0;

    while error>=1e-12
```

C-2-25-4
```matlab
% First guess for flash calculations of the asphaltene mole fraction
    step=step+1;
    if step==1
        kwilson=(PC(3)/p)*exp(5.37*(1+AF(3))*(1-(TC(3)/T)));
        kas=1/(kwilson^(1/3));
        xa=1/kas;
        x=(1-xa)*xperim(j,:);
        x=[x xa];
        nas=(x(3)*sum(nmperim(j,:)))/(1-x(3));


% Modification of the mole fraction calculation, step 2 to step n
    else
        xa=x(3)*(fugacityas/fugacityl(3));
        x=(1-xa)*xperim(j,:);
        x=[x xa];
        nas=(x(3)*sum(nmperim(j,:)))/(1-x(3));
    end


## C-2-25-5
% Volume calculation of the CPA EoS for oil phase
    bmixliq=Bmix(x,b);
    amixliq=Amix2(x,a,n);
    vliqguess=1.1*bmixliq;
    output=vcpamixture_ECR(vliqguess,b,epsilon,betta,R,T,amixliq,bmixliq,p,x,n,sij);
    m1=m1+1;
    if sum(output)==20000
        fugacityl(3)=fugacityas;
        k=50;
    elseif m1>100
        fugacityl(3)=fugacityas;
        k=50;
    elseif nas>=nastotal(j)
        fugacityl(3)=fugacityas;
```

```
        k=50;
    elseif kk==50
        fugacityl(3)=fugacityas;
        k=50;
    else
        vliq=output(1);
        xnonliq=[output(2) output(3) output(4)];


% Fugacity calculation of the CPA EoS for oil phase
        itliq=output(5);
        zliq=p*vliq/(R*T);
        lnphil=fugacitycoeff_mix(x,xnonliq,vliq,bmixliq,amixliq,b,a,R,T,zliq,n);
        phil=exp(lnphil);
        fugacityl=x.*phil*p;


    end
    error=(1-(fugacityas/fugacityl(3)))^2;
    end
```

C-2-25-6
```
% Error calculations
    if k==50
        xasphaltene(j)=1e36;
        naspre_calc(j)=1e36;
    else
        xasphaltene(j)=x(3);
        naspre_calc(j)=nastotal(j)-nas;
    end
end
naspre=[naspre_exp' naspre_calc'];
xpre=[xEXP(:,3) xasphaltene'];
AARDn=sum(abs((naspre_exp-naspre_calc)./naspre_exp))/nd;


% Plot the results
plot(xEXP(:,3),xasphaltene','*');
xlabel('Experimental mole fraction');
ylabel('model mole fraction');
hold on;
plot(xEXP(:,3),xEXP(:,3));

%%%%%%%%%%%%%%%%%%%%%%%%%%%%%%%%%%%%%%%%%%%%%%%%%%%%%%%%%%%%%%%%%%%%%%%%%%%
```

C-2-26

```
% Flash Calculations CPP EoS; a sample code with all the parameters for the
asphaltene precipitation using n-C6 as precipitant at temperature 308
K
```

C-2-26-1

```matlab
% R = universal gas constant, J.mol-1.K-1
% TC = critical temperature (K)
% PC = critical pressure (pascal)
% AF = acentric factor
% n = number of components
% epsilon = association energy
% betta = association volume


clear
clc
format long
warning ('off','all')

n=3;
% nC6 (Precipitant) is component 1
% HC is component 2
% Asphaltene (A) is component 3
% R is j/mol.k
R=8.314;
%  Temperature unit is kelvin and TC is critical temperature of components [3,4]
TC=[507.5 1426.75836506728 1740.01142509225];
% Pressure unit is pascal and PC is critical pressure of components
PC=1e5*[30.31 13.4878030350856 9.63655994130257];
% AF is acentric factor and is unitless
AF=[0.299 0.873897311316050 1.05223796413750];

% Parameter calculation of the Cubic EoS, Eq 3-4, 3-5, 3-6. 3-7
for i=1:n-1
    a00(i)=0.42748*(((R*TC(i))^2)/PC(i));
    b0(i)=0.08664*((R*TC(i))/PC(i));
    c0(i)=0.48+1.574*AF(i)-0.176*(AF(i)^2);
end


% Adjustable parameters of the CPA EoS, "u" matrix includes a0, b, c1, np, and miu.
"qq" is binary interaction parameters


U= [1.75818783778295,0.00795761680162180,1.83984712636527,1.04840488173193];

qq=[0.9825    -0.3072    -0.1401    -0.4711    -0.9719    0.9954];

b0(asp)=u(1);

b=[b0 b0(asph)];
np=u(2);
miu=u(3)*3.33569e-30;
T=308;
for i=1:n-1
    amm(i)=a00(i)*((1+c0(i)*(1-sqrt(T/TC(i)))).^2);
end

amm(asp)=u(4);
am=[amm amm(asp)];
```

```matlab
% binary interaction parameters adjusted for the equilibrium
kij=[0          qq(1)    qq(2)
     qq(1)   0          qq(3)
     qq(2)   qq(3)    0 ];


lij=[0          qq(4)    qq(5)
     qq(4)   0          qq(6)
     qq(5)   qq(6)    0 ];

a=aij(kij,am,n);
bi=bij(lij,b,n);


% Precipitated asphaltene (experimental data if available for validation)
% naspre_exp = amount of asphaltene precipitation
% nd = number of experimental data
% PEXP = experimental pressure (pascal)
% nastotal = initial oil asphaltene content
% nmperim = oil component fractions


naspre_exp=[0.0000192 0.0000636 0.0001194 0.0002382 0.000291 0.0003168 0.0003186];
nd=numel(naspre_exp);
PEXP=(6894.76*14.7)*ones(1,nd);
% nastotal is number of total moles of asphaltne in each data series
nastotal=0.0003908*ones(1,nd);
nmperim=[0.0957646790000000,0.00854300000000000;0.123126015000000,0.00854300000000000
;0.171008355000000,0.00854300000000000;0.331756208000000,0.00854300000000000;0.489083
894000000,0.00854300000000000;0.704554421000000,0.00854300000000000;0.831100603000000
,0.00854300000000000];
nm=[nmperim (nastotal-naspre_exp)'];
```

C-2-26-2
```matlab
% experimental mole fractions in oil phase
xEXP=ones(nd,3);
for j=1:nd
    xEXP(j,:)=nm(j,:)./sum(nm(j,:));
end


xperim=ones(nd,2);
for j=1:nd
    xperim(j,:)=nmperim(j,:)./sum(nmperim(j,:));
end


% Flash calculations of the asphaltene phase
```
C-2-26-3
```matlab
for j=1:nd
```

```
        p=PEXP(j);

        kk=1;
        A=Acapital(R,am(3),b(3),T,p);
        B=Bcapital(R,am(3),b(3),T,p);
```

% volume and fugacity calculations for precipitated phase
```
        vliqguess=1.1*b(3);
        output=vcpppolar(vliqguess,b(3),T,p,am(3),R,np,miu);
        if sum(output)==6000
            fugacityas=1e36;
            kk=50;
        else

            vliq=output(1);
            miupolarliq=output(2);
            zliq=p*vliq/(R*T);
            lnphil=fugacitycoeff(zliq,A,B,miupolarliq);
            phias=exp(lnphil);
            fugacityas=phias*p;
            fu(j)=fugacityas;
        end
```

C-2-26-4
```
        error=1;
        k=1;
        m1=1;
        step=0;
```
% First guess for flash calculations of the asphaltene mole fraction
```
        while error>=1e-12

        step=step+1;
        if step==1
            kwilson=(PC(3)/p)*exp(5.37*(1+AF(3))*(1-(TC(3)/T)));
            kas=1/(kwilson^(1/3));
            xa=1/kas;
            x=(1-xa)*xperim(j,:);
            x=[x xa];
            nas=(x(3)*sum(nmperim(j,:)))/(1-x(3));

        else
```
% Modification of the mole fraction calculation, step 2 to step n
```
            xa=x(3)*(fugacityas/fugacityl(3));
            x=(1-xa)*xperim(j,:);
            x=[x xa];
            nas=(x(3)*sum(nmperim(j,:)))/(1-x(3));
        end
```

C-2-26-5
% Volume and fugacity calculation of the CPA EoS for oil phase

```matlab
        bmixliq=Bmix2(x,bi,n);
        amixliq=Amix2(x,a,n);
        vliqguess=1.1*bmixliq;

        output=vcubic(vliqguess,R,T,amixliq,bmixliq,p);
        m1=m1+1;
        if sum(output)==20000
            fugacityl(3)=fugacityas;
            k=50;
        elseif m1>100
            fugacityl(3)=fugacityas;
            k=50;
        elseif nas>=nastotal(j)
            fugacityl(3)=fugacityas;
            k=50;
        elseif kk==50
            fugacityl(3)=fugacityas;
            k=50;
        else
            vliq=output(1);
            zliq=p*vliq/(R*T);
            lnphil=fugacitycoeffmix(x,vliq,bmixliq,amixliq,a,R,T,zliq,n,bi);
            phil=exp(lnphil);
            fugacityl=x.*phil*p;
        end
% Error calculations
        error=(1-(fugacityas/fugacityl(3)))^2;
        end


C-2-26-6
        if k==50
            xasphaltene(j)=1e36;
            naspre_calc(j)=1e36;
        else
            xasphaltene(j)=x(3);
            naspre_calc(j)=nastotal(j)-nas;
        end
end
naspre=[naspre_exp' naspre_calc'];
xpre=[xEXP(:,3) xasphaltene'];
AARDn=sum(abs((naspre_exp-naspre_calc)./naspre_exp))/nd;


% Plot the results
plot(xEXP(:,3),xasphaltene','*');
xlabel('Experimental mole fraction');
ylabel('model mole fraction');
hold on;
plot(xEXP(:,3),xEXP(:,3));

%%%%%%%%%%%%%%%%%%%%%%%%%%%%%%%%%%%%%%%%%%%%%%%%%%%%%%%%%%%%%%%%%%%%%%%%%%%%
C-2-27
% Binary attractive energy parameter calculation for oil phase, this
```

```
parameter later is used to calculate the cubic parameter of the EoS,
Chapter 3, Eq 3-6 and [6]


% bij (D2) = binary attractive energy parameter
% BIP (d1)= binary interaction parameter
% bi (d2) = cubic EoS parameter of component i
% n (d3) = number of components


function D2=bij(d1,d2,d3)
for i=1:d3
    for j=1:d3
        D2(i,j)=0.5*(d2(i)+d2(j))*(1-d1(i,j));
    end
end
%%%%%%%%%%%%%%%%%%%%%%%%%%%%%%%%%%%%%%%%%%%%%%%%%%%%%%%%%%%%%%%%%%%%%%%%%%
```

Reference

1. Kontogeorgis, G.M. and G.K. Folas, Thermodynamic models for industrial applications: from classical and advanced mixing rules to association theories. 2009: John Wiley & Sons.

2. Larsen, B., J. Rasaiah, and G. Stell, Thermodynamic perturbation theory for multipolar and ionic liquids. Molecular Physics, 1977. 33(4): p. 987-1027.

3. Riazi, M.R. and T.A. Al-Sahhaf, Physical properties of heavy petroleum fractions and crude oils. Fluid Phase Equilibria, 1996. 117(1-2): p. 217-224.

4. Akbarzadeh, K., Alboudwarej, H., Svrcek, W. Y., & Yarranton, H. W., A generalized regular solution model for asphaltene precipitation from n-alkane diluted heavy oils and bitumens. Fluid Phase Equilibria, 2005. 232(1-2): p. 159-170.

5. Kontogeorgis, Georgios M., Epaminondas C. Voutsas, Iakovos V. Yakoumis, and Dimitrios P. Tassios., An Equation of State for Associating Fluids. Industrial & Engineering Chemistry Research, 1996. 11 (35): p. 4310–18.

6. Jalaei Salmani, Hossein, Mohammad Nader Lotfollahi, and Seyed Hossein Mazloumi., Phase Equilibria Modeling of Polar Systems with Cubic-plus-Polar (CPP) Equation of State. Journal of Molecular Liquids, 2020. 297, 111879.

7. Shahriari, Reza, Mohammad Reza Dehghani, and Bahman Behzadi., A Modified Polar PHSC Model for Thermodynamic Modeling of Gas Solubility in Ionic Liquids. Fluid Phase Equilibria, 2012, 313: p. 60–72.

8. Danesh, A., PVT and phase behaviour of petroleum reservoir fluids. 1998: Elsevier.

Appendix D; MD calculations

To reduce the number of adjustable parameters of the EoS, MD calculations are used. Therefore, the dipole moment of the asphaltene molecule is calculated using MD simulation. Dipole moment refers to the measure of the separation of electric charges within a molecule, which results in a net electrical dipole. It is a vector quantity that has both magnitude and direction. Dipole moment can be determined through experiments or theoretically. From the experimental point of view, dipole moment can be measured by applying dielectric constant measurement, infrared (IR) spectroscopy, nuclear magnetic resonance (NMR) spectroscopy, X-ray crystallography, and electrochemical methods. However, conducting experiments can be a time-consuming and costly process. However, an analytical calculation can provide an efficient way to calculate the dipole moment of a molecule, as it avoids the need for time-consuming and costly experimental measurements.

The MD calculations were performed in this research using Gaussian 09 and Gaussview 05. Therefore, the following steps are followed to calculate the dipole moment of the asphaltene molecule.

1. One asphaltene molecule are designed using Gaussview 05. The asphaltene molecules used in this research are depicted in figure 4-3.
2. From the job type in the Gaussian 09 simulator, optimization is chosen.
3. Ground state and Hartree Fock are selected for the calculation method.
4. No solvation is picked since pure component calculations are needed.
5. Molecule optimized to calculate physical properties, e.g., dipole moment.